MONASH University

A novel epigenetic modification regulating telomeric chromatin assembly

Vinod Benjamin

BBmedSc (Hons)

A thesis submitted for the degree of ***Doctor of Philosophy*** at

Monash University in *2021*

Biochemistry and Molecular Biology

Copyright notice

Abstract

Aurora Kinase B (AURKB) is a serine/threonine kinase that localises to the centromeric region to maintain proper mitotic progression. This thesis demonstrates the novel localisation of AURKB at the telomere of embryonic stem (ES) cells. The maintenance of telomere chromatin is dynamic and is critical in protecting the genome and preventing aberrant transcription. *In vitro* kinase experiments identified that AURKB mainly interacted with S404 on TERF1, a telomere specific protein, to maintain telomere integrity. The loss of either AURKB or TERF1 resulted in aberrant telomere structures. The overexpression of either phospho-null (Serine to Alanine, S404A)-TERF1 or phospho-mimic (Serine to Glutamic acid, S404E)-TERF1 in ES cells resulted in fragile telomere formation. Interestingly, homodimerization of S404E-TERF1 and endogenous TERF1 resulted in their loss of binding at the telomeres, causing aberrant telomere lengthening. These findings demonstrate that AURKB plays a unique role at the telomers of ES cells to regulate telomere structural integrity.

Another protein targeted by AURKB is Histone H3 where AURKB phosphorylates H3 Serine 10 (H3S10) and H3 Serine 28 (H3S28). In addition to Serine 10 and Serine 28, AURKB also phosphorylates the Serine 31 residue on the histone variant H3.3. Histone H3.3 is evolutionarily conserved across species and is loaded into chromatin by its chaperone α-Thalassemia X-Linked Mental Retardation (ATRX) and Death Domain Associated Protein (DAXX) at DNA repeats, including the telomeres and pericentric DNA, to form a compacted and transcriptionally silenced heterochromatin. In mammalian cells, the lack of either H3.3 or ATRX fails to form heterochromatin, accompanied by increased transcriptional activities at these repeats.

Unique to histone H3.3 is a serine residue at position 31 (alanine in canonical H3). This serine residue of H3.3 is phosphorylated (H3.3S31ph) at telomeres and pericentric repetitive DNA region during mitosis. Given the role of H3.3 in telomeric repeat silencing, we hypothesise that H3.3S31ph is a histone mark associated with heterochromatin silencing and is essential for maintaining telomere chromatin integrity. To test our hypothesis, endogenous-H3.3-null S31-H3.3 phospho-null (Serine to Alanine, S31A-H3.3) and endogenous-H3.3-null S31-H3.3 phospho-mimic (Serine to Glutamic acid, S31E-H3.3) mutant ES cell lines were generated. Consistent with our hypothesis, the S31A-H3.3 mutation resulted in reduced ATRX binding and H3K9me3 level at the telomeres, indicating a disruption in heterochromatin maintenance at the telomeres. In contrast, the S31E-H3.3 mutation led to gains in ATRX and H3K9me3 level at the telomeres, indicating a gain in the capacity for the formation of heterochromatin. Additionally, S31A-H3.3 mutant ES cells showed an increase in the binding of KDM4B, a histone H3K9 and H3K36 demethylase, at the telomeres. This indicated that the increased KDM4B binding and activity could drive the loss of heterochromatin marks at telomeres in S31A-H3.3 cells. In line with this, RNAi knockdown experiments show that the depletion of KDM4B restored ATRX and H3K9me3 levels at the telomeres in S31A-H3.3 ES cells. This thesis investigates, shows, and proposes a model of which H3.3S31ph regulates KDM4B binding and, its crucial role in regulating heterochromatin silencing at the telomeres. In addition, this thesis proposes that H3.3S31ph is a vital component of a heterochromatin silencing pathway at other DNA repeats across the genome.

Declaration

This thesis is an original work of my research and contains no material which has been accepted for the award of any other degree or diploma at any university or equivalent institution and that, to the best of my knowledge and belief, this thesis contains no material previously published or written by another person, except where due reference is made in the text of the thesis.

Publications during enrolment

CHAN, F. L., VINOD, B., NOVY, K., SCHITTENHELM, R. B., HUANG, C., UDUGAMA, M., NUNEZ-IGLESIAS, J., LIN, J. I., HII, L., CHAN, J., PICKETT, H. A., DALY, R. J. & WONG, L. H. 2017. Aurora Kinase B, a novel regulator of TERF1 binding and telomeric integrity. *Nucleic Acids Res,* 45**,** 12340-12353.

UDUGAMA, M., HII, L., GARVIE, A., CERVINI, M., VINOD, B., CHAN, F. L., DAS, P. P., MANN, J. R., COLLAS, P., VOON, H. P. J. & WONG, L. H. 2021. Mutations inhibiting KDM4B drive ALT activation in ATRX-mutated glioblastomas. *Nat Commun,* 12**,** 2584.

UDUGAMA, M., VINOD, B., CHAN, F. L., HII, L., GARVIE, A., KALITSIS, P., COLLAS, O., MANN, J. R., VOON, H. P. J. & WONG, L. H. Histone H3.3 phosphorylation promotes heterochromatin formation by inhibiting histone demethylase. *In preparation.*

Acknowledgements

This research was supported by the Monash Postgraduate Discovery Scholarship (MPDS) provided by Monash Biomedicine Discovery Institute, Monash University.

I would like to acknowledge the guidance of the Lee Wong Laboratory (EpiC Lab) for their assistance throughout my PhD candidature. In particular, I would like to acknowledge the assistance, guidance and motivation provided by Assoc. Prof. Lee Wong, Dr. Lyn Chan, Dr. Hsiao Voon, Dr. Maheshi Udugama, and Linda Hii without which, this milestone of my life would have been unattainable. Furthermore, I would like to acknowledge the inputs by collaborators such as Assoc. Prof Jeffery Mann and Prof. Philippe Collas, without which some ideas would have been lost.

In addition to their support academically, I would like to acknowledge the EpiC lab for being there for me in times of crisis, including the COVID-19 pandemic. Together with my family and friends, for mental and emotional support, I was able to complete this thesis in an otherwise taxing time.

Table of Contents

List of Figures

List of Tables

List of Abbreviations

ALT	Alternate lengthening of telomere
APB	ALT-associated promyelocytic leukaemia (APB)
APH	Aphidicolin
ATM	Ataxia telangiectasia mutated
ATR	ATM and Rad3-related
ATRX	Alpha Thalassemia Mental retardation syndrome X-linked
AURKA	Aurora Kinase A
AURKB	Aurora Kinase B
CDK1	Cyclin-dependent kinase 1
CENP-A	Centromere Protein A
CFP	Cyan fluorescent protein
ChIP	Chromatin immunoprecipitation
CHK1	Checkpoint Kinase
Daxx	Death associated protein 6
DNA	Deoxyribonucleic Acid
DNMT	DNA methyltransferase
DSB	Double-stranded breaks
ES cells	Embryonic stem cells
FACS	Fluorescence-activated cell sorting
GFP	Green fluorescent protein
H3.3G34R	Histone H3.3 glycine 34 to arginine
H3.3S31A/S31A-H3.3	Histone H3.3 serine 31 to alanine
H3.3S31D	Histone H3.3 serine 31 to aspartic acid
H3.3S31E/S31E-H3.3	Histone H3.3 serine 31 to glutamic acid
H3.3S31ph	Histone H3.3 serine 31 phosphorylation
H3K27me1	Histone 3 lysine 27 mono-methylation
H3K27me2	Histone 3 lysine 27 di-methylation
H3K27me3	Histone 3 lysine 27 tri-methylation
H3K9ac	Histone 3 lysine 9 acetylation
H3K9me1	Histone 3 lysine 9 mono-methylation
H3K9me2	Histone 3 lysine 9 di-methylation
H3K9me3	Histone 3 lysine 9 tri-methylation
H3S10ph	Histone H3 serine 10 phosphorylation
H3S28ph	Histone H3 serine 28 phosphorylation
H4K20me1	Histone 4 lysine 20 mono-methylation
H4K20me2	Histone 4 lysine 20 di-methylation
H4K20me3	Histone 4 lysine 20 tri-methylation
HA	Human influenza hemagglutinin
HAT	Histone acetyltransferases
HDAC	Histone deacetylases
HDMT	Histone demethylases

HDR	Homology-directed repair
HMET	Histone methyltransferases
HP1	Heterochromatin protein
HR	Homologous Recombination
IKKα	IκB Kinase α
JmjC	Jumonji C
JmjN	Jumonji N
KDM3	Lysine demethylase 3
KDM4	Lysine demethylase 4
KDM7	Lysine demethylase 7
MEF	Mouse embryonic Fibroblast
MTS	Multiple telomeric signals
NHEJ	Non-homologous end-joining
PHD	Plant homeodomain
PIKK	Phosphoinositide 3-kinase-related protein kinase
PLK1	Polo-like kinase 1
PML-NBs	Promyelocytic nuclear bodies
POT1	Protection of telomere
PTMs	Post-translational modifications
RAP1	TERF2 interacting proteins
RNA	Ribonucleic acid
S404A-TERF1	Serine 404 to alanine on TERF1
S404E-TERF1	Serine 404 to glutamic acid on TERF1
Tel-FISH	Telomere fluorescence *in-situ* hybridisation
TERF1	Telomeric repeat binding factor 1
TERF2	Telomeric repeat binding factor 2
TIN1	TERF1 interacting nuclear factor 2
TPP1	Tripeptidyl peptidase I
WT	Wild-type
YFP	Yellow fluorescent protein
γH2AX	Histone H2AX serine 139 phosphorylation

Chapter 1: Introduction

1.1 Functions of Chromatin

1.1.1 Properties of chromatin

Eukaryotes have enormous genomes. For example, the human genome measures 2 metres long, lined up end to end, yet must fit inside a cell nucleus approximately 10 microns in diameter. To safely and efficiently store this vast amount of genetic material within the nucleus, eukaryotic cells have developed a packaging system known as chromatin. Chromatin is a complex of Deoxyribonucleic Acid (DNA) and specialised proteins called histones. DNA wraps around a complex of histones, like beads on a string, and this 'string' is folded back upon itself several times to enable a higher-order organisation, eventually forming discrete structures known as chromosomes. In addition to packaging and storing DNA, chromatin is also essential in regulating other critical nucleic acid transactions, such as transcription during gene expression, DNA replication and DNA repair (Goodarzi and Jeggo, 2012, Venkatesh and Workman, 2015).

The chromatin organisation is essential for influencing the stability of DNA and gene-expression patterns (Cheutin et al., 2003). This organisation is maintained by chemical modifications of either histones or DNA, which regulates access to chromatin factors such as transcriptional factors and replicational machinery to the DNA (Hirota et al., 2005, Francis et al., 2004, Gilbert et al., 2007, Grewal and Jia, 2007).

1.1.2 Types of heterochromatins

Chromatin includes both heterochromatin and euchromatin. Euchromatin consists of 'open' chromatin and comprises the transcriptionally active parts of the genome. In contrast, heterochromatin consists of gene-poor regions of the genome, which are highly compacted and transcriptionally silent. Heterochromatin, which consists of a large part of the genome, is further classified into either constitutive or facultative heterochromatin.

Constitutive heterochromatin consists of repetitive DNA regions such as the centromeres, pericentric DNA and telomeres. Constitutive heterochromatin acts as a genome stabiliser that prevents gene rearrangements between highly similar genetic sequences, ensuring efficient chromosomal segregation. These regions localise predominantly at the periphery of the nucleus and are enriched in histone post-translational modifications (PTMs) including Histone 3 Lysine 9 tri-methylation (H3K9me3) and Histone 4 Lysine 20 tri-methylation (H4K20me3). These histone PTMs are essential for forming a compacted chromatin structure and maintaining transcriptional silencing (**Figure 1.1**). Unlike constitutive heterochromatin, facultative heterochromatin is enriched with a different histone PTM, namely, Histone 3 Lysine 27 tri-methylation (H3K27me3). However, it exerts a similar function by promoting transcriptional silencing (**Figure 1.1**). Facultative heterochromatin is established in a developmentally regulated manner and can be found on gene promoters (Trojer and Reinberg, 2007, Young et al., 2011). It ensures the epigenetic silencing of genes in a specific cell type or tissue and is an essential mechanism for developmental programming and cell fate. However, with specific developmental signalling cues, facultative heterochromatin can be de-repressed and become transcriptionally active. An example of facultative heterochromatin is the inactive X-Chromosome, where the X chromosome is active in males and inactive in females (Trojer and Reinberg, 2007, Chen and Dent, 2014).

Overall, both constitutive and facultative heterochromatin form repressive chromatin structures and are associated with transcriptional silencing.

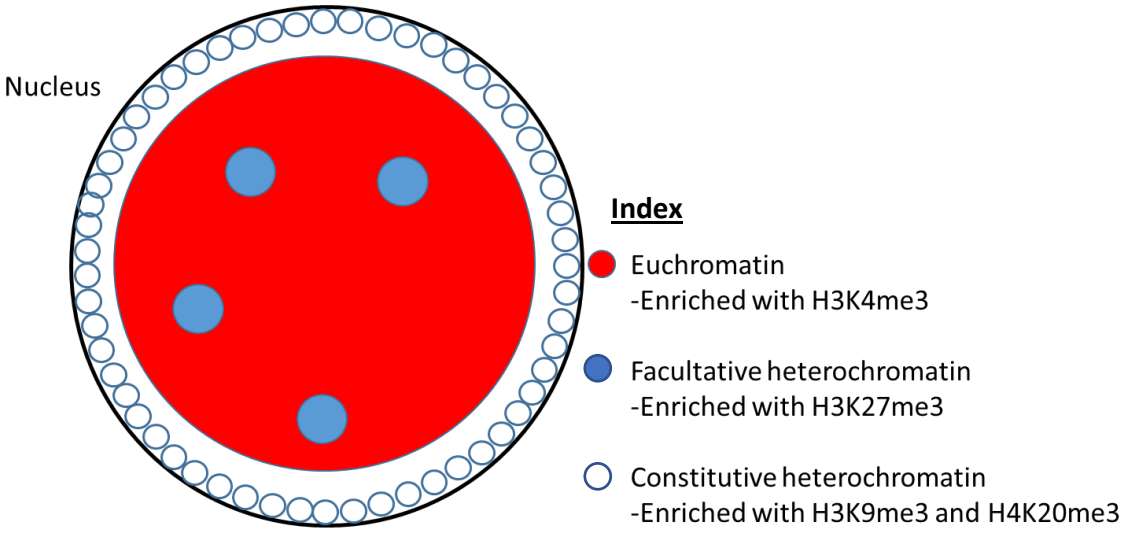

Figure 1.1 An overview of the location of euchromatin and heterochromatin within the nucleus.

Both euchromatin (red) and facultative heterochromatin (dense chromatin region; blue) are located throughout the genome, while constitutive heterochromatin is located mainly at the periphery of the nucleus (blue circles).

1.2 Histones post-translational modifications and histone variants

1.2.1 Properties of histones

Chromatin encompasses DNA and proteins such as histones which are highly conserved among eukaryotes (Baxevanis and Landsman, 1996). Two units of each histone H2A, H2B form two dimers while two units of each H3 and H4 forms a tetramer. Together, these subunits form an octamer. The octamer is wrapped by approximately 146 base pairs of nucleotide in a 1.67 left-handed super-helical turn to form the nucleosome, an essential subunit of chromatin (Van Holde et al., 1974). These histone subunits are rich in positively charged basic amino acids, allowing for interaction with the negatively charged DNA (Kornberg, 1974, Luger et al., 1997). Each histone monomer comprises a histone core region and an N-terminal tail that protrudes from the histone core (**Figure 1.2**) (Davey et al., 2002, Luger et al., 1997). Histone tails are subjected to a variety of PTMs and they play key roles in altering chromatin structure and function (Bannister and Kouzarides, 2011).

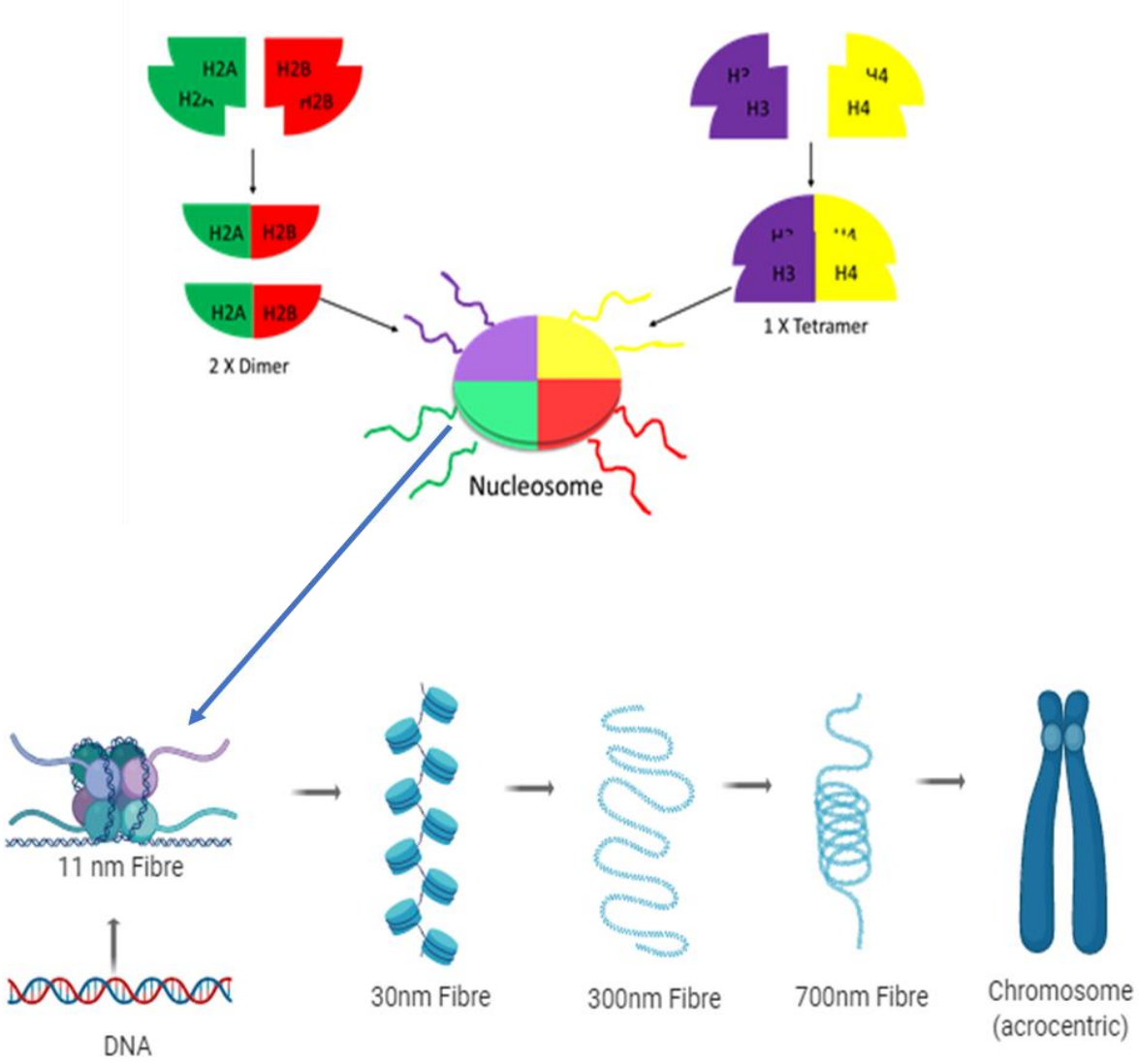

Figure 1.2: Nucleosomes and the compaction of chromatin

Two units of H2A and H2B form 2 dimers. 2 units of each H3 and H4 form a tetramer. These units then interact to form the octamer. The unique feature of the nucleosome is the protrusion of the N-terminal tail of each histone monomer. These N-terminal tails are subject to post-translational modifications which regulate the chromatin state. The DNA wraps around the nucleosomes to form higher-order structures to compact DNA within the nucleus.

1.2.2 Post translational modification of histones

Histone tails are subjected to various PTMs such as acetylation, methylation, and phosphorylation (**Figure 1.3**). Such PTMs act as a histone code to alter chromatin function by creating or removing binding sites for chromatin-associated proteins, such as histone methyltransferases (HMT), histone acetyltransferases (HAT), histone demethylases (HDM) and histone deacetylases (HDAC). A summary of histone PTMs and their regulators are shown in **Table 1.1.**

On histone H3, various residues are subjected to PTMs. For example, Histone 3 Lysine 9 acetylation (H3K9ac) is associated with active promoters and transcriptional activation (Karmodiya et al., 2012). H3K9ac, together with H3K14ac and H3K4me3, are hallmarks of active transcription (Karmodiya et al., 2012). The enrichment of H3K9ac and H3K14ac were observed at the promoter and enhancer regions of active genes (Karmodiya et al., 2012). The acetylation of H3K9 is regulated by the HAT, GCN5 (Jin et al., 2011), and deacetylated by the HDAC, Sirt6 (Michishita et al., 2008). In ES cells, H3K9ac and H3K14ac co-occur with other active histone modifications including H3K4me3. In addition to H3K9ac, H3K4me3 and H3K14ac, active chromatin is also characterised by other PTMs including H3K27ac, H3K36me3 and H3 and H4 acetylation at enhancers, promoters and gene bodies of active genes (Liang et al., 2004, Deckert and Struhl, 2001, Creyghton et al., 2010, Myers et al., 2001, Pokholok et al., 2005). These active modifications maintain an “open chromatin state”, allowing for transcription through regulating the interaction between transcriptional factors and chromatin.

H3K4me3 is catalysed by SETD1A, SETD1B, MLL1, MLL2, MLL3, and MLL4 in mammalian cells and is distributed along the promoter and TSS regions (Sims et al., 2003, Zhang et al.,

2015). At these regions, HAT binds to H3K4me3 through the tudor domain at gene promoters and the deletion of the HAT results in the loss of H3K9ac (Bian et al., 2011). In addition, various studies have shown that HAT complexes contain PHD fingers that preferentially bind H3K4me3 to regulate HAT and HDAC activity in the genome (Doyon et al., 2004, Taverna et al., 2006). In fact, the loss of SET1 and loss of H3K4me3 showed a loss of both H3 acetylation and transcriptional activation (Hsu et al., 2012, Clayton et al., 2006). Thus, the targeting of H3K4me3 by HATs and HDACs facilitate the turnover of histone acetylation and indicates that the regulation of acetylation is essential in ensuring proper transcriptional maintenance.

In addition to active histone modifications, chromatin is also enriched with repressive histone modifications. H3K9me3 and H4K20me3 are hallmarks of constitutive heterochromatin (Saksouk et al., 2015). H3K9me3 is enriched on inactive genes including promoters of CpG islands (Ohm et al., 2007) and short tandem repeats, such as the telomeres (Mikkelsen et al., 2007, Udugama et al., 2015, Barski et al., 2007). H3K9 is tri-methylated by SUV39H (Dang-Nguyen et al., 2013) and is recognised by the chromodomain of heterochromatin protein 1α (HP1α) (Lehnertz et al., 2003) which play roles in heterochromatin formation, chromatin compaction and gene repression (Bannister et al., 2001, Nakayama et al., 2001). This indicates the importance of H3K9 PTM in regulating constitutive heterochromatin.

Histone 4 Lysine 20 tri-methylation (H4K20me3), another hallmark of heterochromatin, is a constitutive heterochromatin mark regulated by SUV4-20 (Benetti et al., 2007). H4K20me3 is enriched at heterochromatic regions including repetitive elements such as the pericentric regions (Schotta et al., 2004) and the telomeres (Benetti et al., 2007) where it facilitates

transcriptional repression (Karachentsev et al., 2005, Schotta et al., 2008, Schotta et al., 2004, Fodor et al., 2010). This indicates a specialised H4K20 PTM function.

Unlike the constitutive heterochromatic marks, the different levels of the facultative heterochromatin mark, H3K27 methylation, is involved in transcriptional activation and inactivation. For example, H3K27me1 is involved with transcriptional activation while H3K27me2/3 is associated with transcriptional inactivation (Zhang et al., 2015). The enrichment of H3K27me3 is mutually exclusive to H3K9me3. The depletion of SUV39H, a H3K9 HMT, resulted in a loss of H3K9me3 and a subsequent increase in H3K27me3, indicating that these marks may compensate for each other and, that H3K9me3 prevents H3K27me3 establishment (Cooper et al., 2014, Peters et al., 2003). Together with the loss of H3K9me3 and increased H3K27me3, DNA methylation is also decreased (Cooper et al., 2014). Thus, the methylation of H3K27 is important in maintaining transcriptional regulation and may act as a heterochromatin substitute.

Another common histone PTM is the phosphorylation of serine and threonine residues. Phosphorylation of critical residues on different histones is associated with various chromatin function. An example of histone phosphorylation is Histone 3 Serine 10 phosphorylation (H3S10ph). H3S10ph, which is observed in various organisms including *maize* (Kaszas and Cande, 2000), *tetrahymena* (Wei et al., 1999), *C. elegans* (Speliotes et al., 2000) and eukaryotes (Wei et al., 1998, Wei et al., 1999), has been suggested to be a mitotic specific mark. In *Tetrahymena*, H3S10ph is associated with mitotic chromosome condensation and segregation, however, the loss of H3S10ph does not affect chromosomal condensation in *C. elegans* (Speliotes et al., 2000). Furthermore, in maize, H3S10ph has been found to play a role in maintaining proper sister chromatid cohesion during meiosis,

instead of condensation of chromatin (Kaszas and Cande, 2000). Together, these studies indicate that H3S10ph is a mitosis-specific mark, but its primary function remains unclear and requires further investigation.

The enrichment of H3S10ph during mitosis was also observed across various species, including mammals (Hendzel et al., 1997) and *Xenopus* (de la Barre et al., 2000). Interestingly, H3S10ph was shown to be associated with transcriptional activation (Johansen and Johansen, 2006) where it facilitates the dissociation of HP1α from heterochromatin (Hirota et al., 2005). H3 Serine 10 is phosphorylated by kinases such as Aurora Kinase B (AURKB) and dephosphorylated by phosphatases such as Protein Phosphatase 1 (Wei et al., 1999). AURKB, found predominantly at the centromere, is a key regulator of mitosis. In fact, AURKB is known to phosphorylate other residues such as Histone 3 Serine 28 (Goto et al., 2002), suggesting its role as an essential regulator of histone phosphorylation.

Interestingly, these modifications may affect the modifications on adjacent residue. This phenomenon is known as histone crosstalk. An example is the crosstalk between H3S10ph and H3K14ac at the promoters (Cheung et al., 2000, Lo et al., 2000). *In vitro* and *in vivo* studies showed that phosphorylation of H3S10 increased the activity of GCN5, a HAT. GCN5 is known to regulate H3K14 acetylation, which in turn regulates transcriptional elongation (Johnsson et al., 2009). This enhanced activity was lost with a mutation of H3S10 to alanine and resulted in the loss of H3K14ac (Lo et al., 2000). A similar phenotype was seen with the mutation of H3S10, where transcription of genes was impaired (Lo et al., 2000). However, H3K14ac did not affect H3S10 phosphorylation. In fact, GCN5 preferentially binds to phosphorylated H3S10, compared to unphosphorylated H3S10 *in*

vitro, to promote H3K14 acetylation (Lo et al., 2000). This indicates the importance of crosstalk between histone PTMs and their roles in regulating chromatin functions. Of the histone PTMs, the phosphorylation of H3.3 Serine 31 is of importance to this project.

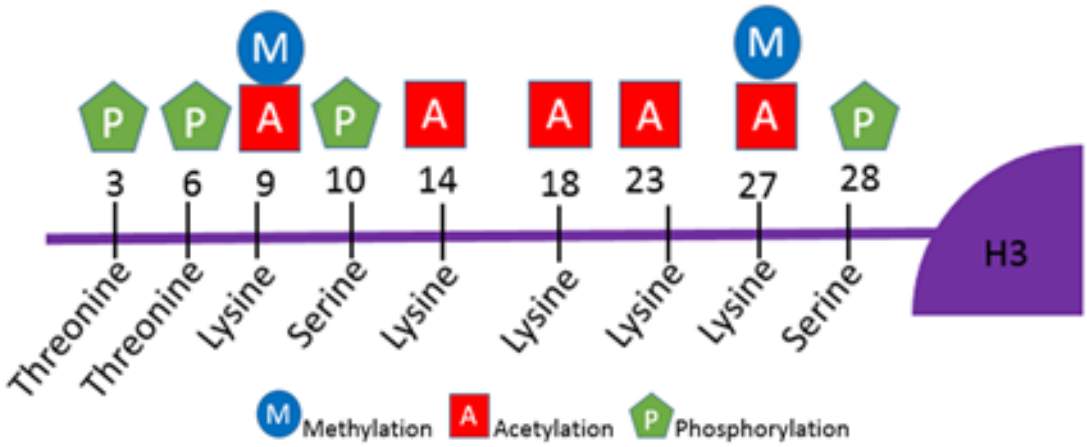

Figure 1.3: Post translational modifications of Histone H3

The N-terminus tail on Histone H3 shows the various residues that can be covalently modified. Residues such as Lysine 9 can be methylated (blue circles) or acetylated (red square), whereas the Serine and Threonine residues such as the Serine 10 and Threonine 3 can be phosphorylated (green pentagon). The numbers denote the position of amino acid residues on Histone H3.

Table 1.1: Examples of residues on histones that may be post translationally modified

Residue	Modification	Writer	Function
H4R3	Mono-methylation Di-methylation	PRMT1	Transcriptional repression (Xu et al., 2010)
H3K14	Acetylation	GCN5	Transcriptional elongation (Johnsson et al., 2009)
H4K16	Acetylation	hMOF	Transcriptional activation (Taylor et al., 2013)
H4K20	Tri-methylation	SUV420	Transcriptional silencing (Wongtawan et al., 2011, Becker et al., 2016)
H3K9	Tri-methylation	SUV39, SETDB1	Transcriptional repression (Becker et al., 2016)
H3K27	Di-methylation Tri-methylation	EZH2	maintains facultative heterochromatin (Hon et al., 2009)
H2AXS139	Phosphorylation	ATM/ATR	Facilitate DNA damage repair (Chowdhury et al., 2005)
H2AY142	Phosphorylation	WSTF-SNF2h	DNA damage regulation (Xiao et al., 2009, Cook et al., 2009)
H3S10	Phosphorylation	AURKB/MSK1/CHK1	Chromatin organisation (Johansen and Johansen, 2006)
H3T11	Phosphorylation	CHK1	Regulation of DNA damage (Shimada et al., 2008)

1.2.3 Histone variants

In addition to the regulation of histones by post-translational modifications, canonical histone subunits may be replaced with variants for specialised function (Table 1.2). An example is H2AX, a variant of histone H2A. H2AX is a substrate of several phosphoinositide 3-kinase-related protein kinases (PIKKs), such as ATM (ataxia telangiectasia mutated) and ATR (ATM and Rad3-related). The phosphorylation of Serine 139 on H2AX, known as γH2AX, is regulated by ATM in response to the formation of double stranded breaks (DSB) and, ATR in response to single-stranded DNA breaks during replication stress (Podhorecka et al., 2010). γH2AX then recruits repair factors such as 53BP1 and repairs DNA through Non-Homologous End Joining (NHEJ) and Homologous Recombination (HR) to prevent DNA damage and defects in DNA damage repair (Celeste et al., 2003, Xie et al., 2004).

H2AZ, another variant of H2A, also plays an important role in regulating centromere function and heterochromatin formation, where its loss leads to defects in heterochromatin formation, centromere cohesion and structural change in pericentric heterochromatin (Rangasamy et al., 2004) and, transcriptional activation in humans (Barski et al., 2007). Recently, a study showed that GCN5, a histone acetyltransferase, regulates acetylation of H2AZ at the promoters of transactivated genes. Together with the XPC–RAD23–CEN2, a DNA repair complex which act as a transcriptional coactivator, GCN5 regulates H2AZ acetylation to alter promoter landscape (Semer et al., 2019).

Another critical example is Centromere Protein A (CENP-A), a variant of H3, which localises specifically to the centromeres of mammalian chromosomes (Yoda et al., 2000, Sullivan et al., 1994) and is required to recruit proteins for kinetochore function during chromosome segregation (Black et al., 2004, Black et al., 2007). CENP-A is also known to establish and

maintain the identity of the centromere (Black et al., 2007, Logsdon et al., 2015). This illustrates how the incorporation of histone variants allow for specialised function in the regulation of chromatin. Of importance to this thesis is H3.3, a histone H3 variant.

Table 1.2: A summary of histone variants and their specialised functions and locations.

Canonical Histone	Variant	Tissue/Genomic localisation	Function
H2A	H2A.B	Testis	Transcription upregulation, splicing, DNA synthesis and spermiogenesis (Tolstorukov et al., 2012, Sansoni et al., 2014, Gonzalez-Romero et al., 2008)
	H2AX	DNA damage regions (Seo et al., 2012)	Regulation of DNA damage response (Podhorecka et al., 2010)
	H2AZ	Promoters and enhancers (Chen et al., 2014, Obri et al., 2014)	Early development, establishing chromatin structures, controls localisation of HP1α (Ridgway et al., 2004b, Iouzalen et al., 1996, Faast et al., 2001, Rangasamy et al., 2004, Ridgway et al., 2004a)
	MacroH2A	Inactive X chromosome (Costanzi and Pehrson, 1998)	X chromosome inactivation (Costanzi and Pehrson, 1998)
H2B	hTSH2B	Testes and sperm	Protein present in mature human sperm cell indicating a role in sperm cell regulation and/or fertilisation (Zalensky and Zalenskaya, 2007)
	H2BQ (Bonenfant et al., 2006)	Unknown	Unknown
H3	H3.t	Testis	Involved in spermatogenesis (Maehara et al., 2015, Tachiwana et al., 2010, Ueda et al., 2017)
	CenpA	lowly or non-transcribed (centromeric region) genomic regions (Kang et al., 2016)	Maintenance and establishment of Centromere (Van Hooser et al., 2001)
	H3.3	Promoters, Gene bodies and repeats (Chen et al., 2014, Goldberg et al., 2010, Wong et al., 2010)	Involved in embryonic development, cellular differentiation, and spermatogenesis (Krimer et al., 1993, Castiglia et al., 1994, Jang et al., 2015)

1.3 Functions of H3.3

1.3.1 H3.3, a histone H3 variant

Evolutionarily, the canonical H3.1 and H3.2 were derived from H3.3 (Postberg et al., 2010). The presence and conservation of H3.3 between organisms indicate the importance of H3. Compared to H3.3, H3.1 and H3.2 differ by 5 and 4 amino acids, respectively (**Figure 1.4**) (Hake and Allis, 2006). The amino acid changes in the globular region (residue 87, 89 and 90) are critical for the replication-independent loading of H3.3 (Lewis et al., 2010). This was shown by a mutagenesis study on H3, where these residues were mutated to the corresponding H3.3 residues. This resulted in H3 attaining the ability to load independent of replication in *Drosophila melanogaster* (Ahmad and Henikoff, 2002). In addition to the amino acid changes on the globular region, H3.3 consist of a serine at residue 31 on the N-terminal tail, whereas canonical H3.1/2 consist of alanine. This gives rise to a new site ready for phosphorylation.

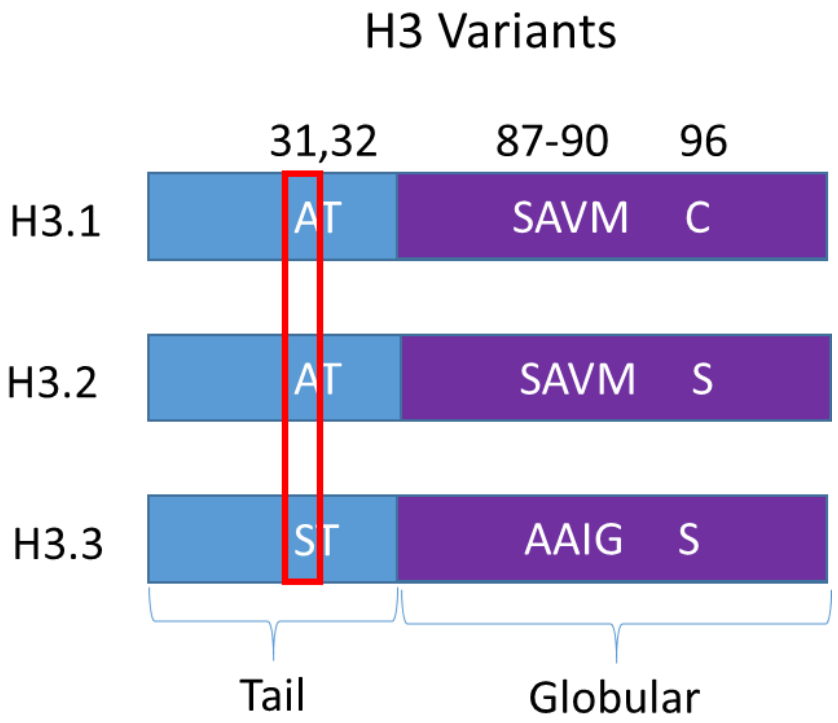

Figure 1.4: Amino Acid differences between H3 variants

Shown are the differences in H3 variant residues. Most differences are in the core region. The residue of interest is serine 31 on the histone H3.3 tail.

1.3.2 The regulation of histone H3.3 by chaperones

Unlike most proteins, H3.3 is encoded by two genes: *h3f3a* and *h3f3b* (Akhmanova et al., 1995, Wells et al., 1987). Although these two genes encode an identical protein, they are found on different chromosomes, have different nucleotide sequence, and have a different gene structure, suggesting that these two genes may be regulated differently (Akhmanova et al., 1995, Wells et al., 1987).

H3.1 and H3.2 are expressed highest during S phase, where they are required for incorporation into the chromatin of newly replicated DNA (Szenker et al., 2011, Osley, 1991). This allows for proper nucleosome assembly during S phase (Szenker et al., 2011, Osley, 1991). Unlike their canonical counterparts, H3.3 is expressed in a replication-independent manner and incorporated into chromatin (Hake et al., 2005, Brush et al., 1985, Garcia et al., 2005, Hake and Allis, 2006, Hake et al., 2006).

In addition to the difference in expression between canonical H3 and H3.3, they employ different histone chaperones to regulate their loading into chromatin. An essential difference between the H3 and H3.3 is their loading into the chromatin by histone chaperones. H3.1/2 is loaded by Chromatin assembly factor 1 (Garcia et al., 2005, Hake and Allis, 2006) while H3.3 is loaded by HIRA at euchromatic regions (Elsaesser and Allis, 2010) and Alpha Thalassemia Mental retardation syndrome X-linked/Death associated protein 6 (ATRX/DAXX) at heterochromatic regions (Elsaesser and Allis, 2010, Wong et al., 2010) (**Figure 1.5**).

The ATRX gene contains an ATPase and helicase domain and is a member of the SWItch/Sucrose Non-Fermentable (SWI/SNF) family of chromatin remodeler. ATRX was

first discovered in *ATRX* syndrome and, thus, was termed ATRX (Gibbons et al., 2008). However, it was later discovered that ATRX was a chaperone of H3.3 (Lewis et al., 2010, Wong et al., 2010). The loss of ATRX contributed to the loss of H3.3, H3K9me3 and H4K20me3 at heterochromatic regions (Udugama et al., 2015, Wong et al., 2010). Recent findings have shown that ATRX recognises H3.3K9me3 to deposit newly synthesised H3.3 into chromatin (Udugama et al., 2015). In addition, another study identified the importance of H3.3 loading at endogenous transposable elements by ATRX/Daxx, where H3K9me3 levels and silencing of these regions are maintained by recruitment of repressors in mouse ES cells (Elsasser et al., 2015). Similarly, DAXX was initially discovered as a Fas death receptor-binding protein that caused apoptosis through the JNK pathway (Yang et al., 1997). The knockout of Daxx was shown to cause embryonic lethality and apoptosis, an unexpected phenotype as the presence of Daxx was thought to cause apoptosis (Michaelson et al., 1999). Furthermore, the loss of Daxx resulted in a decrease in H3.3 loading in the pericentric regions (Drane et al., 2010). Nonetheless, ATRX/Daxx forms a complex with H3.3, where Daxx binds directly to H3.3 and plays an essential role in H3.3 loading at heterochromatic regions (Tang et al., 2004, Xue et al., 2003, Lewis et al., 2010).

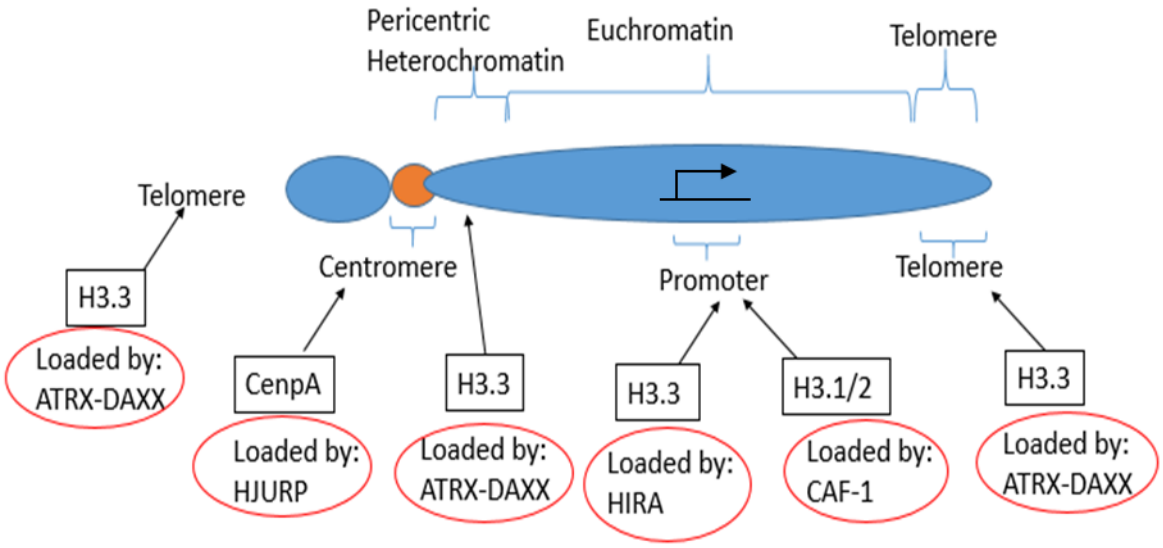

Figure 1.5: Loading of Histone H3 and variants by chaperones

Loading of the Histone H3 variants (Boxed in black) to their respective positions (Indicated by arrows) with the aid of chaperones (Circled in red). Histone CenpA is loaded at the centromeric region by HJURP. Histone H3.1/2 is loaded by CAF1 at promoter regions. H3.3 is loaded at euchromatic regions such as the promoters by HIRA and at heterochromatic regions such as the telomeres and centromeres by ATRX/Daxx.

1.3.3 Role of H3.3 in development

H3.3 plays many roles, such as controlling gene expression, embryonic development, cellular differentiation, and spermatogenesis (Krimer et al., 1993, Castiglia et al., 1994, Jang et al., 2015). For example, in *Drosophila melanogaster*, the deletion of both *h3f3a* and *h3f3b* resulted in reduced viability and sterility in males and females (Sakai et al., 2009, Hodl and Basler, 2009). Interestingly, in *Xenopus Laevis*, gastrulation defects were caused by knockdown of H3.3, while knockout of *h3f3a* in zebrafish caused a loss of head skeletal structure (Szenker et al., 2012, Cox et al., 2012). In mammals such as mice, the complete removal of *h3f3a* and *h3f3a* leads to primary oocyte failure and rapid cell death (Bush et al., 2013, Jang et al., 2015, Tang et al., 2015, Tang et al., 2013a). Interestingly, the knockout of *h3f3a* results in embryonic lethality, reduced growth rate and partial male sterility, while the knockout of *h3f3b* showed similar but more severe phenotypes (Tang et al., 2015, Jang et al., 2015). In addition, although a study showed that the complete loss of *h3f3a* also causes foetal death (Tang et al., 2015), another study suggested that some *h3f3a* knockout mice could reach adulthood (Bush et al., 2013). Additionally, the deletion of both *h3f3a* and *h3f3b* genes in mouse embryonic fibroblasts, through *Cre*-mediated knockout, resulted in chromosomal defects such as aberrant sister chromatid exchange, polyploidy, aneuploidy and DNA damage (Jang et al., 2015).

1.3.4 Role of H3.3 in transcription

H3.3 was initially observed at actively transcribed regions such as gene bodies (Daury et al., 2006) and promoters (Chow et al., 2005, Goldberg et al., 2010, Ahmad and Henikoff, 2002). However, H3.3 was also observed to be enriched at heterochromatic regions such as the telomeres (Wong et al., 2009) and pericentric regions (Drane et al., 2010). Moreover,

recent studies have identified the localisation of H3.3 at other heterochromatic regions including, endogenous retroviral repeats (Elsasser et al., 2015), imprinted differentially methylated regions and selected intragenic methylated CpG islands (Voon et al., 2015). Overall, these studies indicate the importance of H3.3 in development, chromatin function and maintenance and, genomic stability.

1.3.5 Role of H3.3 in cancer

In addition to these roles, the mutation of various residues on H3.3 has been associated with cancer (Lowe et al., 2019, Yuen and Knoepfler, 2013). In fact, in human tumours, all H3.3 mutations occur on the H3F3A gene, leading to single codon changes within the N-terminal tail of the H3.3 protein. This codon change is critical as it changes interactions between H3.3 and chromatin remodelling enzymes or chaperones, causing aberrant mutant H3.3 incorporation which leads to improper chromosomal segregation and loss of genome integrity (Bush et al., 2013, Lin et al., 2013).

Some of the prominent mutations on H3.3 associated with tumour and cancer growth are the H3.3 Lysine 27 mutation to methionine (H3.3K27M) and H3.3 glycine 34 to either arginine or valine (H3.3G34R/V). These mutations were discovered through the exome sequencing of 48 paediatric glioblastoma multiforme samples (Schwartzentruber et al., 2012, Wu et al., 2012). Interestingly, the H3F3A heterozygous mutation of H3.3K27M and H3.3G34R/V, together with other mutations such as ATRX/DAXX, TP53 and IDH1, was sufficient for tumour formation (Schwartzentruber et al., 2012, Voon et al., 2018, Udugama et al., 2021). Furthermore, the H3.3K27M and H3.3G34R/V mutations showed a distinct gene expression profile and DNA methylation pattern (Schwartzentruber et al., 2012). The

localisation of tumours is unique to the specific mutation in which H3.3K27M localises to regions such as the spinal cord while H3.3G34R/V localises to the cerebral hemispheres (Bjerke et al., 2013, Sturm et al., 2012). In addition, H3.3K27M is predominant in patients aged 5-29 years, while H3.3G34R/V is predominant in patients aged 9-42 years (Sturm et al., 2012, Schwartzentruber et al., 2012). Thus, the localisation and prevalence of these mutations in specific age groups show the importance of H3.3 in development at different time points.

In human diffuse intrinsic pontine glioma (DIPG), the expression of H3.3K27M reduces global levels of H3K27me3 (Silveira et al., 2019, Chan et al., 2013) Biochemical and structural studies have shown that H3.3K27M binds with a greater affinity to the catalytic subunit, EZH2, of the polycomb repressive complex 2 (PRC2). As a result, H3.3K27M competes with the normal lysine 27 on histone H3.3 and sequesters PRC2 complex from its normal biding sites in the genome. This in turn prevents the establishment and spreading of H3K27me3 (Justin et al., 2016, Fang et al., 2018, Harutyunyan et al., 2020). Although H3K27me3-silenced regions are reduced in H3.3K27M mutant cells, H3K27me3 and PRC2 levels have been found to be high in the remaining domains. This suggests that PRC2 activity is still functional and certain silent domains may escape misregulation by H3.3K27M (Sarthy et al., 2020). Several recent studies have also reported that H3.3K27M affects H3K27ac levels, resulting in aberrant gene expression and promoting oncogenic transcriptional programs in DIPG (Krug et al., 2019, Silveira et al., 2019, Fang et al., 2018). Thus, these reports indicate that the misregulation of H3.3 is associated with various aggressive cancers.

Recent studies have investigated the molecular mechanism of H3.3G34R mutation in paediatric gliomas (Voon et al., 2018, Udugama et al., 2021). The H3.3G34R mutation is found to inhibit the function of the KDM4 family of K9/K36 demethylases, which in turn leads to increased H3K9me3 and H3K36me3 levels across the genome. In line with this finding the H3.3G34R mutation is found to inhibit the function of the KDM4 family, which in turn leads to increased H3K9me3 and H3K36me3 levels across the genome. H3K9me3 and H3K36me3 profiles in H3.3G34R mutants closely resemble a KDM4 A/B/C triple-knockout (Voon et al., 2018). This shows that the mutation of H3.3 dysregulates chromatin remodelling enzymes which is a cause for tumour formation.

1.4 Phosphorylation of H3.3 Serine 31

1.4.1 The localisation and enrichment of H3.3S31ph

The phosphorylation of H3.3 Serine 31 was first discovered in HeLa and HEK293 cells through the generation of H3.3S31ph specific antibodies (Hake et al., 2005). Like other histone phosphorylation marks such as H3S10ph and H3S28ph, H3.3S31ph is a mitosis-specific modification (Goto et al., 2002, Hake et al., 2005). The phosphorylation of H3.3 Serine 31 was also identified in other cell types and organisms including mouse ES cells, mouse embryonic germ cells, mouse somatic cells and urochordate, indicating the evolutionary conservation of the serine residue and its phosphorylation (Schulmeister et al., 2007, Wong et al., 2009).

In human and mouse cells, H3.3S31ph is detectable during late prometaphase, enriched during metaphase and is lost by anaphase (Hake et al., 2005). Although H3.3 is present throughout the chromosomes during interphase and mitosis, only a subset of H3.3S31 is

phosphorylated. The absence of H3.3S31ph during interphase suggests a specific function of H3.3S31ph during mitosis (Wong et al., 2009, Hake et al., 2005). H3.3S31ph is explicitly enriched during mitosis at the pericentric regions of urochordate, human cells and mouse cells (Hake et al., 2005, Schulmeister et al., 2007). However, an interesting study also identified the unique enrichment of H3.3S31ph at the telomeres, in addition to the pericentric regions, of mitotic mouse embryonic stem and germ cells (Wong et al., 2009). Nonetheless, these studies showed that H3.3S31ph is enriched at heterochromatic sites, suggesting a role of H3.3S31ph in heterochromatin maintenance during mitosis.

1.4.2 CHK-1 and AURKB: regulators of H3.3S31ph

Recently, two studies have shed light on the kinases that drives the phosphorylation of H3.3S31. Checkpoint Kinase 1 (CHK1) was the first identified kinase that phosphorylates H3.3S31 in alternate lengthening of telomere (ALT) cancer cells (Chang et al., 2015). CHK1 is a Serine/Threonine kinase involved in DNA damage response signalling. Also, CHK1 is known to phosphorylate H3 on Threonine 3, Serine 10 and Threonine 11 (Shimada et al., 2008, Liokatis et al., 2012). Like H3S10ph and H3S28ph, H3T3ph and H3T11ph are enriched during mitosis. Consistent with its role in phosphorylating H3S10 and H3T11 in response to DNA damage (Shimada et al., 2008) it is not surprising that CHK1 also phosphorylates H3.3S31 in ALT cancer cells which show high levels of genomic instability and DNA damage. In ALT cancer cell models such as U2OS, W138-VA13/RA and GM847, the distribution of H3.3S31ph was observed on the chromosomal arms in addition to the pericentric regions (Chang et al., 2015). As ALT-cancer cells have persistent DNA damage and instability, the regulation of H3.3S31ph by CHK1 was investigated. CHK1 was shown to phosphorylate H3.3S31 in ALT-cancer cells *in vitro* and *in vivo* (Chang et al., 2015).

Furthermore, siRNA inhibition and drug-mediated inhibition of CHK1 resulted in a loss of H3.3S31ph on chromosome arms of ALT-cancer cells, indicating that CHK1 phosphorylates H3.3S31 *in vivo* (Chang et al., 2015). Despite the inhibition of CHK1, H3.3S31ph was observed at the pericentric region, suggesting that there are other kinases that regulate H3.3S31ph. This was verified by other studies, which showed that CHK1 does not phosphorylate H3.3S31 in human somatic cells, mouse ES cells and monkey somatic cells (Li et al., 2017a, Hinchcliffe et al., 2016, Martire et al., 2019). Together, these studies show that various kinases could be involved in regulating H3.3S31ph.

Consistently, another study showed that AURKB phosphorylates H3.3S31 (Li et al., 2017a). This was an exciting discovery as AURKB was previously suggested to be the unlikely kinase that phosphorylates H3.3S31 due to the sequence preference of AURKB and its lack of colocalisation with H3.3S31ph (Hake et al., 2005). AURKB, a member of the chromosomal passenger complex, is a master regulator of mitosis (Hochegger et al., 2013, Ditchfield et al., 2003, Andrews et al., 2004). AURKB is known to phosphorylate Histone H3 on residues such as H3S10 and H3S28 (Goto et al., 2002). The identification of AURKB as an H3.3S31ph regulator was performed using kinase inhibitor libraries and siRNA library for kinases where AURKB was selected and tested for its effects on H3.3S31 *in vivo* and *in vitro* (Li et al., 2017a). Using drug-mediated inhibition and siRNA mediated knockdown of AURKB in HEK293F cells, a drastic reduction of H3.3S31ph positive cells was observed. Furthermore, this loss of H3.3S31ph was rescued with the expression of siRNA resistant AURKB (Li et al., 2017a). In addition, *in vitro* kinase assays also showed the enzymatic activity of AURKB on H3.3S31 (Li et al., 2017a). Altogether, this identified that AURKB phosphorylates H3.3S31.

Altogether, these studies have identified the kinases that phosphorylate H3.3S31. Nonetheless, other kinases may regulate H3.3S31 (Armache et al., 2020). With the kinases known to phosphorylate H3.3S31, it is prudent to understand the molecular mechanism of H3.3S31ph and its functions.

1.4.3 The function of H3.3S31ph

One of the possible functions of H3.3S31ph was reported to be necessary for ALT-cancer cell survival (Chang et al., 2015). Inhibition of CHK1 in ALT-cancer cells resulted in increased DNA damage response on the chromosome arms and telomeres. Interestingly, prolonged treatment of CHK1 inhibition caused ALT-cancer cell death (Chang et al., 2015). This implicates H3.3S31ph in ALT-cancer cell chromatin maintenance and survival.

H3.3S31ph is enriched at the telomeres of only mitotic ES cells (Wong et al., 2009). This enrichment of H3.3S31ph is lost at the telomeres and gained at the pericentric region after differentiation. The increase of H3.3S31ph at the pericentric region was coupled with an increase of heterochromatic marks such as H3K9me3 and H4K20me3 at heterochromatic regions (Wong et al., 2009). This may indicate that H3.3S31ph may have a unique role in regulating heterochromatin. Also, the presence of H3.3S31ph at the long telomeres of mitotic mouse ES cells may suggest the importance of H3.3S31ph in telomere length maintenance. However, H3.3S31ph levels at the telomeres of human somatic cells with long (HT1080) and short telomeres (human primary fibroblasts) were undetectable (Wong et al., 2009). In addition, human telomerase positive A549, HT29 and HT1080 did not show H3.3S31ph at the telomeres (Chang et al., 2015). Altogether, these finiding indicated that H3.3S31ph at the telomeres might regulate heterochromatin instead of telomere length.

H3.3 is loaded at the telomeres of mitotic mouse ES cells during telomere replication and processing (Wong et al., 2009). This was shown using a telomere replication marker, ATMS1981ph (Sanchez-Molina et al., 2011). Further suggesting a role of H3.3 in telomere maintenance, RNAi knockdown of H3.3 showed increased telomere dysfunction induced foci (Wong et al., 2009). However, further studies need to be conducted to determine if the H3.3 Serine 31 residue is related to telomere replication and the increase in telomere dysfunction induced foci.

A possible function of H3.3S31ph is the rescue of defective replication fork progression after UV irradiation (Frey et al., 2014). H3.3 knockout chicken DT40 cells showed increased sensitivity to UV damage. The expression of phospho-null H3.3S31A mutant showed similar UV hypersensitivity compared to the H3.3 knockout DT40 cells. This indicates that H3.3S31 may be necessary for UV damage resistance (Frey et al., 2014). When exposed to UV irradiation, DT40 cells knocked out of H3.3 showed reduced replication fork progression. This phenotype was rescued with the expression of phospho-null H3.3S31A mutant (Frey et al., 2014). Although this suggests a possible role of H3.3S31 in defective replication fork progression, further studies need to be conducted (Frey et al., 2014).

H3.3S31ph was indicated to be essential for p53-mediated cell cycle arrest (Hinchcliffe et al., 2016). In monkey (cos7) and human (RPE-1) cells, misaligned chromosomes during anaphase cause an increase of H3.3S31ph on chromosome arms (Hinchcliffe et al., 2016). Together with this increase, nuclear accumulation of p53 was also observed. Despite the inhibition of CHK1, H3.3S31ph enrichment on misaligned chromosomes was not lost. Interestingly, microinjection of H3.3S31ph antibodies into anaphase cells blocked the activation of p53 (Hinchcliffe et al., 2016). Although it was shown that H3.3S31ph is essential

for p53-mediated cell cycle arrest, further understanding of the mechanism of how H3.3S31ph affects cell cycle arrest is required.

In addition to the various possible functions of H3.3S31ph, recent studies have shown its role in development and transcriptional regulation (Sitbon et al., 2020, Armache et al., 2020). In mouse macrophage cells and other immune cells, H3.3S31 is phosphorylated along rapidly induced genes in response to stimulation such as stress, immune system process and cellular response to chemical stimulus (Armache et al., 2020). Interestingly, due to its localisation to H3.3S31ph genes in response to stimuli, the kinase that regulates H3.3S31ph was suggested to be IKKα (Armache et al., 2020). However, further binding and phosphorylation studies are required to confirm the role of IKKα in regulating H3.3S31 phosphorylation. Interestingly, the inhibition of RNA polymerase II led to a loss of H3.3S31ph at rapidly induced genes, suggesting a role of H3.3S31ph in transcriptional regulation. Furthermore, H3K36me3, a mark associated with active transcription, was also enriched with H3.3S31ph at stimulation-induced genes. Interestingly, the activity of SETD2 is enhanced by H3.3S31ph. Thus, as ZMYND11, a transcriptional corepressor and tumor suppressor that localises to gene bodies, reads H3K36me3 with the unmodified S31 (Guo et al., 2014, Wen et al., 2014), the role of H3.3S31ph was suggested to eject ZMYND11 from chromatin. Altogether, this report showed that H3.3S31ph plays a role in transcriptional activation.

Another study showed the importance of H3.3S31ph in transcriptional activation for proper embryonic development in *Xenopus laevis* (Sitbon et al., 2020). The depletion of H3.3 in *Xenopus laevis* prevented blastopore closure, indicating the importance of H3.3. (Sitbon et al., 2020, Szenker et al., 2012). Interestingly, the depletion of endogenous H3.3 was rescued

by the expression of phospho-mimic H3.3 serine 31 to aspartic acid mutation (H3.3S31D) while the expression of phospho-null H3.3 serine 31 to alanine mutation (H3.3S31A) did not rescue endogenous H3.3 depletion during *Xenopus laevis* early development (Sitbon et al., 2020). This showed that H3.3 is critical for proper development in *Xenopus laevis*. Interestingly, as previously reported on H3.3S31D, H3.3K27ac was enriched (Sitbon et al., 2020, Martire et al., 2019). However, H3K36me3 was not enriched although this enrichment was reported in another study (Sitbon et al., 2020, Armache et al., 2020). Furthermore, H3.3S31D attracted factors involved with transcriptional activation of key developmental genes in interphase cells and repulsed factors involved in chromosome condensation in mitotic cells (Sitbon et al., 2020, Clevers, 2006, Liu and Millar, 2010), identifying its importance in chromatin regulation. This study showed that H3.3S31ph is important in transcription for the development in *Xenopus laevis*.

1.4.4 Interacting partners of H3.3S31ph

H3.3S31ph acts through its interaction with proteins such as ZMYND11 (Wen et al., 2014, Guo et al., 2014). ZMYND11 acts as a co-repressor of cellular transcription factors and may act as a tumour suppressor (Ansieau and Sergeant, 2003, Ladendorff et al., 2001, Hateboer et al., 1995). ZMYND11, which interacts with H3.3, has multiple histone reading domains such as the plant homeodomain (PHD) domain, bromodomain and PWWP domain. These domains are essential for the binding between H3K36me3 and ZMYND11 (Wen et al., 2014). In addition, the crystal structure of H3.3 and ZMYND11 interaction showed that H3.3S31 and H3.3 Threonine 32 bound to a specific pocket in the Bromo-ZnF-PWWP valley (Wen et al., 2014). Further indicating the importance of the H3.3S31 residue, an increased binding affinity was observed between ZMYND11 and H3.3 compared to ZMYND11 and

H3.1 (Wen et al., 2014). ChIP/seq analyses of ZMYND11, H3K36me3 and H3.3 showed a clear overlap, indicating that ZMYND11 interacts preferentially with H3.3K36me3 (Wen et al., 2014). Therefore, it is possible that unphosphorylated H3.3S31, coupled with H3K36me3, may regulate H3.3 binding to ZMYND11. Thus, further investigation is needed to determine if the phosphorylation of H3.3S31 may prevent its binding to ZMYND11 (Wen et al., 2014, Guo et al., 2014).

Another recent study has identified a role of H3.3S31ph in stimulating histone acetylation (Martire et al., 2019). In H3.3 knockout mouse ES cells, a global H3K27ac loss was observed through immunoblotting, mass spectrometry and ChIP/seq analysis (Martire et al., 2019). Similarly, in HIRA knockout mouse ES cells, but not ATRX knockout mouse ES cells, global loss and enhancer specific loss of H3K27ac was observed (Martire et al., 2019). This showed that HIRA-dependant loading of H3.3 is required for the regulation of H3K27ac. The loss of H3K27ac was rescued with the expression of either wildtype H3.3 and phospho-mimic H3.3 (H3.3S31E; serine 31 to glutamic acid) mutant but not phospho-null H3.3S31A mutant (Martire et al., 2019). This suggested that the phosphorylation of H3.3S31 was necessary for the regulation of H3K27ac. The inhibition of CHK1 but not AURKB resulted in a decrease of H3.3S31ph and a loss of H3K27ac at enhancers (Martire et al., 2019). *In vitro* kinase assays concluded that phosphorylated H3.3S31 stimulates histone acetyltransferase, p300, and increased acetylation (Martire et al., 2019). This finding is interesting as previous studies only identified the enrichment of H3.3S31ph at heterochromatic regions. Nonetheless, despite being identified in 2005, there has been little progress in understanding the function and role of H3.3S31ph in chromatin maintenance.

In this project, we aim to elucidate the function of H3.3S31ph in regulating heterochromatin regulation. As a model to study H3.3S31ph, we used the telomeres of mouse ES cells as our lab has extensively worked on H3.3 at the telomeres and, as H3.3S31ph is enriched at the telomeres of mouse ES cells.

1.5 The chromatin of telomeres

1.5.1 The importance of telomere ends

Telomeres are structures located at the ends of linear chromosomes. Telomeres consist of kilobases of hexametric TTAGGG (5'-3') repeat in mammals, with a single-stranded G-rich overhang (Wright et al., 1997). Depending on the cell type, the length of telomeres in humans varies between 5 kb to 15 kb (Wang et al., 2013), whereas telomere length in mice varies between 25 kb to 50 kb (Kipling and Cooke, 1990). This sequence is bound by a complex of telomere specific proteins known as the Shelterin complex (de Lange, 2005). Typically, cells would recognise linear ends of chromosomal DNA as double-stranded breaks and mount DNA damage responses to target them for repair. Interestingly, telomeres are liberated from being recognised as double-stranded breaks, thus protecting the integrity of the genome. Telomeres accomplish this by forming a secondary structure known as the telomere loop (t-loop) and, the telomere specific Shelterin complex (Luke-Glaser et al., 2012, Wang et al., 2004). This shield telomere ends from being recognised as double-strand breaks by DNA damage response machinery, which, if triggered, could result in uncontrolled DNA degradation and loss of the internal coding sequence on the chromosome.

1.5.2 Protection of telomere and genome integrity – maintaining telomere length

An integral function of the telomere is to protect the genome. Telomere ends in differentiated cells (somatic cells), shorten after each cell division due to the incomplete replication of the 5' end of DNA by eukaryotic DNA polymerases (Harley et al., 1990). As a result, the length of telomeres decreases at an estimated rate of 30 bp per cell doubling (Martens et al., 2000). This gradual decrease in length eventually leads to a loss of binding between the Shelterin complex and telomeric DNA and the loss of the t-loop structure (Liu et al., 2004a). This activates DNA damage response which ultimately leads to cellular senescence or cell death. By itself, the Shelterin complex protects telomere integrity. The Shelterin complex regulates telomere length by controlling the access of telomerase, a reverse transcriptase enzyme that synthesises telomere DNA *de novo,* to the telomeres (Greider and Blackburn, 1985, Smogorzewska et al., 2000, van Steensel and de Lange, 1997). In addition, the Shelterin complex protects telomeres by repressing DNA damage response and regulating telomere length renewal to ensure genome integrity (Palm and de Lange, 2008). For example, Telomeric repeat binding factor 1 (TERF1), a component of the Shelterin complex, protects the telomeres from ataxia telangiectasia and Rad3-related protein (ATR) dependent DNA damage response and promotes efficient replication of telomeres through helicases (Sfeir et al., 2009).

1.5.3 Protection of telomere and genome integrity - Telomere capping and suppression of DNA damage response

In most organisms, an exclusive feature of telomere ends is the single-stranded telomere DNA, otherwise known as the 3' single-stranded G-rich overhang (Cimino-Reale et al., 2001, Oganesian and Karlseder, 2011). This 30 to 500 nucleotide long single-stranded G-rich

overhang (Cimino-Reale et al., 2001, Oganesian and Karlseder, 2011, Wright et al., 1997) has been shown to sustain telomere functions such as capping and repressing the activation of DNA damage response (Tsai et al., 2007).

To facilitate capping, telomere DNA folds back upon itself to allow the 3' single-stranded G-rich overhang to invade duplex telomere DNA to form a noose-like structure known as the t-loop (**Figure 1.6**). This displaces the G-rich strand of the duplex telomere DNA, forming a triple-stranded structure known as the Displacement loop (D-loop) (Griffith et al., 1999). The t-loop structure disguises and prevents linear telomere ends from being recognised as a double-stranded break by DNA damage response machinery (Wang et al., 2004). Furthermore, the t-loop structure has been identified in other organisms, including *trypanosomes* (Munoz-Jordan et al., 2001, Murti and Prescott, 1999). Hence, its role has been suggested to be conserved, portraying its vital role in protecting the genome from degradation.

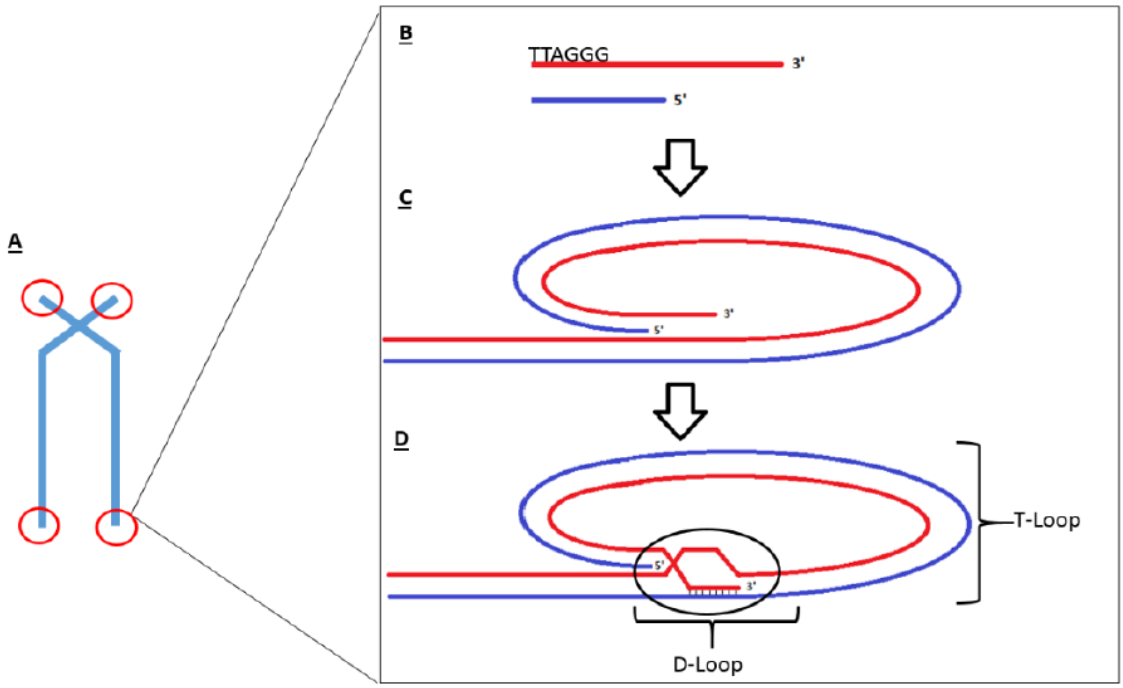

Figure 1.6: Formation of the t-loop

A *shows an image of a chromosome. The red circles identify the telomeres.* ***B*** *shows both strands of the telomere DNA. Additionally, the 3' single-stranded G-rich overhang can be seen. The hexametric repeat of TTAGGG is indicated on the 3' strand.* ***C*** *shows the formation of a noose-like structure by the looping of telomere DNA.* ***D*** *shows the duplex telomere DNA dissociation by the invasion of the single-stranded 3' G-rich overhang into the duplex DNA, forming the D-loop (circled). The single-stranded 3' G-rich overhang binds to the 5' C-rich strand of the duplex DNA, forming a triple-stranded structure. The end resulting noose-like structure is known as the t-loop.*

1.5.4 Protection of telomere and genome integrity – the function of Shelterin end protection problem

In addition to the t-loop formation, the telomere-specific protein complex, known as Shelterin, is required for various aspects of telomere function. Such functions include telomere structure maintenance, telomere length maintenance and, most importantly, preventing telomeres from being recognised as double-stranded DNA breaks (Palm and de Lange, 2008). Double-stranded DNA breaks are unstable and are targeted by the DNA repair pathways. A study that prevented the binding of the Shelterin complex to telomere DNA, through the deletion of TERF1 and TERF2, revealed that the Shelterin complex was required to repress DNA damage repair pathways such as NHEJ, HDR and, DNA damage-induced kinases such as ATM and ATR signalling (Sfeir and de Lange, 2012). The Shelterin complex binds the TTAGGG repeats at the telomeres (Liu et al., 2004a). In addition, the components of the Shelterin complex also precisely localise to telomeres and are present at telomeres throughout the cell cycle (Bilaud et al., 1997, Liu et al., 2004b, Broccoli et al., 1997, Li et al., 2000, Shen et al., 1997, Ye et al., 2004). The Shelterin complex is made of 6 specific proteins: TERF1 (Zhong et al., 1992), Telomeric repeat binding factor 2 (TERF2) (Bilaud et al., 1997, Broccoli et al., 1997), TERF2 interacting proteins (RAP1)(Li et al., 2000), TERF1 interacting nuclear factor 2 (TIN2) (Kim et al., 1999), Tripeptidyl peptidase I (TPP1) (Houghtaling et al., 2004) and Protection of telomere 1(Baumann and Cech, 2001) (POT1; **Figure 1.7**).

Various studies have shown the importance of the individual Shelterin subunits on telomere maintenance (Sfeir and de Lange, 2012, Palm and de Lange, 2008, de Lange, 2005). TERF1 is vital for regulating telomerase binding to telomere DNA (van Steensel and de Lange, 1997). The lack of TERF1 binding to telomere DNA, through the expression of a

dominant-negative TERF1, led to an increase in telomerase binding and subsequently, the lengthening of telomeres. In addition, knockout of TERF1 led to a loss of telomere structural integrity and replication fork stalling at the telomeres (Sfeir et al., 2009). Like the importance of TERF1 in maintaining telomere function, TERF2 prevents chromosome end fusions and the activation of ATM-dependent DNA damage response through the recruitment of proteins such as RAP1 (van Steensel et al., 1998, Sfeir et al., 2010). In addition, the deletion of TERF2 led to a reduction of t-loop formation and maintenance, suggesting that TERF2 is vital for the remodelling of linear telomere DNA into t-loop (Stansel et al., 2001). Finally, POT1 prevents telomere erosion, which in turn prevents the activation of ATR-mediated repair at the telomeres (Veldman et al., 2004, Gong and de Lange, 2010).

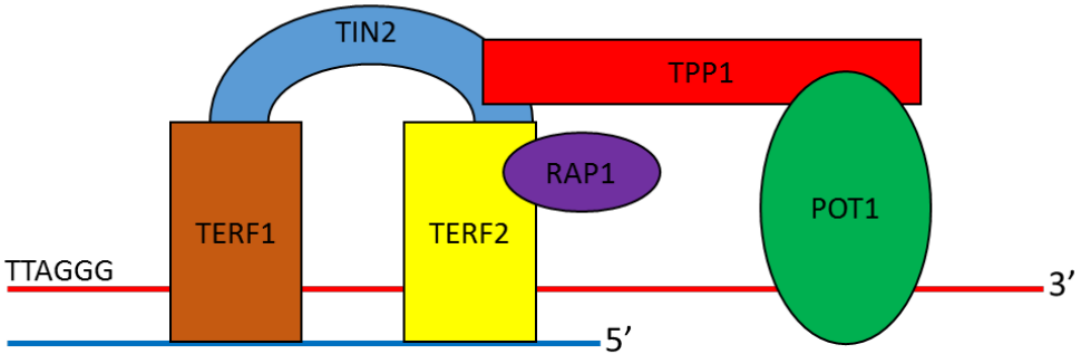

Figure 1.7: A simplified diagram of the Shelterin complex and telomere DNA.

TERF1 and TERF2 bind to duplex telomere DNA. POT1 binds to only the 3' single-stranded G rich overhang. TIN2 acts as a connector between TERF1 and TERF2. TPP1 binds to TIN2 and POT1. Finally, RAP1 binds to TERF2. Only a single Shelterin complex is depicted. In vivo, multiple Shelterin complexes bind to the telomere DNA.

1.6 Telomeres chromatin in somatic cells and pluripotent ES cells

In addition to the unique set of proteins and structure, telomere chromatin is constitutively heterochromatic. The telomeric and sub-telomeric regions show low levels of acetylated histones and are enriched with H3K9me3 and H4K20me3 marks (Garcia-Cao et al., 2004), which are suggestive of a compact, repressed genomic region. The presence of H3K9me3 recruits HP1α, which regulates chromatin compaction. The binding of histone methyltransferases such as SUV39H1 and SUV39H2 further identifies the telomeres as heterochromatin. The loss of these heterochromatic marks through the deletion of SUV39H1 and SUV39H2 in mouse ES cells, porcine ES-like cells and porcine embryonic fibroblasts led to a loss of H3K9me3 levels, which resulted in abnormal telomere DNA elongation and recombination (Garcia-Cao et al., 2004, Benetti et al., 2007). In addition, the deletion of SUV420H1 and SUV420H2 led to a loss of H4K20me3 levels which subsequently also led to telomere DNA elongation and recombination (Benetti et al., 2007).

In addition to histone demethylation, DNA methyltransferase ([DNMT]; DNMT1, DNMT3a and DMNT3b) regulates DNA methylation. Although telomeres lack CpG methylation site, their sub-telomeric region is hyper-methylated. Indicating the importance of DNMT in maintaining telomere integrity and the regulation of heterochromatin, the loss of DMNT (DNMT1 or both DMNT3a and DMNT3b) results in telomere elongation. Furthermore, the loss of DMNT gave rise to an increase in recombination events at the telomeres (Gonzalo et al., 2006). These studies show the importance of heterochromatin maintenance at the telomeres.

The regulation of heterochromatin in telomeres are essential for telomere integrity maintenance. Unlike their somatic cell counterparts, the chromatin of ES cells comprises an

overall more open (active) chromatin state (Meshorer and Misteli, 2006). Compared to somatic cells, ES cells show presence of low levels of heterochromatic marks such as H3K9me3 and H4K20me3 at telomeres, suggesting that in ES cells, open chromatin is compatible with telomere function (Wong et al., 2009). In addition, telomere chromatin is enriched with proteins such as H3.3, a histone H3 variant usually associated with active chromatin. The depletion of H3.3 through ribonucleic acid (RNA) interference resulted in telomere dysfunction, indicating that H3.3 has an essential role in maintaining telomere function in ES cells (Wong et al., 2009). Additionally, telomeric H3.3 is phosphorylated at Serine 31 (a residue unique to H3.3). This H3.3S31ph mark is not seen at the telomeres of somatic cells (Wong et al., 2009). Furthermore, the chromatin remodeler ATRX/DAXX, which functions to deposit H3.3 at the telomeres, is enriched at the telomeres of ES cells (Wong et al., 2010, Wong et al., 2009). The depletion of ATRX led to a loss of H3.3S31ph at telomeres in mouse ES cells and increased DNA damage at the telomeres. Due to the unique properties of the telomeres of ES cells, we will study the function of H3.3S31ph in regulating heterochromatin at telomeres in these pluripotent cells.

1.7 Aims and sub aims

The aims of this thesis are a) to investigate the role of histone variant H3.3 serine 31 phosphorylation (H3.3S31ph) in heterochromatin assembly, particularly, in telomeric chromatin assembly and b) to identify interacting protein(s) of H3.3S31ph at the telomere.

The aim of Chapter 3 was to uncover the function of AURKB, which is a mitotic kinase that phosphorylates H3.3S31, in regulating TERF1 binding to maintain telomeric DNA integrity in mouse ES cells. The unpublished data from our lab shows that AURKB localises to the telomere during mitosis in ES cells and it phosphorylates both H3.3S31 and TERF1 at the telomere. To investigate the role of AURKB at the telomere, I investigated the impact of the loss of AURKB on telomere function in mouse ES cells. This was achieved through siRNA knockdown of AURKB expression and drug inhibition of its kinase activity. In mouse ES cells, the loss of AURKB function resulted in the loss of telomere integrity, a phenotype also found in cells subjected to siRNA mediated depletion of TERF1 expression. *In vitro* protein binding assay and kinase experiments were performed to investigate the interaction between AURKB bind TERF1, and to identify the putative AURKB target sites. Finally, the importance of these candidate residues on TERF1 was determined by overexpressing the phospho-null and phospho-mimic substitutions in cells, and analysis of the effects on telomere maintenance.

The aim of Chapter 4 was to generate mutant mouse ES cell lines carrying H3.3S31 substitutions to study the importance of H3.3S31 and its phosphorylation (H3.3S31ph) in heterochromatin maintenance, particularly, at telomeres. To achieve this, I employed a two-step strategy to obtain mouse ES cells expressing only either the wild-type (WT) H3.3S31, mutant H3.3S31A (serine to alanine) or mutant H3.3S31E (serine to glutamic acid) protein.

The A31 substitution mimics H3.1/2 and is non-phosphorylatable, mimicking a non-phosphorylated state. In contrast, the glutamic acid E31 substitution is a structural mimic of a phosphorylated serine and mimics a phosphorylated state.

The aim of Chapter 5 was to determine the function of H3.3S31ph in heterochromatin regulation at the telomeres using the S31A and S31E-H3.3 mouse ES cell lines generated in Chapter 4. Although previous studies have shown the presence of H3.3S31ph at the telomere (Wong et al., 2009) and the involvement of AURKB and CHK1 kinases in phosphorylating H3.3S31, the function of H3.3S31ph in heterochromatin assembly has not been defined (Chang et al., 2015, Li et al., 2017a). Thus, using the S31A and S31E-H3.3 mouse ES cell lines, I sought to determine if H3.3S31 and its phosphorylated form is required for H3.3 deposition by ATRX and maintenance of heterochromatin at telomeres, and if H3.3S31 substitutions affect telomere length regulation and protection.

The aim of Chapter 6 was to determine if histone H3K9me3 and K36me3 demethylase, KDM4B, was an interacting partner of H3.3S31ph. Findings from Chapter 5 show that heterochromatin structure at the telomere was disrupted in H3.3S31A phospho-null mutant cells. In consideration of the previous findings from our lab that KDM4B localises to the telomeres of ES cells where it is responsible for regulating H3K9me3 level (Udugama et al., 2021, Voon et al., 2018), I hypothesised that H3.3S31ph is a key regulator of KDM4B binding at the telomere and the loss of H3.3S31ph in H3.3S31A resulted in the increased binding of KDM4B demethylase and thereby, loss of heterochromatin at the telomere. To address these hypotheses, *in vitro* demethylase assay and *in vivo* binding assays were performed to determine the interaction between KDM4B and H3.3. In addition, rescue experiments were

performed by depleting KDM4B levels to investigate if the depletion of KDM4B should rescue heterochromatin in H3.3S31A cells.

The implications of these results are discussed in chapter 7, with a focus on potential function of H3.3S31ph, and future possibilities for the understanding and H3.3S31ph in heterochromatin regulation.

Chapter 2: Materials and methods

2.1 Cell culture and transient transfection

2.1.1 Cell culture and maintenance

All mouse ES cell lines (ES129.1), *h3f3a*$^{flox/flox}$ *h3f3b*$^{flox/flox}$ (Tang et al., 2013a) and mutant ES cells lines were cultured at 37°C with 5% CO2 in Dulbecco's Modified Eagle Medium (DMEM) with 4.5 g/L Glucose + 2 mM L-Glutamine that was supplemented with 12% heat-inactivated FCS (v/v), 1000 units/ml leukaemia inhibitory factor, 0.1 mM β-mercaptoethanol, 0.1 mM non-essential amino acids (Gibco) and 1% Penicillin/Streptomycin (v/v).

All somatic (Mouse embryonic fibroblasts, NIH3T3 and human embryonic kidney 293T cells) and cancer cells (HT1080 (fibrosarcoma) (Cristofari and Lingner, 2006), super-telomerase HT1080 (Cristofari and Lingner, 2006), Alternative lengthening of telomere (ALT) positive SKLU1 (lung adenocarcinoma), GM847 (SV40-transformed fibroblast)) were cultured at 37°C with 5% CO_2 in DMEM (with 4.5 g/L Glucose) supplemented with 10% heat-inactivated FCS (v/v) and 1% Penicillin/Streptomycin (v/v). Passaging of adherent cells involved a wash with 1X PBS (137 mM NaCl, 5.4 mM KCl, 10 mM NA_2HPO_4, 5 mM $NaH_2PO_4H_2O$, 1 mM $Na_2EDTA\text{-}2H_2O$ pH to 7.4 with HCl), 5 minutes incubation with 0.025% (w/v) trypsin-EDTA at 37°C to detach cells from cell culture plate and resuspension in fresh complete DMEM every 3-4 days or as necessary.

2.1.2 Cell count

Cells were harvested by trypsinisation with trypsin-EDTA at 37°C for 5 minutes and resuspended in a volume fresh medium equivalent to the volume of trypsin. Then, 200 µl of cell suspension was added to an equal volume of Trypan Blue (Life technologies, dilution

factor =2) and mixed by gentle pipetting. Finally, the cell suspension was added to the hemocytometer and cells counted.

2.1.3 Cell-cycle arrest

Cells were arrested at the G1/S boundary by adding a final concentration of 2.5 mM Thymidine (Sigma Aldrich) to the media for 16 hours. To arrest cells at metaphase, cells were washed three times in pre-warmed PBS supplemented with 2.5 μM deoxycytidine (Sigma Aldrich) before releasing into fresh cell culture media containing 100 ng/ml Nocodazole (Sigma Aldrich) for 10 hours. To enrich for anaphase cells, cells arrested at metaphase were washed three times in pre-warmed PBS and released into fresh media containing 10 ng/ml cytochalasin B (Sigma Aldrich) for 1 hour.

2.1.4 Transient transfection

Cells were seeded at the appropriate concentration for the specific experiment. After 24 hours, cells were transfected with DNA using Lipofectamine 2000 (Invitrogen) at a Reagent:DNA ratio of 4:1. The 4 μl Lipofectamine 2000 reagent and 1 μg of plasmid DNA were diluted in 50 μl of Opti-MEM media (Gibco) separately before being mixed together, followed by a 45-minute incubation at room temperature to form the lipid-DNA complex. This lipid-DNA mix was then added to 2 x 10^5 mammalian cells containing cell culture media lacking penicillin and streptomycin. Culture media was changed after 8 hours.

2.1.5 siRNA transfection

siRNA oligonucleotides were commercially synthesised (GenePharma), and 40 nM of the siRNA was transfected into cells with Lipofectamine 2000 (Invitrogen) as described in

section 2.1.4 with the following changes. The lipid-siRNA complex, prepared at a Lipofectamine:siRNA ratio of 2:1, was added into 2 x 10^5 mammalian cells containing cell culture media lacking penicillin and streptomycin. A set of scramble siRNA (provided by GenePharma) was used as a control for all experiments. The cells were harvested and examined after 24 hours and 48 hours of transfection. Knockdown efficiency was analysed by real-time PCR as described in **Section 2.7**. The siRNA sequences used in this thesis are shown below.

Table 2.1: siRNA and the sequences used in this thesis

Gene Name	Sequence		Company
	Forward（5'-3'）	Reverse（5'-3'）	
Kdm4b-mus-2703	GCAGCGAUGGAAACUGAAATT	UUUCAGUUUCCAUCGCUGCTT	GenePharma
Kdm4b-mus-2933	GCCAGAUCGUCAUCACCAATT	UUGGUGAUGACGAUCUGGCTT	
Kdm4b-mus-3478	CCUGUCCCACUGUAGGUAATT	UUACCUACAGUGGGACAGGTT	
Kdm4b-mus-4552	CCUCCAGUUCAGUAUCAAUTT	AUUGAUACUGAACUGGAGGTT	
Mouse AURKB	SMARTpool: ON-TARGETplus siRNA		Dharmacon
Mouse AURKB	s74513		Ambion
Mouse TERF1	SMARTpool: ON-TARGETplus siRNA		Dharmacon
Mouse TERF2	SMARTpool: ON-TARGETplus siRNA		Dharmacon

2.2 Expressing H3.3S31 wild type and mutants in *h3f3a*$^{-/-}$ *h3f3b*$^{-/-}$ mouse ES cells

2.2.1 Generating H3.3S31 wild type and mutant plasmids

Plasmids containing Human influenza hemagglutinin (HA) tagged and untagged H3.3 (accession number: P84243) wildtype, H3.3S31A and H3.3S31E were commercially synthesised with *Nco*I and *EcoR*I restriction sites at the 3’ and 5’ ends, respectively

(Integrated DNA Technologies). HA tagged and untagged H3.3 wildtype, H3.3S31A and H3.3S31E constructs, together with pHL-EF1α-SphcCas9-iP-A vector (Addgene #60599) were digested with *Nco*I (NEB, 10,000 U/ml) and *EcoR*I (NEB, 20,000 U/ml) at 37ºC overnight to generate pHL-EF1α-SphcCas9-iP-A vector backbone (~5300 bp) and H3.3/H3.3-HA constructs (~400 bp) with sticky ends. These digested fragments with sticky ends were purified by agarose gel electrophoresis and extracted from the agarose gel using Wizard® SV Gel and PCR Clean-Up System (Promega). Sticky end ligation with T4 DNA ligase (NEB) was performed at 16ºC overnight. The ligation mix was transformed into chemically competent DH5α cells at 42ºC for 45 seconds and grown on Luria Broth-agar plate supplemented with 100 µg/ml ampicillin (Sigma Aldrich) at 37ºC overnight. Colonies were cultured and screened for clones containing H3.3 by 3-hour digestion with *Sma*I (NEB, 20,000 U/ml) and *EcoR*I (NEB, 20,000 U/ml) restriction enzymes at 37ºC before separation by agarose gel electrophoresis according to the presence of a 1927 bp and a 3866 bp band of H3.3-HA constructs and a 1900 bp and 3866 bp band for H3.3 constructs. Clones carrying the H3.3 constructs were further validated by capillary sequencing using BDT BigDye 3.1 (Micromon Sequencing Facility, Monash University, Clayton). The vector maps for pHL-EF1α-SphcCas9-iP-A and, HA-tagged and untagged H3.3 is shown in **Figure 2.1**.

2.2.2 Stable transfection of H3.3S31 wildtype and mutant plasmids into *h3f3a*$^{flox/flox}$ *h3f3b*$^{flox/flox}$ mouse ES cells

Confirmed HA tagged and untagged H3.3 wildtype, H3.3S31A and H3.3S31E constructs were linearised with *Fsp*I digestion (NEB, 10,000 U/ml) at 37ºC overnight and transfected into *h3f3a*$^{flox/flox}$ *h3f3b*$^{flox/flox}$ mouse ES cells by electroporation using the MicroPulser Electroporator (BioRad). Cells were trypsinized and washed once with PBS and

resuspended in 400 ul PBS and transferred to the Micropulser Electroporation cuvettes. 10 µg of linearised plasmid DNA was then added to 2 x 10^6 cells before electroporation at 0.25kV, 500uF. Cells were then replated into cell culture media lacking penicillin and streptomycin. To select for H3.3S31 wildtype, H3.3S31A and H3.3S31E transfected cells, 2 µg/ml puromycin (Sigma Aldrich) was supplemented to the ES media after 24 hours. Single colonies were then picked, cultured, and screened for the presence of exogenous HA tagged and untagged H3.3 by immunoblotting (**Section 2.4**), immunofluorescence (**Section 2.6**), and qRT-PCR (**Section 2.7**).

2.2.3 Knockout of *h3f3a* and *h3f3b*

To knockout endogenous H3.3, *h3f3a*$^{flox/flox}$ *h3f3b*$^{flox/flox}$ mouse ES cells expressing H3.3 wildtype, H3.3S31A and H3.3S31E constructs were co-transfected with 10 µg CAG-*Cre* plasmid (Addgene #13775) and 2 µg of pZeoSV2(+) plasmid (Invitrogen; confers resistance to Zeocin) using Lipofectamine 2000 (Invitrogen) as described in **Section 2.1.4.**. Zeocin (Sigma Aldrich) was used at 100 µg/ml to select for clones co-transfected with CAG-*Cre* plasmid. Single colonies were picked, cultured, and screened for the loss of endogenous H3.3 by immunoblotting (**Section 2.4**), Fluorescence-activated cell sorting (FACS, **Section 2.5**), Immunofluorescence (**Section 2.6**), and southern blotting (**Section 2.9**).

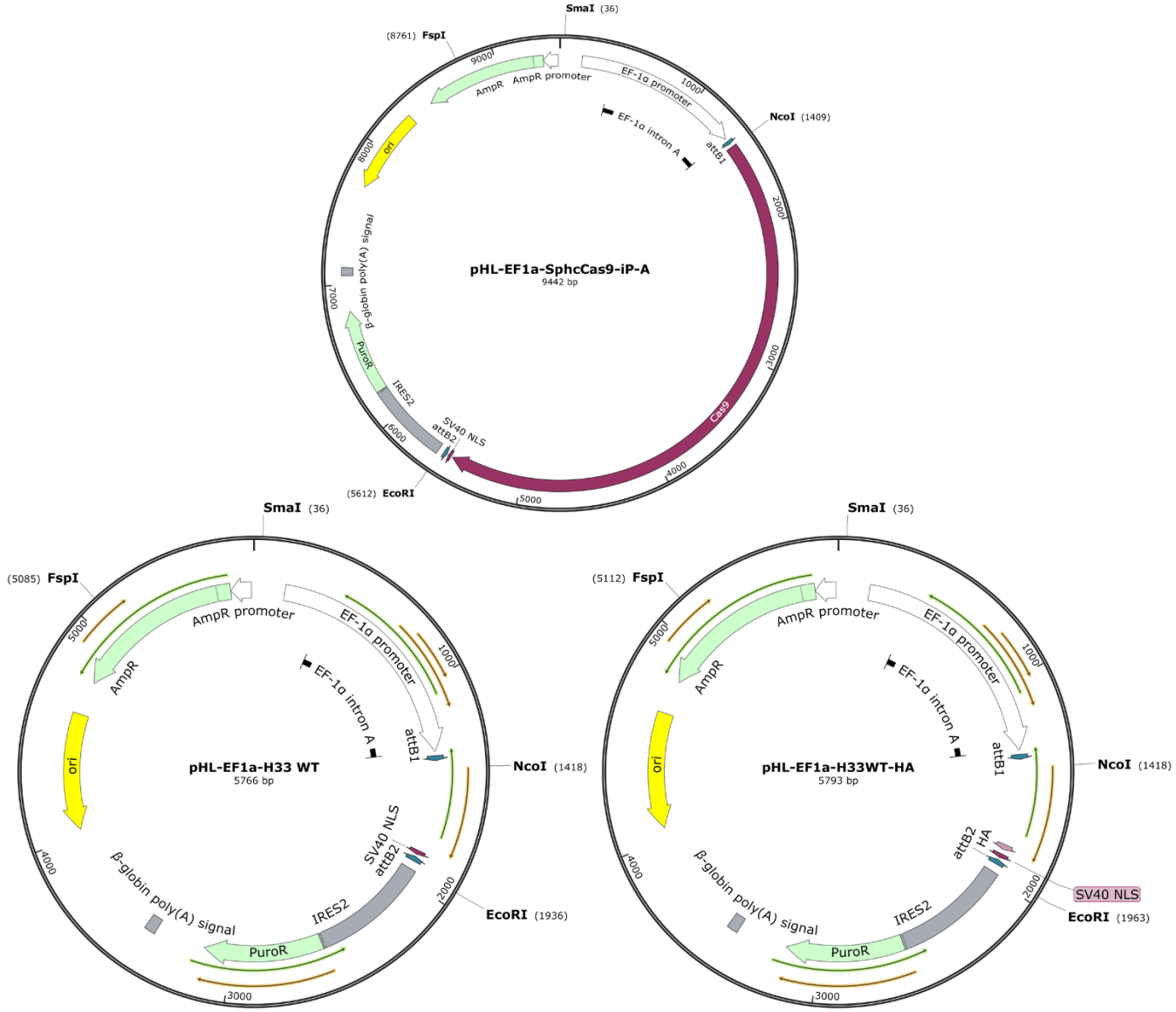

Figure 2.1: Plasmid maps of pHL-EF1α-SphcCas9-iP-A, untagged and HA-tagged H3.3

The plasmid maps of pHL-EF1α-SphcCas9-iP-A, untagged and HA-tagged H3.3 in pHL-EF1α backbone are shown. The plasmid size, significant features and restriction sites of interest are included.

2.3 Expression GFP- TERF1 wildtype and mutant constructs in mouse ES cells

2.3.1 Generating GFP-TERF1 wildtype and mutant plasmids

gBLOCK DNA fragments corresponding to the N- (amino acid 2 - 257) and C- (amino acid 258 - 421) terminus of TERF1 (accession number: P70371) and Myc-HA-tagged TERF1 and TERF2 (accession number: O35144) were purchased from Integrated DNA Technologies. The C-terminus fragments contained either wildtype or mutant (T343A, S344A, S261A, T403A, S404A, S261E and S404E) TERF1 cDNA sequences. The N- and C-terminus of TERF1 were cloned into pEGFP-C1 (Gibco) plasmid using the Gibson Assembly Kit (New England Biolabs). These constructs were used for the transient expression of wild-type and mutant green fluorescent protein (GFP)-TERF1, as described in **section 2.1.3**. DNA fragments of Myc-HA-TERF1, Myc-HA-TERF2, GFP-tagged wildtype and mutant (S261A, S261E, S404A and S404E) TERF1 were cloned into pHL-EF1α-SphcCas9-iP-A (Addgene #60599) at *Nco*I and *EcoR*I sites. Restriction enzyme digest with *Nco*I (NEB, 10,000 U/ml) and *EcoR*I (NEB, 20,000 U/ml) at 37^{o}C overnight was used to generate pHL-EF1α-SphcCas9-iP-A vector backbone (~5300 bp) and, GFP-TERF1 (~ 2000 bp), Myc-HA-TERF1 (~1400 bp) and Myc-HA-TERF2 (~1708 bp) inserts with sticky ends. These digested fragments with sticky ends were purified by agarose gel electrophoresis and extracted using Wizard® SV Gel and PCR Clean-Up System (Promega). Sticky end ligation with T4 DNA ligase (NEB) was performed at 16^{o}C overnight. The ligation mix was transformed into chemically competent DH5α cells at 42^{o}C for 45 seconds and grown on Luria Broth-agar plate supplemented with 100 µg/ml ampicillin at 37^{o}C overnight. Colonies were cultured and screened for clones containing GFP-TERF1, Myc-HA-TERF1/2 by overnight digestion using *Nco*I and *EcoR*I restriction enzymes at 37^{o}C before separation by agarose gel electrophoresis according to the presence of a 2021 bp and 5234 bp bands for

TERF1 and a 1708 bp and 5234 bp band for TERF2. Positive clones carrying the respective constructs were further validated by capillary sequencing using BDT BigDye 3.1 (Micromon Sequencing Facility, Monash University, Clayton). The vector maps of pHL-EF1α-GFP-WT-TERF1, pHL-EF1α-Myc-HA-TERF1 and pHL-EF1α-Myc-HA-TERF2 are shown in **Figure 2.2**

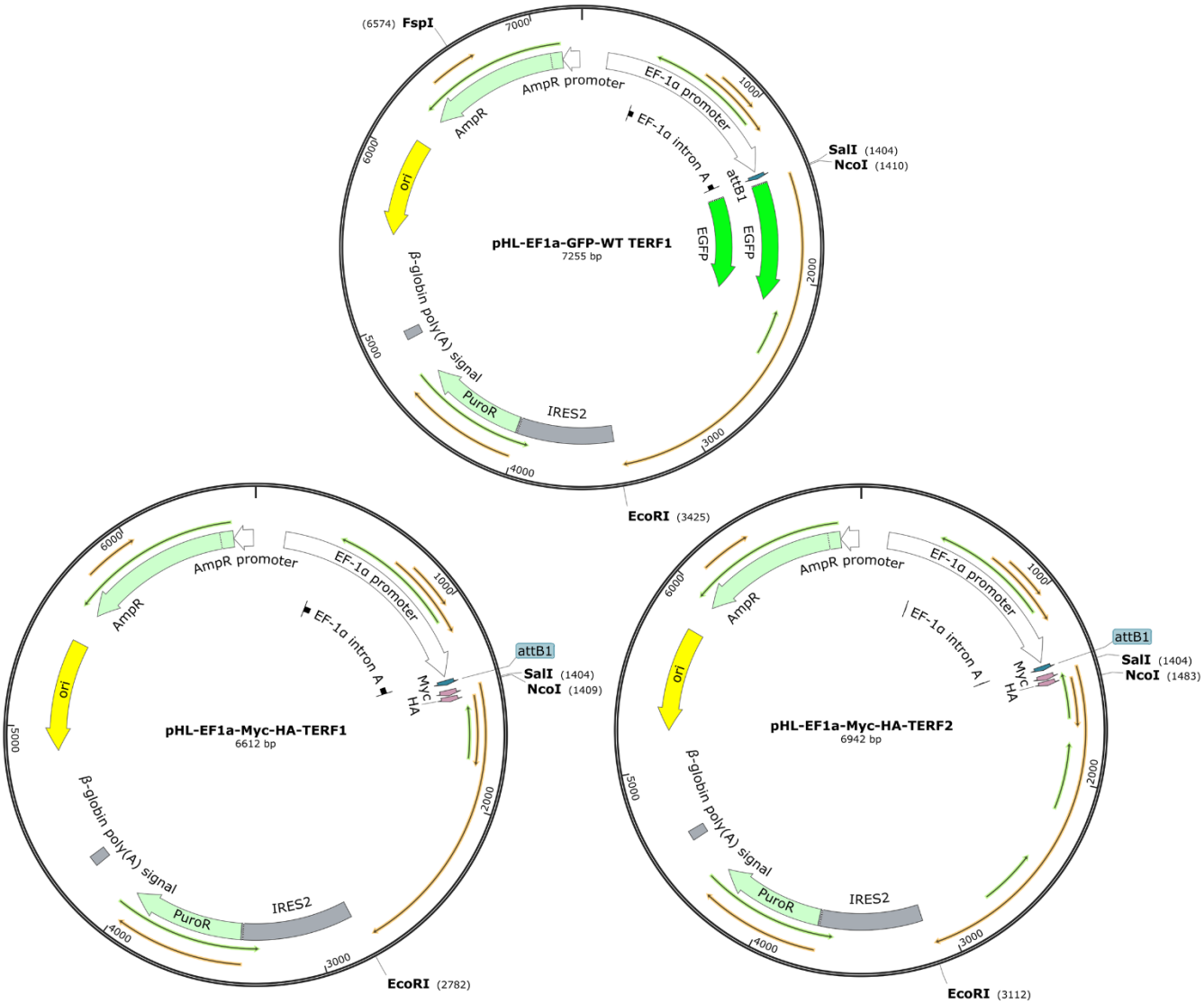

Figure 2.2: Plasmid maps of GFP-TERF1 and siRNA resistant Myc/HA tagged TERF1 and TERF2

The Plasmid maps of GFP-TERF1 and siRNA resistant Myc/HA tagged TERF1 and TERF2 in pHL-EF1α backbone are shown. In addition, the plasmid size, significant features and restriction sites of interest are included.

2.3.2 Stable transfection of GFP-TERF1 wildtype and mutant plasmids into mouse ES cells

TERF1 wildtype and mutant plasmids were linearised with *Fsp*I (NEB, 10,000 U/ml) at 37ºC overnight and transfected into to 2 x 10^6 ES129.1 mouse ES cells by electroporation using the MicroPulser Electroporator (BioRad). Cells were trypsinized and washed once with PBS and resuspended in 400 ul PBS and transferred to the Micropulser Electroporation cuvettes. 10 µg of linearised plasmid DNA was then added before electroporation at 0.25kV, 500uF. Cells were then replated into cell culture media lacking penicillin and streptomycin. To select for GFP-TERF1 wild-type and mutant-transfected cells, 2 µg/ml puromycin (Sigma Aldrich) was supplemented to the ES media after 24 hours. Single colonies were then picked, cultured, and screened for the presence of GFP-TERF1 by immunoblotting (**Section 2.4**), immunofluorescence (**Section 2.6**), and qRT-PCR (**Section 2.7**).

2.4 Immunoblotting and protein analyses

2.4.1 Cell Lysates preparation and SDS-PAGE

Cells were lysed in cold RIPA buffer (150 mM NaCl, 50 mM Tris-HCl at pH 7.5, 0.25% sodium deoxycholate, 0.1% NP40, 0.05% SDS, 1 mM NaF, 1mM sodium orthovanadate, supplemented with mammalian protease inhibitors), followed by a 10-second pulse sonication at amplitude 8 (Qsonica, Q700). After a 5-minute centrifugation at 16,000 *g*, the supernatant was collected. PAGE sample buffer (50 mM Tris pH 6.8, 2% (v/v) SDS, 0.1% bromophenol blue, 10% glycerol 2.5% β–mercaptoethanol) was added to each sample and boiled for 5 minutes at 95ºC. Samples were loaded onto a 4-12% SDS-PAGE gel in a Mini-PROTEAN Tetra Vertical Electrophoresis Cell (Bio-Rad). Running buffer (25 mM Tris base, 190 mM glycine 0.1% SDS) was used for electrophoresis and gel was run at 80 volts for 1

hour. Pre-Stained SDS-PAGE Standards (Bio-rad) was used as a molecular weight marker. SDS-PAGE Gel was then either transferred for immunoblotting (**section 2.4.2**). or stained with Coomassie blue stain (**Section 2.4.3**).

2.4.2 Immunoblotting

Proteins from the SDS-PAGE gel was transferred in a Mini-PROTEAN Tetra Vertical Electrophoresis Cell (Bio-Rad), using transfer buffer (25 mM Tris, 192 mM glycine, 20% ethanol), onto a Polyvinylidene fluoride (PVDF) membrane (Immobilon, Millipore) through a wet/tank electroblotting procedure at 90 volts for 3 hours. Before transfer, membranes were activated in methanol and equilibrated in transfer buffer. Following transfer, the PVDF membrane was blocked either in 2% (w/v) Bovine Serum Albumin (Sigma Aldrich) or 5% (w/v) skim milk in PBS with 0.2% (v/v) Tween 20 solution (MP biochemicals) at room temperature for 1 hour. A primary antibody specific to the target protein was incubated with the membrane at 4^{o}C overnight; the horseradish peroxidase (HRP) conjugated secondary antibody was incubated with the membrane at room temperature for 3 hours. After each round of antibody incubation, the membrane was washed three times in PBS-Tween 20 solution. Protein signals were detected using the SuperSignal West Pico Chemiluminescence HRP substrate detection kit (Thermo Scientific). Results were analysed using ChemiDoc imaging systems (BioRad).

2.4.3 Coomassie blue staining for recombinant protein expression analysis

The SDS-PAGE gel was stained in Coomassie blue staining buffer (45% methanol, 10% glacial acetic acid, 45% dH2O, 0.25% Coomassie blue R250 (Sigma Aldrich) per litre) at room temperature for 2 hours. Following the first de-staining with Solution 1 (50% methanol,

10% glacial acetic acid in distilled water) for 2 hours, the gel was further destained with Solution 2 (5% methanol, 1% glacial acetic acid in distilled water) at room temperature. Coomasie stained gels were then imaged using the ChemiDoc imaging systems (BioRad).

2.5 FACS analyses

2.5.1 Detection of fluorescent proteins

Cells were harvested and washed once in the ice-cold FACS buffer (1% BSA and 2 mM EDTA in PBS), then spun with pellets resuspended in Propidium iodide (PI) (1 ug/ml) in PBS. Cells were analysed on a FACS LSR Analyzer (BD Biosciences, Flowcore, Monash University) and FloJo Software (FlowJo LLC).

2.5.2 Cell cycle analysis

1 hour before harvesting, cells were incubated with 10 µM BrdU (Sigma Aldrich), then washed in ice-cold PBS and fixed in 70% ethanol for another hour. Cells were pelleted at 300 g for 5 minutes and permeabilised with 2 N HCl/0.5% Triton X-100 for 30 minutes. Cells were then incubated 0.1 M NaB_4O_7 (pH8.5) for 30 minutes before pelleting and resuspension in 0.5% Tween 20/1% BSA/PBS containing antibody against BrdU prior to incubation at room temperature for 30 minutes. Cells were washed with 1% BSA/PBS and incubated with secondary antibody for 30 minutes. Cells were washed, resuspended in a solution comprising 10 µg/ml PI and 300 µg/ml RNase A (Cell Signalling, 4087S) and incubated in the dark for 30 minutes, before analyses on a FACS LSR Analyzer (BD Biosciences, Flowcore, Monash University). Data were analysed using FlowJo (FlowJo LLC).

2.6 Immunofluorescence and FISH analysis

2.6.1 Cell preparation and image acquisition

To enrich for mitotic cells, cells were treated with a microtubule disrupting agent, Colcemid (Life Technologies), at a final concentration of 0.1 µg/ml for 1 hour before harvesting for immunofluorescence analysis (**Sections 2.6.2** and **2.6.3**) or Tel-FISH analysis (**Section 2.6.4**). Images were collected using a Zeiss Imager M2 fluorescence microscope linked to an AxioCam MRm CCD camera system. Microscopy analyses were processed using the Zen software 2011(Carl Zeiss Microscopy).

2.6.2 immunofluorescence of cytospun preparations

For immunofluorescence preparations, cells were subjected to hypotonic treatment in 0.075 M KCl and loaded onto a cytofunnel (Fisher Scientific) before being cytospun onto glass slides using a cytocentrifuge at 1,000 *g* (Thermo Scientific™ Cytospin™ 4) . Slides were incubated in KCM buffer (120 mM KCl, 20 mM NaCl, 10 mM Tris-HCl pH 7.5, 0.5 mM EDTA, 0.1% (v/v) Triton X-100) for 5 minutes. Cells were extracted with 0.5% (v/v) Triton X-100 in KCM for 5 minutes and blocked in KCM buffer containing 1% (w/v) BSA before incubation with relevant primary and secondary antibodies at 37^{o}C for 1 hour. After each round of antibody incubation, slides were washed three times in KCM buffer. Slides were then fixed in KCM with 4% (v/v) formaldehyde and mounted with Vectashield (Vector Lab) supplemented with DAPI at 250 ng/ml. Images were taken and processed as described in **section 2.6.1**.

2.6.3 Immunofluorescence of pre-fixed cells

Cells were fixed in 1% formaldehyde/phosphate-buffered saline (PBS) before being cytopsun onto glass slides as in **Section 2.6.2**. Samples were extracted with 0.5% Triton X-100/PBS, blocked with 1% BSA in PBS and incubated with the relevant primary and secondary antibodies at 37°C. After each round of antibody incubation, slides were washed three times in 0.2% Tween-20/PBS. Slides were fixed in PBS with 4% (v/v) formaldehyde and mounted with Vectashield (Vector Lab) supplemented with DAPI at 250 ng/ml. Images were taken and processed as described in **section 2.6.1**.

2.6.4 Fluorescence *in-situ* hybridisation (FISH) analysis

For Telomere-FISH (Tel-FISH) analyses, cells were diluted in hypotonic solution (75 mM KCl) then were fixed in ice-cold methanol/acetic acid (3:1 ratio). Cells were dropped onto slides and dried overnight. Slides were rehydrated in PBS, treated with 0.5 µg/ml RNase A (Roche), fixed in 4% formaldehyde/PBS followed by serial ethanol dehydration (75%>85%>100%). Chromosome preparations were hybridized with 0.5 µM telomere C-strand AlexaFluor® 488-conjugated telomere PNA (peptide nucleic acid) probe (PNA Bio Inc.); or in conjunction with 0.5 µM CENP-B box Cy5-conjugated centromere PNA probe (PNA Bio Inc.) in hybridization solution (10 mM Tris–HCl pH 7.2, 70% deionized formamide (ThermoFisher), 1% salmon sperm DNA (Thermofisher)) at 80°C for 3 minutes. After 2 hours of incubation in the dark at room temperature, slides were sequentially rinsed in FISH buffer I (10 mM Tris–HCl pH 7.2, 70% formamide, 0.1% BSA) and FISH buffer II (100 mM Tris–HCl pH 7.5, 0.15 M NaCl, 0.08% Tween-20) before carrying out another round of serial ethanol dehydration. Images were taken and processed as described in **section 2.6.1**.

2.7 Nucleic acid extraction and PCR analyses

2.7.1 RNA extraction

RNA was prepared according to the manufacturer's protocol (Roche) and treated with DNAse using the Promega RQ1 reagent (Promega). Briefly, cells were lysed in lysis buffer and the lysates were transferred to a High Pure Filter Tube. Samples were spun down through the High Pure Filter Tube and incubated with DNase I for 15 minutes at 25^{o}C before being washed. RNA was eluted from High Pure Filter Tube with elution buffer and stored at -80^{o}C. cDNA was synthesised with oligo d(T)12-18 (Life Technologies) using the cDNA Reverse Transcriptase kit (Life Technologies). The cDNA amount equivalent to 7.5 ng of RNA was amplified with 250 nM of the respective primers and qPCR performed with the FastStart DNA Green Sybr (Roche) using the LightCycler© (Roche) as described in **Section 2.7.3**.

2.7.2 DNA extraction

Cells were lysed in cell lysis buffer (50 mM Tris-HCL pH 8, 100 mM EDTA pH 8, 100 mM NaCl, 1% SDS), and protein precipitated with a final concentration of 2.5 M ammonium acetate. The solution was mixed and spun down at 16,000 *g* for 20 minutes at 4^{o}C. Next, the supernatant was extracted and mixed with equal volumes of isopropanol to precipitate DNA. Precipitated DNA was spun down at 16,000 *g* for 20 minutes at 4^{o}C, washed with 70% ethanol, air-dried and finally dissolved in TE buffer (10 mM Tris-HCL pH 8, 1 mM EDTA pH 8). Samples were stored at -20^{o}C. 100 ng of DNA was used for amplification with 250 nM of respective primers and qPCR performed with the FastStart DNA Green Sybr (Roche) using the LightCycler© (Roche) as described in **Section 2.7.3.**

2.7.3 PCR analyses

The Lightcycler® 96 system (Roche) was used to run PCR analyses of DNA and cDNA samples. All data analyses were calculated using the comparative cycle threshold method (CT). The comparative cycle threshold method uses CT values obtained from two different experimental RNA samples are normalised to a housekeeping gene and then compared. The difference between the Ct values (ΔCt) of the gene of interest and the housekeeping gene (GAPDH) is calculated for each sample. Then, the difference in the ΔCt values between the experimental and control samples ΔΔCt is calculated. The fold-change in expression of the gene of interest between the two samples is then equal to and expressed as $2^{(-\Delta\Delta Ct)}$.

2.8 Chromatin immunoprecipitation (ChIP) analyses

Cells were crosslinked with either a final concentration of 1% formaldehyde in PBS for 10 minutes or a final concentration of 1.5 mM EGS (Thermofisher) for 45 minutes, followed by final concentration of 1% formaldehyde for 20 minutes at room temperature. The reaction was quenched with the addition of final concentration of 250 mM glycine for 10 minutes. Crosslinked cells were pelleted at 300 g for 5 minutes and lysed in cold cell lysis buffer (10 mM Tris pH 8, 10 mM NaCl, 0.2% NP40 and mammalian protease inhibitors). Nuclei were collected, resuspended in resuspension buffer (50 mM Tris pH 8, 10 mM EDTA and 1% sodium dodecyl sulphate (SDS)) and sonicated for 20 minutes (high power mode, 30 sec on / 30 sec off) in Diagenode Biorupter® sonicator to obtain chromatin fragments of 500 bp or less. The chromatin suspension was diluted in dilution buffer (20 mM Tris pH 8, 2 mM EDTA, 150 mM NaCl, 1% Triton X-100 and 0.01% SDS) and precleared with Protein A sepharose beads (Sigma Aldrich) at 4°C for 1 hour with rotation. Pre-cleared chromatin was immunoprecipitated with antibody-bound beads at 4°C

overnight with rotation. 5% of cleared lysate was kept as input at -20°C. For each reaction, 2-5 µg of antibody and 25 µl of Protein A sepharose beads (50% slurry) were used. The immunoprecipitated material was washed (once in low salt buffer (10 mM Tris-HCl pH 8, 2 mM EDTA, 0.1% SDS, 1% Triton X-100, 150 mM NaCl) twice in dilution buffer, once in high salt (10 mM Tris-HCl pH 8, 2 mM EDTA, 0.1% SDS, 1% Triton X-100, 500 mM NaCl) and twice in TE buffer pH 8) and eluted in 200 ul elution buffer (100 mM $NaHCO_3$ and 1% SDS). The eluted material was reverse crosslinked with NaCl at a final concentration of 0.3M and a final concentration of 100 µg/mL RNase A and 200 µg/ml Proteinase K and reverse-crosslinked at 65°C overnight. DNA was extracted using equal volumes of phenol/chloroform and precipitated in 1ml of 100% EtOH with 500 µg/ml tRNA and 500 µg/ml glycogen as carriers. Fractions of the purified ChIP DNA was used as a template for qPCR with appropriate primers and GAPDH (negative control) while inputs at varying concentration (undiluted, 1 in 10 dilution, 1 in 100 dilution, 1 in 1,000 dilution and 1 in 10,000 dilution) were used to generate a standard curve. In addition, ChIP qPCR values of H3 ChIP using primers to (GAPDH) was also tabulated (with standard curve). ChIP qPCR values from targeted purified ChIP DNA were expressed as relative to input and normalised against purified H3 ChIP DNA to cater for variations in chromatin amounts between sample numbers.

2.9 Southern Blotting

Genomic DNA was resuspended in TE buffer and 10 mg of DNA was digested with *Sac*I restriction enzyme (NEB, 20,000 U/ml) in a minimum volume at 37ºC overnight. 1 mg/well for repetitive targets or 5 µg/well for single-copy targets of digested DNA was mixed in DNA loading buffer (6x, NEB) loaded at and separated by 1% agarose gel electrophoresis. As a DNA marker, 1kb plus DNA ladder (Life Technologies) was used. To prepare the gel for

southern blotting after agarose gel electrophoresis, the gel was rinsed in distilled water, immersed in depurination buffer (0.25 M HCl) for 15 minutes, rinsed in distilled water, immersed in denaturing buffer (1.5 M NaCl, 0.5 M NaOH) for 1 hour before replacing the denaturing buffer with neutralizing buffer (0.5 M Tris–HCl, 1.5 M NaCl. pH 7.3) for 90 minutes. To prepare the southern blot apparatus, the casting tray was placed upside down in a large plastic tray to support the gel. Four layers of filter paper (Whatman) over the casting tray for the wick. 20X SSC (3M NaCl, 0.3M Sodium Citrate, pH 7.2) was poured on the filter paper and saturated the base of the tray. The agarose gel was then placed on the blotting base and a piece of Hybond XL membrane (Amersham) was soaked in 2X SSC before being placed on top of the agarose gel. Four layers of filter paper were soaked in 2X SSC and layered on the blot followed by a stack of paper towels and a glass plate and 500 g weight. The blot was left overnight. The Hybond XL membrane was rinsed in 2X SSC and blot dried with filter paper before 5 minutes UV treatment to fix the DNA on the membrane. The blot was Pre-hybridized in hybridization solution (5X SSPE (0.75 M Sodium Chloride, 0.04 M Sodium Hydrogen Phosphate, 0.004 M EDTA pH of 7.4), 5× Denhardt's solution (0.1% ficoll (Sigma Aldrich), 0.1% polyvinylpyrrolidone (Sigma Aldrich), 0.1% BSA), 1% SDS) at 65ºC for 2 hours. Megaprime DNA labelling system, dCTP (GE Heathcare) was used to label PCR product with dCTP-^{32}P (Perkin Elmer). Briefly, primers at a final concentration of 0.2 µM was added to 25 ng of PCR product and incubated at 95 ºC for 2 minutes before incubation with labelling buffer, 10 pmoles of dCTP-32P (Perkin Elmer) and 10 U of Klenow fragment polymerase (Cytiva) at 37ºC for 15 minutes. The labelled probes were denatured at 100°C for 5 minutes adding to 10 ml hybridization solution. The hybridization solution on the blots were replacing with the hybridization solution with denatured probed and incubated at 65°C overnight. Blots were washed twice (15 minutes, 65ºC) with 0.2X SSC, 0.5 % SDS (single-copy targets) or 0.1X SSC, 0.5 % SDS (repetitive

targets) before air-drying. The labelling of the blot was performed using the Typhoon phosphorimager (GE healthcare) at 100 µ scanning resolution. The sequences of probes are shown below. Expected bands with H3F3a probe: WT: 2.9 Kb, H3f3a$^{flox/flox}$: 5.3 Kb, H3f3a$^{-/-}$: 3.9 Kb, and H3F3b probe: WT: 3.9 Kb, H3f3b$^{flox/flox}$: 7.32 Kb, H3f3b$^{-/-}$: 4.9 Kb

Probes	Size	Probe sequence
H3F3A	218 bp	GTCGAGCAGTGGGATAGTGTCTAAGCAGTATGTCCGTGTAATTTAACAGGAAGATAGTCAT ACTTTTTGCTATGGGGAAAAGATGTTTCTCTCTTTTGAATGATTATTACTACTTGAATATGTAT GCATATGTTTGTGAACACATGTATCTTAGTATTCAGTTTGATAGATAACATTACATTTTGAAG CTGTAATCTGATCTAAAAGCCTAAAAAGTC
H3F3B	377 bp	GGAGTGCTAGTGTGCATAAATATAAAAATGGACCCGAGTCTATTCAGCAAGGCATTCTAGT GAAGCTTTAGTAGCTAAAGAAGTGTAAGAGTTTGCATGTATCCCAGACTGGCTTACCCTTCT CAGTCTCCTGAGGAGAAGTTACAAGGTGTGTACTGCCACACCTAGAACTTTAGGTCCCTTTG GATAAGTATGTACCTCAATGGACATGGTATTAATTAGAAGGGGCAGTAGCATAGTCTAGTAC AATGAAAACAGTTCTGACCACATTGTTTTATGTTGGGCTGAGTAAAGTCTGAGGCAGCCCTGA GCGACTGGCTTGTTGAGTTGCTACCTATAGTAACCAAGTCTGTGGCTTGGAGCATGTTGGTTATTGG

2.10 Protein expression and binding

2.10.1 Construction and expression of GST tagged constructs

N- (amino acids 2-251) and C-terminal GST-TERF1 (amino acid 252-421) and KDM4B (accession number: O94953) constructs were generated by cloning N- and C-terminal fragments of TERF1 (Integrated DNA Technologies) and, KDM4B (Integrated DNA Technologies) into pGEX-2T (GE Healthcare Life Sciences) or pGEX4T-1 (Amersham) plasmids, respectively. N- and C-terminal fragments of TERF1 were cloned into pGEX-2T using BamHI and EcoRI sites. N- and C-terminal fragments of KDM4B were cloned into pGEX-4T-1 using *Sal*I and *Not*I sites as described in **section 2.2.1** and **2.3.1**. These plasmids were digested with the respective restriction enzymes at 37^{o}C overnight to generate backbone and inserts with sticky ends before separation by agarose gel

electrophoresis and extraction using Wizard® SV Gel and PCR Clean-Up System (Promega). Sticky end ligation with T4 DNA ligase (NEB) was performed at 16^{o}C overnight. The ligation mix was transformed into chemically competent BL21 bacterial cells at 42^{o}C for 45 seconds and grown on Luria Broth-agar plate supplemented with 100 µg/ml ampicillin at 37^{o}C overnight. Selected colonies were grown at 37^{o}C for 6 hours and protein expression was induced using a final concentration of 1 mM Isopropyl-β-D-thiogalactoside (IPTG) for 6–8 hours at 16^{o}C. Bacterial cells were lysed in ice-cold TNE buffer (10 mM Tris–HCl pH 7.8, 1% (v/v) NP40, 150 mM NaCl, 1 mM EDTA, 1% (v/v) Triton X-100 and protease inhibitors) and induction was confirmed by SDS-PAGE (**Section 2.4.1**) followed by coomassie staining (**Section 2.4.2**). GST-fusion proteins were purified using Glutathione Sepharose beads (GE Healthcare Life Sciences). GST-fusion proteins were eluted using reduced glutathione (50 mM Tris, 10 mM reduced glutathione, pH 8.0) and stored at -80^{o}C.

2.10.2 *In vivo* binding assay

GST-fusion proteins were bound to Glutathione Sepharose beads (GE Healthcare Life Sciences) while antibodies against FLAG were bound to Protein A beads (Sigma Aldrich) before incubation with mouse ES cell lysates for 4 hours at 4°C. Mouse ES cell lysates were obtained as described in **Section 2.4.1**. After 4 hours incubation, protein A beads were washed thrice in ice-cold RIPA buffer (150 mM NaCl, 50 mM Tris–HCl at pH 7.5, 0.25% sodium deoxycholate, 0.1% NP40, 0.1% SDS, 1 mM NaF, 1 mM sodium orthovanadate and protease inhibitor), and boiled in SDS-PAGE sample buffer before SDS-PAGE (**Section 2.4.1**) and immunoblotting (**Section 2.4.2**) using relevant antibodies.

2.11 *In vitro* demethylase assay

250 ng of H3.3 WT K36me3, H3.3 S31ph K36me3, H3.3 A31 K36me3 or H3.3 E31 K36me3 peptides (Chinapeptides) were incubated with 50 nM KDM4B recombinant protein (Active Motif) in reaction buffer (50 µl) containing 50 mM HEPES pH 7.5, 0.02% Triton X-100, 100 µM 2OG, 100 µM Ascorbate, 50 µM $(NH_4)_2Fe(SO_4)_2 \cdot 6(H_2O)$, 1 mM TCEP for 2 hours at room temperature. Samples were co-spotted onto an MTP anchorChip 800/384 TF MALDI target plate with Matrix solution of 10 mg/ml a-cyano-4-hydroxycinnamic acid (Laser BioLabs, Sophia-Antipolis, France) in 50% acetonitrile 0.1% TFA. Samples were analysed on a Bruker Daltonics (Bremen, Germany) ULTRAFLEX MALDI TOF/TOF in reflector mode with an *m*/*z* range of 1200–3500 Da, using Smartbeam parameter set 4, and detector gain 2.5× for 1000 shots. The data was processed using Flexanalysis (Bruker, Version 3.4, build 50). The spectra were externally calibrated against a 4700-peptide mix standard including angiotensin (1296 *m*/*z*), Glu-Fibrinopeptide B (1570 *m*/*z*), ACTH (2093 *m*/*z*), ACTH (2465 *m*/*z*) and ACTH (3657 *m*/*z*) which were spotted on adjacent calibration wells.

Table 2.2: Peptides used for in vitro demethylase assay

Peptides	Full peptide sequence (amino acids 21-44 on H3.3)
H3.3	ATKAARKSAPSTGGVK(Me3) KPHRYRPG-GK(Biotin)
H3.3S31ph	ATKAARKSAPS(ph)TGGVK(Me3) KPHRYRPG-GK(Biotin)
H3.3S31A	ATKAARKSAPATGGVK(Me3) KPHRYRPG-GK(Biotin)
H3.3S31E	ATKAARKSAPETGGVK(Me3) KPHRYRPG-GK(Biotin)

2.12 *In vitro* phosphorylation

1 µg of the peptide 'NWAKILSHYKFNNRTSVMLKDRWRTMKRLK' (TERF1 aa 389-418, Chinapeptides) was incubated with 0.5 µg of recombinant human AURKB protein (Abcam) in the presence of Magnesium/ATP cocktail (Merck Millipore) for 1 hour at 37°C. The *in vitro* kinase assay products were digested in solution with 10 ng Lys-C at 37°C overnight. Digested peptides were desalted and analysed by data-dependent acquisition LC-MS/MS. Raw files were converted to the mzML format and searched with the search engine COMET (Eng, Jahan, & Hoopmann, 2013) against a decoy human protein database (Swissprot; https://www.uniprot.org/), including common contaminants. Methionine oxidation and phosphorylation on serine, threonine and tyrosine were set as differential modifications. Peptide-spectra-matches were statistically validated using the *trans*-proteomic pipeline (Keller, Nesvizhskii, Kolker, & Aebersold, 2002). Peptides found phosphorylated were further investigated by targeted MS-based proteomics using parallel-reaction monitoring (PRM) or multiple-reaction monitoring (MRM) to refine the phosphorylation site localization. PRM and MRM measurements were then analysed and visualized in Skyline (MacLean et al., 2010) (Monash Proteomics & Metabolomics Facility, Monash University).

2.13 Antibodies

The antibodies and their working concentrations are listed in the table below.

Table 2.3: Antibodies and their concentrations used in this thesis

Antibody against	Catalog number	Company	IF (dilutions)	WB (dilutions)	ChIP (µg)	Host
ATRX	SC15408	Santa Cruz	1:200	1:1000	3	Rabbit
Aurora Kinase B	611082	BD biosciences	1:300	1:1000	-	Mouse
BrdU	ab6326	Abcam	1:300 (FACS)	-	-	Rat
CHK1 S317ph	12302	Cell signalling technology	-	1:1000	-	Rabbit

CHK2-Thr68ph	ABE343	Millipore	-	1:1000	-	Rabbit
Daxx	SC7152	Santa Cruz	-	1:1000	-	Rabbit
Flag tag	F1804	Sigma	1:200	1:1000	-	Mouse
GFP tag	11814460001	Roche	1:200	1:1000	3	Mouse
H3	ab1791	Abcam	-	1:1000	2	Rabbit
H3K4me3	ab8580	Abcam	-	1:1000	-	Rabbit
H3K9me3	ab8898	Abcam	1:200	1:1000	3	Rabbit
H3S10ph	9701	Cell signalling technology	1:300	-	-	Rabbit
H3K27ac	7360	Millipore	-	1:1000	-	Mouse
H3K27me3	7447	Millipore	-	1:1000	-	Rabbit
H3K36me3	ab9050	Abcam	1:200	1:1000	3	Rabbit
H3.3	9838	Millipore	-	1:1000		Rabbit
H3.3S31ph	39637	Active motif	1:300	-	-	Rabbit
HP1α	05689	Millipore	1:200	-	3	Mouse
HA tag	3F10	Roche	1:200	1:1000	3	Rat
KDM4B	ab191434	Abcam	-	1:1000	4	Rabbit
PML	MAB3738	Millipore	1:300	-	-	Mouse
RNA pol II (4H8)	ab5408	Abcam	1:200	-	3	Mouse
RNA pol II (H5)	ab24758	Abcam	1:200	-	3	Mouse
Trim25	ab167154	Abcam	-	1:1000	3	Rabbit
β-actin	SC69879	Santa Cruz	-	1:5000	-	Mouse
γH2AX	5636	Millipore	1:1000	1:1000	-	Mouse
Alexa Fluor 488- anti-rabbit IgG	A32790	Molecular Probes	1:1000	-	-	Donkey
Alexa Fluor 488- anti-mouse IgG	A32766	Molecular Probes	1:1000	-	-	Donkey
Alexa Fluor 594- anti-mouse IgG	A32744	Molecular Probes	1:1000	-	-	Donkey
Alexa Fluor 594- anti-rabbit IgG	A32754	Molecular Probes	1:1000	-	-	Donkey
Alexa Fluor 594- anti-human IgG	A11014	Molecular Probes, Life Technologies	1:1000	-	-	Goat
Alexa Fluor 647- anti-rat IgG	A21247	Molecular Probes, Life Technologies	1:1000 (FACS)	-	-	Rat
anti-mouse IgG-(H+L) HRP	31430	Life Technologies	-	1:5000	-	Goat
anti-rat IgG- (H+L) HRP	31470	Life Technologies	-	1:5000	-	Goat
anti-rabbit IgG- (H+L) HRP	31460	Life Technologies	-	1:20,000	-	Goat

2.14 Table of primers

The primers used are listed in the table below.

Table 2.4: Primers and their sequences used

Gene Name	Sequence	
	Forward（5'-3'）	**Reverse（5'-3'）**
Primers Used for qPCR		
TERF1	ACAGCGCCGAGGCTATTATT	GTGTAATACGCTCATCAACT
AURKB	GATCCCAGAACAAGCAGCCT	TCGATTTCGATCTCTCGGCG
TERF2	AAGTGGAACAGCCCTAACGG	TTCACCTGGTGCCTGAACTT
TBX3	GGTAAGGCAGACCCCGAAAT	GCTTGGGAAGGCCAAAGTAAAT
NANOG	TTGCTTACAAGGGTCTGCTACT	ACTGGTAGAAGAATCAGGGCT
ACTIN	TCCCTGGAGAAGAGCTACGA3	AGCACTGTGTTGGCGTACAG
Telomere	GGTTTTTGAGGGTGAGGGTGAGGGT GAGGGTGAGGGT	TCCCGACTATCCCTATCCCTATCCCT ATCCCTATCCCTA
GAPDH	AGAGAGGGAGGAGGGGAAATG	AACAGGGAGGAGCAGAGAGCAC
Csf2ra	GGTCACGACGTGGCGCGAT	AGGCCTCACTCCCCAGCAGT
Polrmt	CGGCCGCGGAAGTCCATGTT	CGCAGCGAGGCCCTGTATCG
Spred2	TGAAGACTACCGGCACGCGC	CCCTTGGCGAAGCGCACGTA
Zfp629	TTGGCTCCTGGTGGCGGAGT	GCCCGGAGAGCTCAGGGTGA
Asxl1	CCACTAGTTCGCTCTTGGGT	GCATAACCACGGGGTCAGAG
Cops7a	CACATGGTGTCTACCGGACG	GAGGTGAGGTCACGTGGG
Hmgn2	TAGAACCGGATTTCACCTCCC	GAGTTTAAACCCCGCCCACG
Fasn	GAGACCGATGCAGACTCAGG	GGGAAGACCCGAACTCCAAG
Eef2	CAAGGCATACCTGCCTGTCAAT	ATTACACAGGCCTTGCAGGTTAT
Csf2ra	GGTCACGACGTGGCGCGAT	AGGCCTCACTCCCCAGCAGT
Primers used for sequencing		
pHL-EF1α primer	TCAAGCCTCAGACAGTGGT	-
H3f3	-	TCTGTTTTGAAGTCCTGAGCA
Full H33 expression	GCTCGTACAAAGCAGACTGCCCGC	AGCACGTTCTCCGCGTATGCG
pEGFPC1	GCGATCACATGGTCCTGCTG	TTAAAGCAAGTAAAACCTCTACAAA
pGEX-2T	TACATGGACCCAATGTGCCTGGATG	CCGGGAGCTGCATGTGTCAGAGG
Primers used for mRNA expression		
Kdm4B ex 5	GGCGTGAATACACCCTACTT	GCAGGTAGTTGATGCTGTAGA
Kdm4B ex 6/7	CCTGGCCATAGGCTTCTTC	CGTACTTCTTCAGGATGATGGG
Kdm4B ex7/8	GCCTTCCTAAGGCACAAGAT	CCCAGCTTCCTGTGTAATCC
Full H33 expression	GCTCGTACAAAGCAGACTGCCCGC	AGCACGTTCTCCGCGTATGCG
H33WT expression	TCGCAAGAGTGCGCCCTC	TCTGTTTTGAAGTCCTGAGCA
H33 S31A expression	TCGCAAGAGTGCGCCCGC	TCTGTTTTGAAGTCCTGAGCA
H33 S31E expression	TCGCAAGAGTGCGCCCGA	TCTGTTTTGAAGTCCTGAGCA
GAPDH expression	GTGGAGTCTACTGGTGTCTTC	GGTTCACACCCATCACAAAC
Primers used to make GST tagged constructs		
KDM4B N-term	GGGTCGACGCGGTAGCGAAGATCAT G	TATGCGGCCGCCTAAAATGTGCTCG GGGCCTGACCT
KDM4B C-term	ATTGTCGACCAAGCAGCGGCGCAGG TCGTA	ATGCGGCCGCTTATTTGTCATCATCA TCC
Primers for southern blotting		
h3f3a probe	GTCGAGCAGTGGGATAGTGTC	GACTTTTTAGGCTTTTAGATCAGA TTACAG
h3f3b probe	GGAGTGCTAGTGTGCATAAAT	CCAATAACCAACATGCTCCAA

Chapter 3: Aurora Kinase B, a novel regulator of TERF1 binding and telomeric integrity

3.1 Introduction

3.1.1 Overview

Shelterin is a protein complex that binds specifically to mammalian telomeres to regulate and maintain their length and protect the chromosome ends from being recognised as sites of DNA damage (de Lange, 2005). Six different proteins make up the Shelterin complex: TERF1, TERF2, TIN2, RAP1, POT1 and TPP1 (de Lange, 2005). Throughout the cell cycle, these subunits function to repress DNA damage response at the telomeres and regulate telomerase activity (Hockemeyer et al., 2006; Wu et al., 2006; Denchi and de Lange, 2007; Wang et al., 2007; Xin et al., 2007).

The Shelterin complex binds to telomeres through its subunit compartments TERF1 and TERF2, which interact with the double-stranded telomeric DNA (Broccoli et al., 1997). TERF1 and TERF2 exist as homodimers and interact with telomere DNA through their Myb-type double-stranded DNA recognition motifs. These motifs enable sequence-specific contacts with DNA major groove (Bianchi et al., 1997, Hanaoka et al., 2005, Fairall et al., 2001, Broccoli et al., 1997). TERF1 negatively regulate telomere length, where the long-term overexpression of TERF1 in telomerase-positive tumour cell lines resulted in telomere shortening (Smogorzewska et al., 2000). Conversely, the expression of a dominant-negative TERF1 mutant was seen to inhibit the binding of TERF1 to the telomeres and resulted in telomere elongation (van Steensel and de Lange, 1997). TERF1 also facilitates DNA replication and maintains telomere integrity where gene deletion of TERF1 results in the loss of telomere structural integrity, as observed by the formation of Multiple Telomeric Signals (MTS) (Sfeir et al., 2009, van Steensel and de Lange, 1997). Furthermore, the deletion of

TERF1 led to the activation of the ATR-mediated DNA damage response (Zimmermann et al., 2014).

Like TERF1, TERF2 protects telomeres from being recognized as sites of DNA damage by repressing ataxia telangiectasia mutated (ATM)-mediated DNA damage response and NHEJ repair pathway. The loss of TERF2 by *Cre*-mediated deletion in mouse cells increases DNA damage markers such as 53BP1 and γH2AX and, increased telomere fusions at G0/G1 of the cell cycle (Denchi and de Lange, 2007, Karlseder et al., 1999, Konishi and de Lange, 2008) Together, these studies show the importance of TERF2 in repressing ATM and NHEJ mediated repair at the telomere.

Unlike TERF1 and TERF2, POT1 binds the 3′ G-overhang single-stranded telomeric DNA (Baumann and Cech, 2001) and associates with TERF1 and TERF2 through interactions with TPP1. In addition, POT1 binds strongly to G-rich telomeric DNA, with preference to telomere DNA of the same species (i.e. human POT1 preferred human telomere DNA) (Baumann and Cech, 2001). POT1 and TPP1 function together to repress ATR signalling and regulate telomerase activity. The knockout of either protein caused increased DNA damage signalling at chromosome ends and, the loss of telomere integrity (Hockemeyer et al., 2006; Wu et al., 2006; Denchi and de Lange, 2007; Wang et al., 2007; Xin et al., 2007). Another Shelterin component, TIN2, is a bridging subunit that interacts with TERF1, TERF2 and TPP1 (O'Connor et al., 2006; Hu et al., 2017). It is a critical subunit that facilitates the assembly of an intact Shelterin complex and contributes to telomere length regulation and protection (Kim et al., 1999; Takai et al., 2011; Frescas and de Lange, 2014; Hu et al., 2017). The sixth Shelterin subunit, RAP1, recruited to telomeres through interaction with TERF2, functions together with TERF2 to inhibit HR-mediated DNA repair. *Cre*-mediated deletion of

TERF2 led to the loss of RAP1 at the telomeres, indicating that TERF2 recruits RAP1 (Celli and de Lange, 2005). Although the loss of RAP1 does not induce DNA damage signalling and loss of telomere integrity at the telomeres, the loss of RAP1 in cells also lacking TERF2 caused an increase in HR and telomeric sister chromatid exchanges (Martinez et al., 2010; Sfeir et al., 2010; Chen et al., 2011; Benarroch-Popivker et al., 2016; Rai et al., 2016). Altogether, the Shelterin complex protects telomere ends from DNA repair mechanisms and regulates telomere activity. In this chapter, we investigate the role of AURKB in regulating the function of TERF1 at the telomeres.

3.1.2 TERF1 knockout and stem cell maintenance

TERF1 is a vital regulator of telomere maintenance and cellular viability. In mouse cells, deletion of TERF1 results in increased DNA damage at the telomeres, rapid telomere shortening, sister chromatid fusion and a loss of telomere integrity (Beier et al., 2012, Martinez et al., 2009). Gene knockout of TERF1 leads to early embryonic lethality in mice (Karlseder et al., 2003, Iwano et al., 2004), while conditional deletion in adult tissue compartments leads to exhausted adult stem cell reserves and premature tissue degeneration (Beier et al., 2012, Martinez et al., 2009). The deletion of TERF1 in bone marrow progenitor cells and hematopoietic progenitor cell compartment resulted in increased DNA damage at the telomeres and induced rapid telomere shortening leading to severe aplasia and bone marrow failure (Beier et al., 2012). Similarly, the deletion of TERF1 in the stratified epithelia also caused severe telomere defects, including increased DNA damage, sister chromatid fusions, and MTS appearance, leading to tissue-specific dysfunction such as reduced skin development in newborn mice (Martinez et al., 2009). In addition to tissue-specific dysfunction, the deletion of TERF1 in the epidermis in mouse also caused the absence of epidermal stem cell compartments, indicating an essential role for

TERF1-mediated telomere maintenance to maintain cellular and tissue viability (Martinez et al., 2009).

A key phenotype associated with the loss of TERF1 function is aberrant telomere structure, as observed by the increase in MTS formation (Sfeir et al., 2009, Martinez et al., 2009, Munoz et al., 2009). This increase in MTS formation is predominantly caused by DNA replication fork stalling at the telomere, which is further exacerbated by treatment with aphidicolin, a DNA polymerase inhibitor (Glover et al., 1984, Sfeir et al., 2009). DNA helicases such as BLM and RTEL1 that associate with telomeres, play important role in suppressing replication fork stalling (Opresko et al., 2002). *Blm* or *Rtel1*-deficient mouse ES cells show increased MTS formation (Ding et al., 2004, Martinez et al., 2009). Furthermore, gene knockdown of either of these helicases, in addition to TERF1 depletion, resulted in a further increase in MTS formation (Sfeir et al., 2009). Importantly, BLM has also been found to directly interact with TERF1 *in vitro* (Lillard-Wetherell et al., 2004). Collectively, these findings indicate that TERF1, BLM and RTEL1 act in cooperation to maintain telomere integrity. Specifically, they work together to regulate replication fork progression at telomeres.

In addition to stem cell telomere maintenance, TERF1 also play a role in the maintenance of cellular pluripotency (Bejarano et al., 2017, Schneider et al., 2013). Compared to differentiated cell compartments, adult stem cell compartments such as the skin and small intestine have increased TERF1 expression (Schneider et al., 2013). The reprogramming of mouse embryonic fibroblasts (MEFs) to induced pluripotent stem cells resulted in increased TERF1 expression levels, further suggesting a role of TERF1 in maintaining pluripotency. The knockout of p53 and TERF1 in MEF cells prevented cellular

reprogramming. Interestingly, the pluripotency-associated factors such as Oct3/4 interact with TERF1 promoter (Schneider et al., 2013), suggesting that Oct3/4 may directly regulate TERF1 expression and that TERF1 is critical for reprogramming of the telomere to generate induced pluripotent stem cells. Altogether, these studies show the importance of TERF1 in maintaining the telomeres of various cells and cellular compartments. Although the molecular mechanism of TERF1 in regulating cellular development and telomere integrity is unknown, these studies show the differential regulation of TERF1 at the telomeres of various cell types. As TERF1 is a critical telomere specific protein, it is unsurprising that one of its functions is telomere length maintenance.

3.1.3 TERF1 regulates telomere length

The ability for stem cells to have long telomeres and unlimited potential for cellular division is due to telomerase. This reverse transcriptase enzyme functions to synthesise telomere DNA *de novo* and maintain telomere length (Szostak and Blackburn, 1982). Interestingly, the Shelterin components regulate the interaction between the telomere DNA and telomerase (Hockemeyer and Collins, 2015). Therefore, the regulation of telomere length by TERF1 is of importance to this study.

The long-term overexpression of TERF1 in telomerase-positive cells and human somatic cells resulted in telomere shortening (van Steensel and de Lange, 1997, Smogorzewska et al., 2000, Ancelin et al., 2002). In contrast, the loss of TERF1 binding to the telomeres facilitated by the expression of a dominant-negative TERF1 lacking the Myb-binding domain resulted in increased telomere length, within both telomerase-positive cells and human

somatic cells. (van Steensel and de Lange, 1997, Ancelin et al., 2002, Smogorzewska et al., 2000).

Interestingly, in induced pluripotent stem cells, high levels of TERF1 overexpression resulted in longer telomeres compared to low levels of TERF1 overexpression (Schneider et al., 2013). This change of telomere lengthening indicates that the upregulation of TERF1 is essential for the maintenance of telomere length. However, TERF1 overexpression or inhibition did not affect telomerase expression and activity (van Steensel and de Lange, 1997, van Steensel et al., 1998, Smogorzewska et al., 2000). This indicates that telomere length maintenance by TERF1 is independent of telomerase levels and function. Altogether, these findings indicate a differential function of TERF1 that may depend on cell type or organism. However, while this is the case, the molecular mechanism of how TERF1 regulates telomere length remains unknown.

3.1.4 Phosphorylation of TERF1

TERF1 is conserved between mouse and human (Martinez et al., 2009). Both analogues of TERF1 consist of an N-terminal TERFH domain which is essential for TERF1 homodimerization (Fairall et al., 2001, Bianchi et al., 1997) and a C-terminal Myb domain which is vital for TERF1 binding to telomere DNA (**Figure 3.1.1**) (Broccoli et al., 1997). The functions of TERF1 are regulated by post-translational modifications (PTMs), including ubiquitination, SUMOylation and phosphorylation (Walker and Zhu, 2012). The phosphorylation of TERF1 is facilitated by a range of kinases, including ATM kinase, Cyclin-dependent kinase 1 (CDK1) and Polo-like kinase 1 (PLK1). Some essential roles of TERF1 phosphorylation are the regulation of TERF1 binding, stability and localization (Walker and

Zhu, 2012). Examples of TERF1 phosphorylation and function are listed in **Table 3.1**. The phosphorylation of Threonine 371 on human TERF1 (T358 in mouse TERF1; which lies adjacent to the Myb-like binding domain) by Cyclin B-dependent kinase prevents binding of TERF1 to the telomeres, indicating that phosphorylation of Threonine 371 on TERF1 negatively regulates TERF1 binding to the telomeres to induce telomere lengthening (McKerlie and Zhu, 2011).

Several residues, including Threonine 122 and Threonine 149, located within the TERFH domain on human TERF1 (T109 and T136 in on mouse TERF1), are also phosphorylated (Kim et al., 2008, Lee et al., 2009). Casein kinase 2, a Serine/Threonine kinase that regulates cell cycle control, phosphorylates Threonine 122 to promote homodimerization, stability and binding of TERF1 to the telomeres (Kim et al., 2008). Conversely, Threonine 149 is a target of Cyclin B-dependent kinase 1 (Lee et al., 2009), and its phosphorylation promotes interaction of TERF1 with PIN1, a prolyl isomerase. Interestingly, PIN1 interacts with Threonine 149 motif in TERF1 through a phosphorylation-dependent manner during mitosis, and this interaction regulates TERF1 stability, telomere maintenance and ageing (Lee et al., 2009). The inhibition of PIN1 renders TERF1 resistant to degradation, leading to enhanced TERF1 binding to telomeres and gradual loss of telomere length in both human and mouse cells (Lee et al., 2009). These studies underline the importance of TERF1 phosphorylation and that the phosphorylation of specific TERF1 residue is responsible for a specific function.

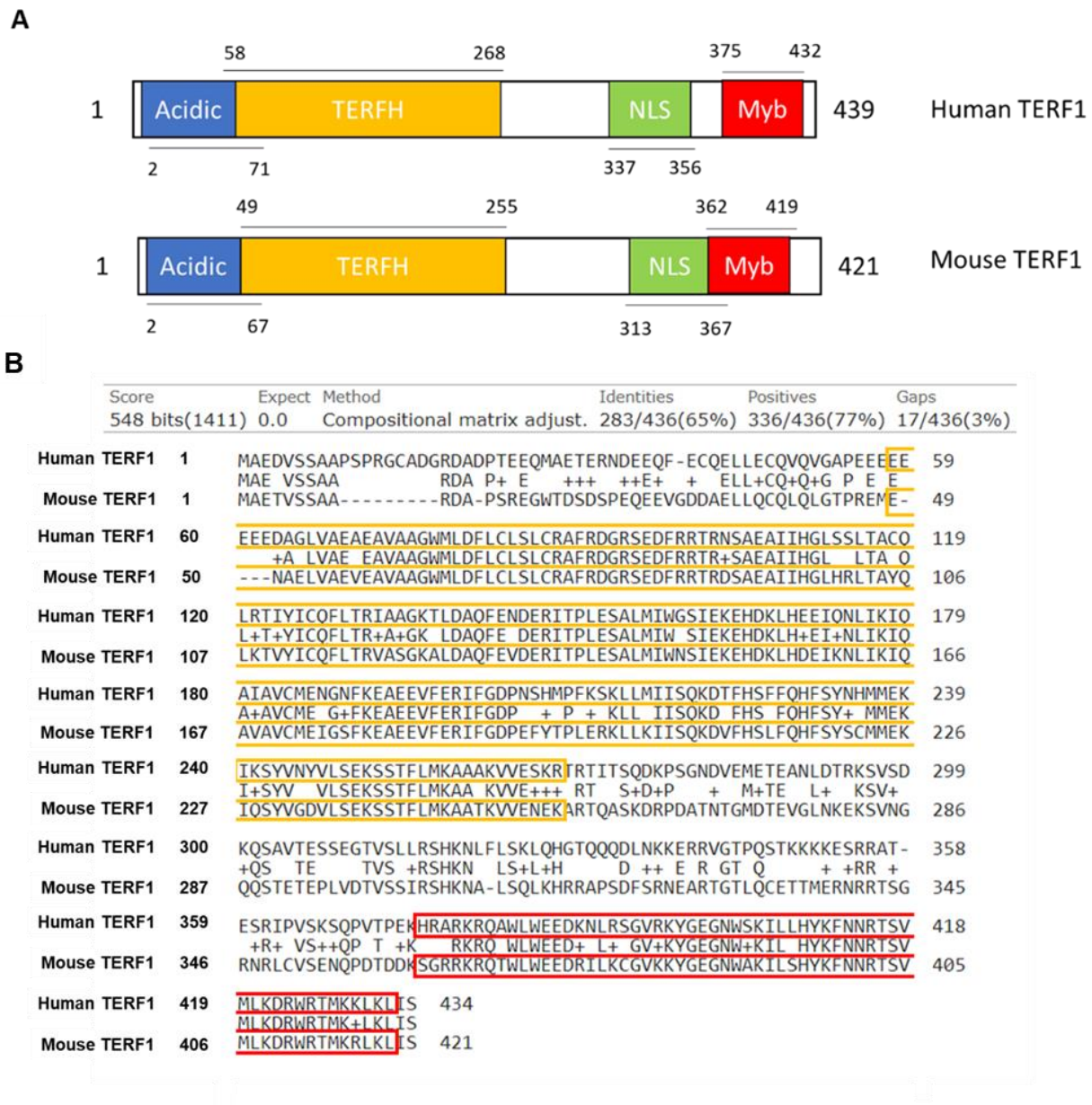

Figure 3.1.1: Overview of human and mouse TERF1 domains

*(**A**) Simplified representation of mouse TERF1 and human TERF1 and their specific domains. Mouse TERF1 is a 421 amino acid protein, smaller than the 439 amino acids human TERF1 protein. Both mouse and human TERF1 have similar structural domains such as the acidic domain (blue), TERF1 homodimerization domain (orange), Nuclear Localisation Signal (green) and a Myb-like DNA binding domain (red). The length of these domains is shown. (**B**) BLASTP (NCBI) was used to identify the similarities in amino acid sequence between human (P54274-1) and mouse (P70371-1) TERF1. Encapsulated in orange and red Is the TERFH domain and Myb domain, respectively.*

Table 3.1: Summary of kinases that regulate TERF1 function

Residue	Kinase	Cell type	Function of phosphorylated residues
T122	Casein Kinase II	Human	Promotes TERF1 stability and binding to telomere DNA (Kim et al., 2008)
T149	Cyclin-dependent kinases	Human	Promotes TERF1 and PIN1 interaction (Lee et al., 2009)
T273	Akt	Human	Negatively regulates telomere length (Chen et al., 2009)
S274	Ataxia-Telangiectasia Mutated	Human	Promotes TERF1 binding to telomere DNA (Wu et al., 2007)
S296	Aurora Kinase A	Human	Promotes and causes mitotic defects (Ohishi et al., 2010)
T344	Cyclin-dependent kinase 1	Human	Prepare TERF1 for phosphorylation by PLK1 (Wu et al., 2008)
S367	Ataxia-Telangiectasia Mutated	Human	Inhibit TERF1 binding to telomeres Mark for TERF1 degradation (McKerlie et al., 2012, Wu et al., 2007)
T371	Cyclin-dependent kinase 1	Human	Prevents TERF1 binding to telomeres (McKerlie and Zhu, 2011)
S435	Polo-Like Kinase 1	Human	Promotes TERF1 binding to telomere DNA (Wu et al., 2008)

3.1.5 Aurora Kinase B

The family of Aurora protein kinase is made of Aurora Kinase A, Aurora Kinase B and Aurora Kinase C. The Aurora Kinase C is only found in mammals due to evolutionary pressure(Seeling et al., 2017), which plays a similar role as AURKB as a chromosome-passenger complex (CPC) protein (Seeling et al., 2017). This family of Serine/Threonine kinase has a conserved kinase domain (Bolanos-Garcia, 2005) where the phosphorylation of Threonine 288 (Aurora kinase A), Threonine 232 (Aurora kinase B) and Threonine 195 (Aurora kinase C), induces a conformation change activating kinase activity (Bayliss et al., 2017, Dodson et al., 2010, Giet and Prigent, 1999, Tang et al., 2017). These kinases mainly localise to the centromere to regulate proper mitotic progression (Li et al., 2015, Liu and Ruderman, 2006, Scrittori et al., 2005). However, little is known about Aurora kinase C. Nonetheless, Aurora kinase A and B are required for the establishment of the bipolar spindle, chromosome alignment and kinetochores anchoring, chromosome separation and cytokinesis (Adams et al., 2001, Adams et al., 2000, Andrews et al., 2004, Bishop and Schumacher, 2002, Carmena et al., 2009, Liu and Ruderman, 2006, Tanaka et al., 2002, Wang et al., 2010). Interestingly, the overexpression of Aurora kinase A and B causes aneuploidy, chromosome instability, chromosome misalignment as well as uncontrolled proliferation and survival (Cahill et al., 1999, Zhou et al., 1998, Dauch et al., 2016). (Li et al., 2015, Liu and Ruderman, 2006, Willems et al., 2018, Carmena et al., 2009, Hochegger et al., 2013, Hegarat et al., 2011, Marumoto et al., 2003, Cahill et al., 1999, Zhou et al., 1998)As such aurora kinases are prime target for its therapeutic effects in the treatment of cancer (Umene et al., 2013, Du et al., 2021).

Of importance to this chapter is AURKB. AURKB is a serine/threonine kinase known for its role in controlling chromosome segregation during mitosis (Hochegger et al., 2013). Through

its highly regulated spatio-temporal association and phosphorylation of an array of interacting proteins at the centromere/kinetochore (CENP-A, inner centromere protein and MCAK), AURKB controls mitotic spindle assembly/checkpoint, chromosome alignment and cytokinesis (Hochegger et al., 2013). The loss of AURKB (through RNAi knockdown, expression of AURKB kinase-dead mutants and AURKB inhibitors (Hesperadin and ZM447439)) resulted in defective mitotic progression and chromosome missegregation, leading to genetic instability (Gimenez-Abian et al., 2004, Buvelot et al., 2003, Ditchfield et al., 2003, Andrews et al., 2004, Gadea and Ruderman, 2005, Hauf et al., 2003, Ruchaud et al., 2007). Recent studies have also linked AURKB to proteins unrelated to chromosome segregation, including factors regulating cellular pluripotency, suggesting that AURKB plays other critical cellular functions apart from its functions for cell cycle progression (Mallm and Rippe, 2015, Lee et al., 2012).

A previous study has shown that Aurora Kinase A (AURKA), another member of the Aurora Kinase family, binds and phosphorylates human TERF1 at Serine 296 *in vitro* (Ohishi et al., 2010). Overexpression of AURKA resulted in mitotic defects, including cytokinetic failure and prolonged mitosis. However, TERF1 depletion prevented cytokinetic failure and prolonged mitosis following AURKA overexpression. Interestingly, the phosphorylation of S296-TERF1 by AURKA induces mitotic defects such as multinucleation. These mitotic defects were prevented following the expression of a S296-phospho-null-TERF1 mutant (S296A-TERF1(Serine to Alanine)) (Ohishi et al., 2010). Overall, this indicates that the phosphorylation of TERF1 causes mitotic defects in human cells overexpressing AURKA.

3.1.6 Aims

Unpublished data from the lab has shown that AURKB localises to the telomeres of ES cells and that the loss of AURKB led to MTS formation, a similar phenotype of TERF1 knockdown. As Aurora kinase A is known to phosphorylate TERF1, we hypothesized that AURKB may phosphorylate TERF1 in ES cells. Considering that Aurora kinase A and B have overlapping functions, the function of AURKB, it is possible that AURKB plays a role in phosphorylating TERF1. This chapter explores the localisation and function of AURKB at the telomeres of ES cells. In addition, this chapter also explores the binding and activity of AURKB on S404-TERF1, and if phosphorylation of S404 affects TERF1 function in regulating telomere maintenance. Finally, this chapter investigates the long-term effects of the phospho-null and phospho-mimic S404-TERF1 on telomere lengthening.

3.2 Results

3.2.1 AURKB localises to the telomeres of interphase and mitotic mouse ES cells

To investigate the localisation of AURKB in mouse ES cells, a range of immunofluorescence staining was performed. The results showed that AURKB localised to the telomeres of both interphase and mitotic ES cells (**Figure 3.2.1A**). In agreement with previous studies (Adams et al., 2000, Andrews et al., 2004), AURKB also localised to the centromeric regions of mitotic ES cells with a similar staining pattern as somatic cells (**Figure 3.2.1A**). To rule out antibody cross-reactivity as a reason for the localisation of AURKB at the telomeres, GFP-tagged AURKB (GFP-AURKB) was expressed in ES cells. The localisation of GFP-AURKB at the telomeres was assessed by immunofluorescence analyses using a GFP antibody and either TERF1 antibody or H3.3S31ph antibody (as a marker used as another telomere marker (Wong et al., 2009)) for the telomeric regions in ES cells. Immunofluorescence analyses using antibody against H3.3S31ph and GFP showed that GFP-AURKB colocalised with H3.3S31ph at both the telomeres and pericentric regions of mitotic cells (**Figure 3.2.1B**).

Next, to study if the cell cycle dynamics of AURKB localisation at the telomere, mouse ES cells were synchronised to the G1/S phase with thymidine treatment. A previous report from our lab showed that ES cells released form G1/S block progressed through S phase after 4 to 6 hours, entered M phase after 8 to 10 hours and re-entered G1 phase after 10 to 12 hours (Wong et al., 2009). Thus, cells were released from G1/S phase and harvested as they progressed through the cell cycle at 0, 2-, 4-, 6-, and 8-hours post thymidine release before immunofluorescence analyses. Foci containing AURKB/TERF1 colocalisation peaked at 4-6 hours post thymidine release (at S phase), with 60-76% of cells showing six

or more colocalising foci (**Figure 3.2.1C**). Together, these results show that AURKB localises to the telomeres during the S phase and remains bound to telomeres during mitosis in mouse ES cells.

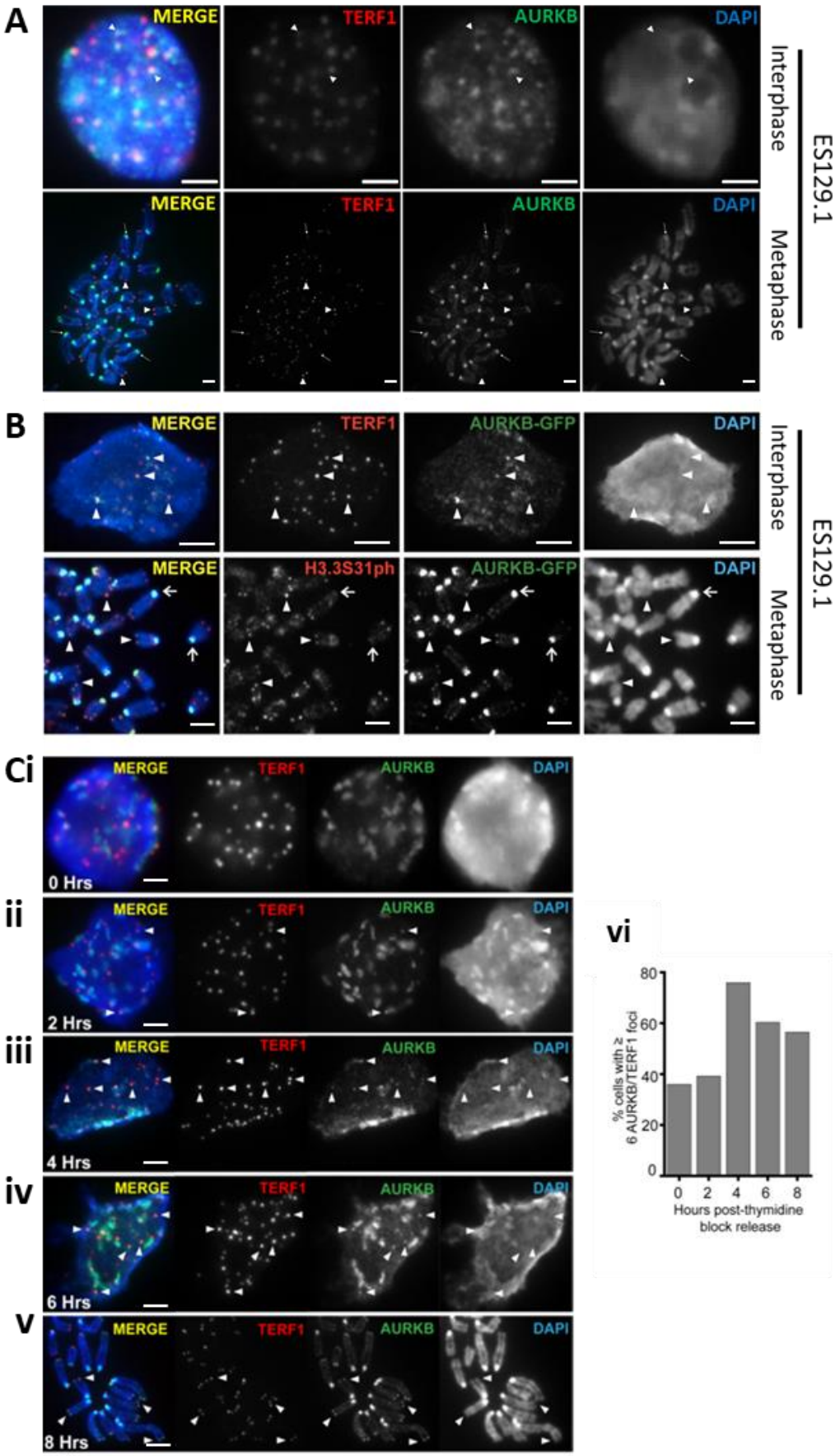
A
MERGE
TERF1
AURKB
DAPI
Interphase
Metaphase
ES129.1
B
MERGE
TERF1
AURKB-GFP
DAPI
Interphase
MERGE
H3.3S31ph
AURKB-GFP
DAPI
Metaphase
ES129.1
Ci
MERGE
TERF1
AURKB
DAPI
0 Hrs
ii
2 Hrs
iii
4 Hrs
iv
6 Hrs
v
8 Hrs
vi
% cells with ≥ 6 AURKB/TERF1 foci
0
20
40
60
80
0 2 4 6 8
Hours post-thymidine block release

Figure 3.2.1: AURKB localises to the telomeres of mouse ES cells during late S phase and mitosis

*(**A**) Immunofluorescence analyses were performed with antibodies against TERF1 (red) and AURKB (green) to determine the distribution of AURKB in mouse ES cells. AURKB colocalised with TERF1 at the telomeres of interphase (**i**) and mitotic cells (**ii**, arrowheads). (**B**) Plasmid containing GFP-AURKB was transfected into mouse ES cells before immunofluorescence analyses with antibodies against TERF1 (red) or H3.3S31ph (red) and GFP (green) were performed to determine the distribution of GFP-AURKB. AURKB colocalised with TERF1 and H3.3S31ph at the telomeres of interphase and mitotic cells (arrowheads), respectively. TERF1 and H3.3S31ph were used as telomere markers. The arrows show the enrichment of AURKB at the centromeres. (**C**) Mouse ES cells were blocked at the G1/S phase with thymidine treatment. Cells were harvested at (**i**) 0 h, (**ii**) 2 h, (**iii**) 4 h, (**iv**) 6 h and (**v**) 8 h post thymidine release. Immunofluorescence analyses with antibody against TERF1 (red) and AURKB (green) were performed to determine the stage of the cell cycle that AURKB localised to the telomeres. Arrowheads show the colocalisation of AURKB and TERF1 at the telomeres. A minimum of 50 cells per time point was analysed and graphed (**vi**). Cells released from thymidine block at 0, 2, 4, 6 and 8 h showed that 36%, 40%, 76%, 60% and 56% of cells, respectively, had 6 or more AURKB/TERF1 colocalisation foci. DAPI was used as a nuclear counterstain (blue). Scale bar represents 4 µm.*

To determine if AURKB localised to the telomeres of non-pluripotent mouse cell types, immunofluorescence analyses of AURKB in somatic mouse NIH3T3 cells were performed (**Figure 3.2.2A**). As reported by other studies (Andrews et al., 2004, Buvelot et al., 2003, Ditchfield et al., 2003), AURKB localised only to the centromere regions of interphase and mitotic cells. This indicated that AURKB may have a specialised function in regulating the telomere function of pluripotent ES cells (Adams et al., 2000, Andrews et al., 2004).

Telomere chromatin undergoes extensive remodelling during cellular differentiation (Wong et al., 2009, Schneider et al., 2013). Thus, to determine if ES cell differentiation causes a loss of AURKB at the telomeres, differentiation was induced by withdrawing Leukaemia inhibitory factor (LIF) and treating ES cells with retinoic acid (RA) (Strickland and Mahdavi, 1978, Wong et al., 2009). To confirm that differentiation was induced by RA treatment, qRT-PCR using primers specific to pluripotency related genes NANOG (Loh et al., 2006) and TBX3 (Lu et al., 2011) was performed. The results showed a loss of NANOG and TBX3 mRNA expression levels after 2, 4, 6, and 8 days after RA treatment, confirming the induction of differentiation (**Figure 3.2.2Dii**).

Immunofluorescence analyses showed that AURKB levels were depleted at the telomeres in ES cells undergoing differentiation (**Figure 3.2.2B**). As expected, the localisation of AURKB at the pericentric region remained unchanged during the differentiation process (**Figure 3.2.2B**). To identify if AURKB at the telomeres were lost after differentiation, cells showing AURKB/TERF1 colocalisation were quantified 0, 2, 4, 6 and 8 days of post differentiation. Before differentiation, 93% of ES cells showed clear colocalisation of AURKB and TERF1 at the telomeres. However, after eight days of differentiation, only 26% of AURKB and TERF1 colocalised at the telomeres (**Figure 3.2.2C**).

It is possible that the expression levels of AURKB may have been altered, rather than the localisation of AURKB to the telomeres. Thus, qRT-PCR was performed to determine the mRNA expression levels of AURKB and TERF1. The results showed no significant change in the mRNA expression levels of AURKB or TERF1 at different time points after differentiation (**Figure 3.2.2Di**). This result indicates that the expression level of either AURKB or TERF1 is unrelated to AURKB binding at the telomeres during differentiation.

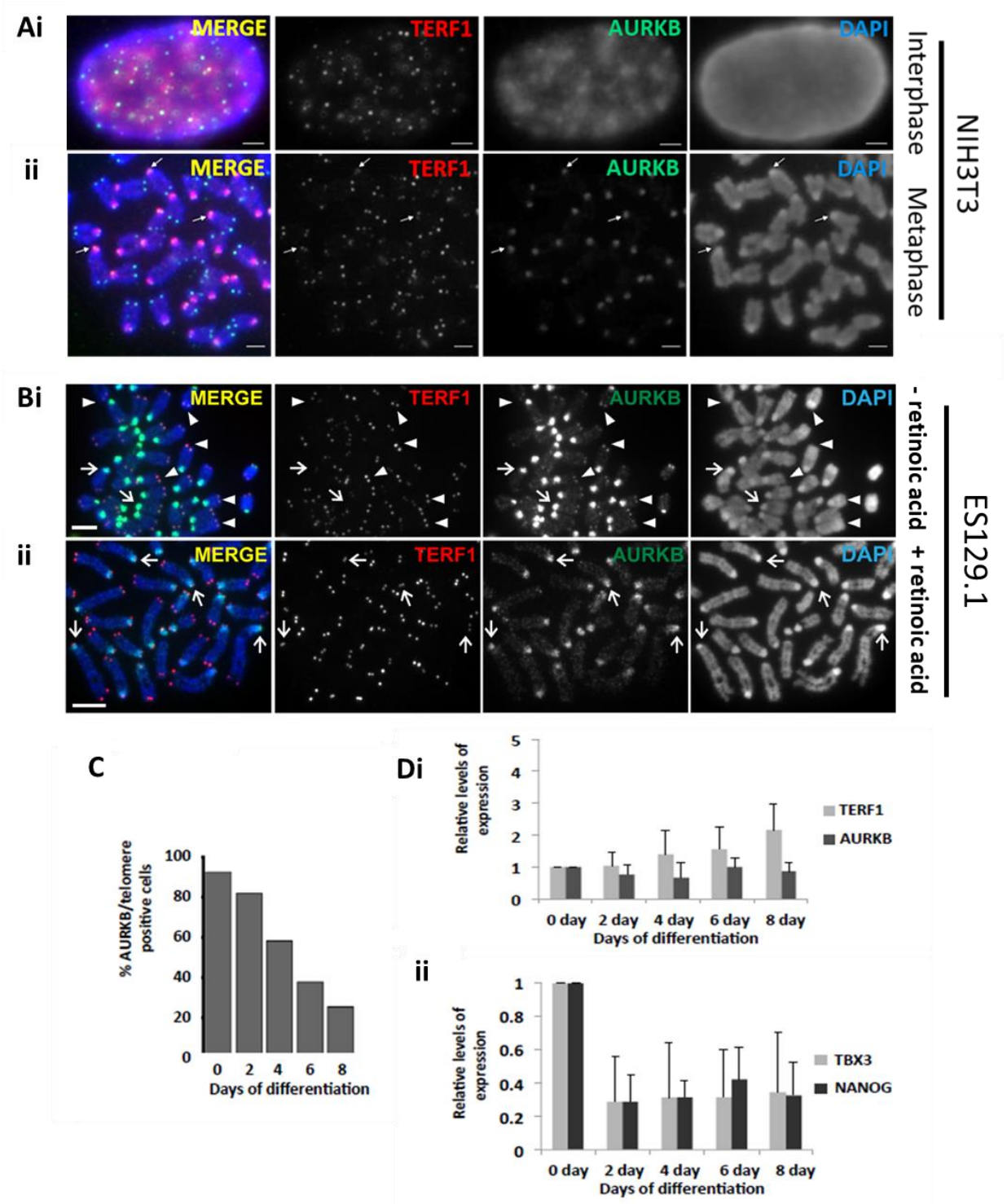
Ai
MERGE
TERF1
AURKB
DAPI
ii
MERGE
TERF1
AURKB
DAPI
Interphase
Metaphase
NIH3T3
Bi
MERGE
TERF1
AURKB
DAPI
ii
MERGE
TERF1
AURKB
DAPI
- retinoic acid
+ retinoic acid
ES129.1
C
% AURKB/telomere positive cells
100
80
60
40
20
0
0 2 4 6 8
Days of differentiation
Di
Relative levels of expression
5
4
3
2
1
0
TERF1
AURKB
0 day 2 day 4 day 6 day 8 day
Days of differentiation
ii
Relative levels of expression
1
0.8
0.6
0.4
0.2
0
TBX3
NANOG
0 day 2 day 4 day 6 day 8 day
Days of differentiation

Figure 3.2.2: AURKB does not localise to the telomeres of differentiated cells

*(**A**) Immunofluorescence analyses were performed in mouse NIH3T3 cells using antibodies against AURKB (green) and TERF1 (red) to determine the distribution of AURKB. TERF1 was used as a telomere marker. AURKB did not colocalise with TERF1 at the telomeres of interphase (**i**) and metaphase cell (**ii**). However, AURKB was present at the centromeres (arrows). (**B**) Leukaemia inhibitory factor (LIF) was withdrawn from ES cells and treated with Retinoic Acid (RA) to induce cellular differentiation. Immunofluorescence analyses were performed with antibodies against AURKB and TERF1 to determine the distribution of AURKB. TERF1 was used as a telomere marker. (**i**) AURKB (green) colocalised with TERF1 (red) at the telomeres (arrowheads) of untreated cells. (**ii**) In RA treated cells, AURKB was not enriched at the telomeres. Instead, AURKB was enriched at the centromere (arrows). DAPI was used as a nuclear counterstain (blue). (**C**) The percentage (%) of AURKB/TERF1 colocalisation in ES cells after 0, 2, 4, 6, and 8 days post cellular differentiation were quantified. In undifferentiated cells, 93% of metaphase spreads showed AURKB colocalisation with TERF1 signals, and this declined to 82%, 58%, 37% and 26% after 2, 4, 6 and 8 days of LIF withdrawal/RA treatment, respectively. A minimum of 50 metaphase spreads were analysed per time point. (**D**) RNA was extracted from pluripotent and differentiated ES cells, and cDNA was generated. qPCR analyses determined the levels of TERF1, AURKB, TBX3 and NANOG expression. Results are relative to GAPDH expression levels. Following differentiation, expression levels of (**i**) TERF1 and AURKB showed no significant change while the expression of pluripotent markers (**ii**) TBX3 and NANOG decreased. Scale bar represents 4 µm. N=4, Error bars represent S.D..*

Mouse ES cells have long telomeres and high levels of telomerase activity (Varela et al., 2011). Thus, to study if AURKB localisation to the telomere in ES cells is associated with long telomeres and/or telomerase activity, AURKB localisation at the telomeres of cells with long telomeres and high telomerase activity such as telomerase overexpressing HT1080 cells (Pickett et al., 2009) or cells with long telomeres with no telomerase activity such as ALT-cancer cells, which maintain their long telomeres through homologous recombination, was investigated. Consistent with the lack of AURKB at the telomeres of differentiated mouse ES cells, AURKB was also not observed at the telomeres of human somatic HT1080 cells (**Figure 3.2.3A**), telomerase overexpressing HT1080 cells (**Figure 3.2.3B**) and ALT positive SKLU1 cancer cells (**Figure 3.2.3C**). However, the localisation of AURKB at centromeres was prominent in all these cells (**Figure 3.2.3**). This result suggests that the localisation of AURKB at the telomeres is independent of telomere length and telomerase status.

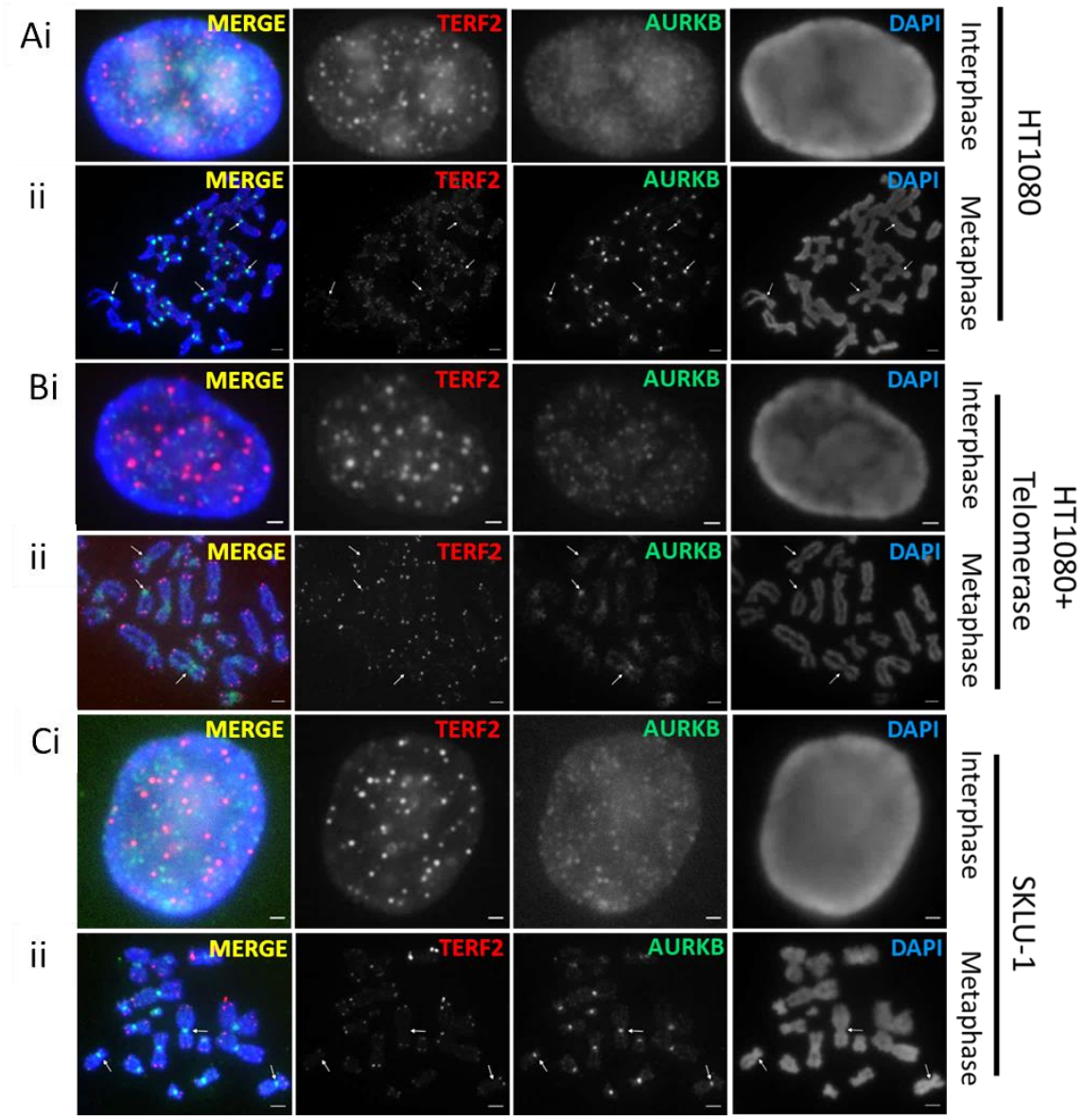

Figure 3.2.3: AURKB does not localise to the telomeres of differentiated cells with long telomeres

*Immunofluorescence analyses were performed on somatic **(A)** human HT1080, **(B)** telomerase overexpressing HT1080 and **(C)** telomerase negative SKLU1 ALT cancer cells with antibodies against TERF2 (red) and AURKB (green). TERF2 was used as a telomere marker. In the respective **(i)** interphase and **(ii)** metaphase cells, AURKB did not localise to the telomeres. However, AURKB was present at the centromeres (arrows). DAPI was used as a nuclear counterstain (blue). Scale bar represents 4 µm.*

3.2.2 AURKB inhibition and knockdown leads to a loss of telomere structural integrity

AURKB is a master regulator of mitosis and plays a vital role in regulating chromosome segregation (Hochegger et al., 2013). The deletion of AURKB in MEF cells and embryos led to an accumulation of prometaphase/metaphase cells, eventually leading to apoptosis (Fernandez-Miranda et al., 2011). However, inhibition of AURKB with a low level of ZM447439, an AURKB inhibitor, avoids deleterious cell-cycle changes in mouse ES cells (Mallm and Rippe, 2015, Umene et al., 2013). Thus, to examine the role of AURKB in regulating telomere function, the impact of a low-level AURKB inhibition by ZM447439 treatment on mouse ES cells was explored.

A well-known protein that AURKB phosphorylates is Histone H3 at Serine 10 (Adams et al., 2001). This mitosis specific marker occurs during prophase and persists to anaphase, where it localises to the outermost peripheral regions of the chromosome (Hake et al., 2005). To identify the optimal concentration and duration of ZM447439 treatment in ES cells, ES cells were treated with 1 µM ZM447439 treatment for 24 hours. Immunofluorescence analyses were performed to examine the loss of H3 Serine 10 phosphorylation (H3S10ph) after AURKB inhibition in mouse ES cells. With 1 µM ZM447439 treatment for 24 hours, the results showed that H3S10ph levels were diminished (**Figure 3.2.4A**), identifying effective inhibition of AURKB activity. However, despite AURKB inhibition, the localisation of AURKB at the pericentric region and the telomeres was unaffected (**Figure 3.2.4A**).

With the identification of 1 µM ZM447439 treatment for 24 hours is effective at inhibition AURKB activity, the changes in telomere structural integrity, a phenotype of aberrant telomere structure, after AURKB inhibition was investigated. Telomere Fluorescent *In-Situ* Hybridization (Tel-FISH) analyses were performed, and MTS formation quantified in mouse

ES cells. In normal cells, a single signal per sister chromatid end is seen with Tel-FISH. However, in cells with aberrant telomere structure multiple signals per sister chromatid end is observed with Tel-FISH (examples shown in **Figure 3.2.4B**). Untreated cells were used as a negative control while cells treated with 0.2 µM aphidicolin (APH), which has been previously reported to induce MTS formation, were used as a positive control (Sfeir et al., 2009, Glover et al., 1984). The results showed that with the inhibition of AURKB, metaphase chromosomes exhibited a significant increase in MTS formation compared to untreated metaphase chromosomes (2.3 MTS/metaphase spread to 8.5 MTS/metaphase spread). This increase was similar to APH treated cells (7.3 MTS/metaphase spread) (**Figure 3.2.4C**). To determine if the formation of MTS observed after AURKB inhibition was specific to mouse ES cells, AURKB was inhibited in the primary non-ES cells MEF, and MTS incidence was quantified. MEF was selected as other immortalised mouse laboratory cell lines had a relatively high background level of MTS (unpublished data). There was no significant change in MTS formation between untreated and AURKB-inhibited MEF cells (**Figure 3.2.4D**). Together, these results show that the role of AURKB in telomere maintenance is unique to pluripotent mouse ES cells.

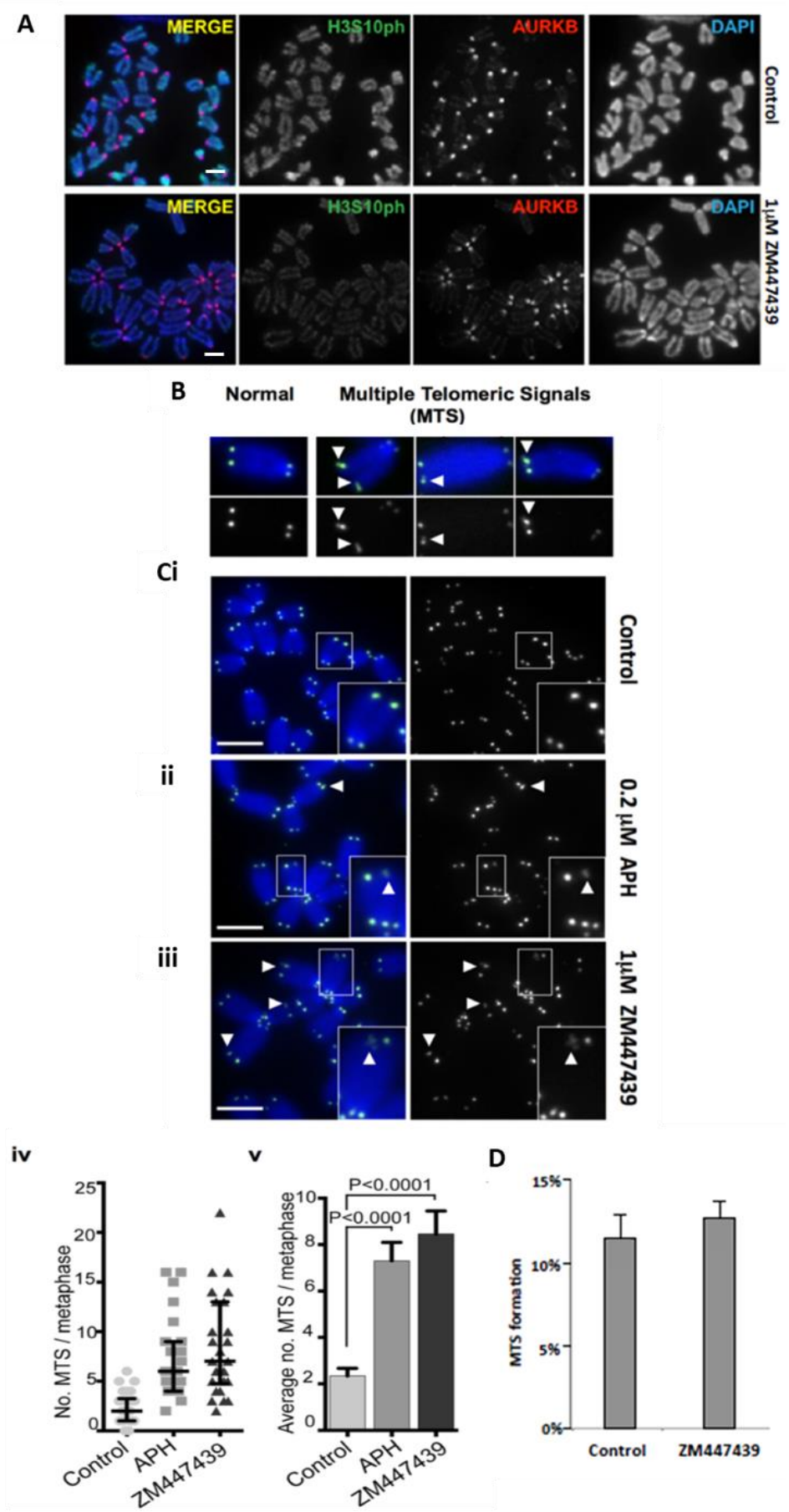
A
MERGE
H3S10ph
AURKB
DAPI
Control
1μM ZM447439
B
Normal
Multiple Telomeric Signals (MTS)
Ci
ii
iii
Control
0.2 μM APH
1μM ZM447439
iv
No. MTS / metaphase
Control
APH
ZM447439
v
Average no. MTS / metaphase
P<0.0001
P<0.0001
D
MTS formation
Control
ZM447439

Figure 3.2.4: Loss of AURKB function results in increased MTS incidence in mouse ES cells

(A) *Mouse ES cells were treated with 1 µM ZM447439 for 24 hours, and immunofluorescence analyses were performed with antibodies against AURKB (red) or H3S10ph (green). (**i**) In control cells**,** H3S10ph was enriched throughout mitotic chromosomes. (**ii**) In cells treated with 1 µM ZM447439, H3S10ph was diminished throughout the mitotic chromosome. In both untreated and treated cells, AUKB localised to the centromere and telomeres of mitotic chromosomes.* ***(B)*** *Examples of standard telomere signal and MTS formation (APH treated, arrowheads) after Tel-FISH analyses are shown.* ***(C)*** *Mouse ES cells were treated with either* ***(ii)*** *0.2 µM APH or* ***(iii)*** *1 µM ZM447439 for 24 h, followed by Tel-FISH analyses. Control untreated cells are shown in* ***(i)****. Tel-FISH signals are shown in green. DAPI was used as a nuclear counterstain.* ***(iv/v)*** *Quantification of MTS identified that untreated cells had an average of 2.3 of MTS/metaphase spread, APH treated cells had 7.3 MTS/metaphase spread ($P < 0.0001$ compared to untreated cells), and ZM447439 treated cells had 8.5 MTS/metaphase spread ($P < 0.0001$ compared to untreated cells). A magnified image of the boxed chromosome is shown in the inset, with MTS indicated by the arrowheads. n = 1000 chromosomes from three biological replicates.* ***(D)*** *MEFs were treated with 1 µM ZM447439 for 12 hrs before Tel-FISH analyses as prolonged treatment resulted in loss of mitotic cells and apoptosis. Quantification of Tel-FISH analyses did not show a significant difference in MTS incidence between control and ZM447439 treated MEF cells. n = 1400 chromosomes from three biological replicates. Each point in the scatterplot* ***(Civ)*** *represents the number of MTS in a single metaphase spread, with error bars showing Q1, Q2 and Q3 values. P-values are indicated in column graphs* ***(Cv)****. Error bars represent S.D****..***

Previous work has reported that MTS formation is closely associated with both APH treatment and the depletion of TERF1 (Sfeir et al., 2009). Thus, the induction of MTS formation is a result of a loss of telomere structural integrity. As MTS is associated with the loss of shelterin component and the loss of AURKB, the association between AURKB and TERF1 was investigated. siRNA against these AURKB and TERF1 were generated. siRNA against TERF2 was also generated and used as a control as it is another member of the Shelterin complex that binds to telomere DNA (Opresko et al., 2002). The knockdown of TERF1 was confirmed by immunofluorescence analyses and qRT-PCR (**Figure 3.2.5A and B**), while the knockdown of AURKB was confirmed by immunofluorescence analyses, qRT-PCR and immunoblotting (**Figure 3.2.5Aii, B, C**)**.** Immunoblotting of TERF1 and TERF2 could not be performed due to poor antibody efficiency. The knockdown of TERF2 did not affect the localisation of AURKB and TERF1 to the telomeres, indicating that TERF2 is not required for either TERF1 or AURKB localisation to the telomeres (**Figure 3.2.5Aiii**). In contrast, the knockdown of TERF1 resulted in a loss of AURKB at the telomeres (**Figure 3.2.5Aii**)**,** while AURKB knockdown did not result in a loss of TERF1 to the telomeres (**Figure 3.2.5Aiv**). These findings suggest that AURKB localisation at the telomeres of mouse ES cells is dependent on the presence of TERF1.

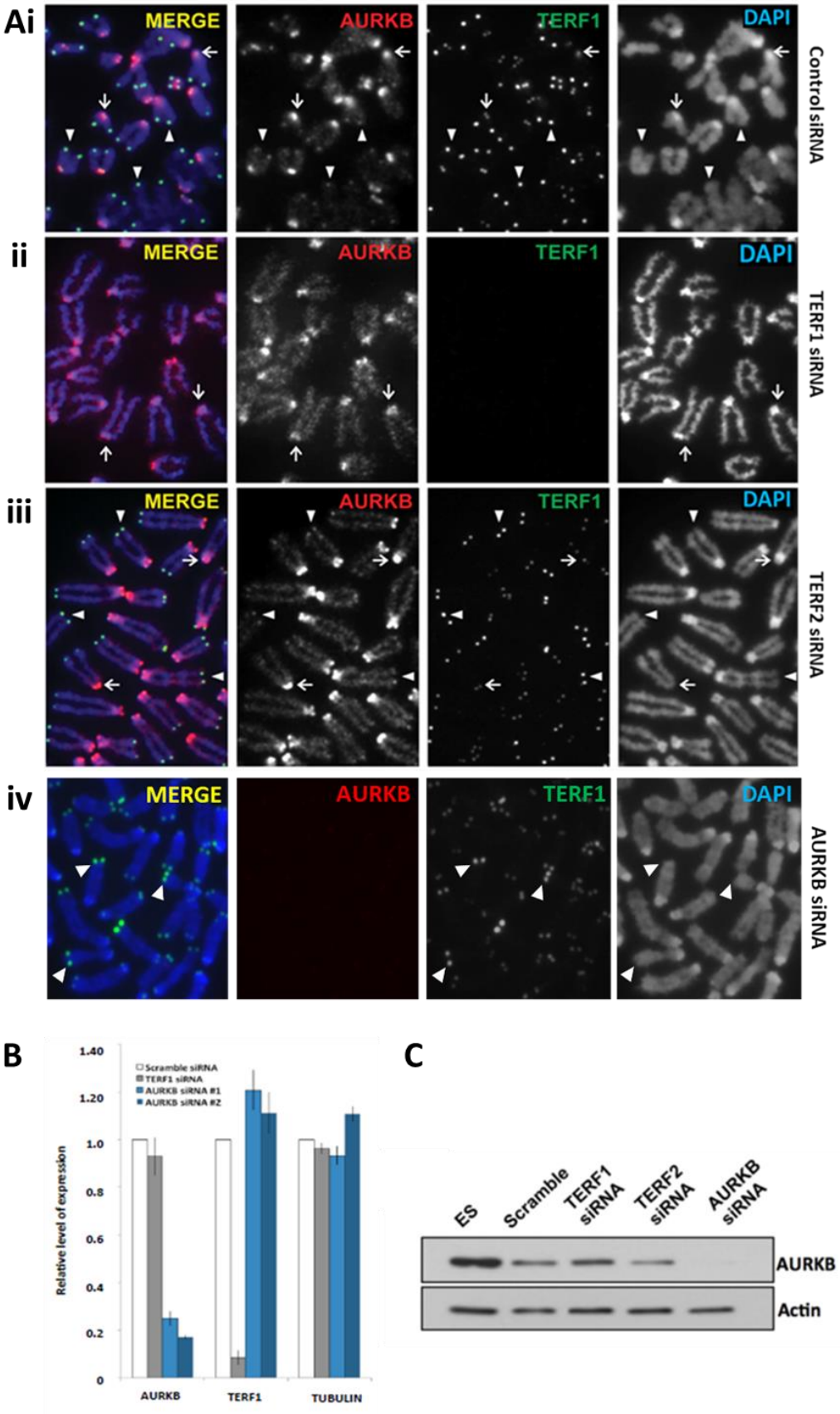
Ai
MERGE
AURKB
TERF1
DAPI
Control siRNA
ii
MERGE
AURKB
TERF1
DAPI
TERF1 siRNA
iii
MERGE
AURKB
TERF1
DAPI
TERF2 siRNA
iv
MERGE
AURKB
TERF1
DAPI
AURKB siRNA
B
Scramble siRNA
TERF1 siRNA
AURKB siRNA #1
AURKB siRNA #2
Relative level of expression
1.40
1.20
1.0
0.8
0.6
0.4
0.2
0
AURKB
TERF1
TUBULIN
C
ES
Scramble
TERF1 siRNA
TERF2 siRNA
AURKB siRNA
AURKB
Actin

Figure 3.2.5: AURKB localisation at the telomeres of mouse ES cells is dependent on the presence of TERF1

(A) *Mouse ES cells were transfected with either control scramble siRNA or siRNAs specific to TERF1, TERF2 or AURKB for 72h before immunofluorescence analyses with antibody against AURKB (red) and TERF1 (green) was performed.* ***(i)*** *In scramble siRNA transfected cells, TERF1 colocalised with AURKB at the telomeres (arrowhead).* ***(ii)*** *With TERF1 knockdown, TERF1 and AURKB at the telomeres were undetectable.* ***(iii)*** *With TERF2 knockdown, AURKB colocalised with TERF1 at the telomeres (arrowhead). AURKB was enriched at the centromere (i, ii, iii; arrow).* ***(iv)*** *With AURKB siRNA transfection, TERF1 was enriched at the telomeres (arrowhead) while AURKB at the telomeres and centromere was lost. DAPI was used as a nuclear counterstain (blue). Scale bar represents 4μm.* ***(B)*** *Mouse ES cells were transfected with either control scramble siRNA or siRNA specific to TERF1 or AURKB for 72h before RNA extraction. qRT-PCR was performed, and the expression level of AURKB, TERF1 and tubulin were determined. Tubulin was used as a negative control. AURKB, TERF1 and tubulin transcript levels were normalised against actin.* ***(C)*** *Mouse ES cells were transfected with either control scramble siRNA oligonucleotides or siRNA oligonucleotides specific to TERF1, TERF2 or AURKB for 24h and harvested for immunoblotting with antibody against AURKB. AURKB levels were depleted in AURKB siRNA transfected cells but not scramble, TERF1 and TERF2 siRNA transfected cells. Actin was used as a loading control.*

To examine if the loss of AURKB caused MTS formation, Tel-FISH analyses were performed on ES cells following RNAi depletion of AURKB or TERF1 (**Figure 3.2.6**). The depletion of TERF1 led to the formation of high levels of MTS compared to the scramble siRNA transfected control (**Figure 3.2.6**). Furthermore, the depletion of AURKB with two independent sets on siRNA (set #1 (**A**) and set #2 (**B**)) showed increased MTS formation (**Figure 3.2.6**).

MTS has previously been reported in cells with aberrant TERF1 dynamics (Sfeir et al., 2009). Thus, to investigate if AURKB associated with TERF1, AURKB was depleted and the changes in TERF1 levels at the telomeres was assessed by immunofluorescence analyses followed by the quantification of TERF1 staining fluorescence intensity at the telomeres of mitotic chromosomes. The result showed that the knockdown of AURKB significantly increased TERF1 fluorescence intensity at the telomeres of AURKB deleted mouse ES cells, indicating that TERF1 binding at the telomeres was increased (66.7% increase compared to control; **Figure 3.2.6C**). Furthermore, ChIP/qPCR analyses of TERF1 levels at the telomeres after AURKB inhibition in ES cells also showed an increase of TERF1 compared to untreated cells (**Figure 3.2.7Di**). However, AURKB inhibition did not affect TERF2 levels and H3 occupancy at the telomeres (**Figure 3.2.6Dii, iii**). These results demonstrate that the inhibition and knockdown of AURKB result in both MTS formation and increased TERF1 binding to the telomeres, identifying a role of AURKB in regulating TERF1 levels at the telomeres of ES cells.

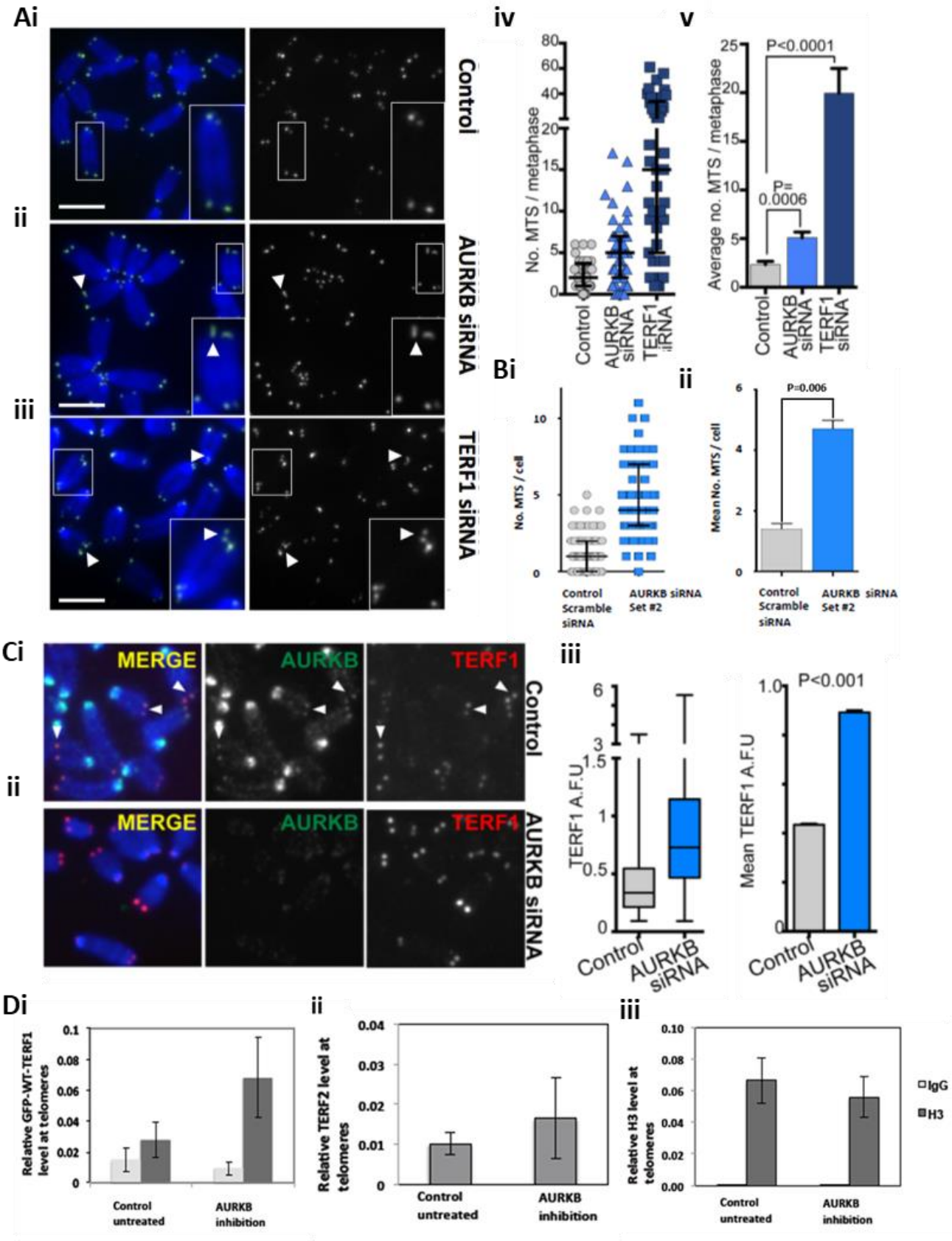
Ai
Control
ii
AURKB siRNA
iii
TERF1 siRNA
iv
No. MTS / metaphase
Control
AURKB siRNA
TERF1 siRNA
v
Average no. MTS / metaphase
P<0.0001
P= 0.0006
Bi
No. MTS / cell
Control Scramble siRNA
AURKB siRNA Set #2
ii
Mean No. MTS / cell
P=0.006
Ci
MERGE
AURKB
TERF1
Control
ii
AURKB siRNA
iii
TERF1 A.F.U
P<0.001
Mean TERF1 A.F.U
Di
Relative GFP-WT-TERF1 level at telomeres
Control untreated
AURKB inhibition
ii
Relative TERF2 level at telomeres
iii
Relative H3 level at telomeres
IgG
H3

Figure 3.2.6: Loss of AURKB results in increased MTS formation and TERF1 at the telomeres

(A) *Mouse ES cells were transfected with scramble control siRNA, AURKB siRNA or TERF1 siRNA for 72 hours, treated with colcemid, and harvested for Tel-FISH analyses. Representative Tel-FISH image of* ***(i)*** *scramble control siRNA,* ***(ii)*** *AURKB siRNA (set #1) or* ***(iii)*** *TERF1 siRNA transfected cells is shown. Tel-FISH signals are shown in green. Magnified images of the boxed chromosomes are shown in the inset, with examples of MTS indicated by the arrowheads. DAPI was used as a nuclear counterstain (blue). Scale bars represent 4 µm. (****iv/v****) Cells transfected with scramble siRNA had an average of 2.3 MTS/metaphase spread. AURKB and TERF1 knockdown cells had an average of 5.1 MTS/metaphase spread (P =0.0006) and 19.95 MTS/metaphase spread (P < 0.0001) respectively. n = 1200 chromosomes from three biological replicates.* ***(B)*** *Mouse ES cells were transfected with scramble control siRNA or AURKB siRNA (set #2) for 72 h and treated with colcemid before Tel-FISH analyses.* ***(i/ii)*** *AURKB depletion resulted in aberrant MTS formation, increasing from an average of 1 MTS/metaphase spread in cells transfected with scramble siRNA to 4 MTS/metaphase spread. P = 0.0006, n = 1200 chromosomes from 3 biological replicates. Each point in the scatterplot* ***(Aiv*** *and* ***Bi)*** *represents the number of MTS in a single metaphase spread, with error bars showing Q1, Q2 and Q3 values. Error bars represent S.D..* ***(C)*** *Mouse ES cells were transfected with either (****i****) scramble siRNA or (****ii****)AURKB siRNA for 72 hours before immunofluorescence analyses were performed with antibodies against AURKB (green) or TERF1 (red). DAPI was used as a nuclear counterstain (blue).* ***(iii)*** *Loss of AURKB led to a 66.7% increase in mean fluorescence staining intensity in TERF1 binding at the telomeres (P < 0.0001, n = >4000 TERF1 foci from three biological replicates). Error bars represent S.E.M., with box and whiskers plot showing Q1, Q2 and Q3 values. P-values are indicated in column graphs.* ***(B)*** *Mouse ES cells stably expressing GFP-WT-TERF1 were treated with 1µM ZM447439 for 72 h, and ChIP/qPCR analyses were performed with antibodies against IgG, GFP and H3. GFP-WT-TERF1 and TERF2 binding was normalised against the level of H3 at the telomeres.* ***(i)*** *GFP-WT-TERF1 was increased by approximately 2-fold when compared to control untreated cells.* ***(ii)*** *TERF2 and* ***(iii)*** *H3 levels at the telomeres were not significantly affected following treatment with ZM447439. N=3. Error bars represent S.D..*

3.2.3 AURKB interacts with TERF1 in mouse ES cells

Next, to investigate if AURKB directly interacts with TERF1, reciprocal co-immunoprecipitation was performed using ES cells expressing GFP-TERF1. Due to the lack of suitable TERF1 antibody, GFP-TERF1 was used. The results showed that GFP-TERF1 co-purified with AURKB (**Figure 3.2.7i**). To identify the region where AURKB interreacted with TERF1, GST-TERF1 fusion proteins containing either the N-terminal TRFH domain (GST-N-TERF1; amino acids 2-251) or the C-terminal Myb domain (GST-C-TERF1; amino acids 240-421) were generated (**Figure 3.2.7ii**). These GST-tagged TERF1 fragments were purified and immobilized onto glutathione agarose beads before incubation with lysates from mouse ES cells. The upper blot in **Figure 3.2.7iii** is probed with a GST antibody to show the presence of GST-N/C terminal TERF1 while the bottom blot is probed with a AURKB antibody to show level of AURKB bound to the respective GST-N/C terminal TERF1 protein fragments. The GST- only control did not bind any AURKB. A higher affinity to the C-terminal was determined by the level of binding between AURKB and GST-N/C terminal TERF1, respectively. GST-C-terminal TERF1 immunoprecipitated significantly more AURKB than the GST-N-terminal AURKB (**Figure 3.2.7iii**). This suggests that AURKB is likely to bind or interact with C terminal of TERF1.

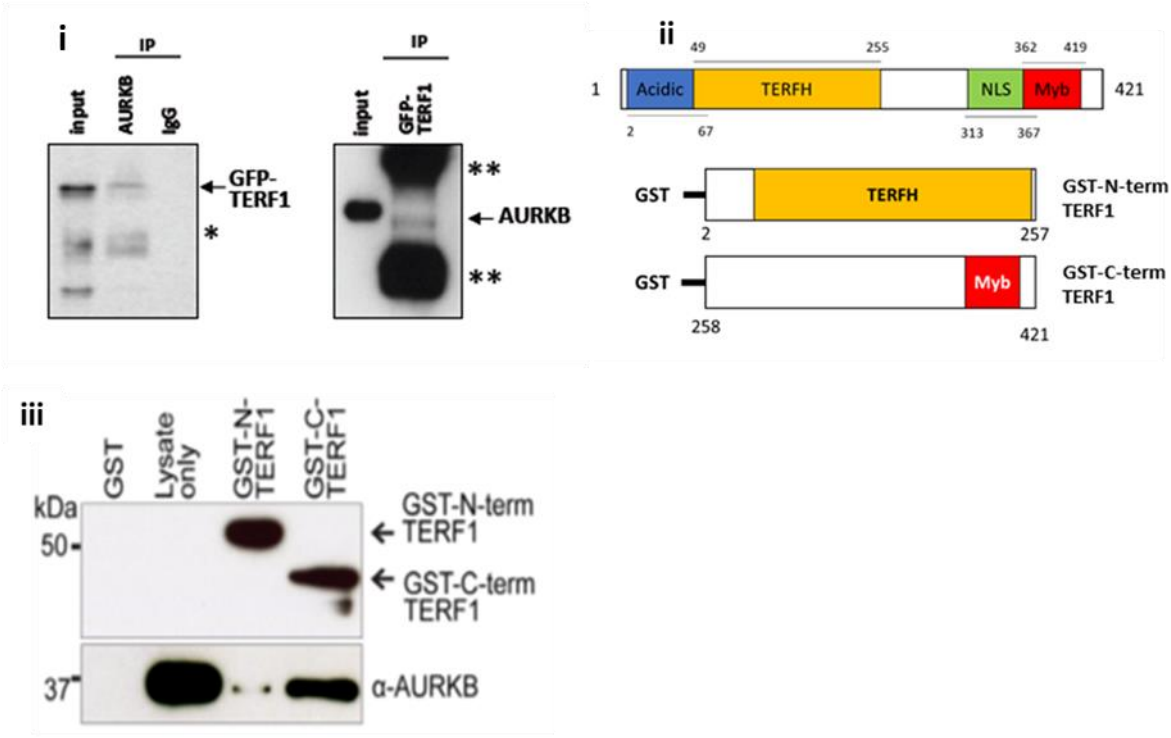

Figure 3.2.7: AURKB directly interacts with TERF1 to regulate TERF1 binding to the telomeres

(i) *GFP-WT-TERF1 stably expressing cells were used in reciprocal co-immunoprecipitation experiments followed by immunoblotting using antibody against GFP and AURKB. GFP-WT-TERF1 co-purified with AURKB immunoprecipitation while AURKB co-purified with GFP-TERF1 immunoprecipitation (arrows). * denotes unspecific band, ** denotes the heavy and light chains of the GFP antibody.* ***(ii)*** *Schematic of GST-N-TERF1 and GST-C-TERF1 used in the in vitro binding assay.* ***(iii)*** *GST-fusion TERF1 fragments were immobilized on glutathione agarose beads and incubated with mouse ES cell lysates before immunoblotting with antibody against GST and AURKB. Immunoblotting with GST showed the presence of GST-N-TERF1 and GST-C-TERF1. GST-TERF1 was not observed in both mouse ES cell lysate and GST-only control. Immunoblotting with AURKB showed interactions between AURKB and both GST-N-TERF1 and GST-C-TERF1. Mouse ES cell lysate showed high levels of AURKB, while GST-only control showed no interaction with AURKB.*

3.2.4 AURKB phosphorylates S404 and T403-TERF1 *in vitro*

GPS2.1, a phosphorylation prediction tool (Xue et al., 2011), was used to identify potential AURKB sites on the C-terminal fragment of TERF1. Of the residues on the C-terminal of TERF1, GPS2.1 identified S404 as a candidate residue (**Figure 3.2.8A**). Thus, *in vitro* kinase assay was performed to determine if AURKB phosphorylates S404-TERF1. Mass spectrometric analyses were undertaken on a 30-amino acid synthetic TERF1 peptide spanning N389 to K418 following incubation with recombinant AURKB in the presence or absence of an AURKB inhibitor. The result showed that S404-TERF1 and T403-TERF1 were phosphorylated. However, the phosphorylation of T403-TERF1 was detected at much lower levels. With the addition of an AURKB inhibitor, the phosphorylation of S404-TERF1 and T403-TERF1 was lost (**Figure 3.2.8B, Supplementary Figure 3.4.1**). This result shows that AURKB phosphorylates T403-TERF1 and S404-TERF1 *in vitro*.

A

Position	Code	Kinase	Peptide sequence	Score	Cutoff
404	S	AURKB	YKFNNRTSVMLKDRW	7.915	6.744

T403-mTERF1

mTERF1	388-	G	N	W	A	K	I	L	S	H	Y	K	F	N	N	R	**T**	S	V	M	L	K	D	R	W	R	T	M	K	R	L	K	-418
hTERF1	401-	G	N	W	S	K	I	L	L	H	Y	K	F	N	N	R	**T**	S	V	M	L	K	D	R	W	R	T	M	K	K	L	K	-431

S404-mTERF1

mTERF1	389-	N	W	A	K	I	L	S	H	Y	K	F	N	N	R	T	**S**	V	M	L	K	D	R	W	R	T	M	K	R	L	K	L	-419
hTERF1	402-	N	W	S	K	I	L	L	H	Y	K	F	N	N	R	T	**S**	V	M	L	K	D	R	W	R	T	M	K	K	L	K	L	-432

Bi

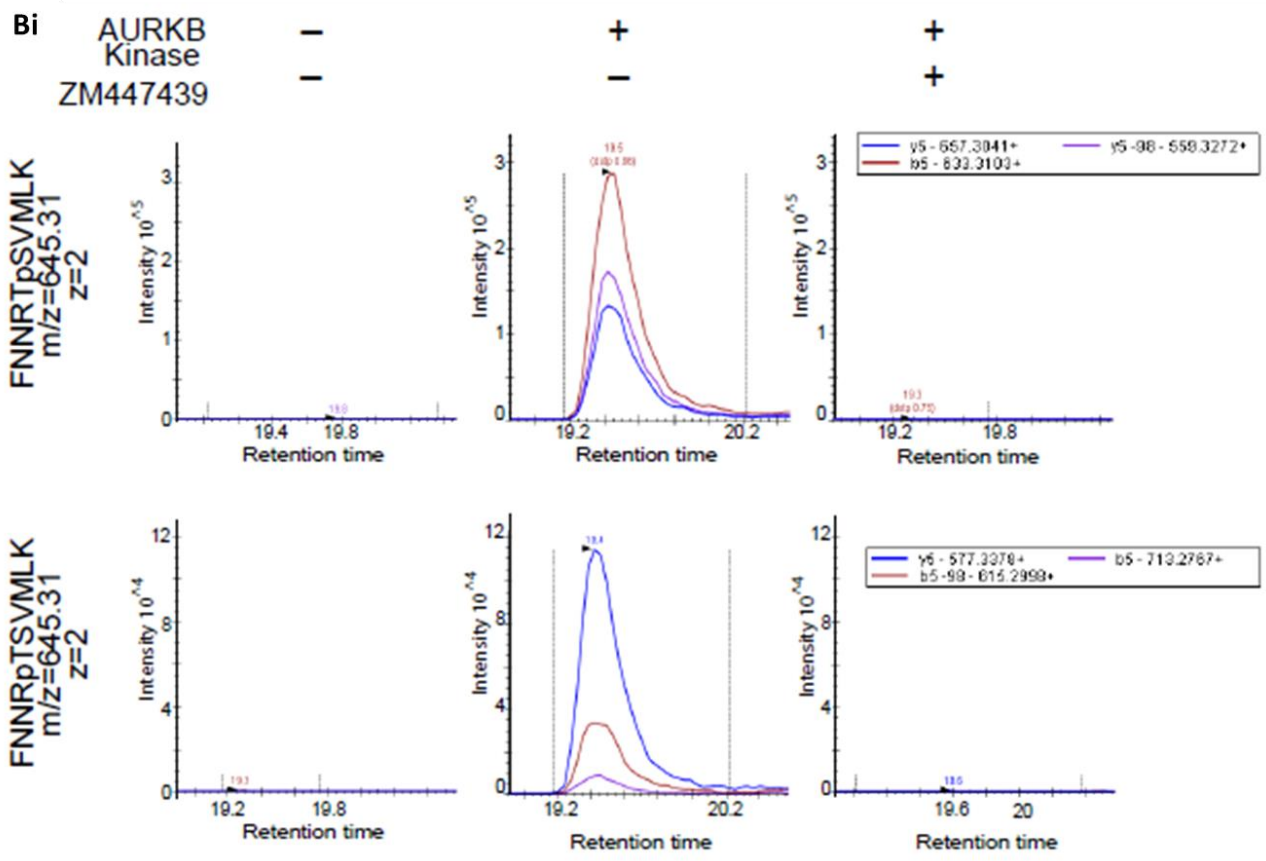

Bii

Ratio pS / pT
(in + kinase / - inhibitor sample)

	Peak Area	Ratio [%]
FNNRT**pS**VMLK	11064377	79.13
FNNR**pT**SVMLK	2917930	20.86

Figure 3.2.8: AURKB phosphorylates TERF1 in vitro

*(**A**) GPS2.1 show that S404 on mouse TERF1 is a likely candidate that is phosphorylated by AURKB (top table). The residue of interest on mouse TERF1 and its human analogue is highlighted in red. The amino acid residues flanking the residue of interest is also shown. In mouse TERF1, S404 and the surrounding region is conserved. mTERF1 represents mouse TERF1, and hTERF1 represents human TERF1. (**Bi**) Targeted MS-based proteomics on a 30-amino acid synthetic peptide spanning N389-K418 of TERF1 incubated with recombinant AURKB in the presence or absence of an AURKB inhibitor in an in vitro kinase assay and digested with Lys-C. Analysis was done by multiple-reaction monitoring (MRM). Only ten amino acid sequence N399-K408 (spanning S404) is shown for clarity. Arrows indicate Lys-C cleavage sites. The theoretical b- and y-ion fragment series after higher-energy collision dissociation (HCD) are indicated above and below the peptide sequence. MRM traces of the peptides FNNRTpSVMLK (Brown trace), FNNRpTSVMLK (Blue trace)* $FNNRTpSVoxMLK$ *(purple trace)* and $FNNRpTSVoxMLK$ *(purple trace) across the three different conditions are shown. The mass-to-charge ratio (m/z), the charge (z) and the monitored transitions are shown for each peptide. (**ii**) A ratio of phosphorylated S404 TERF1/ phosphorylated T403 TERF1 is shown. 79.13% of the observed phosphorylation were located at S404 and 20.86 % at T403.*

3.2.5 T403A-TERF1 regulates TERF1 stability

With T403-TERF1 and S404-TERF1 identified as AURKB targets *in vitro*, phospho-null mutants were generated to study the effect of the loss of phosphorylation at these sites *in vivo*. T403-TERF1 and S404-TERF1 were mutated to alanine (Wu et al., 2007), preventing phosphorylation (**Figure 3.2.9A**). In addition, a GFP tag (Stretton et al., 1998) was added to differentiate between endogenous and exogenous TERF1.

To test the expression of GFP tagged WT, T403A and S404A-TERF1, mouse ES cells were transfected with the relevant plasmids, followed by immunoblotting analysis with an antibody against GFP (**Figure 3.2.9B**). There was a robust expression of GFP-WT and S404A-TERF1 in the cells, however, the expression level of GFP-T403A-TERF1 was barely detectable. The expression of GFP-WT and S404A-TERF1suggested that the GFP tag was not detrimental to the cells while the low level of GFP-T403A-TERF1 protein expression suggests that T403A-TERF1, not the GFP tag, may be unstable or degraded.

Unstable proteins may be targeted for degradation by the proteasome (Janse et al., 2004). To identify if the proteasome degraded GFP-T403A-TERF1, cells were treated for 4 hours with 2μM of MG132, a proteasome inhibitor, before immunoblotting (Rock et al., 1994, Yu et al., 2005). The results showed that GFP-T403A-TERF1 was partially rescued compared to the levels of MG132 treated and untreated GFP-WT-TERF1 after proteasome inhibition (**Figure 3.2.9C**). Thus, the partial rescue of T403A-TERF1 indicated that a fraction of T403A-TERF1 was indeed degraded following expression in mouse ES.

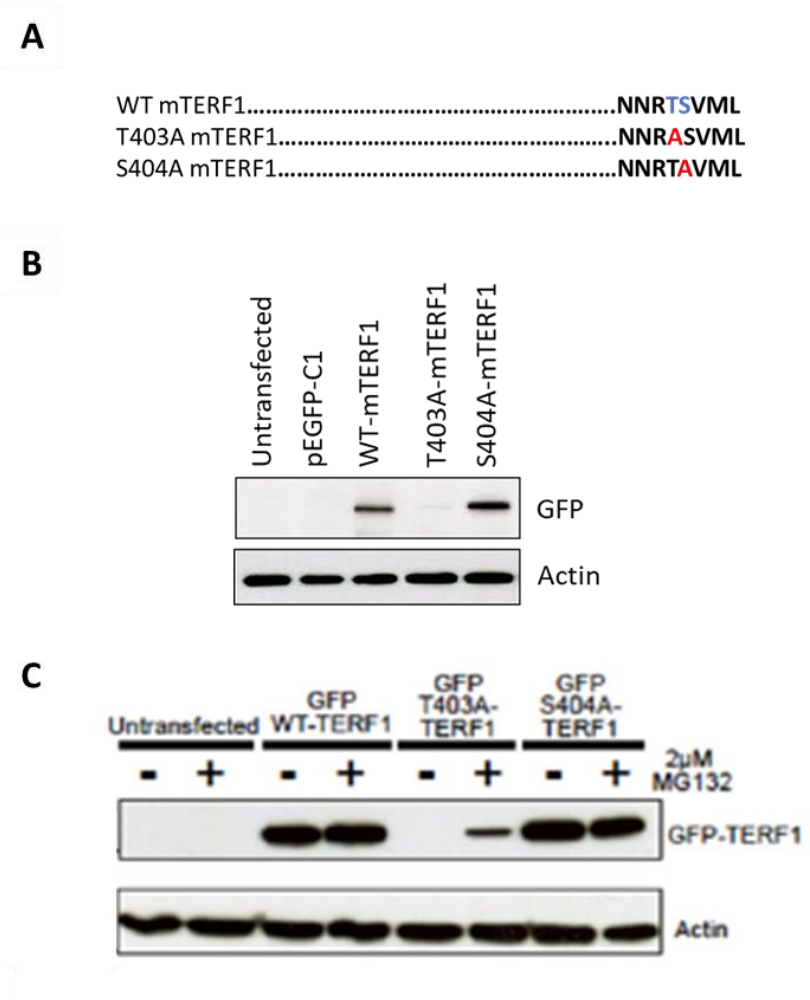

Figure 3.2.9: GFP-T403A-TERF1 is unstable and is degraded by the proteasome.

(A) *WT-TERF1 sequence and the mutation of the respective serine/threonine residues to alanine (red).* ***(B)*** *Mouse ES cells were transfected with pEGFP-C1 and GFP-TERF1 (WT and mutant) plasmid DNA before immunoblotting with antibody against GFP. GFP-TERF1 was not detected in untransfected and pEGFP-C1 transfected cells. GFP-WT and S404-TERF1 were expressed at high levels. The expression of GFP-T403A-TERF1 was barely detectable. (**C**) Mouse ES cells were transfected with GFP-WT-TERF1 or GFP-T403A-TERF1 and treated with 2 μM of MG132 for 4h before immunoblotting with antibody against GFP. GFP-TERF1 was not detected in untransfected cells. GFP-WT-TERF1 was detected at similar levels with or without MG132 treatment. GFP-T403A-TERF1 was undetectable before treatment and was partially rescued (compared to GFP-WT-TERF1) after treatment. Actin was used as a loading control.*

To investigate if GFP-T403A-TERF1 localises to the telomeres of ES cells, immunofluorescence analyses were performed after proteasome inhibition. Following the proteasome inhibition, low level of GFP-T403A-TERF1 was restored and colocalised with endogenous TERF1 at the telomeres of interphase cells (**Figure 3.2.10A**). However, the recruitment of GFP-T403A-TERF1 was too low to be detected at similar levels to wildtype-TERF1. GFP-T403A-TERF1 was undetectable in mitotic cells (**Figure 3.2.10B**). In contrast, the localisation of GFP-WT-TERF1 at the telomeres remained unchanged despite proteasome inhibition in both interphase and mitotic cells. This result suggested that T403-TERF1 may regulate TERF1 stability and abundance within the cells. Further characterisation of the role of T403-TERF1 would provide valuable insight into the function of T403-TERF1 phosphorylation in regulating TERF1 levels. However, the instability and toxicity of the mutation needs consideration. As the expression of T403A-TERF1 was unstable and could not be fully rescued by proteasome inhibition, subsequent analyses focused on S404-TERF1.

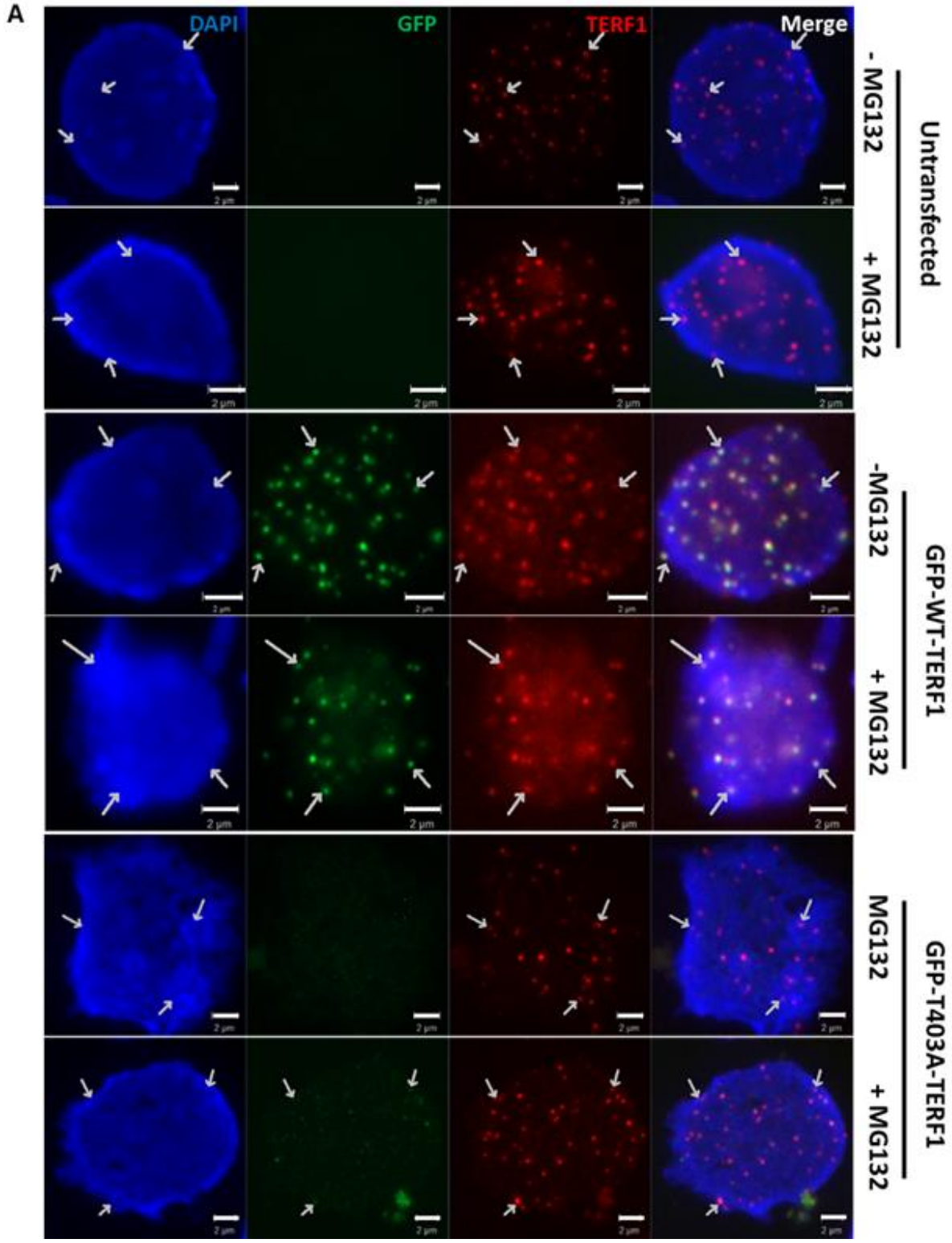
A
DAPI
GFP
TERF1
Merge
Untransfected
- MG132
+ MG132
GFP-WT-TERF1
-MG132
+ MG132
GFP-T403A-TERF1
MG132
+ MG132

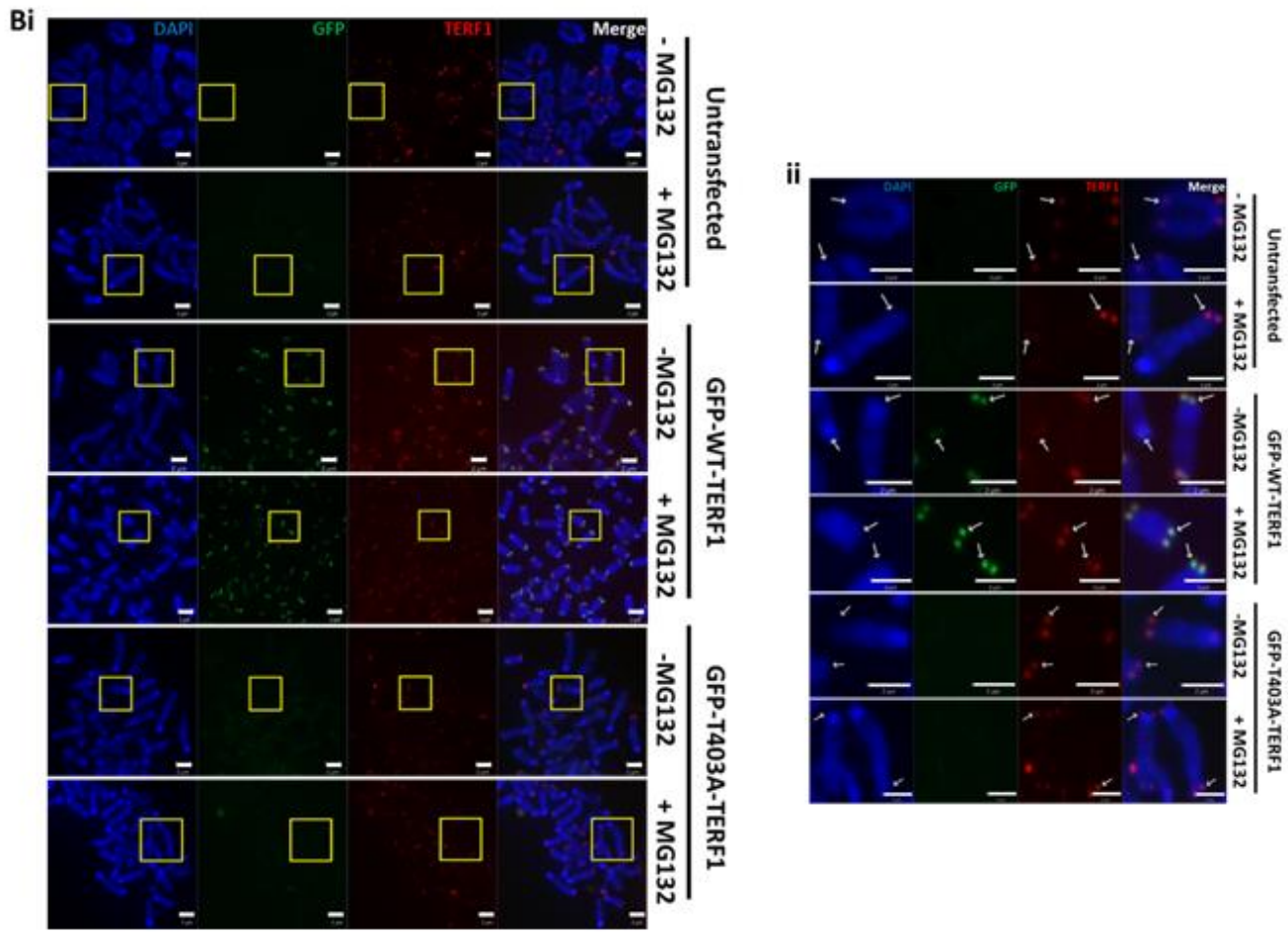

Figure 3.2.10: GFP-T403A-TERF1 is partially rescued and localised to the telomeres of interphase mouse ES cells post proteasome inhibition

*Mouse ES cells were transfected with GFP-WT-TERF1 or GFP-T403-TERF1 and treated with or without 2μM MG132 for 4 hours before immunofluorescence analyses with antibody against GFP (green) and TERF1 (red). Endogenous TERF1 was used as a telomere marker. GFP was undetectable in untransfected interphase and mitotic cells with and without MG132 treatment. However, GFP-WT-TERF1 colocalised with endogenous TERF1 despite MG132 treatment at the telomeres of interphase and mitotic cells (arrows). (**A**) GFP-T403A-TERF1 was partially rescued at the telomeres of interphase cells and colocalised with endogenous TERF1 after MG132 treatment (arrows). (**B**) GFP-T403A-TERF1 was undetectable in metaphase cells despite MG132 treatment. Magnified images of the boxed chromosomes are shown in (**Bii**). DAPI was used as a nuclear counterstain (blue). Scale bar represents 2μm.*

3.2.6 S404E-TERF1 prevents TERF1 binding to telomeres of mouse ES cells

To characterise S404-TERF1 phosphorylation, the phospho-mimic GFP-S404E-TERF1 was also generated (**Figure 3.2.11A**). Mutation to glutamic acid (E) mimics a constantly phosphorylated state (Fink et al., 2007). Next, to investigate if the phospho-null and phospho-mimic S404-TERF1 mutants were expressed in mouse ES cells, immunoblotting was performed after transfection with the respective plasmids. Both S404A and S404E-TERF1 were expressed, similar to GFP-WT-TERF1 expression levels (**Figure 3.2.11B**).

To validate the expression and localisation of S404A and S404E-TERF1 to the telomeres of mouse ES cells, immunofluorescence analyses were performed. Following transfection, S404A-TERF1 localised to the telomeres of both interphase and metaphase cells (**Figure 3.2.11Cii, Dii**). However, despite the robust protein expression of S404E-TERF1, its localisation was detected at lower levels at the telomeres in both interphase and mitotic cells (**Figure 3.2.11Ciii, Diii**). This shows that the recruitment of S404E-TERF1 to the telomeres is reduced in interphase cells and mitotic telomeres. Thus, the robust expression and reduced telomeric binding of S404E-TERF1 suggests that the phosphorylation of S404-TERF1 may function to release TERF1 from the telomeres rather than a signal for TERF1 degradation.

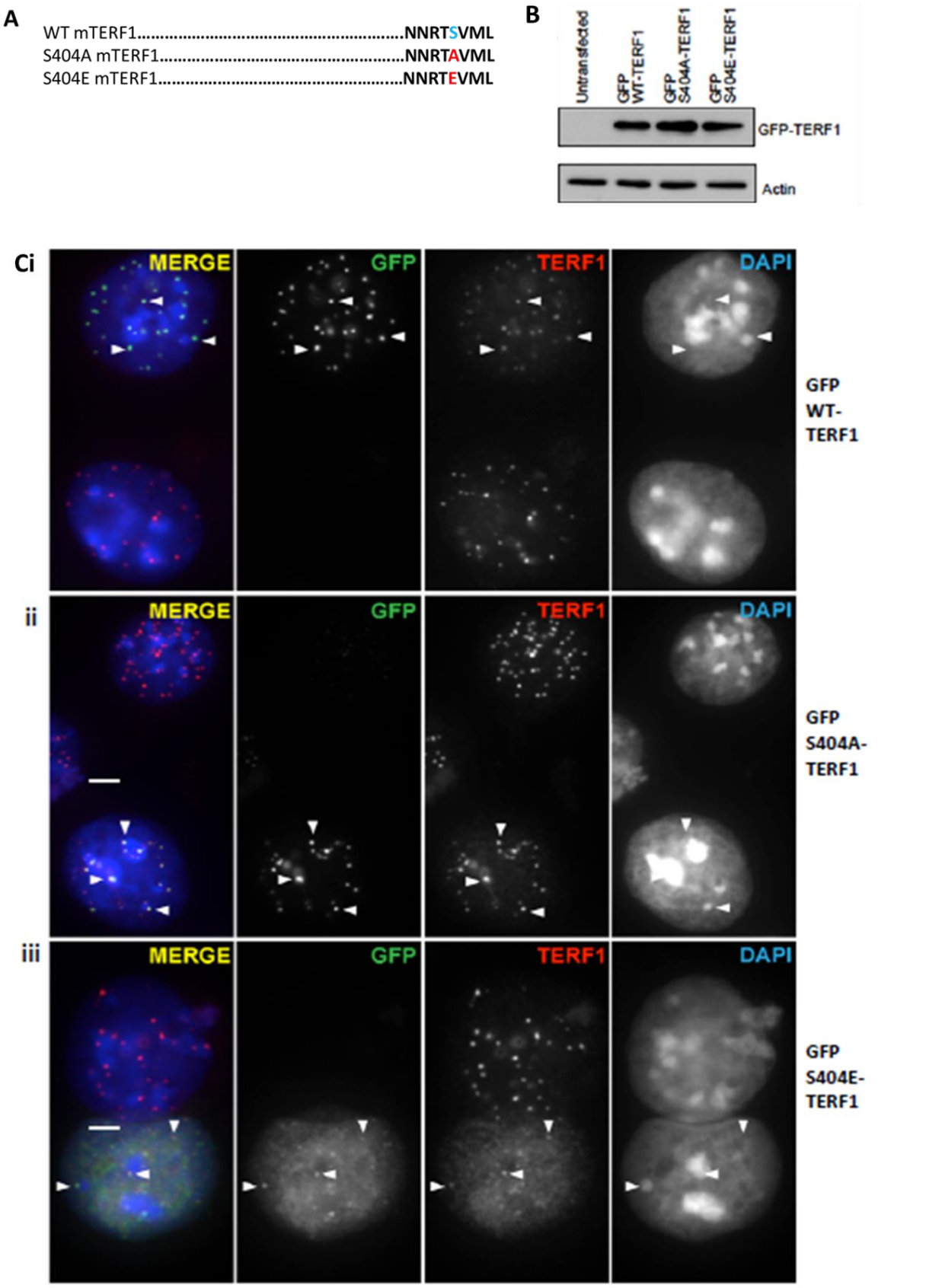
A
WT mTERF1.....NNRTSVML
S404A mTERF1.....NNRTAVML
S404E mTERF1.....NNRTEVML
B
Untransfected
GFP WT-TERF1
GFP S404A-TERF1
GFP S404E-TERF1
GFP-TERF1
Actin
Ci
MERGE
GFP
TERF1
DAPI
GFP WT-TERF1
ii
MERGE
GFP
TERF1
DAPI
GFP S404A-TERF1
iii
MERGE
GFP
TERF1
DAPI
GFP S404E-TERF1

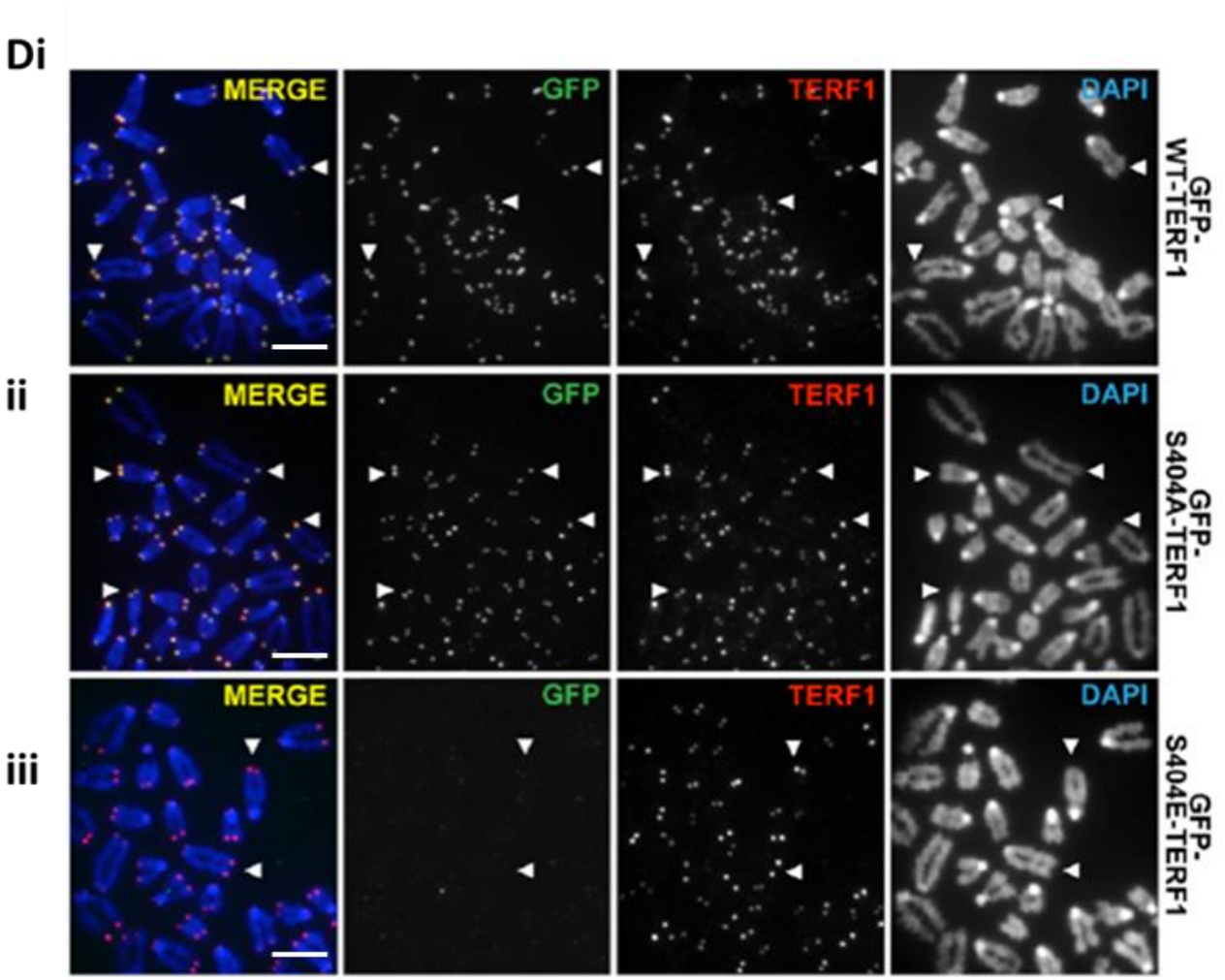
Di
ii
iii
MERGE
GFP
TERF1
DAPI
GFP-WT-TERF1
GFP-S404A-TERF1
GFP-S404E-TERF1

Figure 3.2.11: GFP-S404E-TERF1 does not bind to the telomere

(A) *WT-TERF1 sequence and the mutation of the respective serine/threonine residues to alanine and glutamic acid (red).* ***(B)*** *Mouse ES cells were transfected with GFP-WT, S404A- and S404E-TERF1 plasmid DNA before immunoblotting with antibody against GFP. GFP-WT, S404A- and S404E-TERF1 were expressed at high levels. Untransfected cells showed no expression of GFP-TERF1. Actin was used as a loading control. (**C**/**D**) Mouse ES cells were transfected with GFP-WT, S404A- and S404E-TERF1 plasmid DNA before immunofluorescence analyses with antibody against GFP (green) and TERF1 (red). Endogenous TERF1 was used as a telomere marker. GFP-WT- and S404A-TERF1 were expressed and colocalised with endogenous TERF1 at the telomeres of interphase and mitotic cells (arrowhead; **i**, **ii**). In interphase cells and mitotic cells, GFP-S404E-TERF1 staining at the telomeres was weak but colocalised with endogenous TERF1 (arrowhead; **Ciii; Diii**). GFP-S404E-TERF1 also showed a diffused staining pattern in interphase cells. DAPI was used as a nuclear counterstain (blue). Scale bar represents 2μm.*

To prevent endogenous TERF1 from rescuing the effects of mutant TERF1 expression, HA-tagged siRNA-resistant WT, S404A and S404E-TERF1 constructs were generated by changing the nucleotide sequence on TERF1 but not altering the resultant amino acid codon. These constructs were transiently expressed in mouse ES cells before TERF1 siRNA knockdown. The knockdown of endogenous TERF1 with siRNA was previously shown to be efficient (**Figure 3.2.5B**). Next, to determine if these constructs were resistant to TERF1 siRNA knockdown, immunoblotting was performed against the HA tag after TERF1 siRNA knockdown. Robust expression of siRNA resistant WT, S404A and S404E-TERF1 confirmed that the constructs were indeed resistant to TERF1 siRNA knockdown although lower levels of S404A and S404E-TERF1 were observed compared to WT-TERF1 (**Figure 3.2.12A**).

Next, to investigate if siRNA resistant WT, S404A and S404E-TERF1 to the telomeres of mouse ES cells after TERF1 siRNA knockdown, immunofluorescence analyses using antibody against HA was performed. Consistent with the GFP-TERF1 cells (**Figure 3.2.11C and D**), both HA-WT-TERF1 and HA-S404A-TERF1 localised and bound to the telomeres while HA-S404E-TERF1 failed to localise and bind to the telomeres (**Figure 3.2.12B**). Altogether, these results indicate a role for the phosphorylation of S404-TERF1 in regulating TERF1 binding at the telomeres.

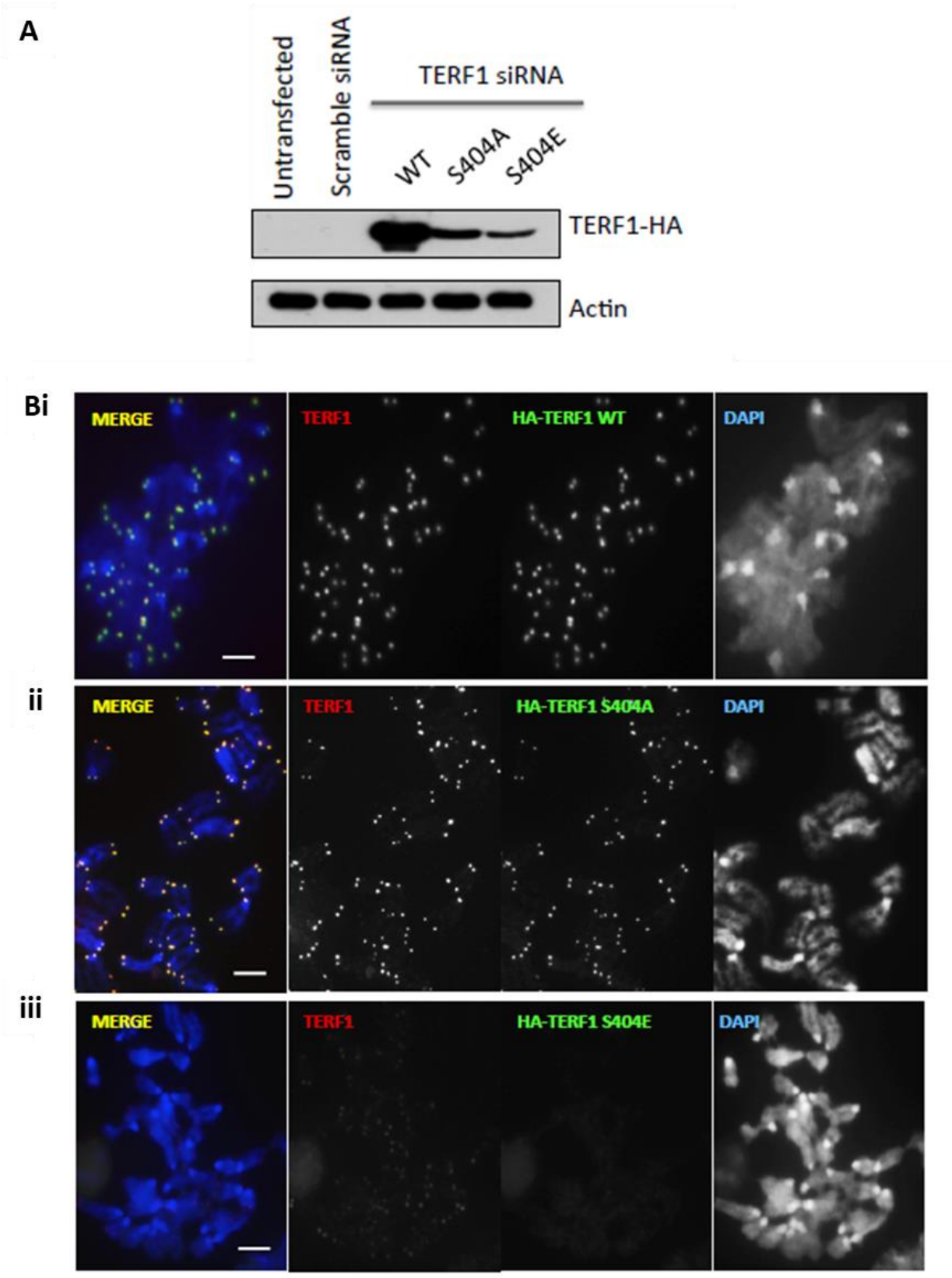
A
Untransfected
Scramble siRNA
TERF1 siRNA
WT
S404A
S404E
TERF1-HA
Actin
Bi
MERGE
TERF1
HA-TERF1 WT
DAPI
ii
MERGE
TERF1
HA-TERF1 S404A
DAPI
iii
MERGE
TERF1
HA-TERF1 S404E
DAPI

Figure 3.2.12: The loss of GFP-S404E-TERF1 binding to the telomeres is not coupled to endogenous TERF1 levels

*Mouse ES cells were subjected to TERF1 siRNA depletion and transfected with siRNA resistant HA-tagged WT, S404A and S404E TERF1 plasmids. (**A**) Immunoblot analyses using antibody against HA showed that HA-TERF1 was not detected in untransfected and scramble siRNA transfected cells. Robust expression of HA-WT-TERF1, HA-S404A-TERF1 and HA-S404E-TERF1 siRNA resistant proteins was detected. Actin was used as a loading control. (**B**) Immunofluorescence analyses with antibody against TERF1 (red) and HA (green) showed that (**i**) HA-WT- and (**ii**) S404A-TERF1 were expressed and localised to the telomeres of mitotic cells. (**iii**) HA-S404E-TERF1 was undetectable at the telomeres. In addition, staining for TERF1 (red) in HA-S404E-TERF1 was weak compared to HA-WT-TERF1 and HA-S404A-TERF1. TERF1 was used as a telomere marker. DAPI was used as a nuclear counterstain (blue). Scale bar represents 5 μm.*

3.2.7 S404-TERF1 phospho-mutants show aberrant MTS formation and binding in mouse ES cells

To study the long-term effects of S404 mutation on TERF1 binding and telomere function, mouse ES cells with stable expression of GFP-S404A and S404E-TERF1 mutants were generated. To determine the expression levels of GFP-WT, S404A and S404E-TERF1, immunoblotting was performed using antibody against GFP. The results showed robust GFP-WT, S404A and S404E-TERF1 expression in mouse ES cells (**Figure 3.2.13A**).

To determine the levels of GFP-WT, S404A and S404E-TERF1 proteins that bound to the telomeres, ChIP/qPCR analyses were performed using an anti-GFP antibody and telomeric DNA specific oligonucleotides. Compared to GFP-WT-TERF1, GFP-S404A-TERF1 showed a moderate increase in telomere binding, while GFP-S404E-TERF1 showed a considerable reduction in telomere binding (**Figure 3.2.13B**). This change in telomere binding further suggests the role of S404-TERF1 phosphorylation in regulating TERF1 binding at the telomeres of mouse ES cells. Cell lines expressing similar levels of GFP-TERF1 protein were selected (WT: clone 1; S404A: clone 2; S404E: clone 1, **Figure 3.2.13 A and B**). To confirm if stably expressed GFP-S404A and S404E-TERF1 mutants localised to the telomeres, immunofluorescence analyses were performed. Consistent with the GFP-TERF1 (**Figure 3.2.11**) and HA-TERF1 cells (**Figure 3.2.12**), the stable expression of GFP-S404A-TERF1 did not affect its ability to localise to the telomeres, whereas S404E-TERF1 failed to localise the telomeres (**Figure 3.2.13C**). Interestingly, endogenous TERF1 levels were depleted at the telomeres of cells with stable expression of GFP-S404E-TERF1 (**Figure 3.2.13Ciii**). This suggests a dominant negative effect of S404E-TERF1, and phosphorylated S404-TERF1.

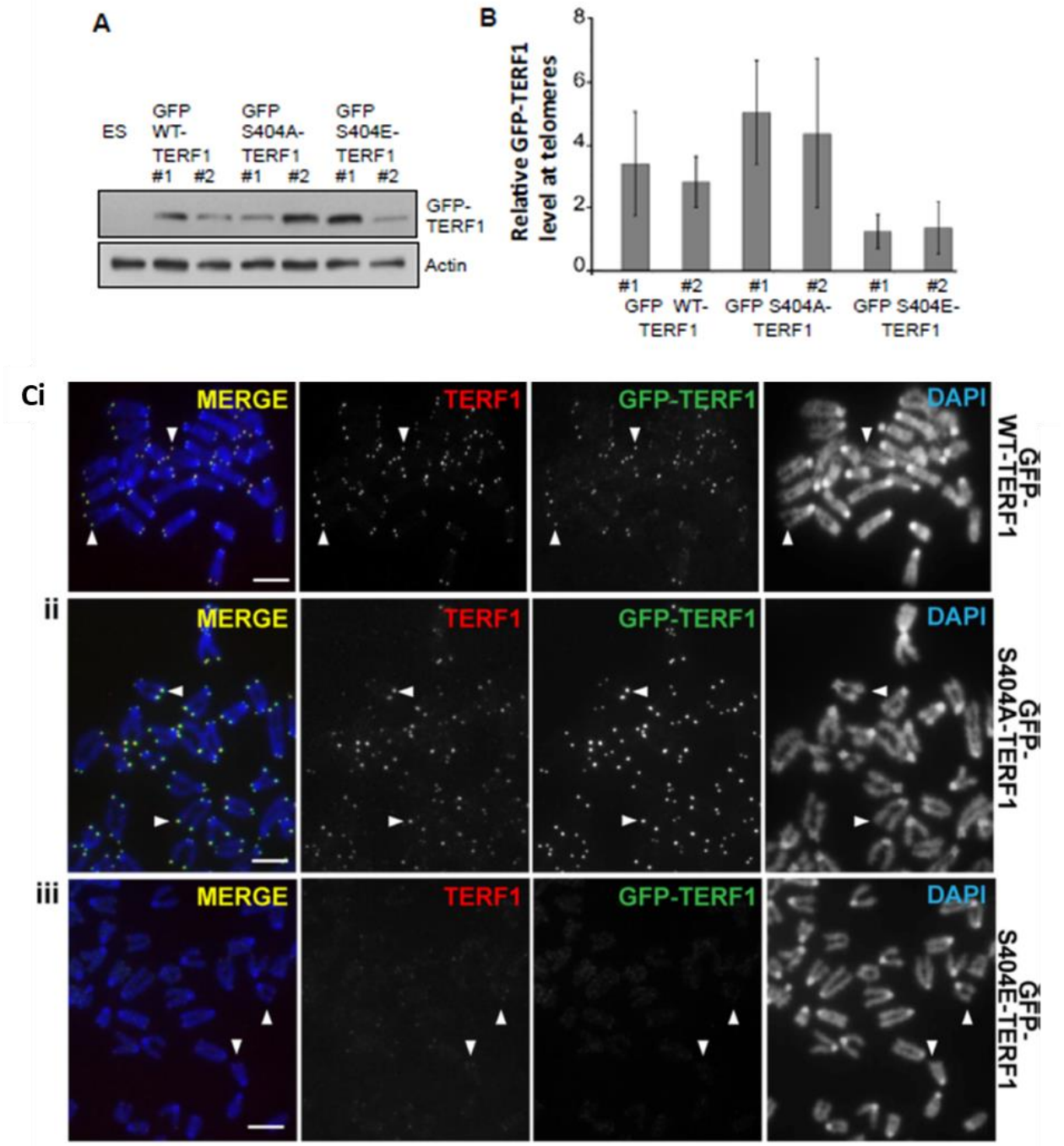

Figure 3.2.13: S404-TERF1 phospho-mutants regulate TERF1 binding at the telomeres

Mouse ES cells with stable expression of GFP-WT, S404A and S404E-TERF1 were generated. ***(A)*** *Immunoblot analyses using antibody against GFP showed that GFP-WT- (clones #1 and #2), S404A- (clones #1 and #2) and S404E- (clones #1 and #2) TERF1 proteins were expressed. GFP-TERF1 was not detected in untransfected cells. Actin was used as a loading control.* ***(B)*** *ChIP/qPCR analyses with antibody against GFP showed that compared to GFP-WT-TERF1, GFP-S404A-TERF1 had approximately 2-fold increased binding while GFP-S404E-TERF1 had an approximately 2-fold decrease in their binding level at the telomeres. Two cell lines for each construct are shown. Results were normalised to H3 levels at GAPDH and are relative to input. Error bars represent S.D..* ***(C)*** *Immunofluorescence analyses with antibody against TERF1 (red) and GFP (green) showed that* ***(i)*** *GFP-WT-TERF1 and* ***(ii)*** *GFP-S404A-TERF1 were expressed and colocalised with endogenous TERF1 at the telomeres of metaphase cells (arrowhead).* ***(iii)*** *GFP-S404E-TERF1 was undetectable at the telomeres and staining for TERF1 in cells expressing GFP-S404E-TERF1 also showed diminished endogenous TERF1 levels at the telomeres. DAPI was used as a nuclear counterstain (blue). TERF1 was used as a telomere marker. Scale bar represents 5μm.*

To assess if S404A- and S404E-TERF1 cells showed compromised telomere integrity, Tel-FISH analyses were performed. In addition, this experiment aimed to identify if AURKB inhibition further aggravate MTS formation in S404A- and S404E-TERF1 cells. This would show that AURKB regulation of this residue was related to MTS formation or if other residues on TERF1 regulated MTS formation. Both GFP-S404A and S404E-TERF1 mouse ES cells showed increased MTS formation when compared to GFP-WT-TERF1 (**Figure 3.2.14A**). Notably, the addition of the AURKB inhibitor, ZM447439, did not result in increased MTS formation in either GFP-S404A or S404E TERF1 mutant cells (**Figure 3.2.14A**). In contrast, the addition of ZM447439 resulted in a significant increase in MTS formation in GFP-WT-TERF1 cells (**Figure 3.2.14A**). Consistent with the increase in MTS formation seen in cells depleted of AURKB function (**Figure 3.2.6**), these results show that S404-TERF1 phosphorylation by AURKB is associated with MTS formation.

In addition, ChIP/qPCR showed an increase in γH2AX levels at the telomere of cells expressing either S404A or S404E-TERF1 compared to WT-TERF1 expressing mouse ES cells (**Figures 3.2.14B**). Immunofluorescence analyses supported this data where γH2AX staining showed increased γH2AX levels following S404A and S404E-TERF1 expression (**Supplementary Figure 3.4.2**). These findings are consistent with previous reports showing dysregulation of TERF1 telomere binding results in MTS formation, which is accompanied by DNA damage marker γH2AX (Martinez et al., 2009, Sfeir et al., 2009). Furthermore, despite minimal levels of GFP-S404E-TERF1 at the telomeres, GFP-S404E-TERF1 cells showed a greater increase in MTS formation. Altogether, these results indicate that AURKB targets S404-TERF1 to regulate telomere structural integrity. Furthermore, the long-term expression of the TERF1 phospho-mimic S404E may act in a dominant-negative fashion,

depleting telomeres of TERF1 binding, resulting in aberrant telomere phenotype as indicated by the MTS formation.

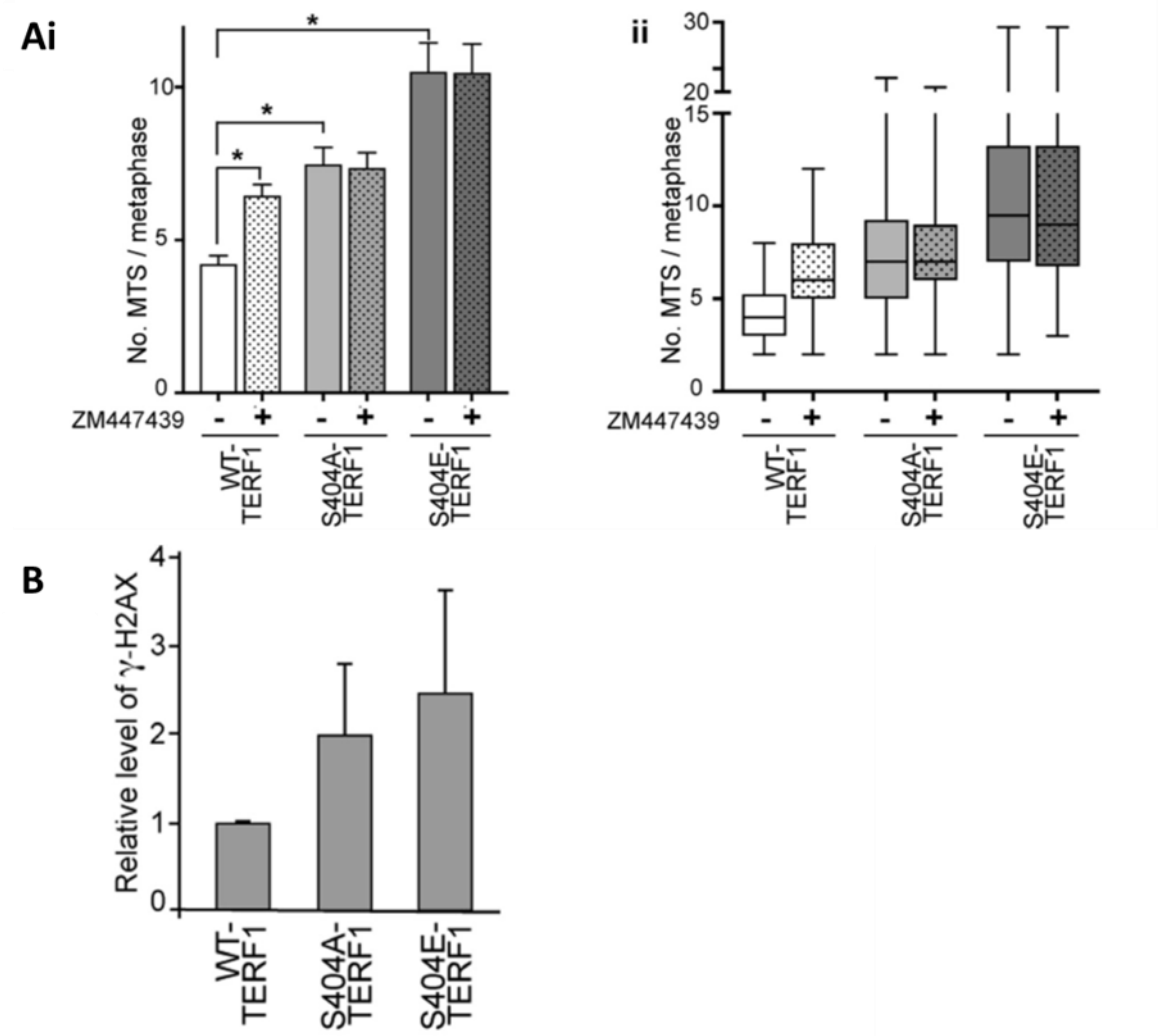
Ai
No. MTS / metaphase
ZM447439
WT-TERF1
S404A-TERF1
S404E-TERF1
ii
No. MTS / metaphase
ZM447439
WT-TERF1
S404A-TERF1
S404E-TERF1
B
Relative level of γ-H2AX
WT-TERF1
S404A-TERF1
S404E-TERF1

Figure 3.2.14: Regulation of S404-TERF1 prevent DNA damage responses and MTS formation at the telomeres

(A) *Tel-FISH analyses were performed on mouse ES cells with stable expression of GFP-WT, S404A- and S404E-TERF1 to assess MTS formation with and without ZM447439 treatment. (**i**) Without ZM447439 treatment and compared to GFP-WT-TERF1 (4.2 MTS/metaphase), GFP-S404A-TERF1 (7.5 MTS/metaphase) and GFP-S404E-TERF1 (10.5 MTS/metaphase) cell lines showed increased MTS formation. (**ii**) With ZM447439 treatment, MTS formation increased from 4.2 to 6.5 MTS/metaphase in GFP-WT-TERF1 cells. MTS formation in GFP-S404A-TERF1 and GFP-S404E-TERF1 cells were unchanged despite ZM447439 treatment. Error bars represent S.E.M.. Asterisk in **(Ai)** indicates P-values < 0.001; N > 1300 chromosomes from over 30 mitotic spreads per condition from three biological replicates. Box and whiskers plot **(Aii)** represents Q1, Q2 and Q3, with the maximum and minimum values plotted.* ***(B)*** *ChIP/qPCR analyses were performed on mouse ES cells with stable expression of GFP-WT, S404A- and S404E-TERF1 with antibody against γH2AX at the telomeres. γH2AX levels were increased in both GFP- S404A and S404E-TERF1, compared to GFP-WT-TERF1. Results were normalised to input and H3 levels at GAPDH. N=3; Error bars represent S.E.M..*

3.2.8 The phosphorylation of S404-TERF1 promotes aberrant telomere lengthening

Compared to GFP-WT-TERF1 cells, GFP-S404A-TERF1 cells showed increased MTS formation (**Figure 3.2.14A**), suggesting that loss of S404-TERF1 phosphorylation is associated with MTS formation, similar to the increase in MTS formation in cells depleted of AURKB function through either ZM447439 treatment or siRNA knockdown (Figures **3.2.4** and **3.2.6**). However, GFP-S404E-TERF1 cells showed an even greater increase in MTS formation (**Figure 3.2.14A**) despite minimal binding of GFP-S404E-TERF1 at the telomeres (Figure **3.2.11C**). In addition to the minimal binding of GFP-S404E-TERF1 at the telomeres, a decrease in the level of endogenous TERF1 binding at the telomeres was observed, suggesting that long-term expression of phospho-mimic S404E mutant, but not S404A mutant, acts in a dominant negative fashion, depleting telomeres of TERF1 binding, resulting in aberrant telomere phenotype as indicated by the MTS formation. A previous study has shown that the loss of TERF1 binding at the telomeres led to increased telomere length (van Steensel and de Lange, 1997, Smogorzewska et al., 2000). Thus, we investigated the length of telomeres by Tel -FISH analyses on GFP-S404E-TERF1 cells after 3 months in culture.

After 3 months in culture, compared to GFP-WT-TERF1 cells, Tel-FISH signals in GFP-S404E-TERF1 increased in intensity (**Figure 3.2.15A**). When normalised against the centromere FISH signal to account for chromatin levels, the overall Tel-FISH signal in GFP-S404E-TERF1 cells was increased by approximately 2.9 folds than that in GFP-WT-TERF1 cells (**Figure 3.2.15B**). This increase in Tel-FISH intensity indicated that the long-term dominant negative effect of S404E-TERF1 results in telomere lengthening in these cells.

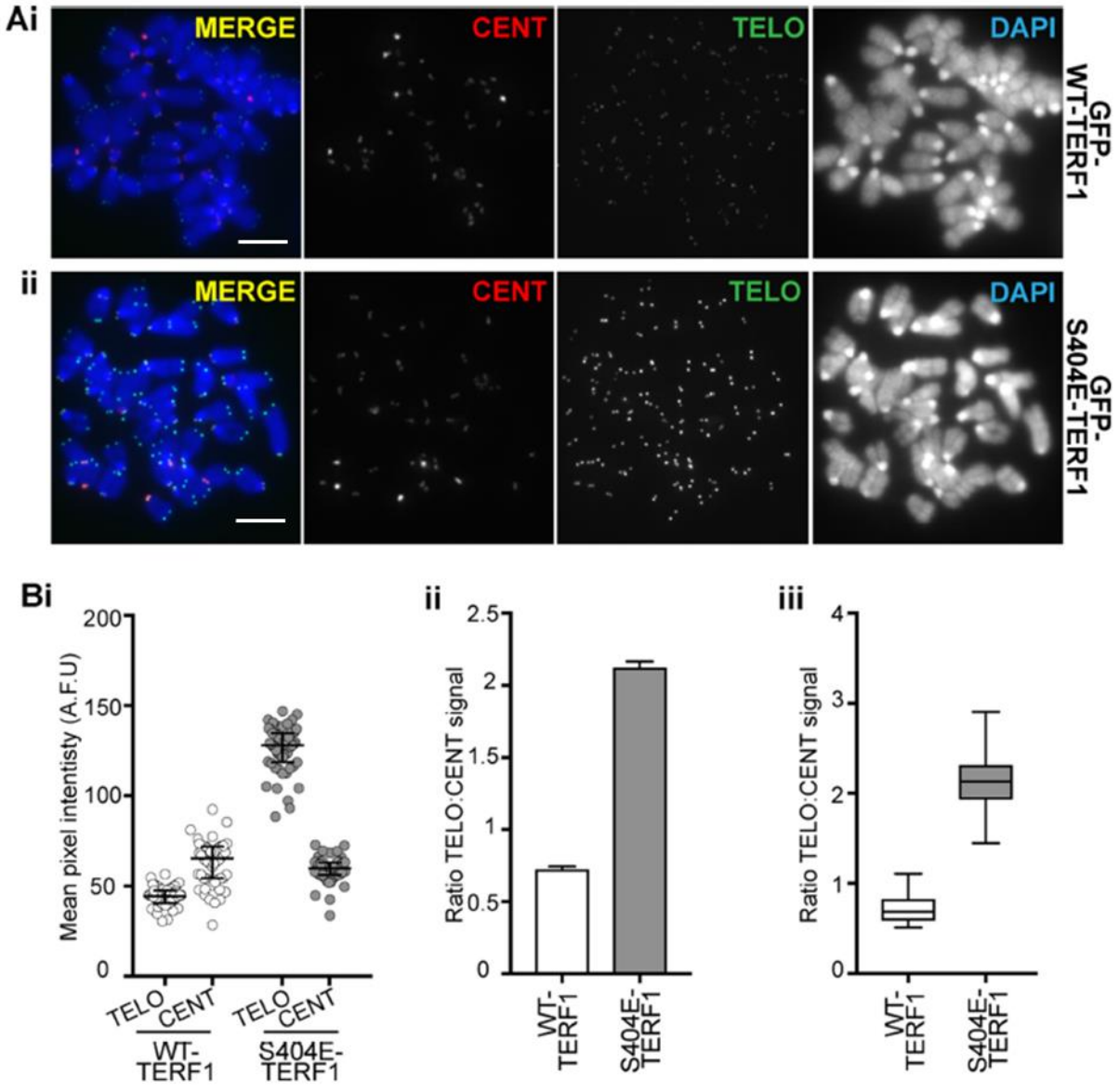
Ai
MERGE
CENT
TELO
DAPI
GFP-WT-TERF1
ii
MERGE
CENT
TELO
DAPI
GFP-S404E-TERF1
Bi
Mean pixel intentisty (A.F.U)
200
150
100
50
0
TELO
CENT
TELO
CENT
WT-TERF1
S404E-TERF1
ii
Ratio TELO:CENT signal
2.5
2
1.5
1
0.5
0
WT-TERF1
S404E-TERF1
iii
Ratio TELO:CENT signal
4
3
2
1
0
WT-TERF1
S404E-TERF1

Figure 3.2.15: Long-term expression of S404E-TERF1 results in telomere lengthening

*(**A**) Telomere (green) and centromere (red)-FISH analyses were performed on mouse ES cells with stable expression of GFP-WT and S404E-TERF1 to assess changes in telomere length. DAPI was used as a nuclear counterstain (blue). Compared to the Tel-FISH signal intensity of (**i**) GFP-WT-TERF1 cells, the Tel-FISH signal intensity of GFP-S404E-TERF1 cells was increased. (**B**) Fluorescence quantification showed increased Tel-FISH signal intensity in GFP-TERF1-S404E compared to GFP-WT-TERF1 cells. **(i)** The scatter plot shows the mean pixel intensities of Telomere and centromere-FISH signals for all metaphase spreads. The centromere FISH signals between the GFP-WT-TERF1 and GFP-S404E-TERF1 cell lines were similar in levels. Tel-FISH signals were normalised against centromere-FISH signals and are shown as (**ii**) column graphs and (**iii**) box and whiskers plots. Tel-FISH signals in GFP-S404E-TERF1 cells were increased by almost three times than those in GFP-WT-TERF1 cells. Error bars in (**Bi**) represent S.E.M. (P = 0.0001, > 50 spreads from three biological replicates were assessed per cell line). Box and whiskers plot shown in (**Bii**) represents Q1, Q2 and Q3, with the maximum and minimum values plotted.*

3.3 Discussion

AURKB is a well-known regulator of mitosis, where it plays critical functions in chromosome segregation through its roles at the centromere and mitotic spindle during mitosis (Carmena et al., 2009, Hochegger et al., 2013). A recent study has shed light on the localisation of AURKB at the pericentric and subtelomeric regions in mouse ES cells (Mallm and Rippe, 2015). AURKB was shown to regulate the generation of non-coding centromeric transcripts (from the centromere regions). These transcripts could, in turn, induce telomerase activity in ES cells (Mallm and Rippe, 2015). However, it is unclear if the association of AURKB with the telomeres correlates with its role in controlling centromeric transcription. Nonetheless, despite its indirect role at the telomeres, the direct function of AURKB at the telomeres has not been uncovered.

This chapter has shown the novel localisation of AURKB at the telomeres of ES cells and investigated its role at the telomeres (**Figure 3.2.1**). The localisation of AURKB at the telomeres is lost with differentiation concomitant with the unique telomere chromatin of ES cells (Wong et al., 2009). Interestingly, loss of AURKB in ES cells results in MTS formation and increased TERF1 binding at telomeres (**Figures 3.2.5 and 3.2.6**). The long telomere lengths and unique telomere chromatin regulation of ES cells are essential for their pluripotency and self-renewal (Huang et al., 2011). In line with this, emerging data show that telomere chromatin of mouse ES cells contain a unique set of proteins. For example, ZSCAN4 (Zalzman et al., 2010) and the unique H3.3S31ph epigenetic mark (Wong et al., 2009) are enriched at the telomeres of pluripotent stem cells. In fact, H3.3S31ph is also regulated by AURKB (Li et al., 2017a). Our results have implicated AURKB as a newly identified protein present in ES cell telomere chromatin and that AURKB function at the telomeres is independent of telomere length maintenance (**Figure 3.2.3**).

With our cell-based binding assays (**Figure 3.2.7**) and *in vitro* kinase assay (**Figure 3.2.8**), we identified S404-TERF1 as the prime candidate for AURKB phosphorylation. However, AURKB may act on other residues on TERF1, similar to its activity on various residues on histone H3 (Goto et al., 2002, Hirota et al., 2005). Although T403-TERF1 was identified as a candidate, the phospho-null mutation, T403A-TERF1, resulted in TERF1 instability, leading to degradation by the proteasome (**Figure 3.2.9 and 3.2.10**). It is possible that T403-TERF1 acts in a similar manner to S367 on human TERF1, where phosphorylation by the ATM kinase disrupts TERF1 binding to telomere and marks TERF1 for degradation (McKerlie et al., 2012). Thus, the phosphorylation of T403-TERF1 may act to prevent degradation. However, further investigation of the kinase that regulates T403-TERF1 and the E3 ligase responsible for proteasome-mediated degradation is required. In addition, experiments, such as mass spectrometry, identifying the cell cycle stage that T403 or S404-TERF1 is phosphorylated will give insights on TERF1 regulation within the cells.

The phosphorylation of S404-TERF1 has not been detected in cells and is a current limitation of this study. Nonetheless, our stable S404-TERF1 mutagenesis studies in mouse cells strongly suggest that S404-TERF1 phosphorylation negatively regulates TERF1 binding to telomeric DNA (**Figure 3.2.11 to 3.2.13**). Furthermore, we have demonstrated that unphosphorylated S404-TERF1 (S404A-TERF1) leads to increased MTS formation, a similar phenotype seen in both AURKB-depleted and TERF1-depleted mouse ES cells (**Figure 3.2.14**). The phosphorylated S404-TERF1 (S404E-TERF1) leads to increased MTS formation together with increased telomere length (**Figure 3.2.14 and 3.2.15**). This is likely caused by a dominant-negative impact of S404E mutation on the endogenous TERF1 function. The MTS formation in both S404A and S404E-TERF1 was accompanied by an increase in DNA damage at the telomeres, indicating the importance of S404-TERF1

phosphorylation in regulating telomere integrity (**Figure 3.2.14**). As our model utilises an overexpression system, TERF1 levels in both S404A and S404E are overexpressed. The overexpression of TERF1 has detrimental effects on the cells including aberrant telomere shortening (van Steensel and de Lange, 1997, Smogorzewska et al., 2000, Munoz et al., 2009) and replication fork stalling which are areas of fragile sites and MTS formations (Ohki and Ishikawa, 2004, Leman et al., 2012). Although the deletion of TERF1 causes aberrant telomere lengthening, it also causes the formation of fragile site and MTS formation (Sfeir et al., 2009, Martinez et al., 2009). Thus, the observed increase in DNA damage in both the S404A and S404E-TERF1 complements previous reports. The loss of TERF1 also leads to increased DNA damage (Beier et al., 2012). Thus, the increased DNA damage observed in S404E-TERF1, compared to S404E-TERF1, may be related to the overall increase in TERF1 protein and the dominant negative binding ability of S404E-TERF1 to telomere DNA, mimicking a TERF1 knockout environment. (Ohki and Ishikawa, 2004, Leman et al., 2012, Sfeir et al., 2009, Martinez et al., 2009). Nonetheless, future work to understand the function of long-term expression of unphosphorylated S404-TERF1 is needed. In addition, the T403 and S404 – TERF1 residues were candidates of AURKB phosphorylation. Although this chapter has shown the mutation of individual residues, a double mutation can be considered for future work to provide insights into TERF1 phosphorylation by AURKB. This would clarify if the presence of a wildtype residue beside a mutated residue partially rescues the phenotype, preventing further deficiencies. Altogether, our study shows the role of AURKB as a novel TERF1 kinase, and it is required for maintaining telomere integrity in mouse ES cells. A model of AURKB function is shown below (**Figure 3.3.1**).

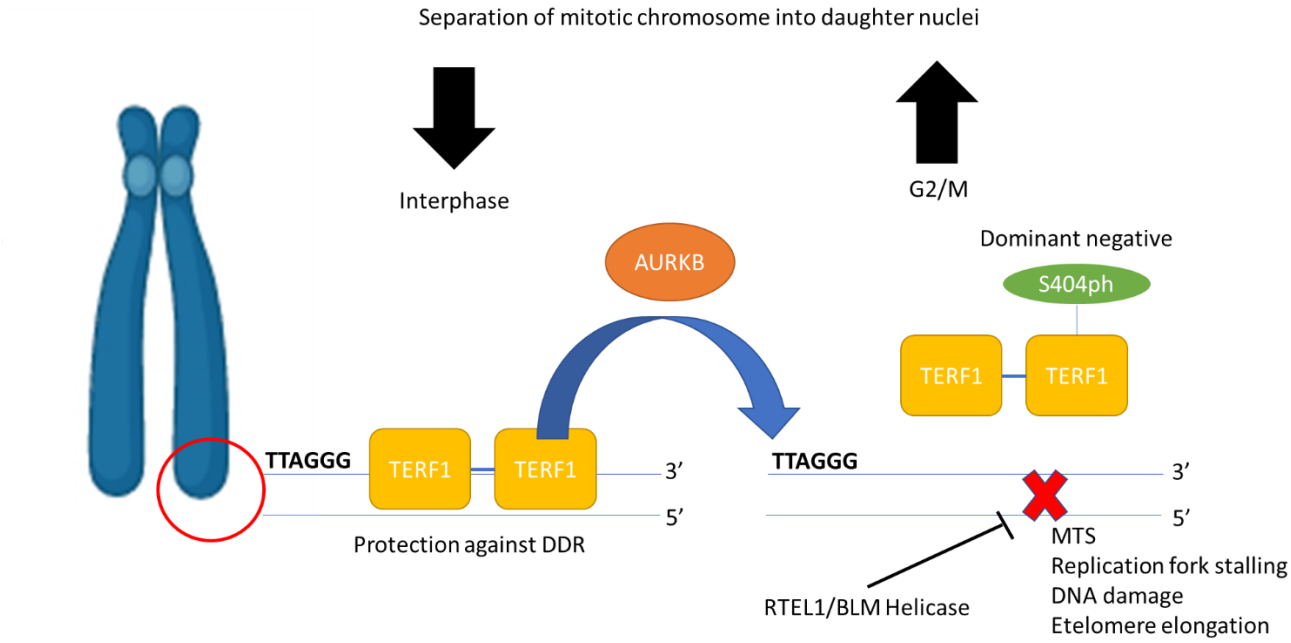

Figure 3.3.1: A model of AURKB function on TERF1

The phosphorylation of S404 by AURKB acts in a dominant negative manner and prevents homodimerized TERF1 from binding to telomere DNA. This causes telomere abnormalities including replication fork stalling, telomere DNA damage and telomere elongation. The presence of MTS formation is indicative of an increase in replication fork stalling at the telomeres. This fork stalling may be rescued by helicases such as BLM and RTEL1. The need for TERF1 detachment may be related to chromosome separation during mitosis.

The binding pattern of TERF1 at the telomeres is dynamic (Mattern et al., 2004). This pattern is regulated through post-translational modification such as phosphorylation (Kim et al., 2008, McKerlie et al., 2012). TERF1 phosphorylation is driven by many kinases, including CDK1, PLK1, ATM and AURKA (McKerlie et al., 2012, Wu et al., 2008, McKerlie and Zhu, 2011). These kinases may act on more than one residue for different functions. For example, phosphorylation of T344 on human TERF1 by CDK1 prepares TERF1 for phosphorylation by PLK1, activating TERF1 binding to telomeric DNA (Wu et al., 2008). In contrast, the phosphorylation of T371 on TERF1 by CDK1 prevents TERF1 binding to the telomere (McKerlie and Zhu, 2011). Here, we have identified AURKB as a novel kinase that targets S404-TERF1, a residue located on the highly conserved Myb DNA-binding domain. The phosphorylation of neither S404-mouse TERF1 nor its corresponding/analogous position on human TERF1 were previously reported. Like CDK1, AURKB may target other residues on TERF1. In line with the possibility of AURKB in phosphorylating other residues on TERF1, previous reports have shown that AURKB phosphorylates various residues on Histone H3 (H3S10 and H3S28) (Goto et al., 2002, Hirota et al., 2005). Nonetheless, the phosphomimic (S404E-TERF1) data suggests that phosphorylation of S404-TERF1 negatively regulates TERF1 binding to the telomere DNA. More importantly, we have shown that AURKB inhibition together with S404-TERF1 phospho-mutants did not further increase MTS formation (**Figure 3.2.14A**), suggesting a link between AURKB-inhibited cells and unphosphorylated S404-TERF1 in mouse ES cells (**Figure 3.2.6 and 3.2.14A**). In addition, TERF1 binding to telomere DNA was increased in AURKB-depleted cells (unphosphorylated S404-TERF1 phenotype) while S404E-TERF1 (phosphorylated phenotype) showed impaired binding of TERF1 to telomere DNA. Thus, we propose that AURKB phosphorylates S404-TERF1 to releases TERF1 from telomere DNA (**Figure 3.2.7, 3.2.13** and **3.3.1**).

Proper telomere maintenance in ES cells is maintained by the regulation of TERF1 binding, through the phosphorylation of S404-TERF1 by AURKB. These data support previous studies that show the importance of a strict TERF1 regulation where both the overexpression (van Steensel and de Lange, 1997, Smogorzewska et al., 2000, Sfeir et al., 2009, Schneider et al., 2013) and loss (Sfeir et al., 2009, Martinez et al., 2009) of TERF1 have harmful effects on the cells such as telomere shortening, activation of DNA damage responses and cell death.

TERF1 is highly expressed in pluripotent cells (Schneider et al., 2013, Varela et al., 2011). Thus, the unique localisation of AURKB and its phosphorylation of S404-TERF1 at the telomere of ES cells may provide additional regulation of TERF1 binding to telomere DNA. This rapid and reversible regulation may be critical as TERF1 is involved in many processes, including telomere length control and telomere DNA replication throughout the cell cycle (van Steensel and de Lange, 1997, Smogorzewska et al., 2000, Sfeir et al., 2009). Interestingly, the inhibition of AURKB led to telomere shortening function (Mallm and Rippe, 2015). A reduction in telomerase activity was observed with either AURKB inhibition or centromere RNA depletion via RNase-H-mediated degradation. *In vitro,* phosphorylation showed that AURKB phosphorylates TERT for telomerase activity, and this activity is enhanced with the expression of centromere RNA function (Mallm and Rippe, 2015). Consistently, we have shown that constant phosphorylation of S404-TERF1, presumably by AURKB, also results in telomere lengthening due to the loss of TERF1 binding (**Figure 3.2.15**). This result was complemented by another study that showed telomere lengthening with a dominant negative TERF1 mutant (van Steensel and de Lange, 1997), further suggesting that S404E-TERF1 acts in a dominant negative manner. Together, these studies and data strongly suggest that AURKB regulates telomere length indirectly.

In conclusion, this study identified AURKB as a novel TERF1 kinase, and the regulation of S404-TERF1 phosphorylation mediates TERF1 binding to telomere DNA and maintains telomere integrity in mouse ES cells. The dynamic function of AURKB is still being investigated where recent studies have identified its association with pluripotency (Lee et al., 2012) and control of telomerase activity (Mallm and Rippe, 2015). This chapter has contributed to understanding AURKB function and pluripotent stem cell biology.

3.4 Supplementary Figures

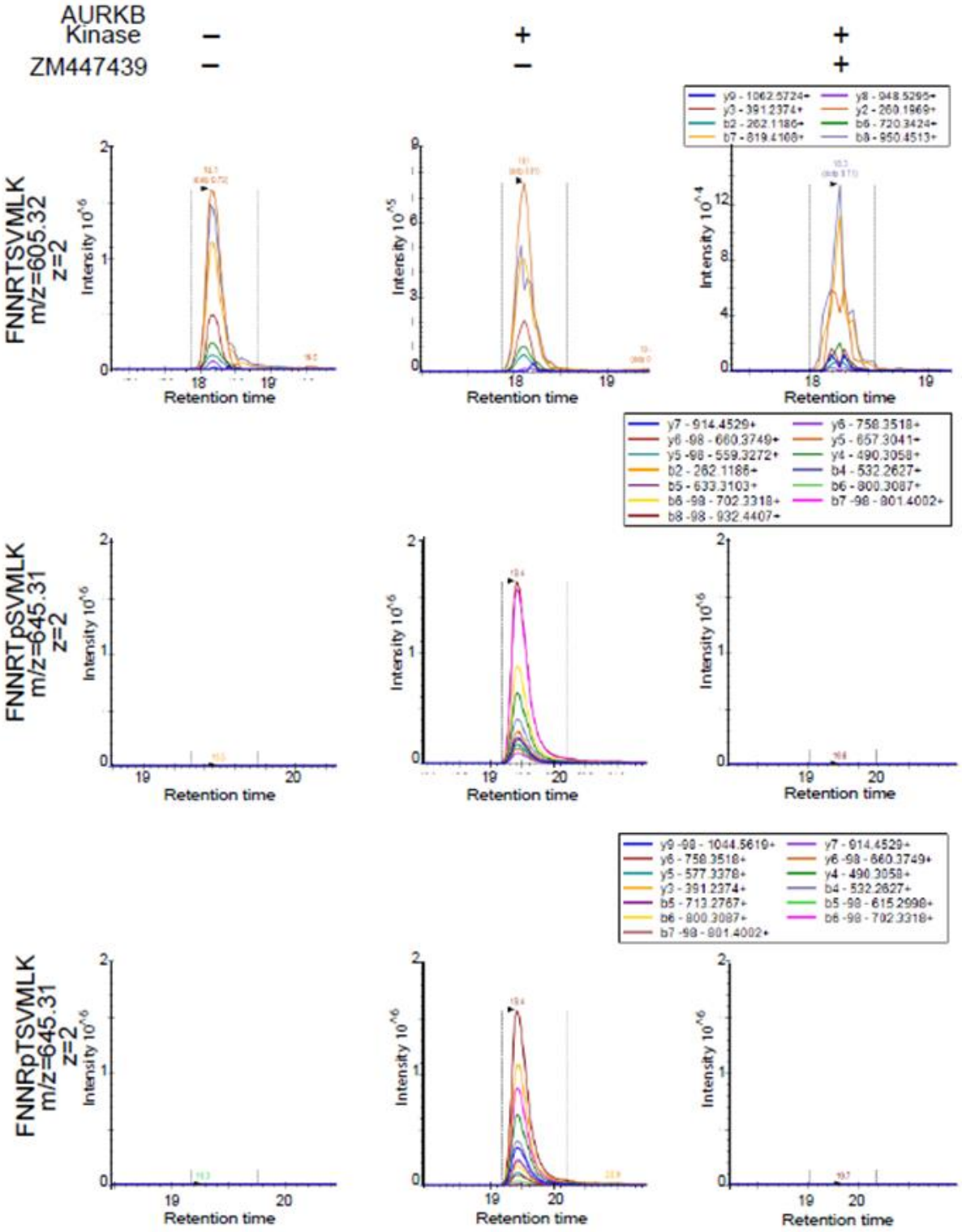

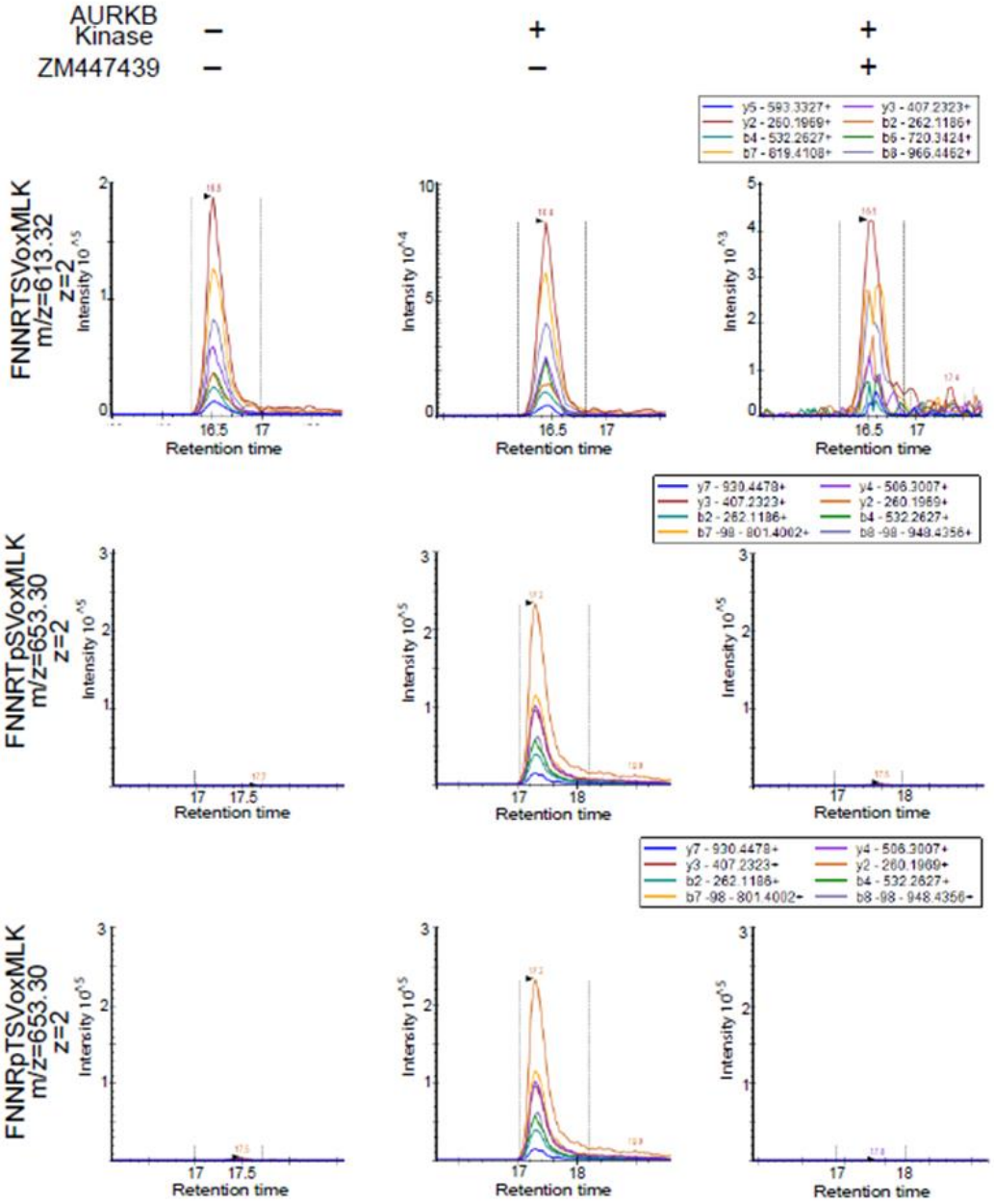

	% of peptide in		
Kinase	-	+	+
Inhibitor	-	-	+
FNNRTSVMLK	91.22	15.55	84.35
FNNRT**pS**VMLK or FNNR**pT**SVMLK	0.01	73.39	7.12
FNNRTSVM[+16]LK	8.74	1.83	4.12
FNNRT**pS**V**ox**MLK or FNNR**pT**SV**ox**MLK	0.03	9.24	3.79

Supplementary figure 3.4.1: Summary of MRM results.

Near 100% of the FNNRTSVMLK peptide was unphosphorylated in the absence of AURKB. Incubation with AURKB resulted in S404 (and/or T403) phosphorylation on approx. 80% of the FNNRTSVMLK peptide, which was inhibited by the addition of the AURKB inhibitor. Moreover, approx. 8-10% of the Methionine residues appeared to be oxidized in each sample. Shown are the MRM traces of the few transitions used to differentiate between FNNRTpSVMLK and FNNRpTSVMLK. The mass-to-charge ratio (m/z), the charge (z) and the monitored transitions are shown for each peptide. The MRM tracAes of six peptides are shown across the three different conditions. These peptides are phosphorylated and oxidized variants of the FNNRTSVMLK peptide. The mass-to-charge ratio (m/z), the charge (z) and the monitored transitions are shown for each peptide. Of note, the oxidation of Methionine, a common post-translational modification known to happen spontaneously during sample preparation, has no significant impact on phosphorylation of the peptide. In addition, only a few transitions can be used to distinguish FNNRTpSVMLK and FNNRpTSVMLK (as well as FNNRTpSVoxMLK and FNNRpTSVoxMLK). Most transitions shown here are common between these variants resulting in nearly identical MRM traces.

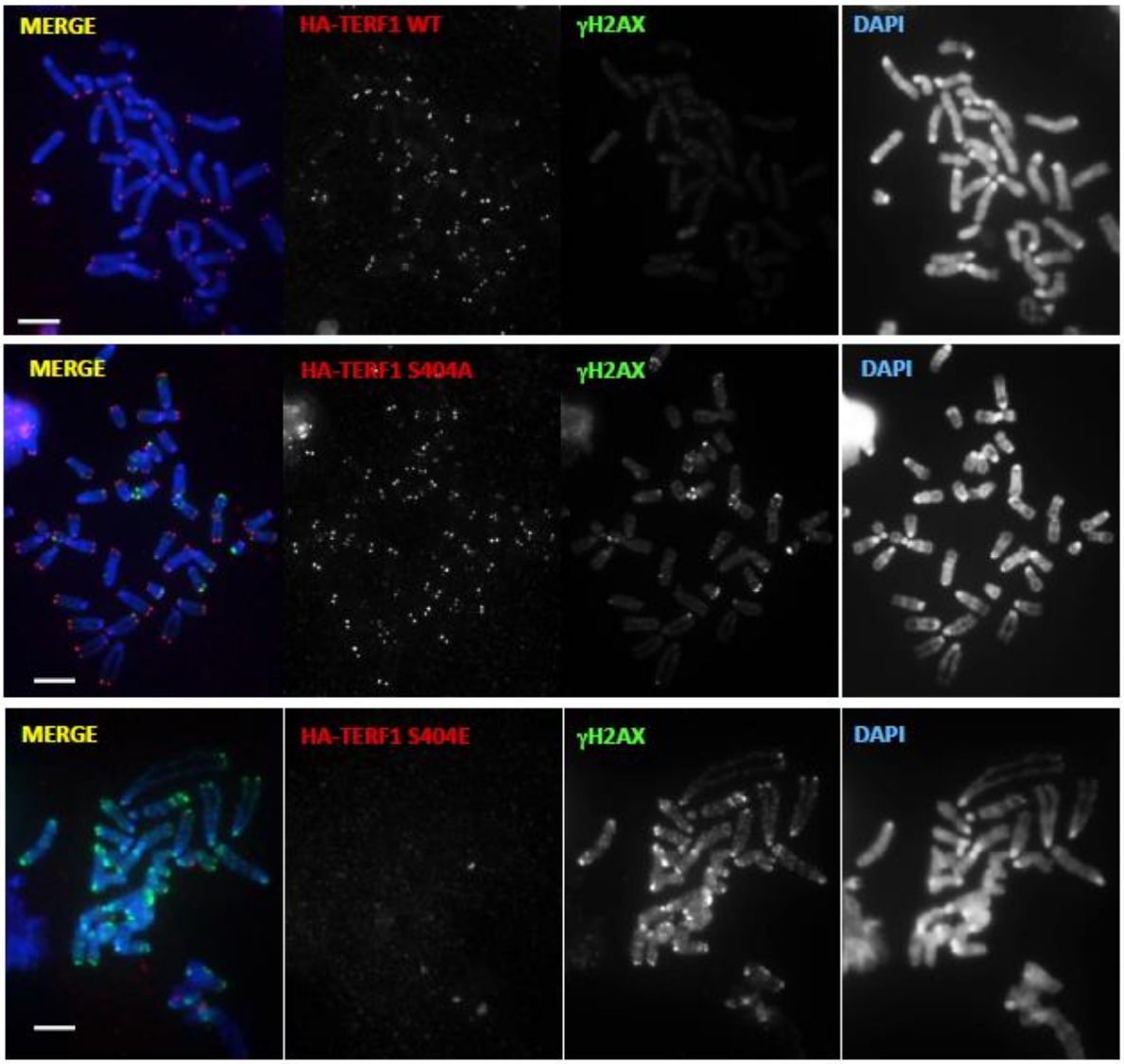

Supplementary figure 3.4.2: S404E-TERF1 induces an increase in γH2AX levels at the telomeres

Mouse ES cells were subjected to TERF1 siRNA depletion followed by transfection with siRNA resistant HA-tagged WT, S404A and S404E TERF1 plasmids. Immunofluorescence analyses with antibody against HA (red) and γH2AX (green) showed that when compared to HA-WT-TERF1 cells, γH2AX levels were increased in HA-S404A-TERF1 and HA-S404E-TERF1 cells. In addition, HA-S404E-TERF1 showed weak staining at the telomeres. DAPI was used as a nuclear counterstain (blue). Scale bar represents 5μm.

Chapter 4: Generation of H3.3S31 mutant mouse Embryonic Stem cell lines

4.1 Introduction

4.1.1 Histone PTMs and their role in chromatin regulation

Nucleosomes are the basic building blocks of chromatin. Each nucleosome comprises a segment of DNA wound around comprises two histone proteins H2A, H2B, H3, and H4 (Kornberg, 1974), known as a histone octamer (Andrews and Luger, 2011). The flexible region of the histones, known as the histone tails, protrude from the nucleosome (Hartzog and Winston, 1997). The N-terminal histone tails are subjected to PTMs, including acetylation, methylation (mono-, di- or tri-methylation) and phosphorylation. These PTMs are critical for controlling nucleosome dynamics and transcription (see **Chapter 1**, **Table 1.1** for an overview of PTMs and functions) (Bowman and Poirier, 2015).

Many of the PTMs on histone, specifically those on the N-terminal histone tail, have been extensively studied (Bowman and Poirier, 2015, Bannister and Kouzarides, 2011). Among them, PTMs on histone H3 is best characterised (Zhang et al., 2015). Examples of PTMs on H3 are shown in **Figure 4.1.1**. These various modifications on histone tails are regulated by chromatin re-modellers, including epigenetics writers (histone methyltransferases, acetyltransferases and kinases) and erasers (histone demethylases, deacetylases and phosphatases), and they play essential roles in transcription regulation. For example, the tri-methylation of H3 Lysine 4 by KMT2 is associated with transcriptional activation (Shilatifard, 2012). In contrast, the tri-methylation of H3 Lysine 9 by Suv39H1/2 is linked to transcriptional repression (Barski et al., 2007, Garcia-Cao et al., 2004). Also, lysine acetylation of histones H3 and H4 tails enhance transcription activation by reducing the affinity between histones and DNA and increasing accessibility to DNA for transcription factors (Fischer et al., 2008).

Phosphorylation is a critical PTM that occurs on histone tails. H3 Serine 10 phosphorylation (H3S10ph) and H3 Serine 28 phosphorylation (H3S28ph) are well-established mitotic markers (Goto et al., 2002, Li et al., 2017b). These residues are phosphorylated at the pericentric heterochromatin during prophase, extend to chromosome arms during metaphase, and are lost by anaphase (Hendzel et al., 1997, McManus and Hendzel, 2006). However, neither the function of H3S10ph nor H3S28ph is well-studied. In *S. cerevisiae*, H3S10ph and H3S28ph appear to be dispensable for cell cycle progression as mutations of individual residues (phospho-null mutation of H3S10 or H3S28 to alanine (H3S10A/H3S28A)) or both H3S10A and H3S28A have no impact on mitotic or meiotic chromosome segregation (Hsu et al., 2000). In contrast, H3S10ph is critical for regulating mitosis and meiosis in *Tetrahymena* as H3S10A results in defective chromosome condensation and segregation, leading to chromosome loss (Wei et al., 1999). Interestingly, a study showed that the phosphorylation of H3S10 in MEF cells by AURKB dissociates HP1α from heterochromatin and forms an open chromatin state (Hirota et al., 2005). Nonetheless, the specific function of H3S10ph and H3S28ph in chromatin regulation remains to be fully understood (Wei et al., 1998, Wei et al., 1999, Goto et al., 2002).

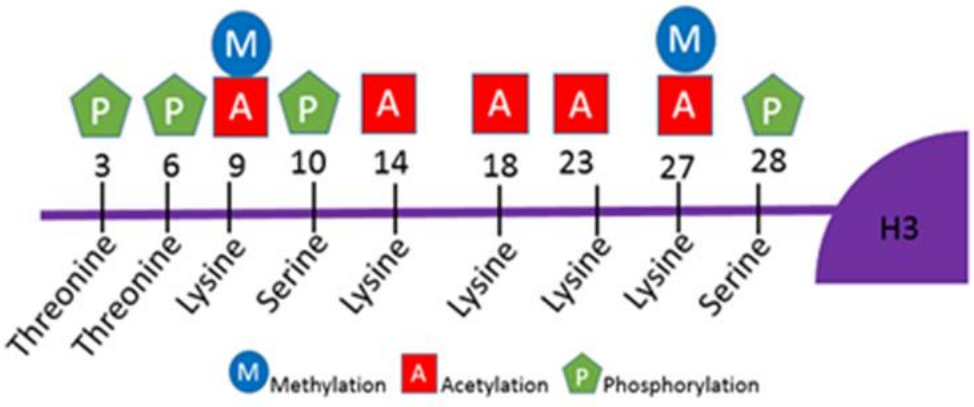

Figure 4.1.1: PTMs on N-terminal tail of Histone H3

Examples of PTMs on the N-terminal tail of H3. Threonine and Serine residues can be phosphorylated (green pentagon), while Lysine residues can be either methylated (blue circles) or acetylated (red square). The numbers indicate the position of the individual residues.

4.1.2 Histone H3.3 and its role in maintaining chromatin integrity

Various studies have identified variants for all histones other than H4 (Bowman and Poirier, 2015, Hake et al., 2006, Sawicka and Seiser, 2012). Similar to the canonical histones, their variants are also subjected to PTMs. Furthermore, these variants play specific roles in various tissues to maintain chromatin integrity (Ueda et al., 2017, Weber and Henikoff, 2014). This thesis will focus on the study of H3.3, a variant of Histone H3 (**Figure 4.1.2A**).

H3.3 is evolutionarily conserved among eukaryotes (Li et al., 2017a, Schulmeister et al., 2007, Wong et al., 2009) and differs from canonical H3.1 by five amino acids (**Figure 4.2.1B**). In addition to the amino acid differences, the histone chaperone that loads canonical H3 differs from the histone chaperone that loads H3.3. H3 is loaded into chromatin by Chromatin Assembly Factor 1 (CAF1) in a replication dependant manner (Tagami et al., 2004). In contrast, H3.3 is loaded in a replication-independent manner by ATRX/DAXX at heterochromatic regions and HIRA at euchromatic regions (Tagami et al., 2004, Wong et al., 2010, Ahmad and Henikoff, 2002).

In mammalian cells, H3.3 is encoded by two distinct genes: *h3f3a* and *h3f3b*. In mouse ES cells, *h3f3b* encodes approximately 70-80% of the total H3.3 protein (Udugama et al., 2015). The homozygous deletion of *h3f3a* in mice identified its importance in testes development and male fertility (Yuen et al., 2014, Tang et al., 2015). Similarly, the homozygous deletion of *h3f3b* in mice also caused detrimental effects such as male sterility, growth deficiency and death at birth (Yuen et al., 2014, Tang et al., 2015). Interestingly, the complete knockout of *h3f3a* and *h3f3b* in mice led to primary oocyte failure and rapid cell death (Bush et al., 2013, Jang et al., 2015, Tang et al., 2015, Tang et al., 2013a). At the cellular level, knockout of both *h3f3a* and *h3f3b* genes in MEF resulted in various chromosomal defects such as

aberrant sister chromatid exchange, polyploidy, aneuploidy and DNA damage (Jang et al., 2015). Together, these studies indicate the importance of H3.3 in embryonic development and chromatin maintenance.

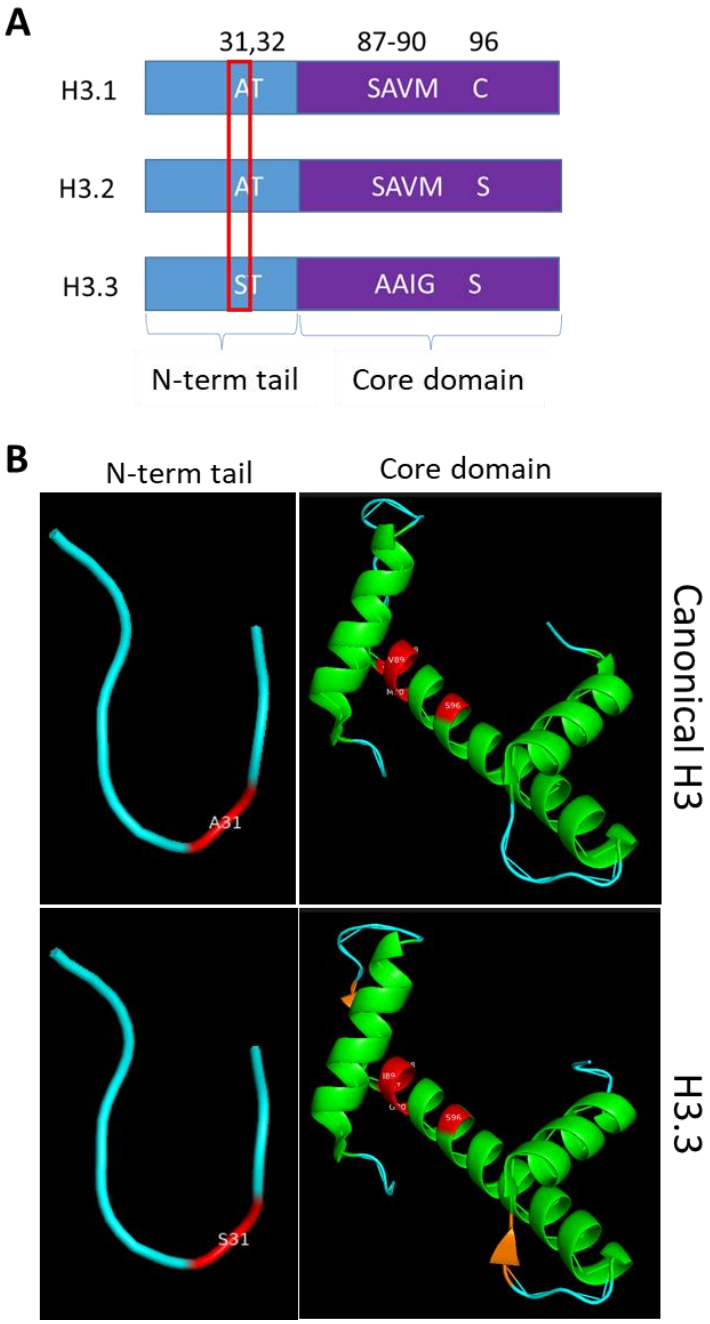

Figure 4.1.2: Amino acid sequence and secondary structure of Histones H3 variants

*(**A**) The differences between amino acid residues in the N-terminal tail (aa 29-35) and globular region (aa 60-135) between canonical H3.1/2 and H3.3 is shown. (**B**) The secondary structures are shown. β sheets – orange; α-helix – red; random loops – cyan. Residues of interest are shown in red. (Canonical H3 - 5bs7 and 4n4h; H3.3 - 5b33 and 4n4i)*

4.1.3 Regulation of H3.3S31 phosphorylation.

The unique serine residue at position 31 in H3.3 is evolutionarily conserved from yeasts to humans (**Table 4.1**) (Elsaesser et al., 2010). Interestingly, in single-cell eukaryotes such as *S. cerevisiae*, H3.3 is present in place of canonical H3 other H3 variants. In contrast, multicellular eukaryotes such as humans utilise H3.3 and other H3 variants to perform specialised functions (Hake et al., 2006).

Various reports have shown the phosphorylation of H3.3S31, enriched specifically during mitosis, in several cell types and organisms, including mouse cells and sea squirts (Hake et al., 2005, Wong et al., 2009, Schulmeister et al., 2007, Hinchcliffe et al., 2016, Sitbon et al., 2020). The alignment of amino acid sequences also shows the evolutionary conservation of H3.3 Serine 31 in various organisms (**Table 4.1**). Furthermore, recent studies have identified AURKB, CHK1 and IκB Kinase α (IKKα) as kinases that phosphorylate H3.3S31 (Li et al., 2017a, Chang et al., 2015, Sitbon et al., 2020, Armache et al., 2020). Interestingly, the enrichment of H3.3 Serine 31 phosphorylation (H3.3S31ph) only localises to the pericentric region of metaphase chromosomes in somatic cells (Hake et al., 2005). In addition to the enrichment of H3.3S31ph at the pericentric region, the enrichment of H3.3S31ph was reported at the telomeres of mitotic chromosomes in ES and embryonic germ cells (Wong et al., 2009). Hence, the localisation of H3.3S31ph at these heterochromatic regions highlight the potential role of H3.3S31ph in heterochromatin maintenance.

Table 4.1: Conservation of H3.3S31 between organisms

Species	N-terminal tail	Histone Core domain	% similarity to human H3.3	Accession no.
Homo sapiens	//KSAPSTGGVK//	//FQSAAIGALQEASEAYL//	-	AAA52654.1
Xenopus laevis	//KSAPSTGGVK//	//FQSAAIGALQEASEAYL//	100	NP_001079375.1
Mus musculus	//KSAPSTGGVK//	//FQSAAIGALQEASEAYL//	100	NP_032237.1
Drosophila melanogaster	//KSAPSTGGVK//	//FQSAAIGALQEASEAYL//	100	CAA57080.1
S. cerevisiae	//KSAPSTGGVK//	//FQSSAIGALQESVEAYL//	90	NP_014367.1
	31	87 90 96		

4.1.4 The function of H3.3 Serine 31 phosphorylation

Most studies of H3.3S31ph have investigated its role during mitosis. H3.3S31ph is vital for cell survival, development, and transcriptional regulation (Chang et al., 2015, Schulmeister et al., 2007, Hake et al., 2005, Sitbon et al., 2020, Armache et al., 2020). One study has demonstrated that H3.3S31ph accumulates along the chromosome arms of lagging or misaligned chromosomes, leading to p53 induction and inhibition of cell proliferation in monkey cells (Hinchcliffe et al., 2016). The masking of H3.3S31ph by antibody microinjection prevented nuclear p53 accumulation on the chromosomes and growth arrest, indicating the importance of H3.3S31ph in cell cycle maintenance and survival.

In another study using chicken DT40 cells, knockout of H3.3 genes results in increased sensitivity to UV light but did not lead to cell death (Frey et al., 2014). Interestingly, this is different from mammalian cells, where knockout of H3.3 led to rapid cell death (Bush et al., 2013, Jang et al., 2015, Tang et al., 2015, Tang et al., 2013a, Frey et al., 2014). Furthermore, when exposed to UV light, DT40 cells lacking H3.3 could not maintain replication fork progression (Frey et al., 2014). However, the expression of phospho-null H3.3S31A mutant

(serine to alanine mutation; phospho-null) in these cells restored fork progression (Frey et al., 2014). Thus, although unphosphorylated H3.3S31 may be necessary for replication fork progression in DT40 cells, further investigation to determine the phenotype of H3.3S31E mutants is required.

Recently, the function of H3.3S31ph in regulation transcription was examined (Martire et al., 2019). The knockdown of H3.3 through shRNA depletion of *h3f3a* and complete knockout of *h3f3b* (Banaszynski et al., 2013) resulted in the reduction of H3.1K27ac, with prominence at the enhancers. Interestingly, inhibition of CHK1 but not AURKB prevented the phosphorylation of H3.3S31, reducing H3K27ac at the enhancers. Further investigation using mass spectrometry identified that H3.3S31ph stimulates p300 activity, a histone acetyltransferase responsible for the acetylation of H3K27 in mouse ES cells. This stimulation resulted in higher levels of H3K27ac at the enhancers (Martire et al., 2019). As many latent enhancers are activated during differentiation, H3.3 knockout cells expressing H3.3S31E were differentiated and showed an increase in H3K27ac at these enhancer regions. This led to an increase in transcription from differentiation-specific genes, indicating that H3.3S31ph is essential for the regulation of chromatin state and transcriptional activation at DNA enhancers

Another study employed a unique method to reduce H3.3 levels within *Xenopus laevis* embryos (Sitbon et al., 2020, Szenker et al., 2012). To knockdown of H3.3 in *Xenopus laevis* embryos, morpholino to target H3.3 specifically was used and resulted in defects during late gastrulation, followed by embryo death (Sitbon et al., 2020, Szenker et al., 2012). The expression of the phospho-mimic mutant H3.3S31D (Serine to Aspartic acid) but not H3.3S31A rescued H3.3 levels. However, only the pulldown of H3.3S31D at gastrulation

showed high levels of H3.3K27ac (Sitbon et al., 2020). The increased H3K27ac was previously reported after H3.3 knockdown with H3.3S31E expression, identifying the importance of H3.3S31ph in transcriptional regulation (Martire et al., 2019).

Another recent study showed the importance of H3.3S31ph in transcriptional regulation (Armache et al., 2020). Clustered regularly interspaced short palindromic repeats (CRISPR) targeting both *h3f3a* and *h3f3b* resulted in the complete knockout of H3.3 in the macrophage cells. Furthermore, the expression of the phospho-mimic, H3.3S31E, in H3.3 knockout macrophage cells but not the phospho-null, H3.3S31A, increased gene expression at regions with high H3.3S31ph levels after stimulation. Interestingly, the H3.3S31E mutant activated SETD2, a histone methyltransferase, to regulate gene expression (Armache et al., 2020). Altogether, these studies show that H3.3S31ph is critical for cellular functions. Furthermore, they demonstrate that H3.3S31ph act to regulate the activity of histone remodellers to maintain gene transcription. To date, H3.3S31ph has been investigated in the context of transcription regulation. Thus, this thesis aims to investigate the function of H3.3S31ph in heterochromatin maintenance.

4.1.5 Aims

H3.3 S31ph is enriched at telomeres of mouse ES cells (Wong et al., 2009). The function of H3.3S31ph at euchromatic regions has been reported. However, its function at heterochromatic regions has yet to be studied. The experiments performed in this chapter aimed to generate HA-tagged and untagged H3.3S31 phospho-null (alanine) and phospho-mimic (glutamic acid) mutations in mouse ES cells void of endogenous H3.3. In Chapter 5, these H3.3S31 phospho-mutant cell lines were used for investigating the impact of the

H3.3S31 mutation on cell survival and heterochromatin maintenance, particularly the role of H3.3S31ph in telomere heterochromatin maintenance.

4.2 Results

4.2.1 Generation of wild-type and mutant H3.3 untagged and HA-tagged expression vectors

In a previous study, a conditional H3.3 knockout mouse ES cell line in which the targeting vector substituted most of exon 2 for *h3f3a* and all of exon 2 for *h3f3b* was established (Tang et al., 2013a). Briefly, the targeting vector contained the *Cre*-LoxP system, which flanked either *h3f3a* or *h3f3b* gene and, a reporter coding sequence. With the expression of *Cre*-recombinase, the knockout of *h3f3a* would result in the expression of yellow fluorescent protein (YFP), while the knockout of *h3f3b* would result in the expression of cyan fluorescent protein (CFP) (Tang et al., 2013a) (**Figure 4.2.1**). The complete loss of endogenous H3.3 is crucial as this will prevent a masking response and directly relate the observed phenotypes with the respective H3.3S31 phospho-mutants. Thus, we aimed to generate H3.3S31 phospho-mutant cell lines in a endogenous H3.3 null background to study the role of H3.3S31ph in heterochromatin maintenance.

Cre-mediated deletion of all *h3f3a* and *h3f3b* genes led to rapid cell death (overview of the process shown in **Figure 4.2.2**). Several studies also reported this phenomenon where knockout of H3.3 in mouse cells led to reduced cell proliferation and cell death (Bush et al., 2013, Jang et al., 2015, Tang et al., 2015, Tang et al., 2013a). Thus, to study the function of H3.3S31ph, H3.3S31 wild-type and mutant histones (Alanine 31 and Glutamic acid 31) were expressed in $h3f3a^{flox/flox}$ $h3f3b^{flox/flox}$ ES cells, respectively, prior to *cre*-mediated knockout of endogenous H3.3.

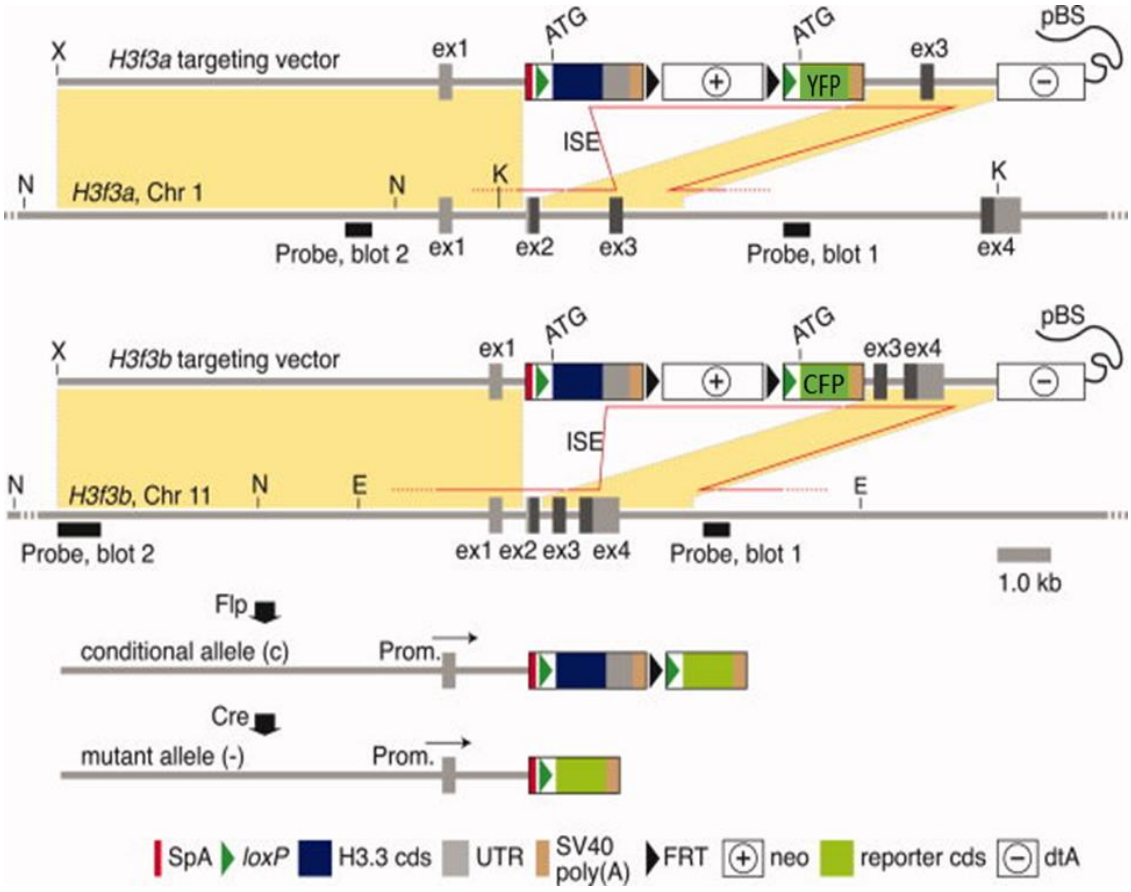

Figure 4.2.1: H3.3 targeting vectors and knocked in strategies.

The core region of cassettes was nearly identical for h3f3a and h3f3b, and the difference was in the UTR, which gives the specificity for homologous recombination. This targeting sequence substituted for much of exon 2 for h3f3a (encoding the first 17 amino acids) and all of exon 2 for h3f3b (encoding the first 41 amino acids). Exposure to Flp recombinase removed the neo selection cassette. The cassette arrangement and positioning of the loxP sites allows for conditional allelic replacement: on Cre-mediated excision of the H3.3 coding sequences (cds), an alternative cds is brought under control of the endogenous promoter; this being the YFP cds for h3f3a, and the CFP cds for h3f3b. The yellow shading marks the regions where strand exchange would be expected to occur. The red line marks a potential and undesired internal strand exchange (ISE) event occurring due to internal regions of homology. Such events would lead to the loss of upstream targeting vector sequence, including the loxP site.

SpA, synthetic splice acceptor; ex, exon; neo, neomycin positive selection cassette; dtA, diphtheria toxin A chain negative selection cassette; E, EcoRI, K, KpnI; N, NheI site; X, XhoI; pBS, pBluescript vector.

Adapted from (Tang et al., 2013b)

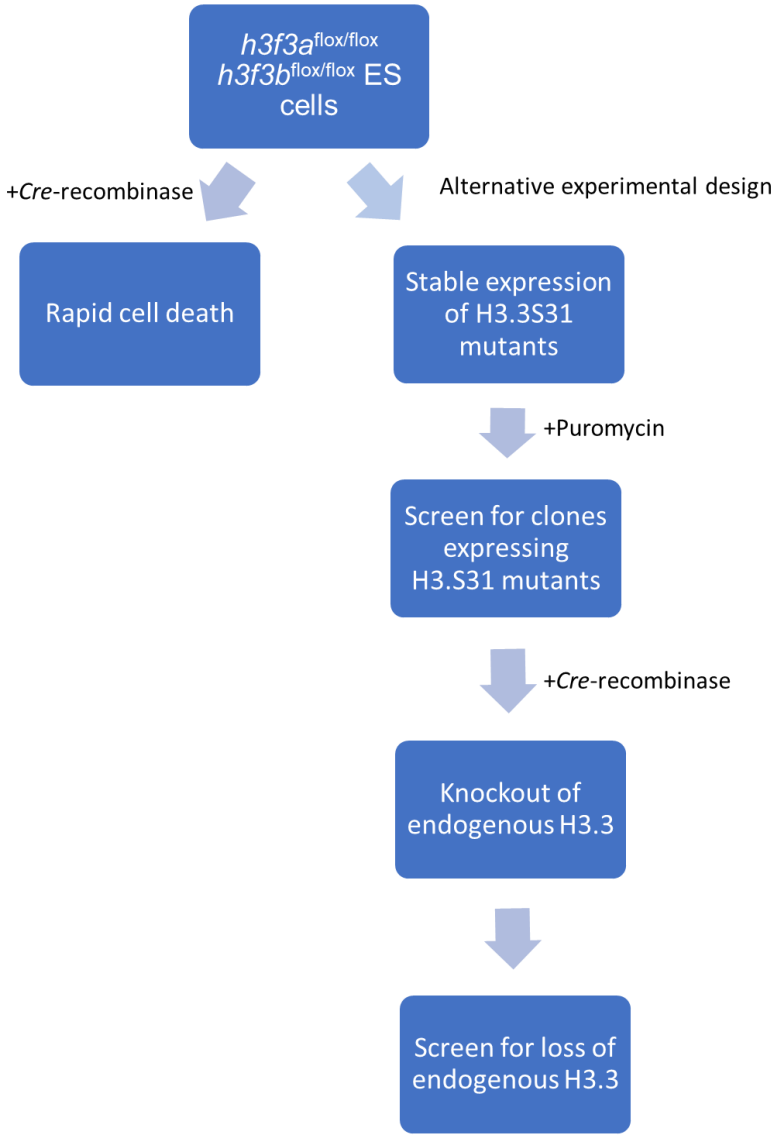

Figure 4.2.2: Overview of experimental design for generating H3.3S31 mutant cell lines

h3f3a$^{flox/flox}$ h3f3b$^{flox/flox}$ ES cells transfected with of Cre-recombinase resulted in rapid cell death (Left). Thus, an alternative experimental design was employed to generate H3.3S31 mutant cell lines. H3f3a$^{flox/flox}$ h3f3b$^{flox/flox}$ ES cells were transfected with wild-type, S31A and S31E expression vectors and clones were selected for resistance to puromycin (right). The expression of H3.3-HA was determined by immunoblotting using an antibody against HA while PCR analyses with specific primers determined the expression of untagged H3.3. Endogenous H3.3 was knocked out by transfection of Cre-recombinase. The loss of endogenous H3.3 in ES cell clones was screened by FACS analyses and immunoblotting with antibody against GFP to determine YFP/CFP expression, southern blotting and, immunofluorescence analyses with antibody against H3.3S31ph.

To study the function of H3.3S31ph, the serine 31 residue of H3.3 was mutated to either alanine (S31A-H3.3, phospho-null) or glutamic acid (S31E-H3.3, phospho-mimic, **Figure 4.2.3A**). As previously discussed in **Chapter 3**, Alanine was selected as it has no charge and cannot be phosphorylated (Li et al., 2017a, Hake et al., 2005, Chan et al., 2017, Armache et al., 2020, Sitbon et al., 2020, Martire et al., 2019). In contrast, glutamic acid was selected as it is negatively charged, allowing it to act as a constitutively phosphorylated serine residue (Chan et al., 2017, Fink et al., 2007, Rios-Doria et al., 2009, Armache et al., 2020, Martire et al., 2019). Although other amino acids, including valine and aspartic acid, have also been used as phospho-null and phospho-mimic substitutions respectively (Dissmeyer and Schnittger, 2011, Aihara et al., 2016, Sitbon et al., 2020), alanine and glutamic acid are commonly used.

Studies have used a wide range of protein tags to determine the localisation of H3.3. These tags include YFP (Goldberg et al., 2010), Myc (Wong et al., 2009), and HA (Sitbon et al., 2020). Thus, a HA tag was selected for this study to identify the localisation and differentiate between endogenous and exogenous H3.3. Furthermore, the HA tag was selected due to its considerably small size of 1 kDa and was fused to the C-terminal of H3.3 (H3.3-HA). Nonetheless, untagged wild-type S31A and S31E-H3.3 clones were also generated presuming that the HA tag was detrimental to the cells. Altogether, 6 different *h3f3a*$^{flox/flox}$ *h3f3b*$^{flox/flox}$ mouse ES cell lines were established: HA-tagged and untagged H3.3 wild-type, S31A and S31E cell lines, respectively.

The S31 mutations were created by substituting the nucleotides TCT on H3.3 wild-type to either GCT for S31A-H3.3 or GAG for S31E-H3.3 (**Figure 4.2.3B**). To determine the successful incorporation of HA tagged and untagged wild-type, S31A and S31E-H3.3 cDNA

into the expression vector, restriction enzyme digests (**Figure 4.2.3Ci**) and sequencing analyses were performed (**Figure 4.2.3D and E**). The results showed that untagged and HA-tagged wild-type, S31A and S31E H3.3 constructs were successfully incorporated into the expression vector. Furthermore, for stable transfection into *h3f3a*$^{flox/flox}$ *h3f3b*$^{flox/flox}$ mouse ES cells, these plasmids were linearised (**Figure 4.2.3Cii**), as previously described in **Section 2.2.2**, prior to transfection.

.

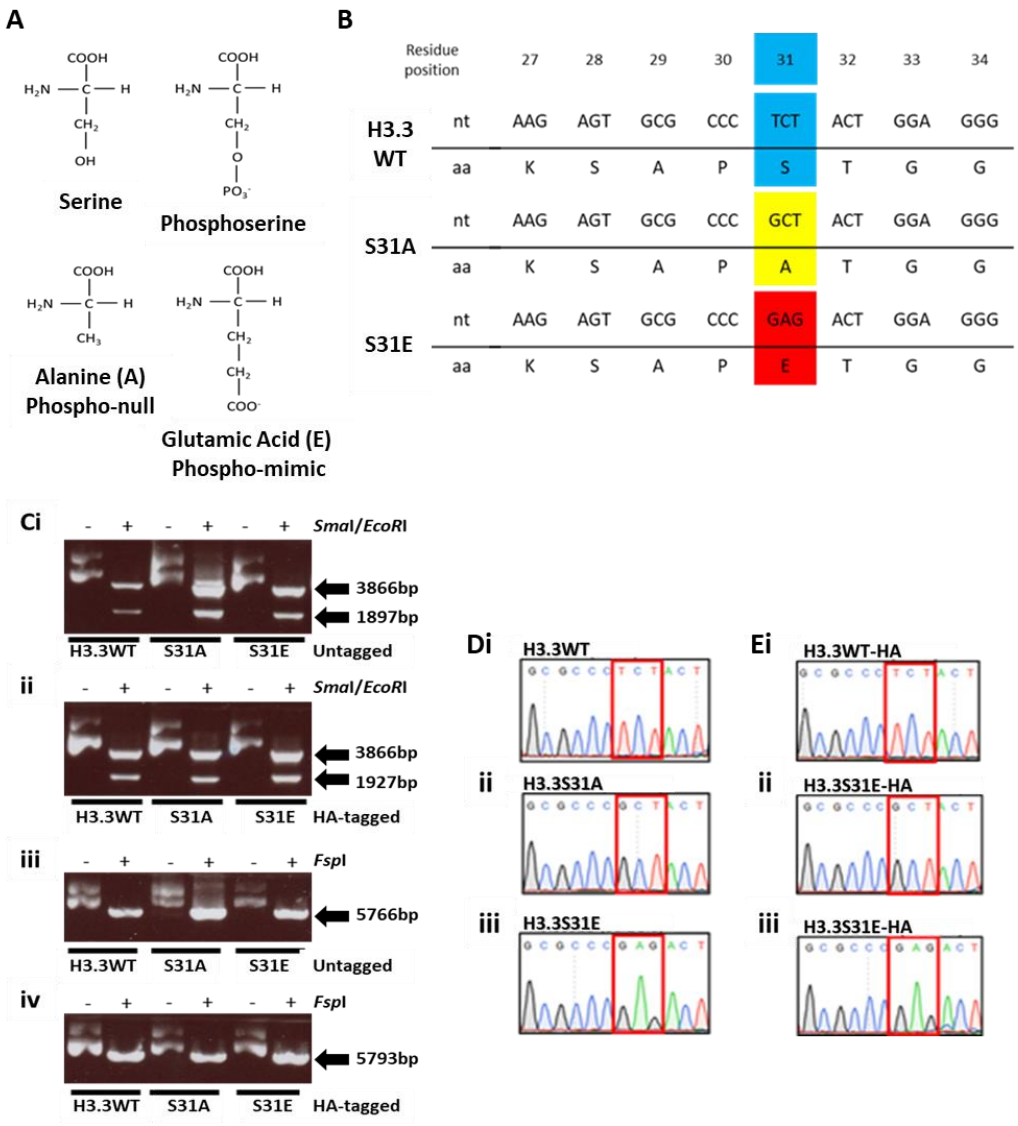

Figure 4.2.3: Generation of H3.3 wild-type, S31A and S31E mammalian expression plasmids

*(**A**) Chemical structure of serine, phosphoserine, alanine (phospho-null) and glutamic acid (phospho-mimic) is shown.. (**B**) A segment of the H3.3 protein sequence, ranging from amino acid residues 23 to 34, is shown. Serine 31 (H3.3 WT, blue) residue is substituted with either an Alanine (H3.3 S31A, yellow) or Glutamic acid (H3.3 S31E, red). Amino acids are shown as single-letter codes. nt - nucleotide, aa – amino acid. (**Ci**) Restriction enzyme digest of pHL-EF1α-GW-iP-A expression plasmid containing H3.3 wild-type and mutants (untagged and HA-tagged H3.3) with SmaI and EcoRI. (**Cii**) Linearization of H3.3 wild-type and mutant plasmids (untagged and HA-tagged H3.3) with FspI. (**D/E**) Chromatograms from sequencing experiments of (**D**) untagged and (**E**) HA-tagged H3.3 showing the substitution (red box) of (**i**) S31 with (**ii**) A31 or (**iii**) E31.*

4.2.2 Expression of HA-tagged wild-type and mutant H3.3 in ES cells

Firstly, to determine if wild-type, S31A and S31E HA-tagged H3.3 were expressed in *h3f3a*$^{flox/flox}$ *h3f3b*$^{flox/flox}$ ES cells, immunoblot analyses using a specific antibody against the HA-tag were performed on ES cell colonies (**Figure 4.2.4A**). The results showed that wild-type (upper panel), S31A (middle panel) and S31E (lower panel) HA-tagged H3.3 were expressed in *h3f3a*$^{flox/flox}$ *h3f3b*$^{flox/flox}$ ES cells (**Figure 4.2.4A**). Compared to S31A-H3.3-HA, wild-type and S31E-H3.3-HA were expressed at greater levels (for example, lanes 5 and 6 of **Figure 4.2.4A**). Nonetheless, the clones expressing similar levels of H3.3S31 mutant proteins were selected for downstream and further experiments (wild-type-H3.3-HA clone 5; S31A-H3.3-HA clone 8; S31E-H3.3-HA clone 2). In addition, immunoblotting was performed to determine if the relative abundance of H3.3 levels were similar to wild-type, S31A and S31E HA-tagged-H3.3 cell lines (**Figure 4.2.4B**). The results indicated that H3.3 and H3.3-HA were expressed at similar levels between cells expressing wild-type, S31A and S31E-HA-tagged H3.3.

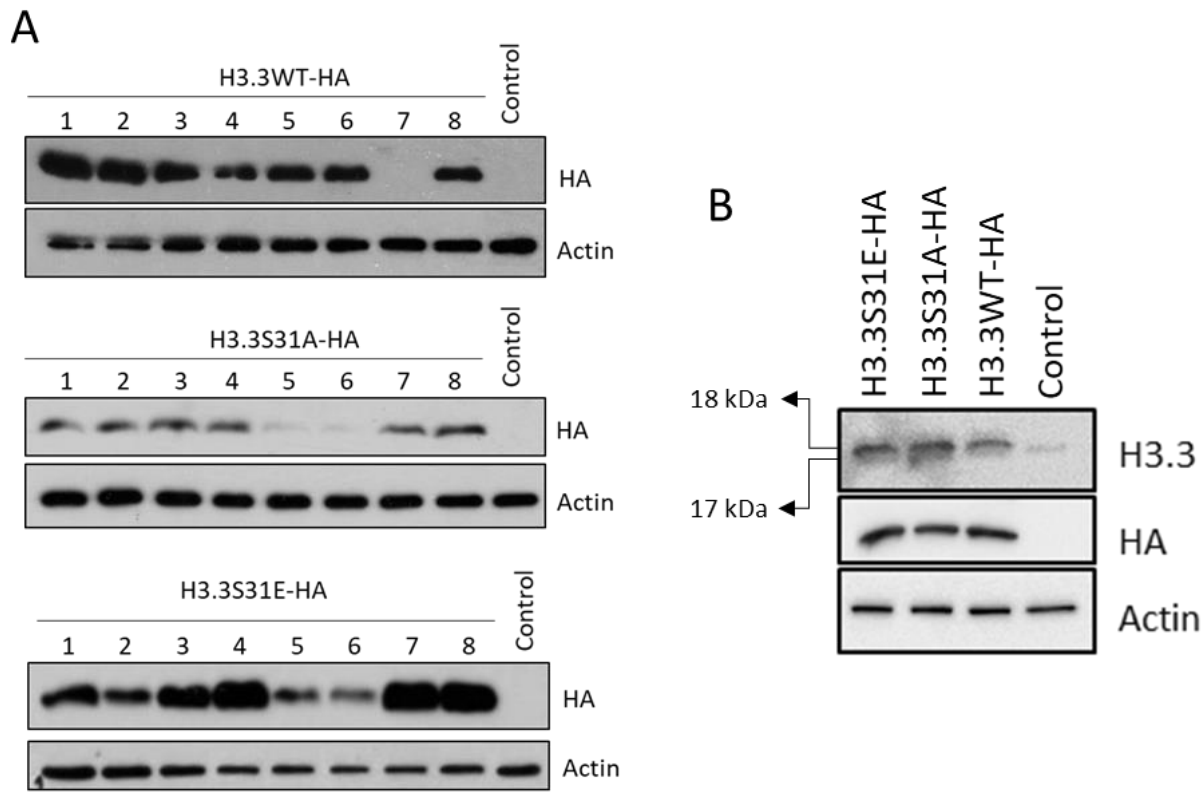

Figure 4.2.4: Expression of wild-type, S31A and S31E HA-tagged-H3.3 in *h3f3a*$^{flox/flox}$ *h3f3b*$^{flox/flox}$ ES cells

(A) *Wild-type, S31A and S31E HA-tagged H3.3 expression plasmids were transfected into h3f3a*$^{flox/flox}$ *h3f3b*$^{flox/flox}$ *mouse ES cells and their expressions in the respective clones were determined by immunoblotting with a specific antibody against HA. Wild-type, S31A and S31E HA-tagged H3.3 were successfully expressed in h3f3a*$^{flox/flox}$ *h3f3b*$^{flox/flox}$ *mouse ES cells. (**B**) Immunoblotting was performed on H3.3 wild-type-HA clone #5, H3.3S31A-HA clone #8 and H3.3S31E-HA clone #2 with antibodies specific to HA and H3.3. Endogenous H3.3 (17KDa) was detected in untransfected and transfected cells lines while wild-type, S31A and S31E HA-tagged H3.3 (18 KDa) were detected only in transfected h3f3a*$^{flox/flox}$ *h3f3b*$^{flox/flox}$ *ES cells. HA-tagged H3.3 was not detectable in untransfected h3f3a*$^{flox/flox}$ *h3f3b*$^{flox/flox}$ *ES cells (control). Actin was used as a loading control.*

Having established the expression of wild-type, S31A and S31E HA-tagged H3.3 proteins in *h3f3a*$^{flox/flox}$ *h3f3b*$^{flox/flox}$ ES cells, their deposition into chromatin and distribution in the genome was next investigated. Immunofluorescence analyses were performed using a specific antibody against HA and ATRX, a histone H3.3 chaperone (Wong et al., 2010). ATRX localises to heterochromatic regions such as the telomeres (punctate signals) and pericentric regions where it deposits H3.3 into chromatin (diffused patterns) (Wong et al., 2010). The results showed that wild-type, S31A and S31E HA-tagged H3.3 were expressed throughout the nucleus and colocalised with ATRX at the telomeres of interphase cells (**Figure 4.2.5A**). In metaphase cells, wild-type, S31A and S31E HA-tagged H3.3 were found to be distributed across the chromosome arms, with enrichment at the telomeres and the pericentric regions (**Figure 4.2.5B**).

To further investigate if wild-type, S31A and S31E HA-tagged H3.3 localised to the telomeres, immunofluorescence analyses were performed using antibodies against HA and TERF1. TERF1 is a telomere specific protein and thus was used as a telomere marker. The results showed that wild-type, S31A and S31E HA-tagged H3.3 colocalised with TERF1 at the telomeres of both interphase and mitotic cells (**Figure 4.2.6**). Together, these results showed that wild-type, S31A and S31E HA-tagged H3.3 were distributed throughout the chromosomes, including the telomeres.

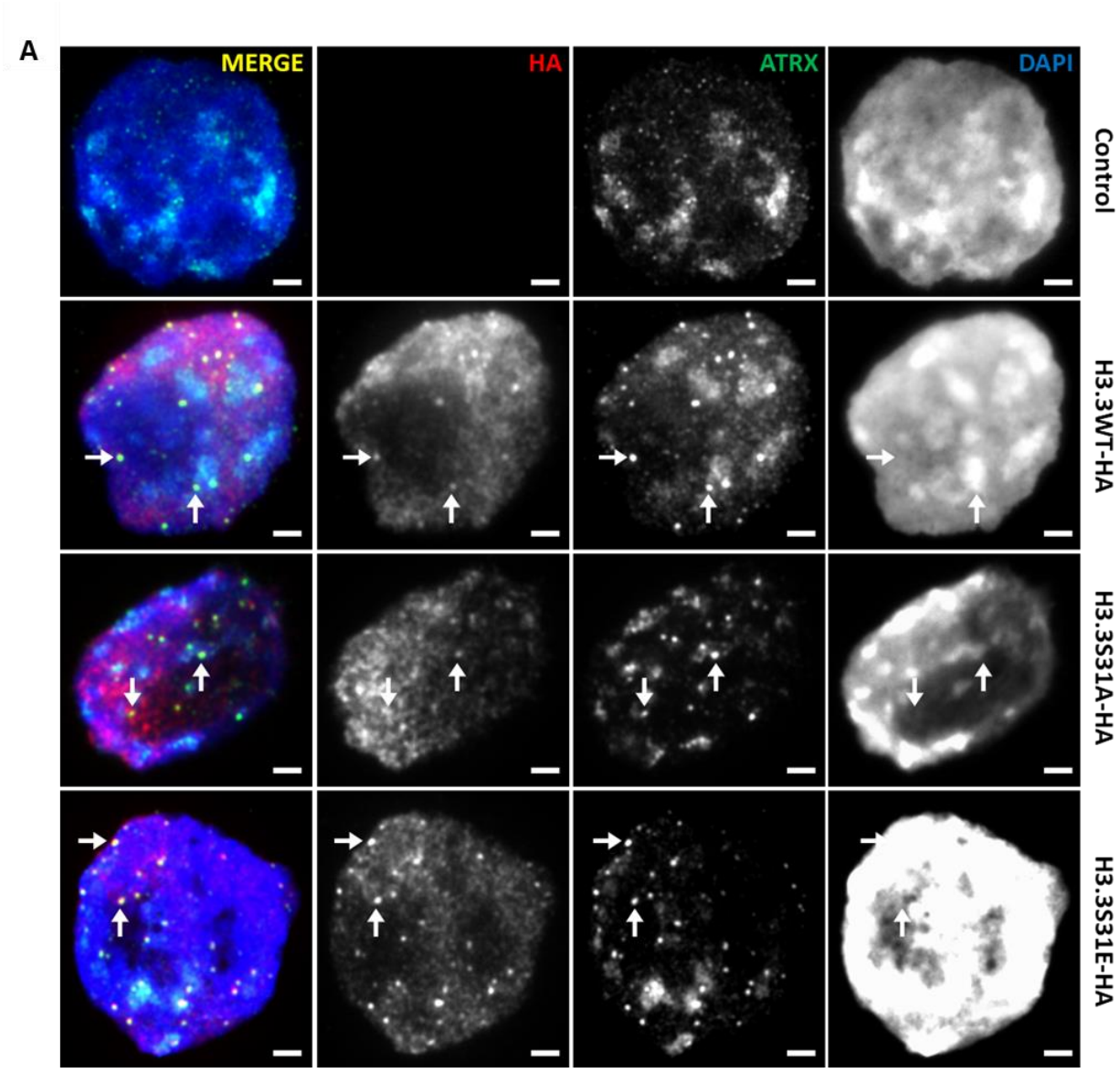
A
MERGE
HA
ATRX
DAPI
Control
H3.3WT-HA
H3.3S31A-HA
H3.3S31E-HA

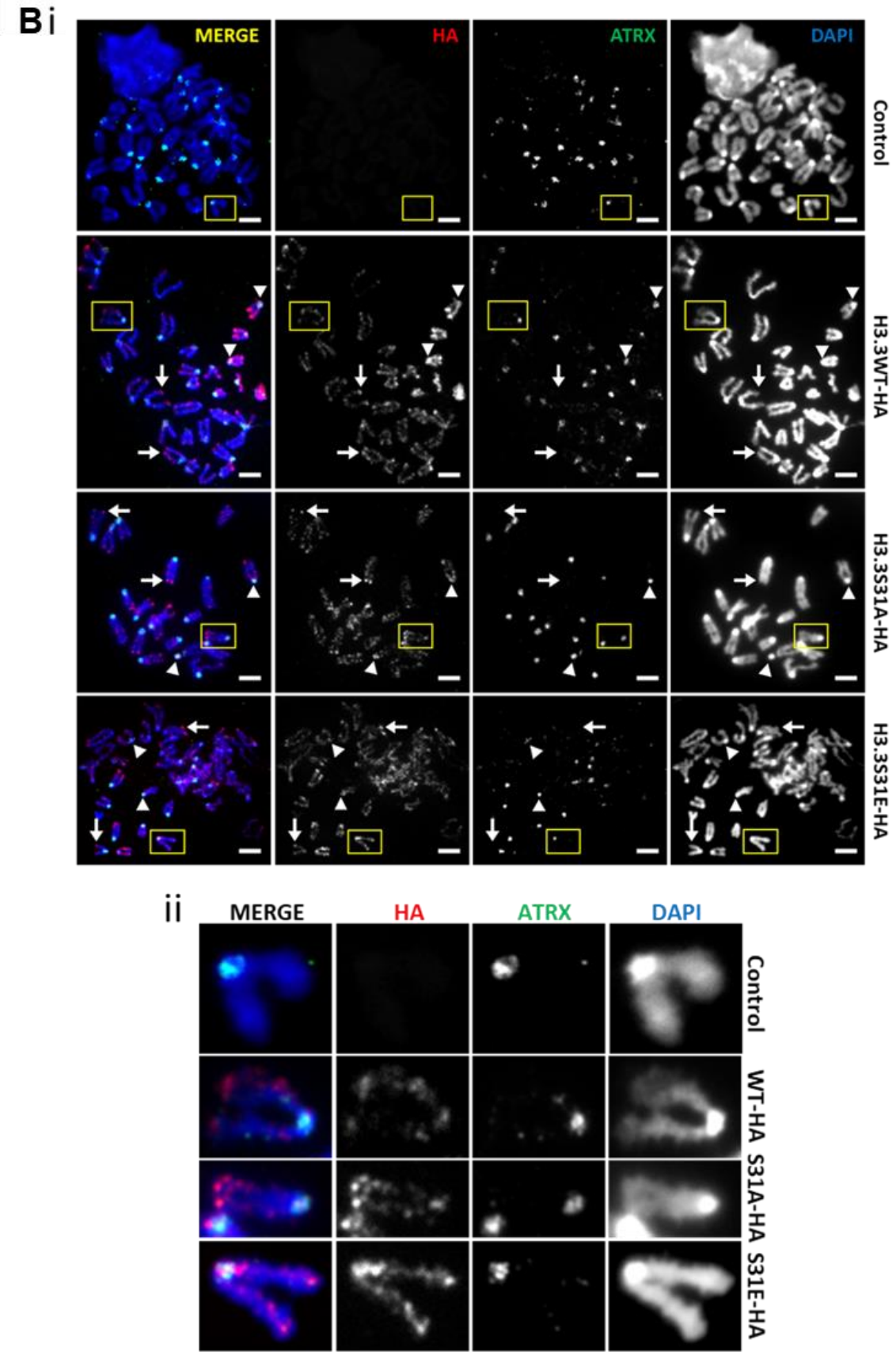
Bi
MERGE
HA
ATRX
DAPI
Control
H3.3WT-HA
H3.3S31A-HA
H3.3S31E-HA
ii
MERGE
HA
ATRX
DAPI
Control
WT-HA
S31A-HA
S31E-HA

Figure 4.2.5: Distribution of wild-type, S31A and S31E HA-tagged H3.3 in ES cells

*(**i**) Immunofluorescence analyses were performed on wild-type, S31A and S31E HA-tagged H3.3 clone with antibodies against HA tag (red) and ATRX (green) to determine their deposition into chromatin. Wild-type, S31A and S31E HA-tagged H3.3 were also distributed throughout the chromatin and, colocalised with ATRX at the telomeres of interphase cell (**A**; arrows) and at the pericentric region of mitotic cells (**B**; arrowhead). The HA/ATRX co-staining signals were weaker in S31A-H3.3-HA cells, but stronger in S31E-H3.3-HA cells, when compared to those in wild-type-H3.3-HA cells. HA staining was undetected in h3f3a$^{flox/flox}$ h3f3b$^{flox/flox}$ ES cells (control). An enlarged image of the selected region (yellow box) is shown in (**ii**). DAPI was used as a nuclear counterstain. Scale bar represents 4 μm.*

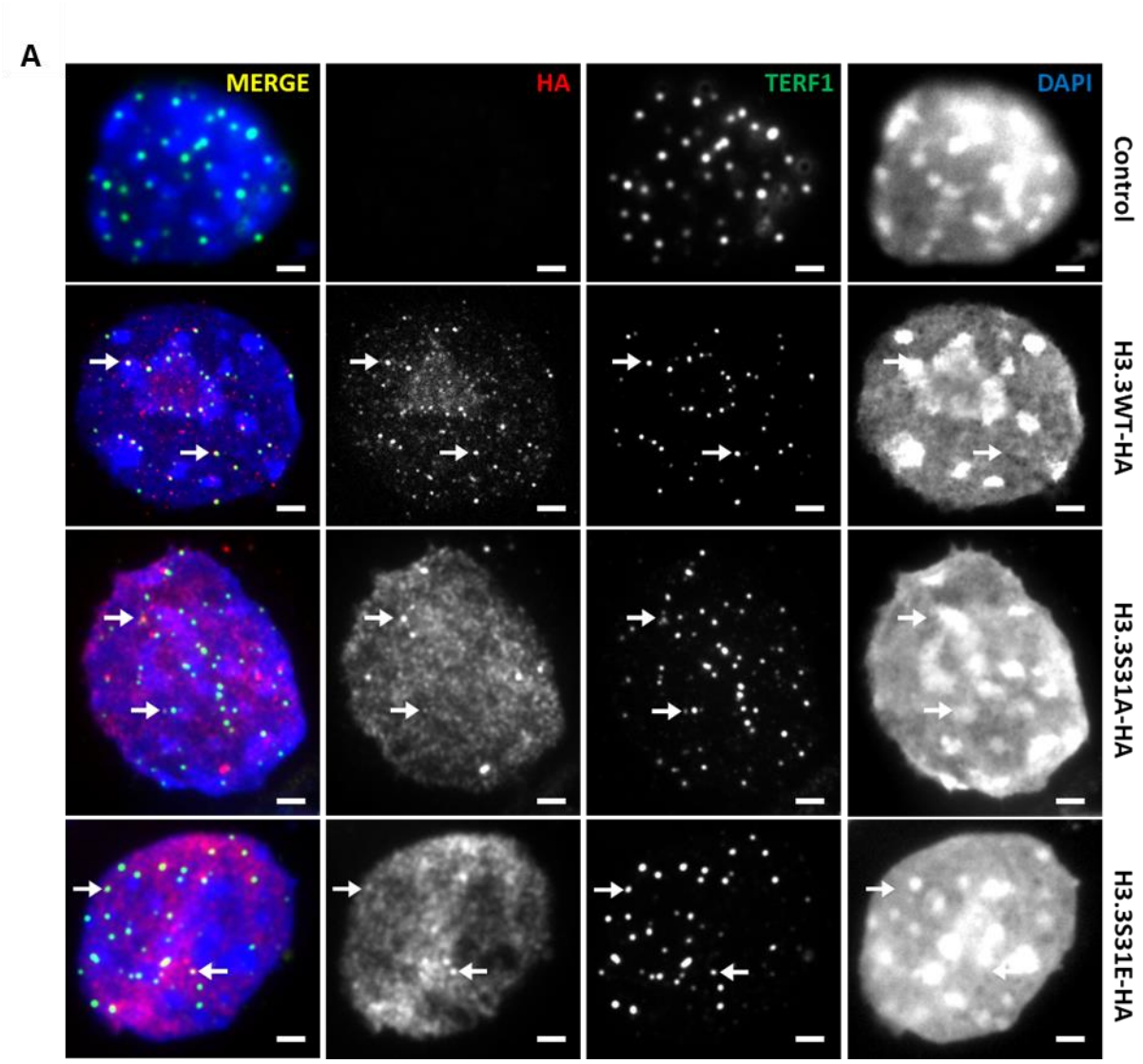
A
MERGE
HA
TERF1
DAPI
Control
H3.3WT-HA
H3.3S31A-HA
H3.3S31E-HA

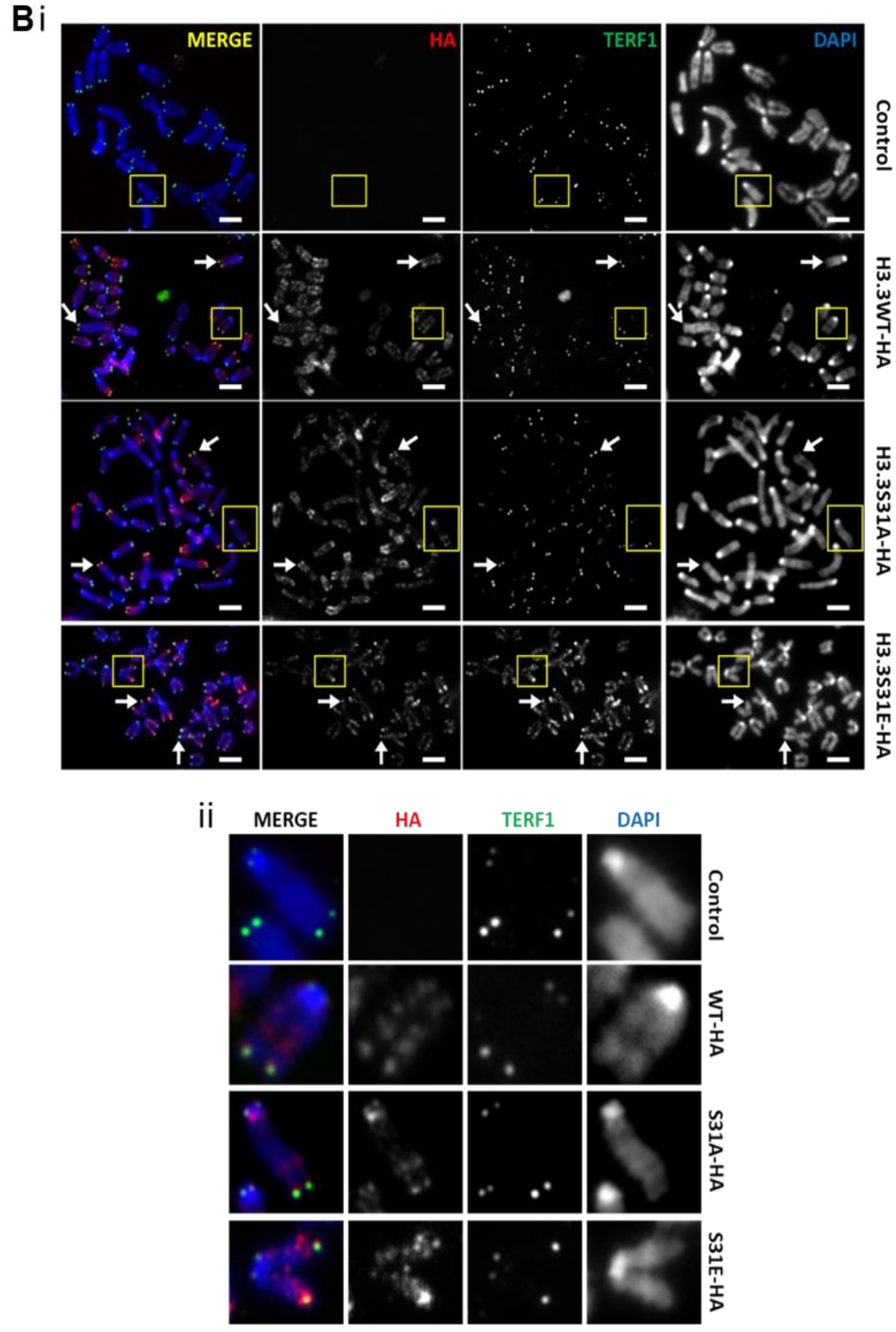
Bi
MERGE
HA
TERF1
DAPI
Control
H3.3WT-HA
H3.3S31A-HA
H3.3S31E-HA
ii
MERGE
HA
TERF1
DAPI
Control
WT-HA
S31A-HA
S31E-HA

Figure 4.2.6: Wild-type, S31A and S31E HA-tagged-H3.3 localise to the telomeres of ES cells

*(**i**) Immunofluorescence analyses were performed on wild-type, S31A and S31E HA-tagged H3.3 ES cell clones with antibodies against HA tag (red) and TERF1 (green) to determine their localisation to telomeres. TERF1 was used as a telomere marker. Wild-type, S31A and S31E HA-tagged-H3.3 colocalised with TERF1 at the telomeres of (**A**) interphase and (**B**) mitotic cells (arrows). HA staining was undetected in h3f3a$^{flox/flox}$ h3f3b$^{flox/flox}$ ES cells (control). An enlarged image of the selected region (yellow box) is shown in **(ii)**. DAPI was used as a nuclear counterstain. Scale bar represents 4 µm.*

Next, to investigate if wild-type, S31A and S31E HA-tagged H3.3 were distributed at H3.3S31ph enriched regions, immunofluorescence analyses were performed using specific antibodies against HA and H3.3S31ph. The antibody against H3.3S31ph is specific and has been tested and verified in our previous studies (Chang et al., 2015, Wong et al., 2009, Chan et al., 2017). In metaphase cells, wild-type, S31A and S31E HA-tagged H3.3 colocalised with H3.3S31ph at the telomeres and pericentric regions (**Figure 4.2.7**). Importantly, cells expressing wild-type and S31E HA-tagged H3.3 showed clear enrichment of H3.3S31ph at the telomeres and pericentric regions, while cells expressing S31A-HA-tagged H3.3 showed less enrichment of H3.3S31ph at these sites. Although both residues are not able to be phosphorylated, a previous report has shown that the antibody against H3.3S31ph antibody can detect H3.3S31E protein. Thus, the increased H3.3S31ph levels in S31E HA-tagged H3.3 expressing cells, could be due to the antibody recognition of the H3.3S31E protein (Sitbon et al., 2020).

Altogether, both wild-type, and mutant, S31A and S31E HA-tagged H3.3, were successfully expressed in *h3f3a*$^{flox/flox}$ *h3f3b*$^{flox/flox}$ ES cells. Specifically, these wild-type, S31A and S31E HA-tagged H3.3 were found deposited at heterochromatic regions, including the telomere (indicated by TERF1 staining) and pericentric DNA repeats (indicated by ATRX staining). In addition to these HA-tagged wild-type, S31A and S31E H3.3, I have also expressed their untagged counterparts in *h3f3a*$^{flox/flox}$ *h3f3b*$^{flox/flox}$ ES cells, in order to avoid any potential detrimental off-target effects caused by the addition of the HA-tag.

i

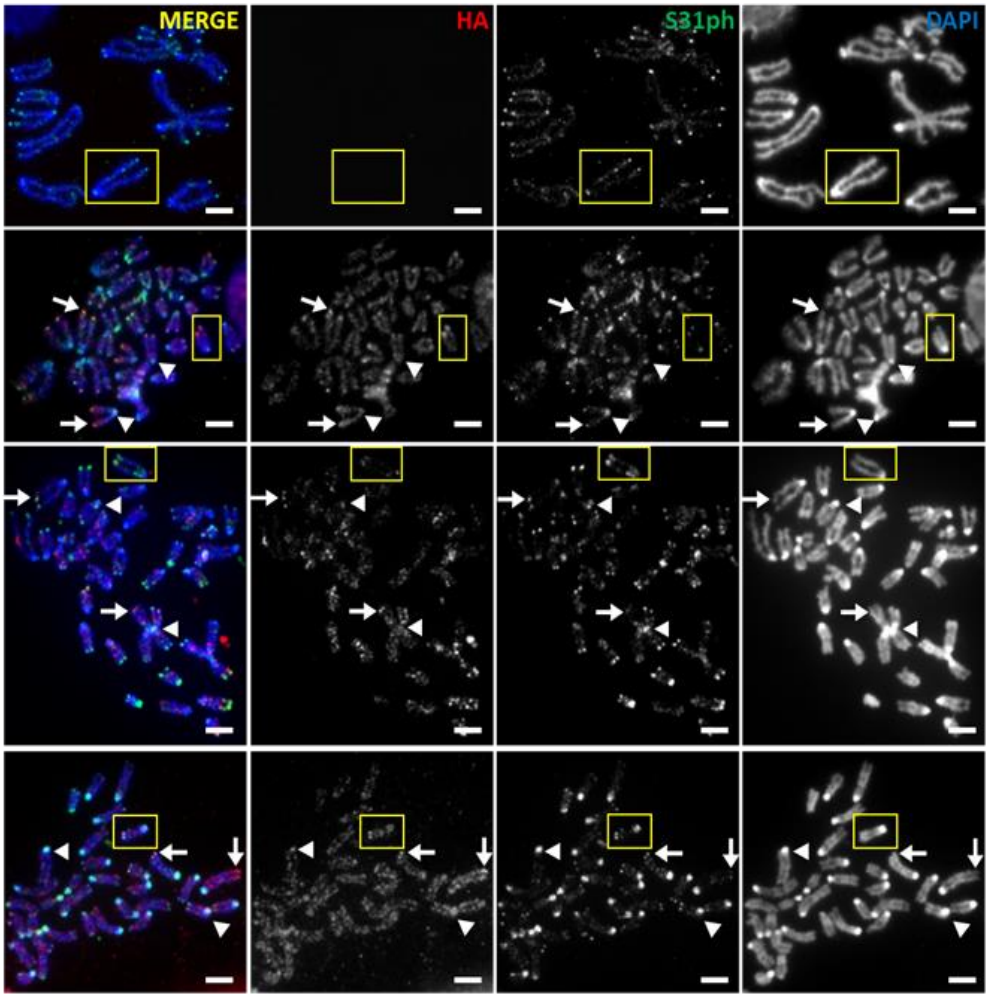
MERGE
HA
S31ph
DAPI
Control
H3.3WT-HA
H3.3S31A-HA
H3.3S31E-HA

ii

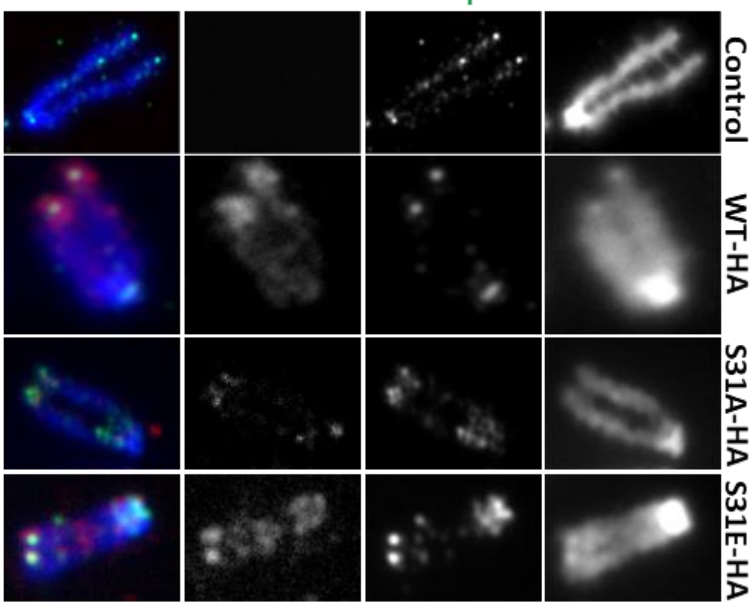
MERGE
HA
S31ph
DAPI
Control
WT-HA
S31A-HA
S31E-HA

Figure 4.2.7: Wild-type, S31A and S31E HA-tagged H3.3 localise to regions enriched with H3.3S31ph in ES cells

*(**i**) Immunofluorescence analyses were performed on wild-type, S31A and S31E HA-tagged H3.3 clones with antibody against HA tag (red) and H3.3S31ph (green) to determine their localisation to H3.3S31ph enriched regions. Wild-type, S31A and S31E HA-tagged H3.3 showed colocalisation with H3.3S31ph at the telomeres (arrow) and pericentric region (arrowhead). HA staining was undetected in h3f3a$^{flox/flox}$ h3f3b$^{flox/flox}$ ES cells (control). An enlarged image of the selected region (yellow box) is shown in (**ii**). DAPI was used as a nuclear counterstain. Scale bar represents 4 µm.*

4.2.3 Untagged H3.3 mutants were expressed in *h3f3a*$^{flox/flox}$ *h3f3b*$^{flox/flox}$ ES cells

Like the HA-tagged H3.3 constructs, linearised untagged wild-type, S31A and S31E H3.3 plasmids were transfected into *h3f3a*$^{flox/flox}$ *h3f3b*$^{flox/flox}$ ES cells to establish stable clones. Single colonies were picked and screened for the expression of H3.3 transcripts as described in **Chapter 2.2.3**. Unlike their HA-tagged counterparts, immunoblotting and immunofluorescence analyses could not differentiate between the endogenous and exogenous H3.3. Thus, qRT-PCR, using primers specifically targeting wild-type, S31A and S31E H3.3 transcripts, was performed to examine the expression of untagged H3.3 (overview in **Figure 4.2.8A**). The results indicated that untagged H3.3 wild-type, H3.3S31A and H3.3S31E transcripts were expressed in *h3f3a*$^{flox/flox}$ *h3f3b*$^{flox/flox}$ ES cells (**Figure 4.2.8B**). The low levels of untagged H3.3 wild-type, when compared to H3.3S31A (**Bii**) and H3.3S31E (**Biii**), may be due to the wildtype primers recognising both endogenous and exogenous H3.3. Nonetheless, this result determined the expression of exogenous untagged wild-type, S31A and S31E H3.3 in *h3f3a*$^{flox/flox}$ *h3f3b*$^{flox/flox}$ ES cells.

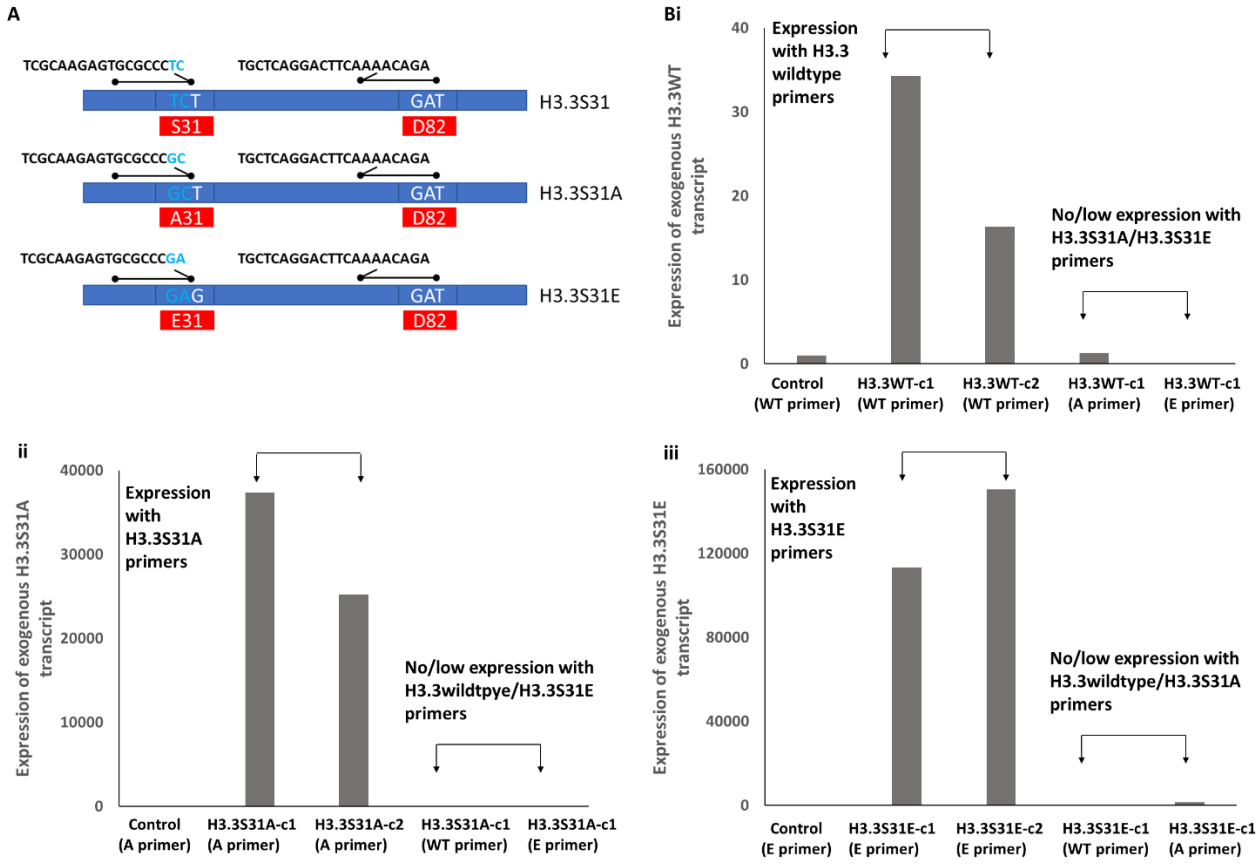

Figure 4.2.8: Expression of untagged H3.3 in h3f3a$^{flox/flox}$ h3f3b$^{flox/flox}$ ES cells

*(**A**) Forward primers were designed specifically for wild-type, S31A and S31E H3.3, where the last two nucleotides of the primer sequence recognise the first two nucleotides of H3.3 wild-type, S31A or S31E H3.3 sequence at codon 31 (cyan). The reverse primer used was the same. (**B**) RNA was harvested from control untransfected and untagged wild-type, S31A, S31E H3.3 transfected h3f3a$^{flox/flox}$ h3f3b$^{flox/flox}$ ES cells. cDNA was synthesised before qPCR analyses determined the level of exogenous untagged (**i**) wild-type, (**ii**) S31A, (**iii**) S31E-H3.3 mRNA. Expression of untagged wild-type, S31A, S31E-H3.3 are shown relative to GAPDH levels and are normalised to control. 2 clones were used for the relevant primers. WTprimer: H3.3WT primer, Aprimer: H3.3S31A primers, Eprimer: H3.3S31E primer. h3f3a$^{flox/flox}$ h3f3b$^{flox/flox}$ ES cells were used as a negative control.*

4.2.4 Knockout of endogenous H3.3 in *h3f3a*$^{flox/flox}$ *h3f3b*$^{flox/flox}$ ES cells expressing HA-tagged H3.3 and untagged H3.3 mutants

With the successful expression of wild-type, S31A and S31E HA-tagged H3.3 in *h3f3a*$^{flox/flox}$ *h3f3b*$^{flox/flox}$ mouse ES cells, *h3f3a* and *h3f3b* genes were next knocked out. To knockout *h3f3a* and *h3f3b* genes, a vector containing *Cre*-recombinase was transiently transfected into these cells. The knockout of either allele of *h3f3a* will result in the expression of YFP, and the knockout of either allele of *h3f3b* will result in the expression of CFP (Tang et al., 2013a).

To determine the loss of endogenous H3.3 proteins, immunoblot analyses were performed using antibody against GFP to detect the presence of YFP/CFP (**Figure 4.2.9A**). As the antibody against green/cyan/yellow fluorescent proteins cross-react and recognise other fluorescent proteins due to their sequence homology, antibody against GFP was used. In addition, antibody against the HA-tag was used to detect wild-type, S31A and S31E HA-tagged H3.3 proteins while antibody against H3.3 was used to determine the levels of total H3.3 after endogenous H3.3 knockout (**Figure 4.2.9A**). The 1 kDa (HA tag) difference between endogenous H3.3 and H3.3-HA is detectable by immunoblotting.

In wild-type-HA-H3.3 expressing clones, the endogenous H3.3 (17kDa) was lost while the wild-type-HA-tagged H3.3 (18 kDa) was present (**Figure 4.2.9A**). In S31A-HA-tagged-H3.3 clones, there were low but detectable levels of endogenous H3.3 and a loss of S31A-HA- -H3.3. Finally, S31E-HA-tagged H3.3 clones retained both endogenous H3.3 and S31A-HA-H3.3 proteins, indicating a failure to knockout the endogenous H3.3 genes. Supporting this, YFP/CFP was detected in wild-type and S31A-HA-H3.3 clones but not in S31E-HA-H3.3 clones (**Figure 4.2.9A**). These results suggest that the endogenous H3.3 alleles were not

completely removed in both S31A-H3.3-HA and S31E-H3.3-HA expressing mutant clones although YFP/CFP was detected. It is likely that the endogenous H3.3 genes were only partially removed. As complete endogenous H3.3 knockout in S31A and S31E-H3.3-HA expressing cells were unattainable, the focus was on the knockout of endogenous H3.3 in untagged wild-type, S31A and S31E H3.3 expressing cells. The loss of S31A-H3.3-HA expression may be due to cell toxicity from combining the S31A mutation and the HA-tag. As complete endogenous H3.3 knockout in S31A and S31E-H3.3-HA expressing cells were unattainable, the focus was on the knockout of endogenous H3.3 in untagged wild-type, S31A and S31E H3.3 expressing cells.

Similarly, to knockout endogenous H3.3 in untagged wild-type, S31A and S31E-H3.3 cells, a vector containing *Cre*-recombinase was transiently transfected into these cells. Immunoblot analyses were performed with antibodies against H3.3 and GFP to determine the loss of endogenous H3.3. YFP/CFP was detected for all untagged wild-type, S31A and S31E-H3.3 clones, indicating a loss of endogenous H3.3 in these cells. However, immunoblotting with H3.3 antibody could not differentiate between endogenous and exogenous H3.3 (**Figure 4.2.9B**). Thus, it was impossible to determine the complete knockout of endogenous H3.3. Nonetheless, due to their relatively similar H3.3 expression levels, wild-type-H3.3 clone #1, S31A-H3.3 clone #2 and S31E-H3.3 clone #2 were selected for further investigation.

Next, to investigate if either *h3f3a* or *h3f3b* was knocked out, FACS was performed to detect the expression of YFP and CFP. The results showed that YFP and CFP were expressed for untagged wild-type, S31A and S31E-H3.3 cells, indicating a loss of at least one allele of *h3f3a* and *h3f3b* (**Figure 4.2.9C**). Altogether, the results from immunoblotting and FACS

confirmed the loss of at least one allele of *h3f3a* and *h3f3b* in these untagged wild-type, S31A and S31E-H3.3 cell lines.

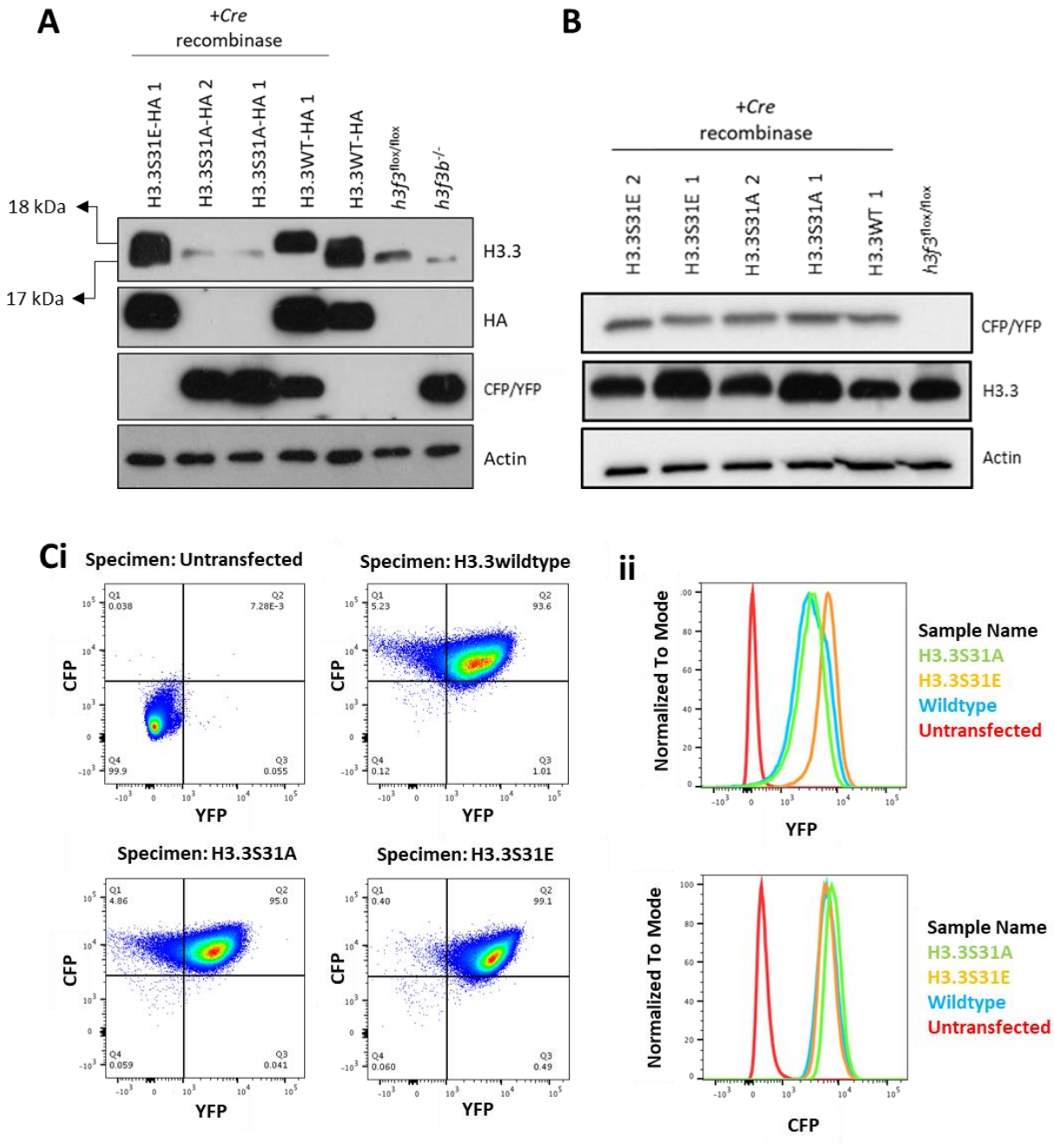

Figure 4.2.9: Partial knockout of endogenous H3.3 in untagged wild-type, S31A and S31E-H3.3 clones after Cre-recombinase expression

(A) *Immunoblot analyses of wild-type, S31A and S31E HA-tagged H3.3 clones after Cre-recombinase transfection using antibody against H3.3, HA and GFP. Wild-type and S31E HA-tagged H3.3 were detected, while S31A HA-tagged H3.3 was undetectable. YFP/CFP was detected for Wild-type and S31A HA-tagged H3.3 clones but not S31E HA-tagged H3.3 clone. h3f3a$^{+/+}$ h3f3b$^{-/-}$ ES cells were used as a positive control for CFP expression.* ***(B)*** *Immunoblot analyses of cell lysates extracted from untagged wild-type, S31A and S31E H3.3 clones after Cre-recombinase transfection using antibodies against H3.3 and GFP. YFP/CFP was detected for all untagged wild-type, S31A and S31E H3.3 clones. H3.3 was detected at high levels for all untagged wild-type, S31A and S31E H3.3 clones. Actin was used as a loading control. Neither HA-tagged H3.3 nor YFP/CFP were detected in untransfected h3f3a$^{flox/flox}$ h3f3b$^{flox/flox}$ ES cell (control).* ***(Ci)*** *FACS analyses were performed to detect CFP or YFP expression in the untagged wild-type, S31A and S31E cells. CFP and YFP were detected for untagged wild-type, S31A and S31E H3.3 clones. Y-axis: CFP, X-axis: YFP* ***(ii)*** *Normalised YFP and CFP levels in untagged wild-type, S31A and S31E H3.3 clones. YFP/CFP signal was undetected in untransfected h3f3a$^{flox/flox}$ h3f3b$^{flox/flox}$ ES cells (control).*

4.2.5 Validation of H3.3 knockout after *Cre*-recombinase expression

Despite identifying the expression of both YFP and CFP, the homozygous loss of *h3f3a* or *h3f3b* was not established. Thus, southern blot analyses were performed on the genomic DNA of untagged wild-type, S31A and S31E-H3.3 cells using specific probes to identify the complete deletion of either *h3f3a* or *h3f3b* genes (refer to **Figure 4.2.1** for complete information on endogenous H3.3 knockout including probe position and restriction sites)(Tang et al., 2013a) (sequence of probes and primers are shown in **Table 2.15**). Analysis was performed on two S31A and S31E-H3.3 clones. The results showed that untagged wild-type, S31A and S31E H3.3 cells were homozygous for the knockout of both *h3f3a* and *h3f3b* genes (**Figure 4.2.10**).

A summary of the H3.3 mutants cell line generation is shown in **Table 4.2.** The number of colonies screened for HA-tagged and untagged H3.3S31A after endogenous H3.3 knockout was significantly high compared to the wild-type and S31E untagged H3.3 under same conditions. The ease of attaining S31E-H3.3 mutants suggests the importance of H3.3S31ph in maintaining cell survival while the knockout of endogenous H3.3 from H3.3 conditional ES cells expressing S31A-H3.3, caused rapid cell death, indicating the importance of the evolutionarily conserved H3.3S31 residue. With the screening of 150 S31A-H3.3 clones after endogenous H3.3 knockout, only 6 clones expressed CFP/YFP reporter proteins, indicating a partial loss of endogenous H3.3. Of which, only 2 showed a compete loss of both *h3f3a* and *h3f3b* genes. This suggest that the H3.3S31 residue is required for normal growth and that the mutation of H3.3S31 to alanine affect ES cell survival.

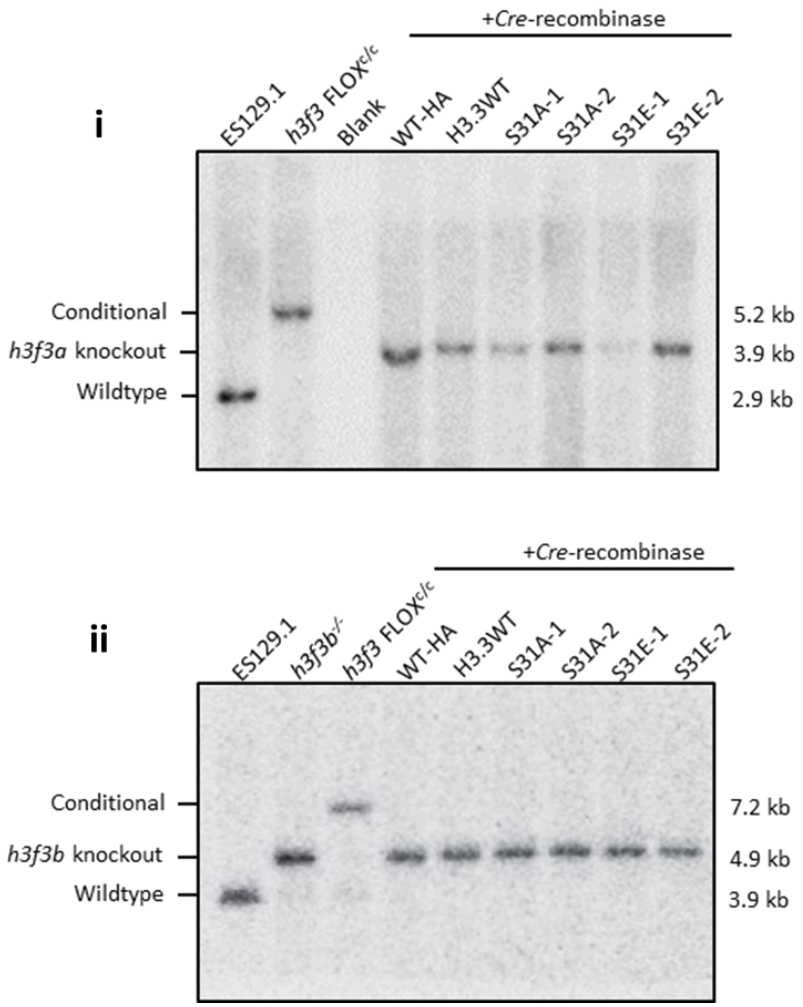

Figure 4.2.10: Complete knockout of h3f3a and h3f3b in wild-type, S31A and S31E H3.3 cells

*Southern blot analyses were performed on h3f3a$^{flox/flox}$ h3f3b$^{flox/flox}$ ES cell (h3f3 FLOX$^{c/c}$), h3f3a$^{+/+}$ h3f3b$^{-/-}$ ES cell (h3f3b$^{-/-}$) and, Cre-recombinase transfected H3.3 wild-type-HA (WT-HA), H3.3 wild-type (H3.3WT), H3.3S31A (S31A) and H3.3S31E (S31E) cells. SacI was used to digest the genomic DNA. Probes specific to either h3f3a or h3f3b were used to detect the presence of the respective sequence. (**i**) All clones tested after Cre-recombinase transfection showed a complete loss of h3f3a (single 3.9 kb band). The control h3f3 FLOX$^{c/c}$ showed no loss of h3f3a (single 5.2 kb band). (**ii**) All clones tested after Cre-recombinase transfection showed a complete loss of h3f3b (single 4.9 kb band). The control h3f3 FLOX$^{c/c}$ showed no loss of h3f3b (single 7.2 kb band). As a positive control, h3f3b$^{-/-}$ cells showed a single 4.9 kb band. ES129.1 was used as a negative control.*

Table 4.2: Summary of H3.3 mutants after knockout of endogenous H3.3

Clone	Total number of clones screened	Number of clones expressing YFP/CFP	H3.3 KO clones confirmed by southern blot
H3.3WT-HA	9	6	1
H3.3S31A-HA	90	23	-
H3.3S31E-HA	2	1	-
H3.3WT	2	2	1
H3.3S31A	150	6	2
H3.3S31E	9	6	2

The expression of S31A-H3.3-HA was lost following the knockout of the endogenous H3.3 genes (**Figure 4.2.9A**). Thus, to investigate if exogenous untagged wild-type, S31A and S31E-H3.3, were expressed after endogenous H3.3 knockout, qRT-PCR analyses were performed. The primers used are as shown in **Figure 4.2.8A**. The results showed robust expression of wild-type, S31A and S31E-H3.3 transcripts, identifying that, unlike the S31A-H3.3-HA counterpart, untagged S31A-H3.3 was expressed after endogenous H3.3 knockout (**Figure 4.2.11**).

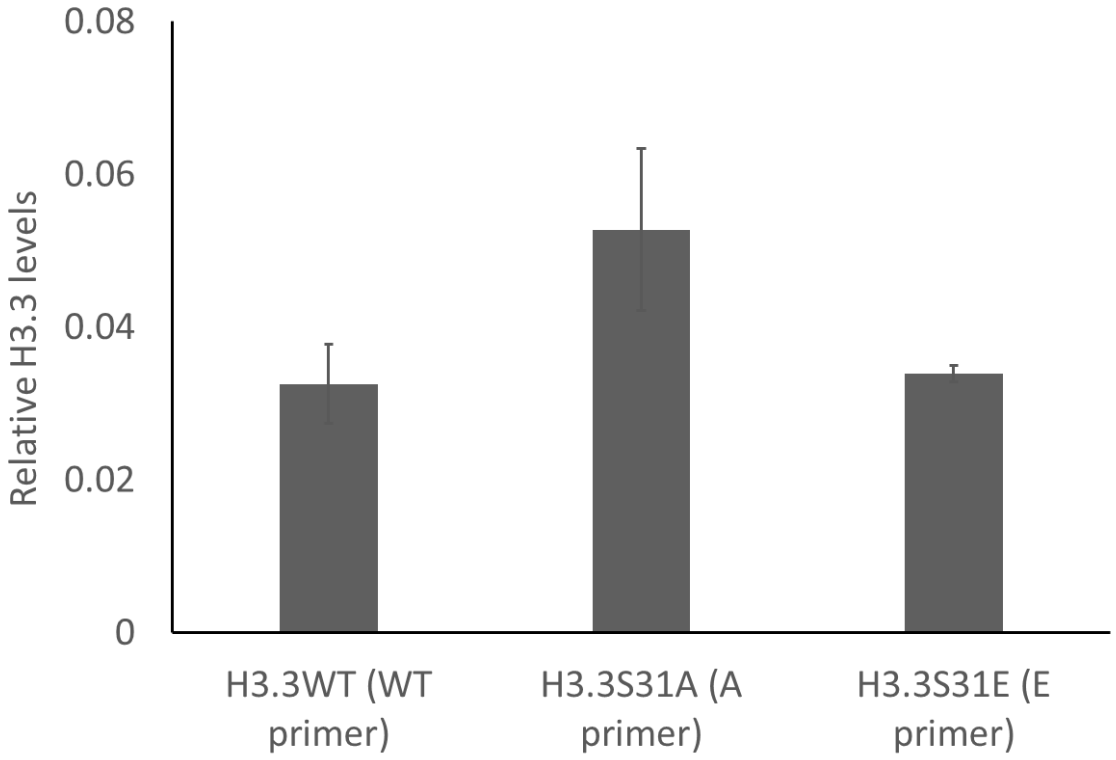

Figure 4.2.11: Expression of untagged H3.3 in after endogenous H3.3 knockout

*RNA was harvested from untagged wild-type, S31A, S31E-H3.3 expressing ES cell clones after cre-mediated knockout of endogenous H3.3 genes. cDNA synthesised before qPCR analyses determined the level of exogenous untagged **(i)** wild-type, **(ii)** S31A, **(iii)** S31E H3.3 mRNA. Expression of untagged wild-type, S31A, S31E H3.3 are shown relative to GAPDH levels. WT primer: H3.3WT primers, A primer: H3.3S31A primers, E primer: H3.3S31E primers.*

To confirm the loss of H3.3, the resultant loss of the H3.3-specific H3.3S31ph mark was investigated. Immunofluorescence analyses using antibody against H3.3S31ph followed by Tel-FISH in untagged wild-type, S31A and S31E-H3.3 clones showed that H3.3S31ph was present in wild-type H3.3 clone. In contrast, H3.3S31ph was not detectable in S31A and S31E-H3.3 expressing ES cell clones (**Figure 4.2.12**). However, results from immunofluorescence analyses, without Tel-FISH, showed the presence of low H3.3S31ph levels in S31E-H3.3 clones but undetectable levels of H3.3S31ph in S31A-H3.3 clones (**Figure 4.2.13A**). This result suggests that the H3.3S31ph antibody has a low affinity to H3.3S31E. As S31E-H3.3 acts as H3.3S31ph, there was potential for H3.3S31E to be recognised by the H3.3S31ph antibody (Sitbon et al., 2020).

The results from immunoblotting showed that H3.3 levels between wild-type, untagged S31A and S31E-H3.3 were similar (**Figure 4.2.13B**). Thus, the loss of H3.3S31ph observed in S31A and S31E-H3.3 cells (**Figure 4.2.12 and 13A**) was likely due to a loss of wildtype H3.3 protein. Altogether, these results complement the results from southern blot analyses to indicate a complete knockout of endogenous H3.3 from untagged wild-type, S31A and S31E-H3.3 clones

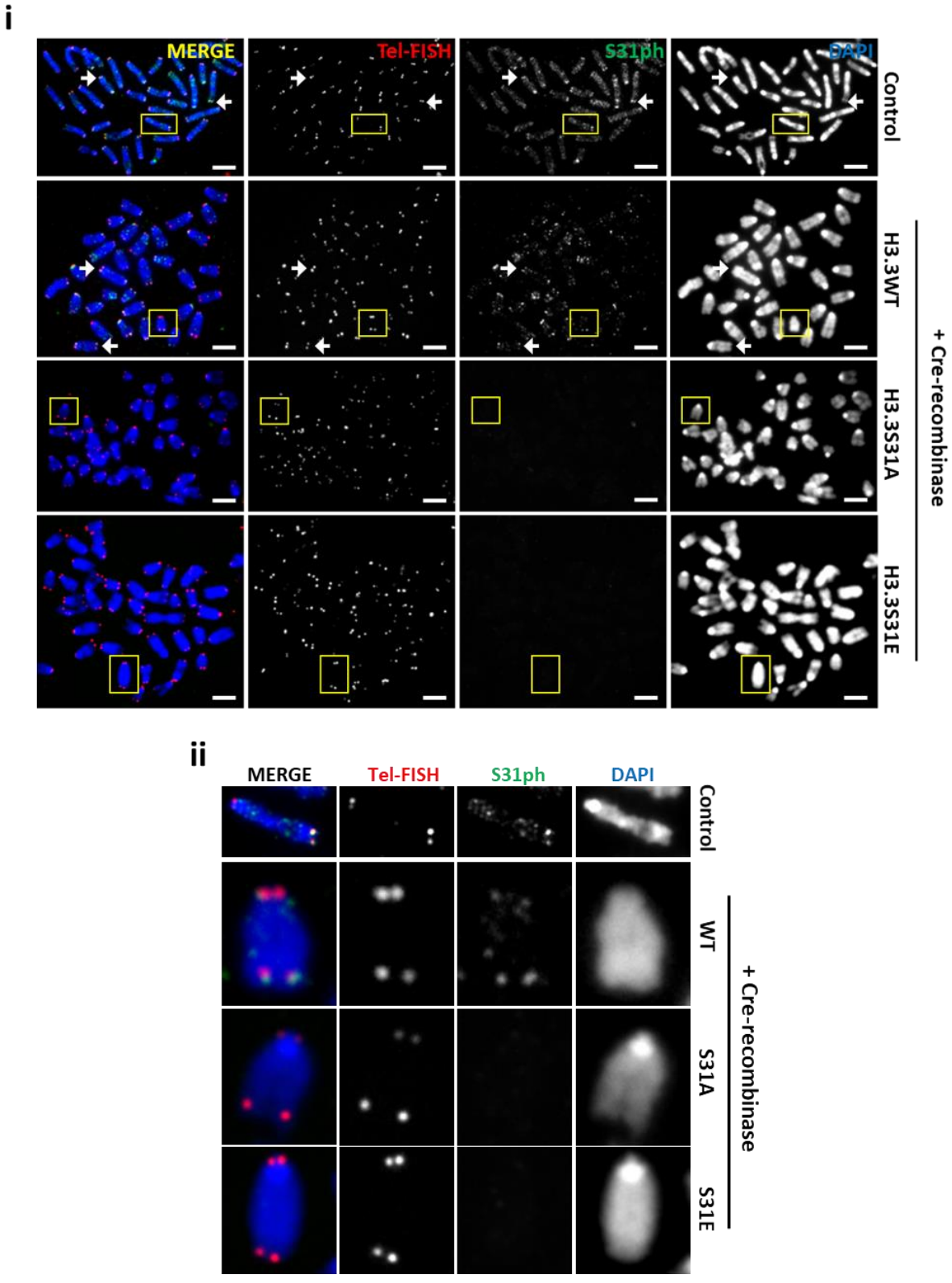
i
MERGE
Tel-FISH
S31ph
DAPI
Control
H3.3WT
H3.3S31A
H3.3S31E
+ Cre-recombinase
ii
MERGE
Tel-FISH
S31ph
DAPI
Control
WT
S31A
S31E
+ Cre-recombinase

Figure 4.2.12: H3.3S31ph is lost in S31A and S31E-H3.3 ES cell clones

*(**A**) Immunofluorescence analyses were performed after endogenous H3.3 knockout on wild-type, S31A and S31E H3.3 expressing ES cell clones with antibody against H3.3S31ph (green) followed by Tel-FISH (telomere marker; red) to determine the presence of H3.3S31ph. Both untransfected h3f3a$^{flox/flox}$ h3f3b$^{flox/flox}$ ES cells (control) and wild-type-H3.3 cells showed enrichment of H3.3S31ph at the telomeres of mitotic cells (arrow). H3.3S31ph signals were undetectable in mitotic S31A and S31E-H3.3 ES cells. An enlarged image of the selected region (yellow box) is shown in (**ii**). DAPI was used as a nuclear counterstain. Scale bar represents 4 µm.*

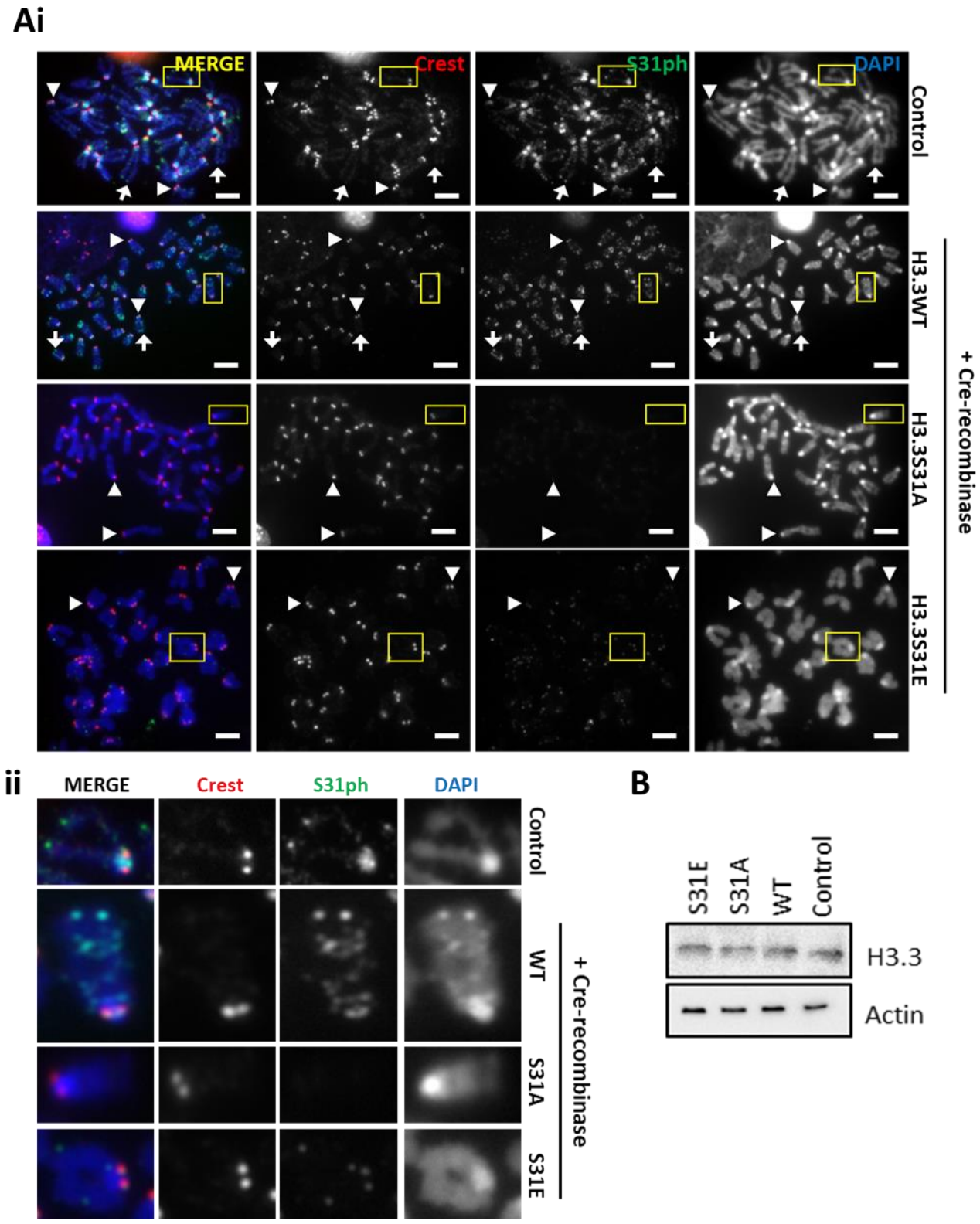
Ai
MERGE
Crest
S31ph
DAPI
Control
H3.3WT
H3.3S31A
H3.3S31E
+ Cre-recombinase
ii
MERGE
Crest
S31ph
DAPI
Control
WT
S31A
S31E
+ Cre-recombinase
B
S31E
S31A
WT
Control
H3.3
Actin

Figure 4.2.13: H3.3S31ph antibody has low affinity to H3.3S31E

*(**Ai**) Immunofluorescence analyses were performed on wild-type, S31A and S31E-H3.3 ES cell clones after the knockout of the endogenous H3.3 genes with antibodies against H3.3S31ph (green) and centromere (CREST6, red) to determine the presence of H3.3S31ph. Both untransfected h3f3a$^{flox/flox}$ h3f3b$^{flox/flox}$ ES cells (control) and H3.3 wild-type mitotic cells showed enrichment of H3.3S31ph at the telomeres (arrow). H3.3S31ph signals were undetectable in mitotic S31A-H3.3 clones. Weak H3.3S31ph levels were observed in mitotic S31E-H3.3 cells. An enlarged image of the selected region (yellow box) is shown in (**ii**). DAPI was used as a nuclear counterstain. Scale bar represents 4 µm. **(B)** Immunoblot analyses of untagged wild-type, S31A and S31E-H3.3 using antibody against H3.3. H3.3 was detected at similar levels between untransfected h3f3a$^{flox/flox}$ h3f3b$^{flox/flox}$ ES cell (control), untagged wild-type, S31A and S31E-H3.3 expressing ES cell clones. Actin was used as a loading control.*

4.3 Discussion

The tail of Histone H3.3 is regulated by PTMs, including acetylation, methylation and phosphorylation (Bowman and Poirier, 2015). However, the lack of an experimental model to study these specific modifications hinder our more profound understandings of the various H3.3 PTMs. In this chapter, H3.3 conditional knockout ES cell line (*h3f3a*$^{flox/flox}$ *h3f3b*$^{flox/flox}$ ES cells), which was previously created (Tang et al., 2013a), were used to generate H3.3S31 phospho-null (S31A-H3.3) and phospho-mimic (S31E-H3.3) mutant ES cell lines in an endogenous H3.3-null background. The successful expression of untagged S31A and S31E-H3.3 proteins in *h3f3a*$^{flox/flox}$ *h3f3b*$^{flox/flox}$ ES cells was confirmed by qPCR using primers specific to the respective mutation (**Figure 4.2.8**). Furthermore, with the expression of *Cre*-recombinase, FACS and immunoblotting for CFP/YFP reporter proteins (**Figure 4.2.9**), southern blotting (**Figure 4.2.10**) and immunofluorescence analyses of H3.3S31ph (**Figure 4.2.12** and **Figure 4.2.13**) confirmed the complete knockout of endogenous H3.3. Although immunofluorescence analyses of H3.3S31ph showed a weak presence of H3.3S31ph in S31E-H3.3 ES cell lines (**Figure 4.2.12**), this detection is likely due to the recognition of H3.3S31E as the H3.3S31ph antibody was previously shown to detect H3.3S31D, another H3.3S31 phospho-mimic mutant (Sitbon et al., 2020). Nonetheless, southern blotting showed the complete loss of both *h3f3a* and *h3f3b* genes in the S31E-H3.3 ES cell lines.

In addition to these untagged H3.3 mutants, HA-tagged S31A-H3.3 (S31A-H3.3-HA) and S31E-H3.3 (S31E-H3.3-HA) were also generated to differentiate between endogenous and exogenous H3.3 proteins. The expression of S31A-H3.3-HA and S31E-H3.3-HA in *h3f3a*$^{flox/flox}$ *h3f3b*$^{flox/flox}$ ES cells was confirmed by and immunoblotting (**Figure 4.2.4**) and immunofluorescence analyses (**Figure 4.2.5, 4.2.6** and **4.2.7**) of the HA protein. However,

with the expression of *Cre*-recombinase, immunoblotting showed that a complete knockout of endogenous H3.3 was not achieved for the S31A-H3.3-HA and S31E-H3.3-HA ES cell lines (**Figure 4.2.9**). Thus, the untagged S31A and S31E-H3.3 cell lines were selected for further studies.

In S31A-H3.3-HA cell lines after knockout of endogenous H3.3, despite screening of 90 clones, none of the clones showed a complete loss of endogenous H3.3. Interestingly, together with rapid cell death, these S31A-H3.3-HA clones also showed a loss of H3.3S31A-HA proteins, suggesting that the substitution of H3.3S31 to alanine, in conjunction with the HA tag, further exacerbate the chances of cell survival. Further indicating increased toxicity to the cells due to the HA tag, only 2 colonies were attained for S31E-H3.3-HA cell line, with only one expressing the CFP/YFP reporter proteins and neither having a complete loss of both *h3f3a* and *h3f3b* genes (**Table 4.2**). This phenomenon may be unique to mammalian cells as another study was able to express H3.3S31A-HA and H3.3S31E-HA in *Xenopus eggs* (Sitbon et al., 2020). Another possibility is the high levels of H3.3-HA proteins, compared to endogenous H3.3 levels (**Figure 4.2.2B**). The increased levels of H3.3 itself may have been detrimental to the cells. Future experiments will identify cells with H3.3-HA levels similar to endogenous H3.3 levels to prevent cell death.

As the HA tag is considerably large (1 kDa) when compared to histone proteins (17 kDa), its tagging to the histone globular domain may affect the total number of DNA wrapped around the nucleosome, leading to genomic defects resulting in rapid cell death. Although another study was able to insert a HA tag on the C-terminal domain of H3.3 in *Xenopus egg* (Sitbon et al., 2020), it is possible that the HA tag on the C-terminal domain of H3.3 may be more detrimental in mammalian cells. Thus, tagging of the N-terminal tail of the histone

protein may be a more viable option. In fact, previous studies using YFP-H3.3 showed a loss H3.3 at endogenous retroviral repeats (Voon et al., 2015, Elsasser et al., 2015) while a study using untagged H3.3 reported increased H3.3 at endogenous retroviral repeats (Sadic et al., 2015). These studies complement the possible dysfunction of a tag in affecting the proper DNA wrapping around nucleosomes, leading to dysregulated genomic integrity. Thus, untagged S31A and S31E-H3.3 ES cell lines were used for further studies investigating the role of H3.3S31ph and its function in heterochromatin regulation.

Chapter 5: H3.3S31 phosphorylation is required for maintaining telomere heterochromatin

5.1 Introduction

5.1.1 Overview

Chromatin functions, including chromatin compaction and accessibility, are regulated by various factors, including histone variants and histone PTM. For example, H2AX, H2AZ and macroH2A are variants of Histone H2A (Talbert and Henikoff, 2021). Compared to canonical H2A, the H2A variants differ mainly at the C-terminal (Marzluff et al., 2002). H2AX contains a C-terminal SQ(D/E]Φ motif (where Φ is a hydrophobic amino acid) (Turinetto and Giachino, 2015, Talbert and Henikoff, 2021) and is loaded into chromatin by the histone chaperone facilitates chromatin transcription (FACT) (Piquet et al., 2018). The H2AX variant is widely known for its role in DNA damage regulation where in response to DNA breaks, the Serine at residue 139 is phosphorylated by ATM or ATR (Podhorecka et al., 2010, Bakkenist and Kastan, 2003). The Serine 139-phosphorylated H2AX, also known as γH2AX, then recruits the DNA repair machinery to repair the double stranded breaks (Celeste et al., 2002).

Another H2A variant, H2AZ is critical for transcriptional regulation and its loading into chromatin is regulated by various chaperones such as SWR1, ANP32E, FACT, Spt6, chz1 and INO80 (Giaimo et al., 2019, Luk et al., 2007, Obri et al., 2014, Jeronimo et al., 2015, Papamichos-Chronakis et al., 2011). H2AZ has been reported to be involved in both gene activation and gene silencing. H2A.Z deposition leads to an abnormal nucleosome structure which decreases nucleosome occupancy and increases accessibility of DNA to transcription factors and chromatin-associated proteins (Hu et al., 2013). H2AZ is enriched at promoters, enhancers and poise genes where is promotes transcription and RNA polymerase II recruitment (Weber et al., 2014, Hu et al., 2013, Adam et al., 2001). H2AZ occupies the

promoter regions of transcriptional factor families including *Fox*, *Sox* and *Tbx* (Burch, 2005, Lehmann et al., 2003, Schepers et al., 2002, Showell et al., 2004). Interestingly, the depletion of H2AZ prevented the expression of differentiation related markers such as *Sox1* which inhibited ES cell differentiation (Creyghton et al., 2008, Hu et al., 2013). Contrary to this study which showed and proposed that H2AZ is not required for ES cell renewal, a more recent study showed that the loss of H2AZ in self renewing ES cells prevented *Oct4* binding to target genes, compromising both heterochromatin and euchromatin regulation (Hu et al., 2013).

H2AZ also plays an important role in regulating centromere function and heterochromatin formation, where its loss leads to defects in heterochromatin, centromere cohesion, structural change in pericentric heterochromatin (Rangasamy et al., 2004) and transcriptional activation (Barski et al., 2007). Recently, a study showed that GCN5, a histone acetyltransferase, regulates acetylation of H2AZ at the promoters of transactivated genes. Together with the XPC–RAD23–CEN2, a DNA repair complex which act as a transcriptional coactivator, GCN5 regulates H2AZ acetylation to alter promoter landscape (Semer et al., 2019). In addition to its function at the promoter regions, H2AZ was found to be enriched along linear chromatin fibres throughout the centromere (Greaves et al., 2007). However, its function at the centromere remains to be discovered.

MacroH2A, another major H2A variant, is unique to other H2A variants as it contains a bulky C-terminal non-histone domain (Chakravarthy et al., 2012). A recent study has shown that macroH2A is loaded into chromatin by Lymphoid Specific Helicas (LSH) and promotes transcriptional repression and silencing (Ni et al., 2020). MacroH2A is preferentially enriched at the inactive X chromosome where it promotes transcriptional inactivation (Costanzi and

Pehrson, 1998). Like H2AX, macroH2A is also phosphorylated in response to DNA damage and regulates DNA repair (Lorkovic et al., 2017). In addition to its function in DNA repair and transcriptional silencing, macroH2A is involved in chromatin structure regulation (Muthurajan et al., 2011), prevents somatic cell reprogramming toward pluripotency (Gaspar-Maia et al., 2013) and acts as a tumor suppressor in a wide range of cancers (Kapoor et al., 2010, Pliatska et al., 2018).

Similar to canonical histone H2A, histone H3 has its own set of variants. The replication dependant Centromere Protein-A (Cenp-A) and replication independent H3.3 are well known variants of histone H3 (Sullivan et al., 1994, Ahmad and Henikoff, 2002). Cenp-A, the centromere-specific H3 variant, functions to maintain proper cell cycle progression. Cenp-A, which is deposited into chromatin by HJURP (Pan et al., 2019), plays a critical role in building kinetochore and maintaining sister chromatid cohesion in eukaryotes (Sullivan et al., 1994, Yoda et al., 2000, Van Hooser et al., 2001).

Unlike the canonical H3, H3.3 is unique such that it is deposited into euchromatin by HIRA and heterochromatin by ATRX/DAXX chaperone complex, respectively (Elsaesser and Allis, 2010, Wong et al., 2010, Law et al., 2010, Drane et al., 2010). Genome-wide mapping of H3.3 showed the colocalization of HIRA and H3.3 at active and repressed genes while ATRX/DAXX is required for Hira-independent localisation of H3.3 at telomeres and for the repression of telomeric RNA (Goldberg et al., 2010). This unique loading by different histone chaperones suggests its specialised roles at euchromatin and heterochromatin. Furthermore, H3.3 has an exclusive serine residue at position 31 compared to canonical H3, and this Serine 31 residue can be phosphorylated (Hake et al., 2005). To study the role of H3.3S31ph in heterochromatin regulation, wild-type, S31A and S31E-H3.3 cell lines

lacking endogenous H3.3 that were successfully generated in **Chapter 4** were used for analysis of the impact of H3.3 S31 substitution on telomeric chromatin maintenance.

5.1.2 The regulation of H3.3S31ph

Compared to the canonical H3, which has an Alanine residue at position 31, H3.3 has a unique Serine residue. This H3.3 Serine 31 residue is evolutionarily conserved from yeasts to humans (Elsaesser et al., 2010, Hake et al., 2006). Like H3S10ph and H3S28ph, multiple studies have shown the enrichment of H3.3S31ph on mitotic chromosomes during mitosis in various cell models, such as sea squirts, yeast, mouse and human (Schulmeister et al., 2007, Wong et al., 2009, Hake et al., 2005). In mammalian cells, the presence of H3.3S31ph is detected on chromosomes from late prometaphase to metaphase, and is lost after the onset of anaphase (Hake et al., 2005). In somatic cells, H3.3S31ph is enriched at the pericentric heterochromatin (Hake et al., 2005, Schulmeister et al., 2007, Frey et al., 2014, Hinchcliffe et al., 2016). In pluripotent mouse ES cells, H3.3S31ph localises predominantly to telomeres (Wong et al., 2009). Upon differentiation of mouse ES cells, H3.3S31ph level decreases at telomeres but increases at pericentric heterochromatin. Interestingly, in the urochordate, *Oikopleura dioica,* H3.3S31ph is present throughout mitotic chromosome (Schulmeister et al., 2007). This shows that the H3.3S31ph is evolutionarily conserved and plays a vital role in cell survival, cell viability and cell cycle progression.

Recent studies identified AURKB, CHK1 and IKKα as kinases that regulate H3.3S31ph (Chang et al., 2015, Li et al., 2017a, Sitbon et al., 2020, Armache et al., 2020). The localisation of H3.3S31ph at heterochromatic regions during mitosis highlight the potential role of H3.3S31ph in heterochromatin maintenance, however, the role of H3.3 S31 at

transcriptionally silent DNA repeat regions remains unknown and further investigation is needed.

5.1.3 H3.3S31ph regulates DNA damage response and controls cell viability

Cancer cells that use ALT are unique as they do not require telomerase to maintain long telomeres. Instead, they employ a recombination-like mechanism to maintain telomere length (Amorim et al., 2016). In most ALT-positive cancer cells, ATRX is inactivated (Lovejoy et al., 2012). Similarly, aberrant H3.3S31ph localisation was seen in ATRX-deficient ALT-cancer cells, with H3.3S31ph enriched not only at the pericentric region but also along the entire chromosome arms (Chang et al., 2015). These ATRX-deficient ALT-cancer cells display a severe delay in mitotic progression, leading to increased H3.3S31ph levels throughout the chromosomes (Chang et al., 2015). Interestingly, in these cells, inhibition of CHK1, a kinase activated by persistent DNA damage, resulted in a loss of H3.3S31ph at the chromosome arms, but not pericentric regions. This indicates that CHK1 is the kinase responsible for the aberrant distribution of H3.3S31ph across the chromosome arms (Chang et al., 2015). Furthermore, the loss of H3.3S31ph, through either the inhibition of CHK1 activity or the expression of H3.3S31A mutants, was shown to lead to an increase in γH2AX levels on chromosome arms, leading to ATRX-deficient ALT-cancer cell death (Chang et al., 2015). This suggests a role of H3.3S31ph in preventing the activation of the DNA damage response throughout the chromosomes of ATRX-mutated ALT cancer cells to maintain cell viability.

In addition to the function of H3.3S31ph in ATRX-deficient ALT-cancer cells, prolonged mitosis led to the enrichment of H3.3S31ph throughout the arms of misaligned or lagging

mitotic chromosomes, suggesting a function of H3.3S31ph in maintaining genome stability (Hinchcliffe et al., 2016, Chang et al., 2015). The targeting and inactivation of H3.3S31ph by microinjecting monospecific anti-H3.3S31ph antibody does not affect cytokinesis but blocks p53 accumulation in daughter cells (Hinchcliffe et al., 2016). This lack of p53 accumulation in G1 prevents the activation of DNA damage pathways by ATM and ATR (Hinchcliffe et al., 2016). Thus, this indicates a possible function of H3.3S31ph in regulating p53 activation and cell cycle checkpoint at G1 to maintain cell viability.

H3.3 is also deposited at sites of UV-induced DNA damage by HIRA, in addition to euchromatic regions, to facilitate transcriptional recovery after repair (Adam et al., 2013). The complete knockout of H3.3 in chicken cells caused hypersensitivity to UV-induced DNA damage. Interestingly, the expression of neither phospho-null H3.3S31A nor phospho-mimic H3.3S31E prevented hypersensitivity to UV-induced DNA damage, indicating that H3.3S31ph was not associated with hypersensitivity to UV-induced DNA damage (Adam et al., 2013). Nonetheless, with exposure to UV irradiation, chicken cells lacking H3.3 were defective for replication fork progression (Frey et al., 2014). Strikingly, the expression of H3.3S31A restored replication fork progression despite UV irradiation (Frey et al., 2014). This suggests that the H3.3S31 residue and the regulation of H3.3S31ph were critical for maintaining replication fork progression in chicken cells. Although the phenotype of H3.3S31E expression and the mechanism of H3.3S31ph in regulating replication fork progression has not been established, this study investigated the importance of the H3.3S31 residue and the regulation of H3.3S31ph for maintaining replication fork progression at heterochromatic regions. Altogether, these studies show the importance of H3.3S31ph in maintaining DNA damage response and cell viability.

5.1.4 Function of H3.3S31 in development

A recent study using *Xenopus laevis* embryos showed that H3.3S31ph was required for *Xenopus* gastrulation (Sitbon et al., 2020). With H3.3 depletion in *Xenopus laevis* embryos using morpholino specific to H3.3 (Szenker et al., 2012), defects during late gastrulation were prominent (Sitbon et al., 2020). The expression of H3.3S31D (mimics phosphorylation gain), but not H3.3S31A (mimics phosphorylation null), rescued H3.3 depletion during early development in *Xenopus*. This rescue by H3.3S31D expression indicated that the negatively charged phosphorylation mark is needed for the function of the H3.3 variant during early development in *Xenopus*. In support of this, mass spectrometry analysis has shown that H3.3S31D attracts transcriptional activation factors that are key for developmental programs, and repulses factors that drive chromosome condensation (Sitbon et al., 2020). Furthermore, H3.3S31D has been shown to promote H3.3K27ac (acetylated H3.3K27) which is associated with transcriptional activation (Sitbon et al., 2020). Altogether, this study highlights a potential role of H3.3S31ph in cell cycle maintenance and the importance of a negatively charged serine 31 residue in regulating the interaction between H3.3 and H3.3-interacting proteins. In addition, it also shows that H3.3S31ph is dynamic, and its tight regulation is essential during different stages of the cell cycle, allowing for interaction with other proteins to maintain cell viability.

5.1.5 Function of H3.3S31 in transcription regulation

Recent studies have also highlighted a role of H3.3S31ph in transcriptional regulation, as the loss of H3.3S31ph resulted in transcription dysregulation (Frey et al., 2014, Martire et al., 2019, Armache et al., 2020, Sitbon et al., 2020). In mouse ES cells and *Xenopus Laevis* embryos lacking H3.3, H3K27ac, a mark associated with transcriptional activation,

levels were reduced at euchromatic regions, such as enhancers (Sitbon et al., 2020, Armache et al., 2020, Martire et al., 2019). Interestingly, in mouse ES cells lacking H3.3, the expression of phospho-mimic H3.3S31E, but not phospho-null H3.3S31A, restored H3K27ac levels. In addition, depletion of H3.3S31ph through CHK1 inhibition resulted in a loss of H3K27ac at the enhancers (Martire et al., 2019). Interestingly *in vitro* analysis using reconstituted H3.1 containing nucleosomes (with phospho-S28) and H3.3 containing nucleosomes (with phospho-S28 and phospho-S31) showed that although H3.1 and H3.3 were substrates for p300, a well-known histone H3K27 acetyltransferase (Pasini et al., 2010, Raisner et al., 2018, Martire et al., 2019), H3.3S31ph did not affect the expression and enrichment of p300 but instead acted to stimulate p300 activity (Martire et al., 2019). This study shows that H3.3S31ph can interact with other proteins and through stimulation, indicating the unique dynamics of H3.3S31ph in regulating transcription at euchromatin.

A recent study showed that the level of H3.3S31ph is increased in mouse bone marrow-derived macrophages after stimulation with bacterial lipopolysaccharide (Armache et al., 2020). H3.3S31ph ChIP/seq analysis revealed that its deposition is specific for stimulation-induced genes, not a general feature of constitutively expressed genes. Furthermore, the increase in H3K36me3 levels correspond to H3.3S31ph levels at gene bodies after stimulation (Armache et al., 2020). The authors found that H3.3S31ph is driven by IKKα kinase and is required for the recruitment of SETD2, a histone methyltransferase that promotes H3K36 methylation. In addition, H3.3S31ph also blocks ZMYND11 transcriptional repressor from binding to stimulation induced genes (Armache et al., 2020). Previous studies have shown that both H3.3K36me3 and unphosphorylated H3.3S31 are crucial for the interaction between ZMYND11 and H3.3 (Guo et al., 2014, Wen et al., 2014). As such, the phosphorylation of H3.3S31 (despite the presence of H3.3K36me3) rejects ZMYND11

from binding to chromatin and promotes transcriptional activation (Armache et al., 2020). Supporting this, the expression of H3.3S31E (mimics phosphorylation gain) increases transcription of stimulation-induced genes in H3.3 knockout mouse bone marrow-derived macrophages, whereas the expression of H3.3S31A (mimics phosphorylation null) leads to reduced gene expression. Finally, inhibition of RNA Polymerase II elongation and RNA Polymerase II stalling abolishes H3.3S31ph, further suggesting a role for H3.3S31ph in transcription regulation (Armache et al., 2020). Altogether, these studies show that H3.3S31ph plays a role in maintaining transcriptional regulation.

5.1.6 Aims

To date, the function of H3.3S31ph in regulating telomere function or heterochromatin has not been well-studied. Our lab previously showed that H3.3S31ph is enriched at the telomeres of ES cells (Wong et al., 2009). This deposition of H3.3 at heterochromatic regions is guided by ATRX/DAXX (Wong et al., 2010, Lewis et al., 2010). H3.3 interacts with DAXX through the “AAIG” motif of H3.3 (Elsasser et al., 2012), while ATRX interacts with unmodified H3.3K4 and H3K9me3 to deposit newly synthesized H3.3 onto chromatin. (Wong et al., 2010, Udugama et al., 2015). Previous studies have suggested that the H3.3S31 residue does not play a role in H3.3-ATRX/DAXX binding (Elsasser et al., 2012). Nonetheless, the enrichment of H3.3S31ph correlates with the loading of H3.3 by ATRX/DAXX at heterochromatic regions (Wong et al., 2010). Thus, the telomeres of ES cells were used as a model to investigate the function of H3.3S31ph. This chapter investigates the importance of H3.3S31ph for cell survival, its role in heterochromatin maintenance and the relative changes to histone PTM. To achieve these aims, endogenous H3.3-null mouse ES cells expressing exogenous wild-type, S31A (phospho-null) and S31E (phospho-mimic) H3.3, previously generated in **Chapter 4,** were used to investigate the impact of S31A and S31E substitution on telomeric chromatin maintenance in mouse ES cells.

5.2 Results

5.2.1 H3.3S31ph is uncoupled with aberrant cell cycle progression

The phosphorylation of H3.3S31 occurs during mitosis (Hake et al., 2005, Wong et al., 2009). To investigate if H3.3S31ph plays a role in cell cycle progression, wild-type, S31A and S31E-H3.3 mouse ES cell lines were seeded at equal densities, and the number of cells was quantified over 5 days. Compared to the wild-type-H3.3 and control cells, neither S31A nor S31E-cell lines showed any detectable difference in the number of cells at all time points investigated (**Figure 5.2.1A**). Next, to determine if S31A or S31E-H3.3 cell lines progressed through the cell cycle stages at different rates, immunofluorescence analyses using antibodies against H3S10ph or AURKB were used to distinguish the different stages of the cell cycle, such as the G1, S, G2 and M phases. A previous study has shown that enrichment of H3S10ph and AURKB in ES cells. H3S10ph and AURKB were absent in the nucleus during G1. In S phase, H3S10ph was enriched near heterochromatic regions, was further enriched at heterochromatic regions in G2 and, throughout mitotic chromosome arms in GM phase. AURKB was homogenously distributed throughout the S phase nucleus and was enriched at the heterochromatic regions during G2 and centromeric regions of mitotic chromosomes during M phase (Mallm and Rippe, 2015). Similar to wild-type H3.3 cell line, S31A and S31E-H3.3 cell lines showed no detectable change in the number of cells for each cell cycle phase (**Figure 5.2.1B**).

A previous report identified that the regulation of H3.3S31ph is required for proper chromosomal segregation in mammalian cells (Hinchcliffe et al., 2016). Therefore, chromosomal abnormalities, including chromosomal fusions and, loss or gain of chromosomes caused by substitution of S31A or S31E on H3.3 was investigated. First,

mitotic cell populations were enriched in cells expressing wild-type, S31A and S31E-H3.3 and the chromosome number was subsequently quantified. A significant change in the number of chromosomes between wild-type, S31A and S31E-H3.3 cells was not observed (**Figure 5.2.1C**). Additionally, end-to-end chromosomal fusion was not observed (data not shown). Next, to identify if S31A and S31E-H3.3 caused chromosomal mis-segregation, cells were enriched for anaphase using a microfilament formation disruptor, cytochalasin B, to examine the presence of lagging chromosomes (Theodoropoulos et al., 1994, Chan et al., 2012). The experimental design is summarised in **Figure 5.2.1D** (see **Chapter 2.1.3**), and representative images of normal and lagging chromosomes are shown in **Figure 5.2.1E**. The number of lagging chromosomes remained unaltered in both S31A and S31E-H3.3 ES cell lines compared to wild-type H3.3 (**Figure 5.2.1F**). Together, these results demonstrate that H3.3S31 substitution does not lead to a significant change in cell cycle progression and chromosomal abnormalities in ES cells.

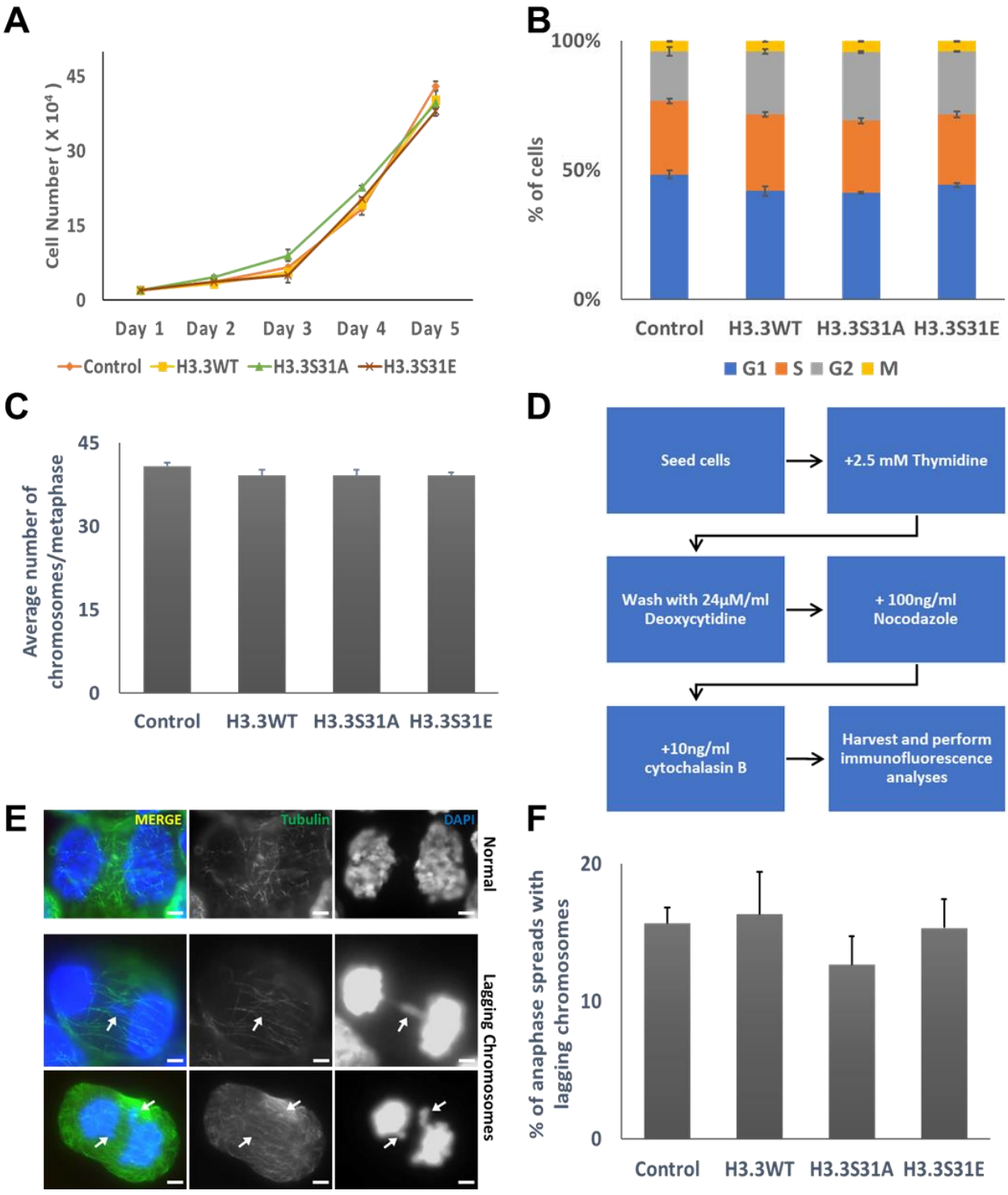
A
Cell Number (X 10⁴)
45
30
15
0
Day 1
Day 2
Day 3
Day 4
Day 5
Control
H3.3WT
H3.3S31A
H3.3S31E
B
100%
50%
0%
% of cells
Control
H3.3WT
H3.3S31A
H3.3S31E
G1
S
G2
M
C
Average number of chromosomes/metaphase
45
30
15
0
Control
H3.3WT
H3.3S31A
H3.3S31E
D
Seed cells
+2.5 mM Thymidine
Wash with 24µM/ml Deoxycytidine
+ 100ng/ml Nocodazole
+10ng/ml cytochalasin B
Harvest and perform immunofluorescence analyses
E
MERGE
Tubulin
DAPI
Normal
Lagging Chromosomes
F
% of anaphase spreads with lagging chromosomes
20
10
0
Control
H3.3WT
H3.3S31A
H3.3S31E

Figure 5.2.1: Wild-type S31A and S31E H3.3 cell lines display similar cell cycle dynamics

*(**A**) Untransfected ES cells (control), wild-type, S31A and S31E-H3.3 cells were seeded at equal densities and counted daily over 5 days. N=3; error bars represent S.E.M.. (**B**) Untransfected ES cells (control), wild-type, S31A and S31E-H3.3 cells were fixed and quantified for percentage (%) of cells in each of the cell cycle phases including G1, S, G2 and Mitosis (M) N=3 (50 cells per N); error bars represent S.E.M.. (**C**) Untransfected ES cells (control), wild-type, S31A and S31E-H3.3 cells were fixed before quantifying the total number of chromosomes. The average number of chromosomes per metaphase spread is shown. N=3 (30 chromosome spreads per N); error bars represent S.E.M (**D**) Overview of cell synchronisation to enrich for anaphase cells. Cells were synchronised to S phase by treatment with thymidine for 16 hours, washed with deoxycytidine and synchronised to mitosis with nocodazole for 10 hours. Cells were then washed and treated with cytochalasin B for 1 hour to enrich for anaphase cells before harvesting for immunofluorescence analyses. (**E/F**) Immunofluorescence analyses were performed with antibody against Tubulin (green) to identify lagging chromosomes. DAPI was used as a nuclear counterstain. Scale bar represents 4µm. Examples of normal anaphase cells (Normal) and abnormal anaphase progression with lagging chromosomes (Lagging chromosomes) are shown in (**E**). Percentages of lagging chromosomes were quantified. N=3 (50 cells per N); error bars represent S.E.M*

5.2.2 H3.3S31ph regulates telomere length maintenance

H3.3S31ph is enriched at the telomeres of ES cells (Wong et al., 2009). Thus, it was possible that H3.3S31ph played a role in regulating telomere length maintenance. Thus, telomere length of long-term cultured wild-type, S31A and S31E-H3.3 ES cell lines was next assessed by Tel-FISH as the intensity of Tel-FISH staining is directly correlated to telomere length (Wong and Slijepcevic, 2004). After 6 (**Figure 5.2.2A**) and 9 (**Figure 5.2.2B**) months of culture, S31A-H3.3 ES cell line showed a decrease in Tel-FISH intensity while S31E-H3.3 ES cell line showed similar Tel-FISH intensity when compared to wildtype-H3.3 ES cell line. To quantify the decrease in telomere length seen in S31A-H3.3 ES cell line, qPCR analyses using primers specific to the telomeres were performed. In line with the findings from Tel-FISH analyses, a decrease in telomere length was observed in S31A-H3.3 ES cells after 6 and 9 months in culture while the telomere length of S31E-H3.3 ES cells remained unchanged (**Figure 5.2.2C**). These results suggest that H3.3S31 and its phosphorylation potentially play a role in telomere length maintenance, and this could be linked to the function of H3.3S31ph in regulating heterochromatin maintenance at the telomeres. Nonetheless, further investigation is required to elucidate the mechanism of H3.3S31ph in regulating telomere chromatin maintenance.

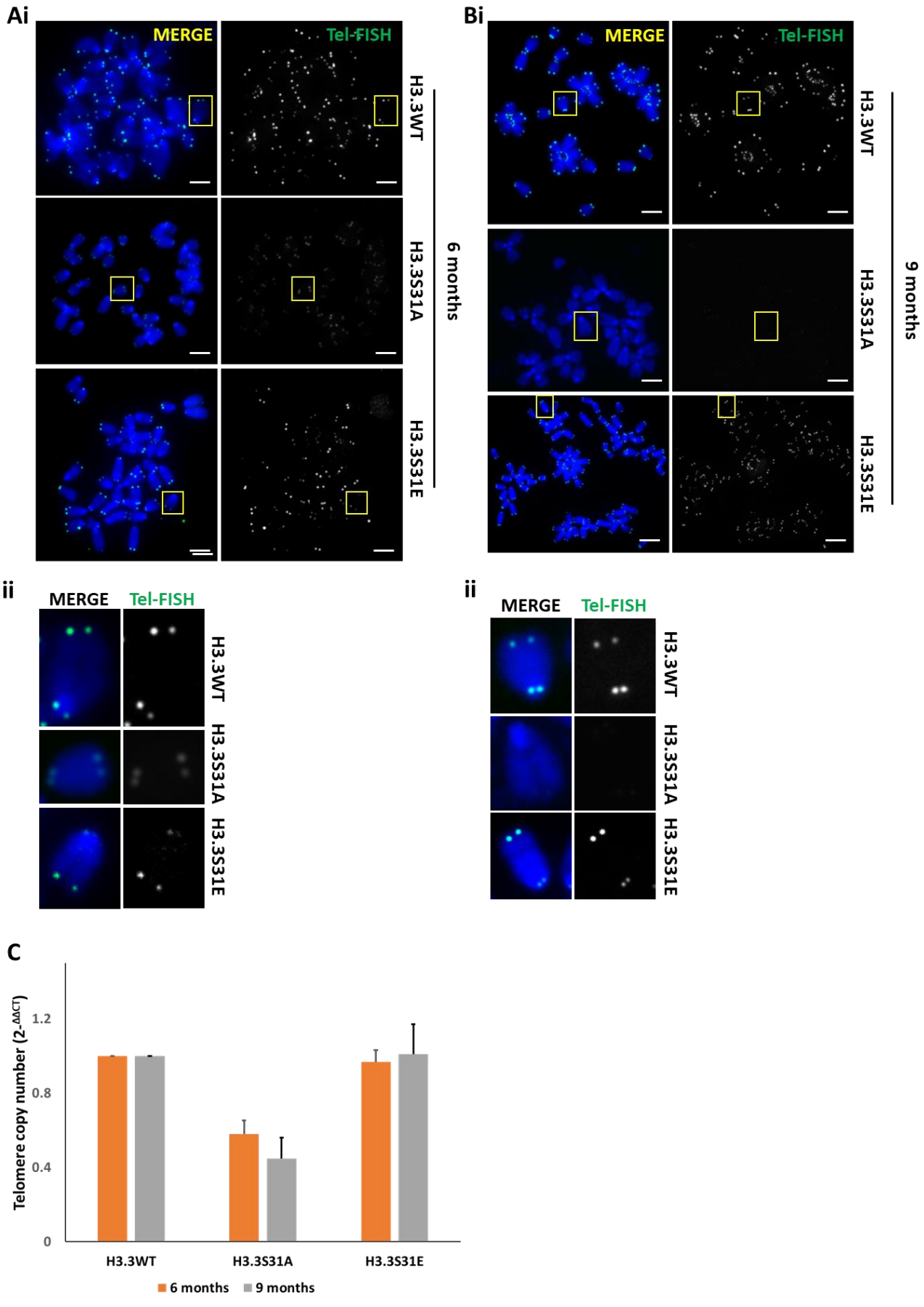
Ai
MERGE
Tel-FISH
H3.3WT
H3.3S31A
H3.3S31E
6 months
Bi
MERGE
Tel-FISH
H3.3WT
H3.3S31A
H3.3S31E
9 months
ii
MERGE
Tel-FISH
H3.3WT
H3.3S31A
H3.3S31E
ii
MERGE
Tel-FISH
H3.3WT
H3.3S31A
H3.3S31E
C
Telomere copy number (2-ΔΔCT)
1.2
0.8
0.4
0
H3.3WT
H3.3S31A
H3.3S31E
6 months
9 months

Figure 5.2.2: H3.3S31 is required for telomere length maintenance

*(**Ai**) Tel-FISH analyses of (**i**) wild-type, (**ii**) S31A and (**iii**) S31E-H3.3 ES cells after 6 and 9 months of culture were performed to determine the changes in telomere length. Tel-FISH signal intensity for S31A-H3.3 cell line were weaker after 6 and 9 months of culture while Tel-FISH signal intensity for S31E-H3.3 cell lines were similar when compared to wild-type-H3.3 ES cell line. DAPI was used as a nuclear counterstain. Scale bar represents 4µm. (**B**) Genomic DNA was harvested from wild-type, S31A and S31E-H3.3 cells after 6 and 9 months of culture before qPCR analyses with telomeres-specific primers were performed. Telomere copy number ($2^{-\Delta\Delta CT}$) was identified with results relative to GAPDH levels and normalised to H3.3 wild-type. Error bars represent S.E.M..*

5.2.3 Histone PTMs are unaffected by H3.3S31 mutations

Previous reports have identified that a crosstalk mechanism on histone tails, or the modification of a residue, may influence other modification on the histone tail (Hirota et al., 2005, Martire et al., 2019, Sitbon et al., 2020). For example, high levels of H3K9me3 are correlated to low levels of H3K4me3 (Lee et al., 2017). In addition, a decrease in H3K27ac levels at enhancer regions was seen following the loss of H3.3S31ph (Martire et al., 2019, Sitbon et al., 2020). Thus, to elucidate if H3.3S31 phospho-mutants altered the global levels of other PTMs, immunoblotting was performed using specific antibody against H3K4me3, H3K9me3, H3K36me3, H3K27me3 and H3K27ac. H3K4me3 was chosen as it is an established mark for transcriptional activation (euchromatin), while H3K9me3 and H4K20me3 were chosen as they are established marks associated with transcriptional repression (heterochromatin) (Kouzarides, 2007). In addition, H3K36me3 was selected due to its proximity to H3.3S31. Finally, H3K27 was investigated as the mutation of H3.3S31 to alanine caused a loss of H3K27ac levels in previous reports (Martire et al., 2019, Sitbon et al., 2020). Immunoblotting showed no noticeable change in the global H3K27ac level (**E**) and in the levels of other PTM including H3K4me3 (**A**), H3K9me3 (**B**), H3K27me3 (**C**), H3K36me3 (**D**) and H3K27ac (**E**) in S31A and S31E-H3.3 cells (**Figure 5.2.3**). Although, densitometry analyses showed noticeable changes in H3K27me3 and H3K27ac levels further biological replicates are required to draw a conclusion (**Figure 5.2.3ii**).

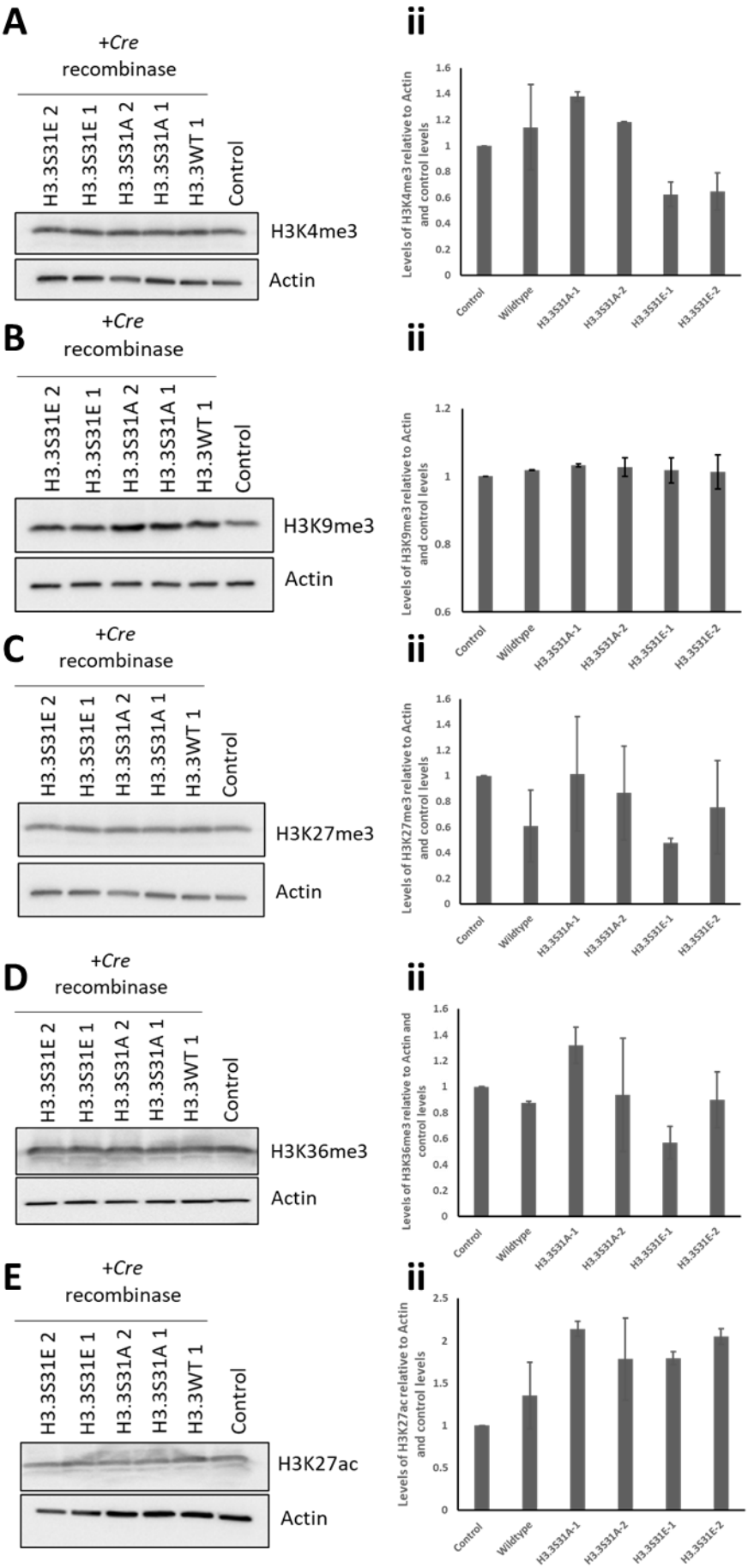
A
+Cre recombinase
H3.3S31E 2
H3.3S31E 1
H3.3S31A 2
H3.3S31A 1
H3.3WT 1
Control
H3K4me3
Actin
ii
Levels of H3K4me3 relative to Actin and control levels
Control
Wildtype
H3.3S31A-1
H3.3S31A-2
H3.3S31E-1
H3.3S31E-2
B
+Cre recombinase
H3K9me3
Actin
Levels of H3K9me3 relative to Actin and control levels
C
+Cre recombinase
H3K27me3
Actin
Levels of H3K27me3 relative to Actin and control levels
D
+Cre recombinase
H3K36me3
Actin
Levels of H3K36me3 relative to Actin and control levels
E
+Cre recombinase
H3K27ac
Actin
Levels of H3K27ac relative to Actin and control levels

Figure 5.2.3: H3.3S31 phospho-mutants did not alter global histone PTM

*Immunoblotting analyses using antibody against (**A**) H3K4me3, (**B**) H3K9me3, (**C**) H3K27me3, (**D**) H3K36me3 and (**E**) H3K27ac were performed on wild-type, S31A and S31E-cell lines. Untransfected ES cells were used as a control. Two different clones were used for S31A and S31E-H3.3 cell lines (denoted as 1 and 2). H3K4me3, H3K9me3, H3K36me3, H3K27me3 and H3K27ac were detected at similar levels between control, wild-type, S31A and S31E-cell lines. Actin levels were used as a loading control. (**ii**) Bands were measured by densitometry by subtracting intensity of band of interest by control actin intensity. The values were then normalised to control cells. N=2*

5.2.4 H3.3S31ph regulates ATRX and PML-NB localisation to the telomeres

The deposition of H3.3 by ATRX/DAXX within PML bodies is known to be dependent on the interaction between ATRX and H3.3K9me3 (Wong et al., 2010, Udugama et al., 2015, Szenker et al., 2011). As it was possible the subtle change of H3K9me3 levels was not detected by immunoblotting and that specific regions may have changes in H3K9me3 levels, the localisation of ATRX within S31A and S31E-H3.3 cell lines was investigated. Strikingly, immunofluorescence analyses using antibody specific to ATRX showed that ATRX levels at the telomeres and pericentric regions of S31A-H3.3 cells were significantly reduced (**Figure 5.2.4i**). In contrast, ATRX levels in S31E-H3.3 cells were increased compared to wild-type-H3.3 cells (**Figure 5.2.4i**). Furthermore, quantification of ATRX/Tel-FISH colocalisation foci showed that S31A-H3.3 cells showed reduced colocalisation foci while S31E-H3.3 cells showed an increase in colocalisation foci (**Figure 5.2.4ii**). To determine if the protein expression of ATRX was a factor in loss of ATRX in S31A-H3.3 cells, immunoblotting with antibody specific to either ATRX or DAXX was performed. The results showed similar levels of ATRX and DAXX between wild-type, S31A and S31E-H3.3 cells (**Figure 5.2.4iii**). This showed that ATRX was unbound to chromatin and is uncoupled with ATRX expression.

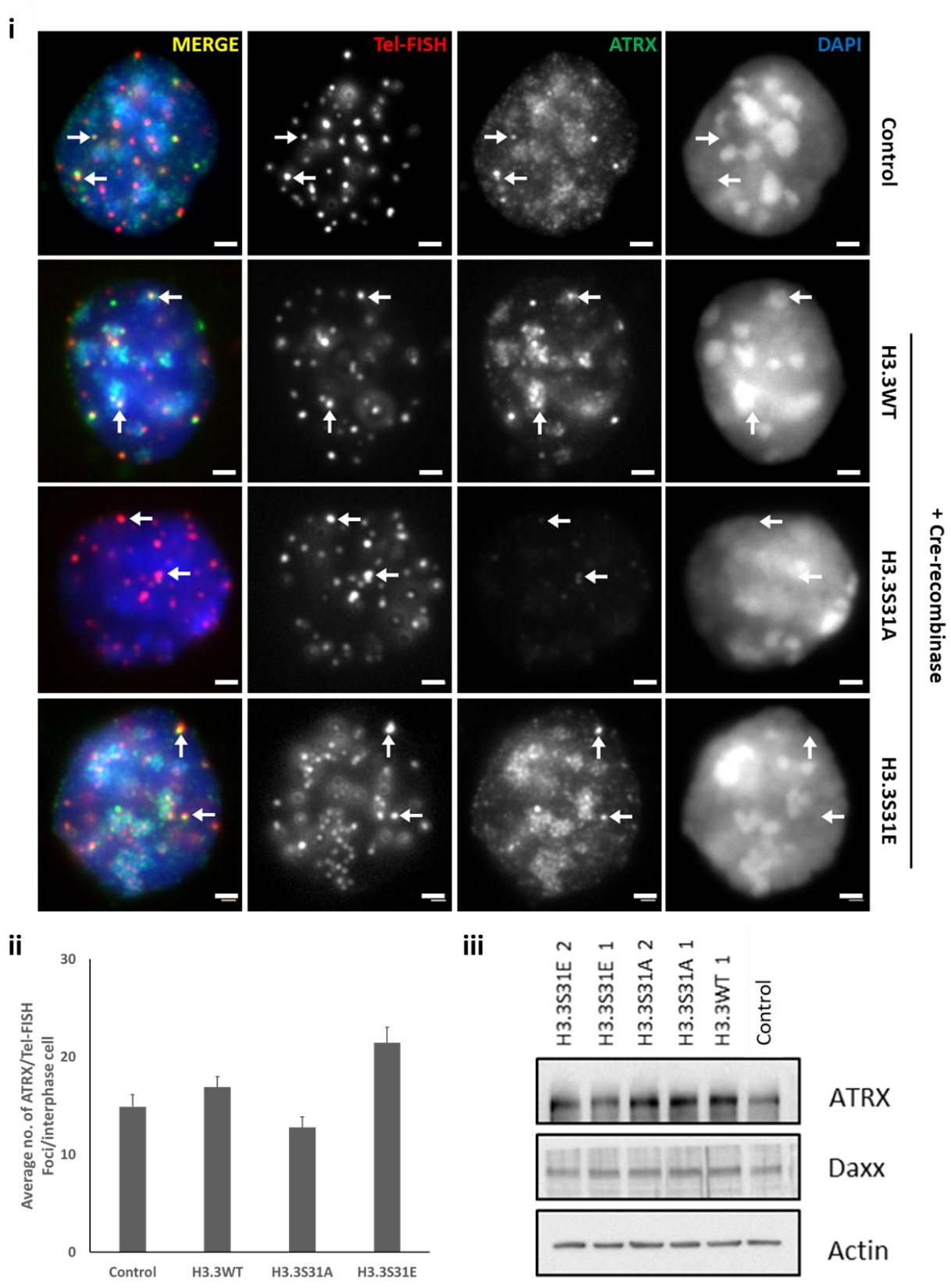
i
MERGE
Tel-FISH
ATRX
DAPI
Control
H3.3WT
H3.3S31A
H3.3S31E
+ Cre-recombinase
ii
Average no. of ATRX/Tel-FISH Foci/interphase cell
30
20
10
0
Control
H3.3WT
H3.3S31A
H3.3S31E
iii
H3.3S31E 2
H3.3S31E 1
H3.3S31A 2
H3.3S31A 1
H3.3WT 1
Control
ATRX
Daxx
Actin

Figure 5.2.4: H3.3S31ph regulates ATRX enrichment and localisation to heterochromatin

*(**Ai**) Immunofluorescence analyses were performed on untransfected cells, wild-type, S31A and S31E-H3.3 cells with antibody against ATRX (green) followed by Tel-FISH (red) to determine the localisation of ATRX. Tel-FISH was used as a telomere marker. ATRX was detected in untransfected ES cells (control), wild-type and S31E-H3.3 cells and was barely detectable in S31A-H3.3 cells. Additionally, ATRX colocalised with Tel-FISH signals at the telomeres of wild-type, S31A and S31E-H3.3 interphase cells (arrows) and were enriched at the pericentric region (DAPI-dense regions). DAPI was used as a nuclear counterstain. Scale bar represents 4 µm. (**ii**) ATRX/Tel-FISH colocalisation foci were quantified. 30 foci per cell was counted. N= 20. Error bars represent S.E.M.. (**iii**) Immunoblotting was performed on untransfected ES cells (control), wild-type, S31A and S31E-H3.3 cell lines to determine the levels of ATRX and DAXX within the cells. For S31A and S31E-H3.3 cell lines, two different clones were used (denoted as 1 and 2). The levels of ATRX and DAXX between wild-type, S31A and S31E H3.3 cell lines were similar to those in control ES cells. Actin was used as a loading control.*

To rule out the possibility that ATRX levels were lost due to a loss of ATRX protein expression, immunofluorescence analyses with antibody specific to ATRX were performed on pre-fixed wild-type, S31A and S31E-H3.3 cells. Compared to the other proteins, ATRX was the only protein that showed minimal staining or loss of binding. Thus, cells were pre-fixed to determine if ATRX levels in the cells. With pre-fixed cells, the cell membrane and proteins within the cells are fixed. In addition, they are not subjected to hypotonic treatment which lyses the cell membrane, removing soluble proteins. Thus, the intact cell membrane prevents unbound proteins from being washed away. The results showed that ATRX was present at similar levels in wild-type, S31A and S31E-H3.3 cells (**Figure 5.2.5**). Together, these results show that the observed loss of ATRX at heterochromatin of S31A-H3.3 cells is uncoupled with ATRX protein expression and, indicate that H3.3S31ph regulates ATRX binding to the telomeres which supports the hypothesis that H3.3S31ph maintains heterochromatin silencing.

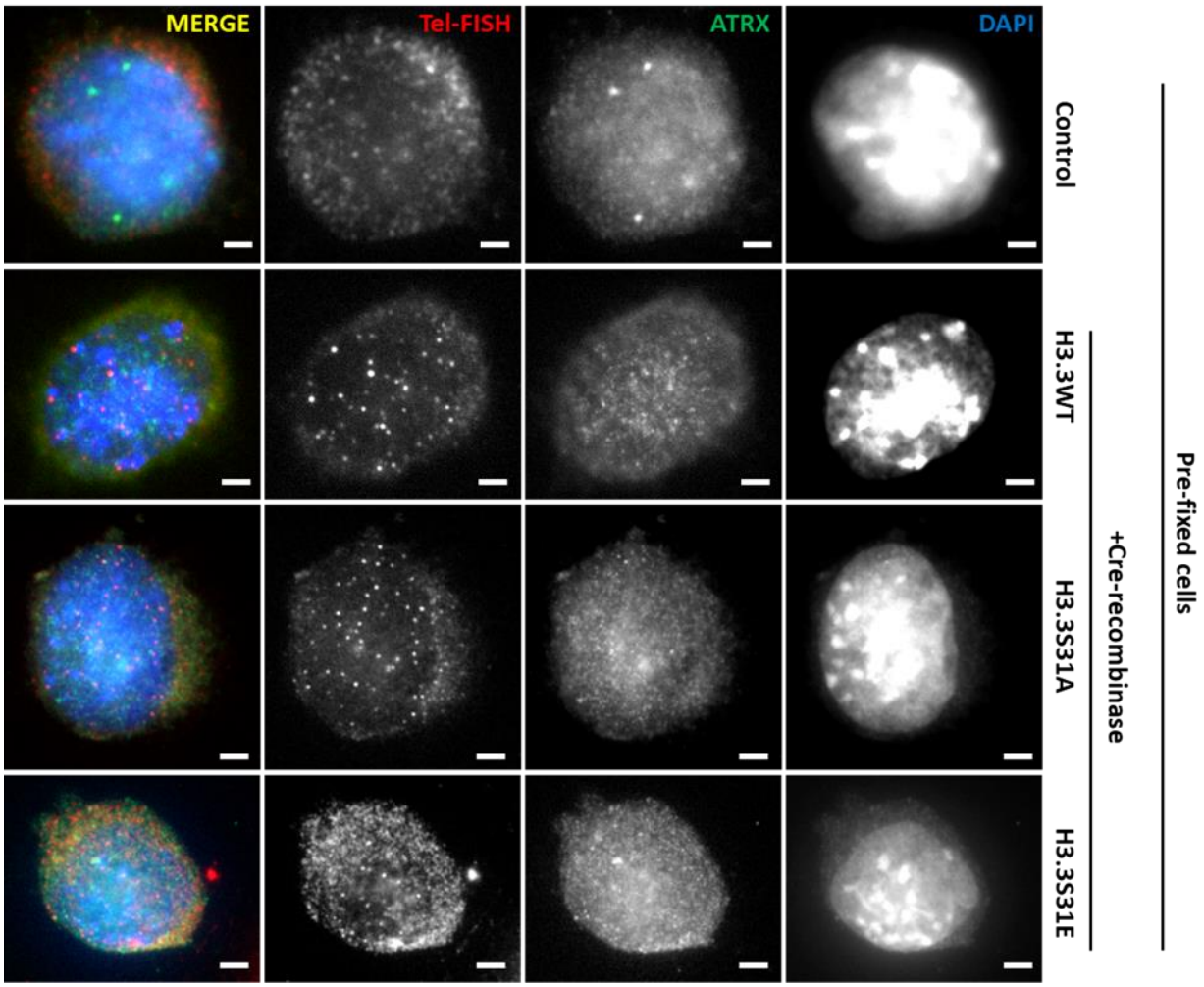

Figure 5.2.5: ATRX expression is unchanged in wild-type, S31A and S31E-H3.3 cell lines

Immunofluorescence analyses were performed on pre-fixed untransfected ES cells (control), wild-type, S31A and S31E-H3.3 cell lines with antibody ATRX (green), followed by Tel-FISH to determine the expression of ATRX. Tel-FISH was used as a telomere marker (red). ATRX levels were similar between wild-type, S31A and S31E-H3.3 cell lines. DAPI was used as a nuclear counterstain. Scale bar represents 4 µm.

ATRX and DAXX are components of promyelocytic nuclear bodies (PML-NBs), which are sites of H3.3 chromatin assembly (Delbarre et al., 2013, Delbarre et al., 2017). The localisation of ATRX, DAXX and H3.3 to PML-NB, is linked explicitly to S phase (Kraushaar et al., 2013, Shastrula et al., 2019). DAXX is known to directly interact with PML-NB (Salomoni and Khelifi, 2006) while PML is recruited during S phase and its depletion increases H3.3 deposition onto chromatin (Shastrula et al., 2019). PML-NBs are required for the regulation of H3.3 chromatin assembly during DNA replication, which has implications for understanding how repressed chromatin is established and maintained (Shastrula et al., 2019).

Thus, the localisation of telomeres to PML-NB in S31A and S31E-H3.3 cells was investigated by immunofluorescence analyses using antibody specific to PML (**Figure 5.2.6**). In wild-type interphase cells, telomeres were enriched at PML-NBs. Interestingly, S31A-H3.3 cell line showed the presence of PML-NBs that were variable in size, and a reduction of telomere localisation to PML-NBs (**Figure 5.2.6**). In contrast to S31A-H3.3 cells, S31E-H3.3 cells showed neither a change in PML-NB size nor a loss of telomeric colocalisation to PML-NBs (**Figure 5.2.6**). These results suggest that H3.3S31ph may act to maintain PML-NB integrity, and localisation of telomeres to PML-NBs.

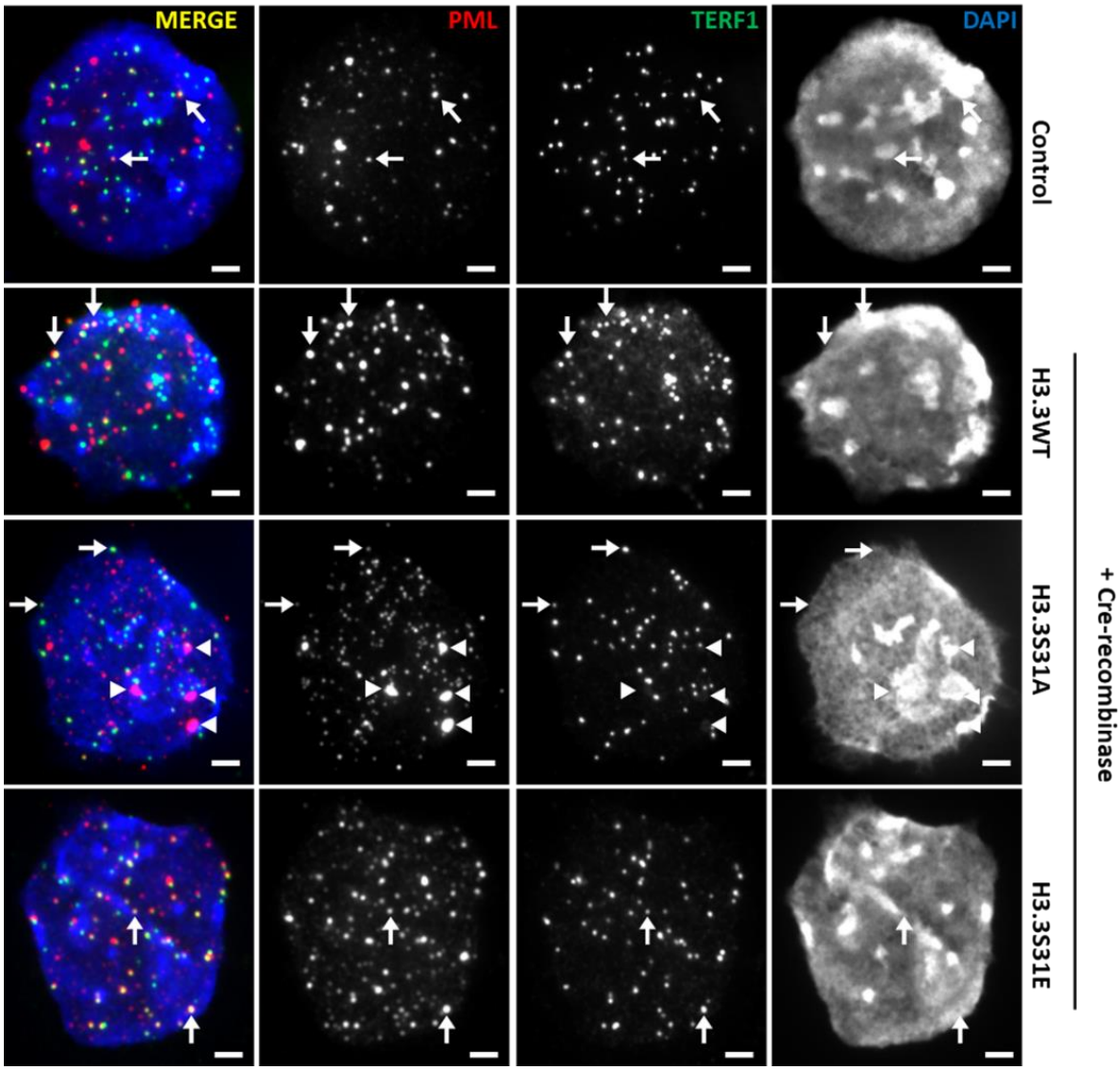

Figure 5.2.6: H3.3S31ph regulates PML-NB integrity and its localisation to the telomeres

*(**A**) Immunofluorescence analyses were performed on wild-type, S31A and S31E-H3.3 cells with antibody against PML (red) and TERF1 (green) to determine the localisation and distribution of PML-NB. TERF1 was used as a telomere marker. PML colocalised with TERF1 signals at the telomeres of control, wild-type, S31A and S31E-H3.3 interphase cells (arrows), S31A-H3.3 cells showed aberrant PML staining pattern (arrowhead). DAPI was used as a nuclear counterstain. Scale bar represents 4 µm.*

As ATRX and DAXX are components of PML-NB, the localisation of ATRX to PML bodies in wild-type, S31A and S31E-H3.3 cells was next investigated by immunofluorescence analyses using antibody specific to PML and ATRX (**Figure 5.2.7i**). ATRX indeed colocalised with PML bodies at the telomeres of wild-type, S31A and S31E-H3.3 interphase cells. In addition to the low levels of ATRX, the aberrant-looking PML staining pattern was also observed for the S31A-H3.3 cells compared to the wild-type H3.3 cells. Furthermore, the quantification of ATRX/PML colocalisation foci showed decreased ATRX/PML colocalisation foci in S31A-H3.3 cells and an increase in S31E-H3.3 cells compared to wild-type-H3.3 (**Figure 5.2.7ii**). These results suggest that H3.3S31ph regulates ATRX localisation to PML bodies. Altogether, the results show that H3.3S31ph regulates ATRX binding and PML-NB recruitment to the telomeres, and this could be linked to H3.3 deposition and heterochromatin formation at the telomeres

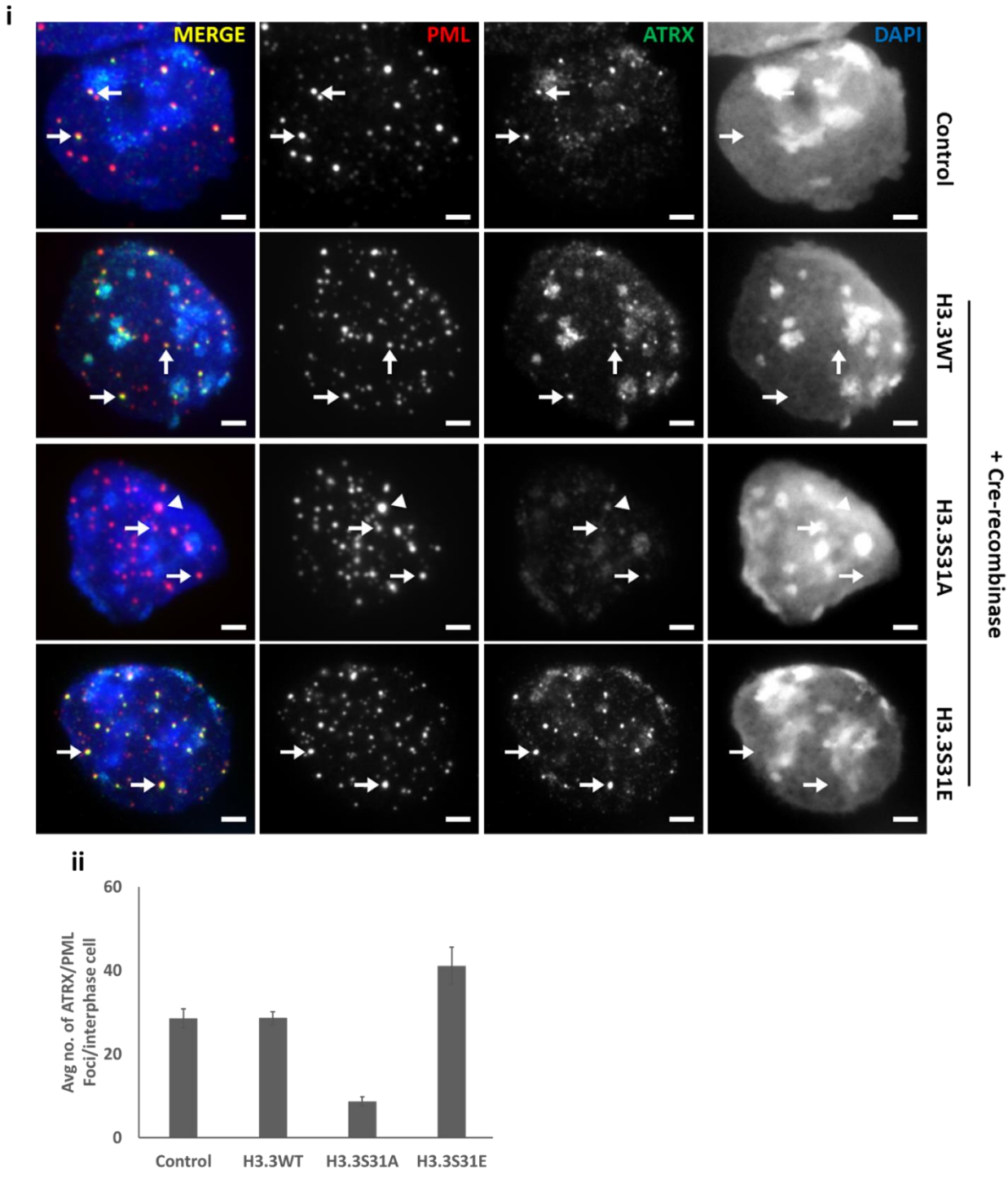
i
MERGE
PML
ATRX
DAPI
Control
H3.3WT
H3.3S31A
H3.3S31E
+ Cre-recombinase
ii
Avg no. of ATRX/PML Foci/interphase cell
60
40
20
0
Control
H3.3WT
H3.3S31A
H3.3S31E

Figure 5.2.7: ATRX and PML colocalise at the telomeres of wild-type, S31A and S31E-H3.3 cell lines

*Immunofluorescence analyses were performed on untransfected ES cells (control), wild-type, S31A and S31E-H3.3 cell lines with antibody against PML (red) and ATRX (green) to determine the colocalisation of ATRX and PML. ATRX levels were similar between the control, wild-type and S31E-H3.3 cells. ATRX levels were barely detectable in S31A-H3.3 cells. PML was detected in control, wild-type, S31A and S31E-H3.3 cells. S31A-H3.3 cell lines showed an aberrant PML staining pattern (arrowhead). ATRX and PML colocalised at the telomeres of control, wild-type, S31A and S31E-H3.3 cell lines. DAPI was used as a nuclear counterstain. Scale bar represents 4μM. **(ii)** ATRX/PML colocalisation foci were quantified. 30 foci per cell was counted. N= 20. Error bars represent S.E.M..*

5.2.5 H3.3S31ph regulates for heterochromatin maintenance at the telomeres

Our lab has previously demonstrated that ATRX recognizes H3.3K9me3 at the telomeres and deposits newly synthesized H3.3 onto telomere chromatin to facilitate heterochromatin maintenance (Udugama et al., 2015). To further investigate if H3.3S31ph regulates ATRX-mediated H3.3 deposition and heterochromatin formation at the telomeres (**Figure 5.2.4**), the levels of ATRX (**iii**), H3K9me3 (**iv**) and H3.3 (**v**) at the telomeres of wild-type, S31A and S31E-H3.3 cells were investigated by ChIP/qPCR analyses using antibody specific to ATRX, H3K9me3 and H3.3 (**Figure 5.2.8**). Compared to the wild-type-H3.3 cells, S31A-H3.3 cells showed lower levels of ATRX, H3K9me3 and H3.3 at the telomeres, whereas these heterochromatin marks were increased at telomeres in S31E-H3.3 cells (**Figure 5.2.8**). These results demonstrate that H3.3S31ph is required for regulating heterochromatin levels at the telomeres.

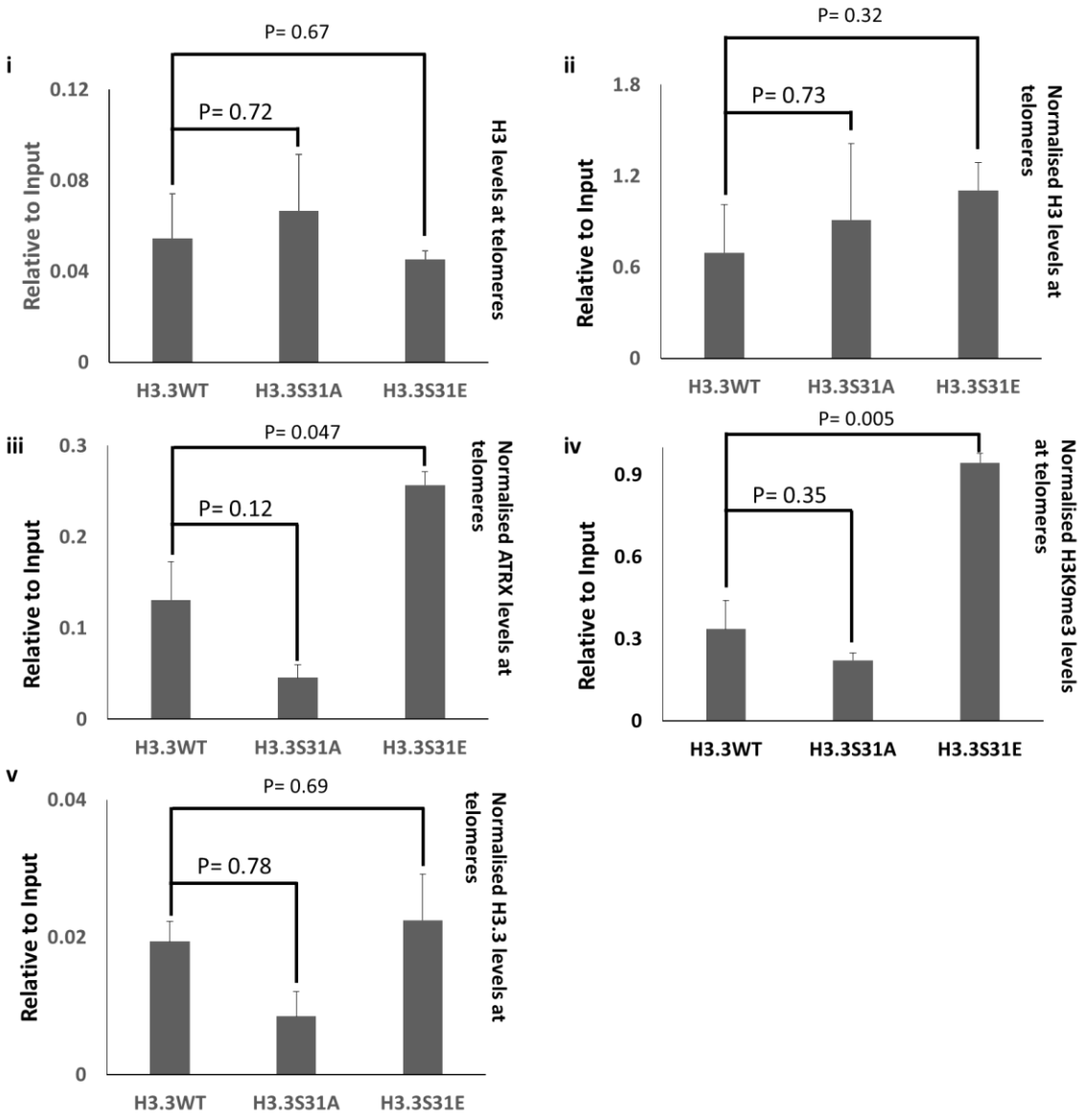

Figure 5.2.8: The regulation of H3.3S31ph is vital for heterochromatin maintenance at the telomeres

*ChIP/qPCR analyses were performed on wild-type, S31A and S31E-H3.3 cell lines with antibody against H3, ATRX, H3K9me3 and H3.3. H3 levels at the telomeres normalised to input are shown in (**i**), H3 levels at the telomeres normalised to input and H3 levels at GAPDH are shown in (**ii**). Results were normalised to input and H3 levels at GAPDH. Compared to wild-type H3.3 cells, ATRX (**iii**), H3K9me3 (**iv**) and H3.3 (**v**) levels at the telomere were decreased in S31A-H3.3 cells and increased in S31E-H3.3 cells. Error bars represent S.E.M.. N=3. P values (shown in graphs) were calculated using two sample t-test.*

5.2.6 H3.3S31ph induces DNA damage at the heterochromatin regions

The loss of heterochromatin has been associated with increased DNA damage and ageing (Lee et al., 2020). Additionally, a previous report showed that the loss of H3.3S31ph and the expression of H3.3S31A in ALT-cancer cells increases DNA damage marker, γH2AX, on chromosome arms, subsequently leading to cell death (Chang et al., 2015). Furthermore, the inactivation of H3.3S31ph prevented p53 accumulation and activated ATM and ATR DNA damage repair pathways (Hinchcliffe et al., 2016). Following this, the regulation of DNA damage response by H3.3S31ph was investigated through immunofluorescence analyses using a specific antibody against γH2AX (Podhorecka et al., 2010). Compared to wildtype-H3.3, S31A-H3.3 cells showed only a slight increase in DNA damage while S31E-H3.3 cells showed a substantial increase in DNA damage at the telomeres in both interphase (**Figure 5.2.9Ai**) and mitotic cells (**Figure 5.2.9Aii**). In S31E-H3.3 mitotic cells, the increased levels of γH2AX were found not only at telomeres but also at the pericentric heterochromatin (**Figure 5.2.9Aii**). In line with the observation made with immunofluorescence analysis, ChIP-qPCR of γH2AX showed increased DNA damage at the telomeres of S31A and S31E-H3.3 ES cells (**Figure 5.2.9B**). This suggest that the maintenance of H3.3S31ph is essential for suppressing DNA damage at the telomeres

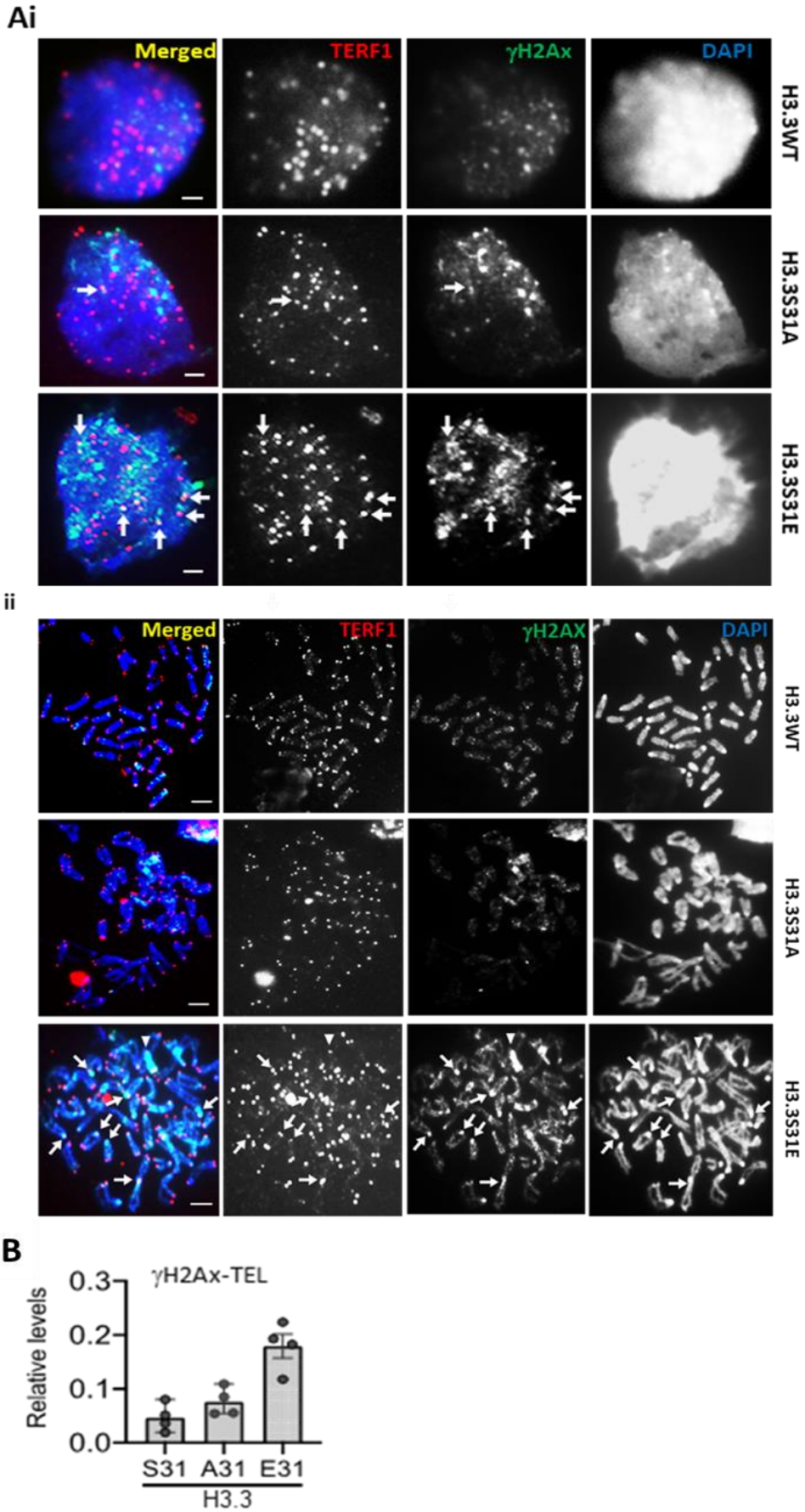
Ai
Merged
TERF1
γH2Ax
DAPI
H3.3WT
H3.3S31A
H3.3S31E
ii
Merged
TERF1
γH2AX
DAPI
H3.3WT
H3.3S31A
H3.3S31E
B
γH2Ax-TEL
Relative levels
0.3
0.2
0.1
0.0
S31
A31
E31
H3.3

Figure 5.2.9: S31E-H3.3 induces DNA damage response at the telomeres

(A) *Immunofluorescence analyses were performed on wild-type, S31A and S31E-H3.3 cell lines with antibodies against TERF1 (red) and γH2AX (green) to determine DNA damage levels at the telomeres. TERF1 was used as a telomere marker. The colocalisation of TERF1 and γH2AX (arrows) showed that when compared to wildtype-H3.3 cells, S31A-H3.3 cells a slight increase in γH2AX levels at the telomere of interphase cells (**i**) while S31E-H3.3 cells had increased γH2AX levels at the telomere of (**i**) interphase and (**ii**) mitotic cells. (**ii**) In mitotic cells, γH2AX levels were increased at the pericentric heterochromatin of S31E-H3.3 and not wild-type and S31A-H3.3 cells. DAPI was used as a nuclear counterstain. Scale bar represents 4μm. (**B**) ChIP/qPCR analyses were performed on wild-type, S31A and S31E-H3.3 cell lines with antibody against γH2AX. Results were normalized to input and H3 levels at the GAPDH. Compared to wild-type H3.3 cells, γH2AX levels at the telomere were increased in both in S31A-H3.3 cells and S31E-H3.3 cells. Error bars represent S.E.M.. N=4.*

H3.3S31ph is enriched at heterochromatic regions including the telomeres and pericentric regions (Ahmad and Henikoff, 2002, Wong et al., 2009, Li et al., 2017a, Schulmeister et al., 2007). With the induction of differentiation, H3.3S31ph is lost at the telomeres of ES cells and is enriched at the pericentric regions during mitosis (Wong et al., 2009)(**Figure 5.2.10A**). Thus, in addition to the telomeres (**Figure 5.2.9**), the increase in DNA damage at other heterochromatin regions such as the pericentric DNA in S31A and S31E-H3.3 cells was also investigated. To address this, immunofluorescence analyses was performed using antibody against γH2AX followed by FISH, with a DNA probe specific to mouse major satellite on differentiated S31A and S31E-H3.3 cells. ES cell differentiation was induced in wildtype, S31A and S31E-H3.3 ES cells by withdrawing leukemia inhibitory factor (LIF) and adding retinoic acid (RA) to the culture media (**Figure 5.2.10A**). The DNA damage at the pericentric regions in S31A-H3.3 cells was similar to the differentiated wildtype-H3.3 cells while the DNA damage level at the pericentric heterochromatin was increased in S31E-H3.3 cells (**Figure 5.2.10B**). These results indicate that H3.3S31ph maintains not only heterochromatin integrity at telomeres but also at other heterochromatic regions or repetitive DNA regions such as the pericentric heterochromatin.

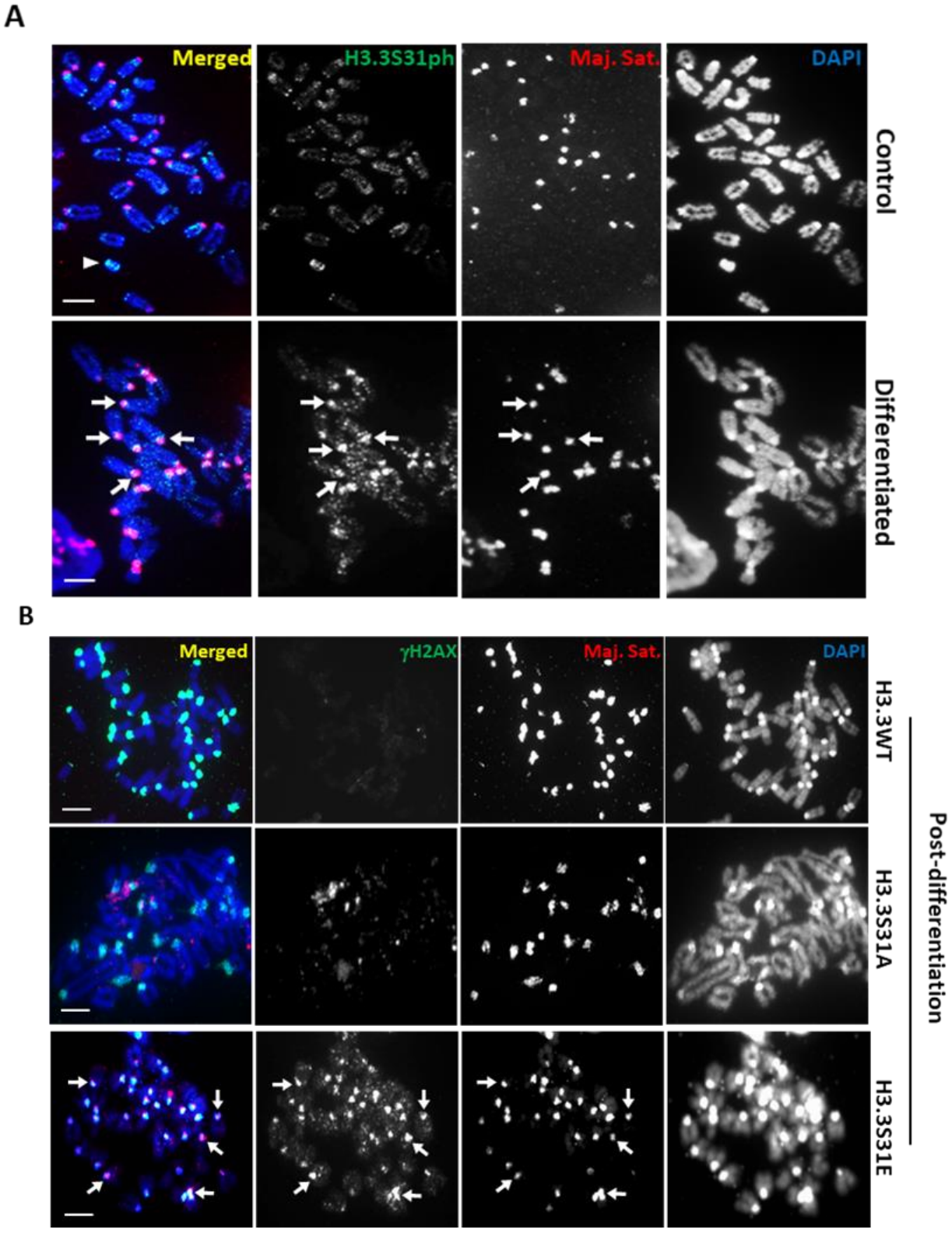

Figure 5.2.10: S31E-H3.3 induces DNA damage response at the pericentric regions

(A) *Differentiation was induced in wildtype, S31A and S31E-H3.3 ES cells by withdrawal of leukemia inhibitory factor from culture media and treatment with retinoic acid 3 for days. Immunofluorescence analyses were performed on untreated and differentiated ES cells with antibody against H3.3S31ph (green) followed by FISH analysis with a DNA probe against mouse major satellite (red). H3.3S31ph was lost at the telomeres and enriched at the pericentric region of mitotic cells after differentiation (arrows). (**B**) Differentiation was induced in wildtype, S31A and S31E-H3.3 ES cells by treatment with retinoic acid and removal of leukemia inhibitory factor from culture media and cultured for 3 days. Immunofluorescence analyses were performed on differentiated wildtype, S31A and S31E-H3.3 ES cells with antibody against γH2AX (green) followed by FISH analysis with a DNA probe against mouse major satellite (red). Compared to wildtype-H3.3, S31A-H3.3 showed a slight increase in γH2AX levels at the major satellite repeat while S31E-H3.3 showed an increase in γH2AX levels at the major satellite repeat. DAPI was used as a nuclear counterstain. Scale bar represents 4μm.*

5.3 Discussion

Telomeres are maintained as a heterochromatin domain and are enriched with heterochromatin markers including ATRX, H3K9me3, and HP1 (Schoeftner and Blasco, 2009). The maintenance of heterochromatin is critical in maintaining telomere length and, preventing telomere recombination and DNA damage response (Cheutin et al., 2003, Hall et al., 2002, Benetti et al., 2007, Dang-Nguyen et al., 2013). The H3.3S31ph mark is present at the telomeres of pluripotent ES cells, including the pericentric repeats as seen in somatic cells (Wong et al., 2009, Ahmad and Henikoff, 2002, Hake et al., 2005). In this chapter, ES cell models carrying substitution of H3.3S31 to alanine (phospho-null) and glutamic acid (phospho-mimic) were used to investigate the effects of H3.3S31 substitution on telomere function.

This chapter has shown that H3.3S31ph does not alter cell cycle dynamics (**Figure 5.2.1**). Interestingly, we have shown evidence that H3.3S31ph plays a role in telomere length maintenance where long-term expression of unphosphorylated H3.3S31 caused telomere attrition while long-term expression of H3.3S31ph maintained telomere length (6 and 9 months) (**Figure 5.2.2**). However, the molecular mechanism of telomere length regulation by H3.3S31ph requires further investigation. Strikingly, S31A-H3.3 cells showed a loss of ATRX while S31E-H3.3 cells showed a gain of ATRX at the telomeres (**Figure 5.2.4 and 5.2.8iii**), indicating a loss of ATRX-mediated deposition of H3.3 and heterochromatin formation in the absence of H3.3S31ph. In consistent with this observation, H3K9me3 (**Figure 5.2.8iv**) and H3.3 (**Figure 5.2.8v**) levels at the telomeres were lost in S31A-H3.3 cells but they were gained in S31E-H3.3 cells. The loss of heterochromatin at the telomeres may affect telomere stability, resulting in the loss of telomere length in S31A-H3.3 cells (**Figure 5.2.2**).

In addition to the losses of ATRX binding and heterochromatin marks, S31A-H3.3 cells also showed reduced telomeric localisation to PML-NBs, indicating that the loss of H3.3S31ph and heterochromatin negatively impacted the deposition of H3.3 into telomeres within PML-NB (**Figure 5.2.6**) (Chang et al., 2013). However, it is surprising that the losses of heterochromatin and PML-NB association did not induce a significant increase in DNA damage at the telomeres of S31A-H3.3 cells. Instead, telomeres in S31E-H3.3 cells showed a substantial increase in DNA damage although heterochromatin was maintained at a high level at the telomeres of these cells (**Figure 5.2.9**). These findings indicate that an aberrant gain of H3.3S31ph can induce DNA damage although H3.3S31ph is required for ATRX binding and heterochromatin formation at the telomeres.

In addition to the increase in DNA damage at the telomeres, DNA damage was also found at pericentric repeats (**Figure 5.2.10**), further linking the gain of H3.3S31ph to DNA damage at heterochromatic regions. The increase in DNA damage was closely correlated with the increase of H3.3S31ph at the pericentric region after differentiation, further indicating the link between H3.3S31ph gain and DNA damage. These results show that H3.3S31ph is critical for regulating proper heterochromatin formation and preventing DNA damage activation at repetitive DNA regions.

Despite being maintained as a silenced domain, we have recently shown that a H3K9/K36 demethylase, KDM4B (lysine (K)-specific demethylase 4B), binds to and removes H3K9me3 (H3.3K9me3) at the telomeres to increase chromatin accessibility and to facilitate replication (Udugama et al., 2021). In mouse ES cells, loss of KDM4B leads to increases in both replication stress and DNA damage at telomeric repeats (Udugama et al., 2021). At the telomeres of ES cells, the loss of KDM4B led to the loss of heterochromatin-associated

proteins including H3K9me3, ATRX and HP1α, resulting in increased replication stress, suggesting that the regulation of KDM4B, possibly by H3.3S31ph, maintains accessibility of telomeric heterochromatin to facilitate DNA replication and heterochromatin maintenance. Based on these findings, there were possibilities that KDM4B binding could be increased at telomeres, thus leading to losses of heterochromatin marks and ATRX binding at telomeres. On the other hand, S31E-H3.3 could prevent KDM4B binding at telomeres, which in turn leads to increases of heterochromatin and chromatin inaccessibility that induce replication stress and DNA damage at telomeres. The relationship between KDM4B binding and H3.3S31ph will be investigated in **Chapter 6**

Chapter 6: H3.3S31ph regulation of KDM4B function at the telomeres

6.1 Introduction

6.1.1 Overview

Eukaryotic DNA is wrapped around by histones to form chromatin, and this is important for the protection of the genome. This chromatin structure exists either as an “open” state, allowing access of transcriptional factors for RNA transcriptional activities, or a “closed” state where DNA is condensed to ensure repression of transcription. The maintenance of chromatin structure in both the “closed” and “open” states is controlled by histone PTMs.

A wide range of PTMs, which mainly target the histone N-terminal tail, regulate chromatin function. Of the numerous PTMs, the reversible incorporation of phosphate, acetyl or methyl groups within histone tails have been widely investigated (Rothbart and Strahl, 2014). These histone PTMs are maintained through activities of writer and eraser proteins that either add or remove PTM marks (Hyun et al., 2017). Further, histone variants and PTMs act in combination by providing binding platforms for reader proteins such as chromatin remodelers, histone chaperones, DNA/histone-modifying enzymes and various transcription factors. The reader proteins contain domains that allow for the recognition of specific binding sites. For example, HP1α reads unphosphorylated H3S10 and H3K9me3 through its chromodomain to promote chromatin compaction and transcriptional repression at heterochromatin (Hirota et al., 2005, Lachner et al., 2001).

Due to this complex regulation of proteins, histone PTMs play a critical role in cellular events such as DNA replication and repair, gene expression, chromatin compaction and cell-cycle maintenance (Kouzarides, 2007, Allis and Jenuwein, 2016, Hyun et al., 2017). Misregulation of histone PTM has been implicated in developmental defects and the pathogenesis of

cancer and diseases, accentuating the importance of proper histone PTM regulation (Wang and Allis, 2009, Allis and Jenuwein, 2016, Greer and Shi, 2012). Of importance to this chapter is the H3.3S31ph mark and its maintenance of heterochromatin through the regulation of KDM4B and H3K9me3.

6.1.2 Histone Lysine Readers Writer and Erasers

On the H3 N-terminal tail, various lysine residues, including H3K4, H3K9, H3K27 and H3K36 are subject to methylation (Black et al., 2012). These residues can exist in unmethylated, mono-methylated, di-methylated and tri-methylated forms (Martin and Zhang, 2005). Although these forms do not change the electronic charge of the amino-acid side chain, these levels of methylation do directly alter chromatin compaction and gene expression (Martin and Zhang, 2005). Thus, methylation functions mainly by reader proteins containing methyl-lysine-binding motifs that specifically recognize the methylated site (Martin and Zhang, 2005). For example, H3K4 and H3K36 tri-methylation are associated with gene activation, whereas H3K9 and H3K27 tri-methylation are linked to gene repression (Rea et al., 2000, Lachner et al., 2001, Dhayalan et al., 2010, Fang et al., 2010, Yuan et al., 2011).

The regulation of histone PTM and its importance in transcription was first reported in 1964. However, the discoveries of the first histone methyltransferase (SUV39H1) (Rea et al., 2000) and demethylase (KDM1A) (Shi et al., 2004) were not made till 2000 and 2004, respectively. Nevertheless, these vital discoveries paved the way for the discoveries of other histone methyltransferases and demethylases by searching for proteins carrying the catalytic SET (Su[var]3–9, Enhancer of Zeste, and Trithorax) and Jumonji C (JmjC) domains, respectively.

The regulation of PTM by writers and erasers creates a dynamic environment for specific reader protein binding (Martin and Zhang, 2005). To read methylated lysine resides, reader proteins require methyl-lysine-binding motifs such as PHD, chromo, tudor and PWWP domains. In addition to these unique sites, reader proteins can distinguish target methyl-lysine based on their methylation state and surrounding amino-acid sequence (Musselman et al., 2014). A summary of reader, writer, and eraser proteins for H3K9me3 and H3K36me3 is shown in **Table 6.1**.

Table 6.1: Summary of H3K9 and H3K36 interacting proteins

	Writer Name	*Diseases*	*Reference*	*Erasers name*	*Diseases*	*Reference*	*Reader name*	*Functions*	*Reference*
H3K9	SUV39H/KMT1A–B	Blood cell defects, chromosome instability	(Song, Jung et al. 2001)(Braig, Lee et al. 2005)	JHDM2A/KDM3A	Malignant colorectal cancer, prostate adenocarcinoma	(Qi, Nakayama et al. 2010, Uemura, Yamamoto et al. 2010)	HP1α/β	Heterochromatin formation	(Bannister, Zegerman et al. 2001)
	G9a/KMT1C	Breast and ovarian cancers	(Mechanic, Raynor et al. 1991, Wozniak, Klimecki et al. 2007)	JHDM2B/KDM3B	Myeloid leukemia	(Kim, Kim et al. 2012)	HP1γ	Transcription elongation	(Vakoc, Mandat et al. 2005)
				JHDM2C/KDM3C	—	=	UHRF1	DNA methylation	(Feldman, Gerson et al. 2006)
	SETDB1/KMT1E	Huntington disease	(Ryu, Lee et al. 2006)	JHDM3A/KDM4A	Bladder and breast cancers	(Kauffman, Robinson et al. 2011, Patani, Jiang et al. 2011)			
	PRDM family	Breast and liver cancers, AML	(Steele-Perkins, Fang et al. 2001, Sasaki, Meguro et al. 2002)	JHDM3B/KDM4B	Peripheral nerve sheath tumor	(Pryor, Brown-Kipphut et al. 2011)			
				JHDM3C/KDM4C	Esophageal and breast cancers	(Yang, Imoto et al. 2000, Liu, Bollig-Fischer et al. 2009)			
				JHDM3D/KDM4D	—	-			
				PHF8/KDM7B	X-linked mental retardation	(Laumonnier, Holbert et al. 2005)			
				PHF2/KDM7C	Breast carcinoma	(Sinha, Singh et al. 2008)			
H3K36	SETD2/KMT3A	Renal cell carcinoma	(Duns, van den Berg et al. 2010)	JHDM1A/KDM2A	—	-	DNMT3A	DNA methylation	(Dhayalan, Rajavelu et al. 2010)
	NSD1/KMT3B	AML, neuroblastoma	(Wang, Cai et al. 2007)(Berdasco, Ropero et al. 2009)	JHDM1B/KDM2B	Leukemia, bladder carcinoma	(He, Nguyen et al. 2011, Kottakis, Polytarchou et al. 2011)	LEDGF	DNA repair (HR)	(Pfister, Ahrabi et al. 2014)

6.1.3 Readers Writer and Erasers of H3K9me3

H3K9 methylation is a well-known heterochromatin marker (Barski et al., 2007). In mammalian cells, H3K9 is methylated by histone methyltransferases such as SUV39H1, SUV39H2 and SETDB1 (Garcia-Cao et al., 2004, Hyun et al., 2017). The regulation by these individual histone methyltransferases have roles in diverse cellular events (Hyun et al., 2017). For example, SETDB1 catalyses the mono-methylation of H3K9 at constitutive heterochromatin and provides a substrate for SUV39H1/2 to produce H3K9me3 (Loyola et al., 2009). However, unlike SETDB1, SUV39H1 and SUV39H2 catalyze the di- and trimethylation in constitutive heterochromatin (Lachner et al., 2001, Dang-Nguyen et al., 2013, Garcia-Cao et al., 2004). The loss of SUV39H1/2 proteins resulted in the loss of H3K9me2 and H3K9me3 but not H3K9me1 (Rice et al., 2003, Dang-Nguyen et al., 2013, Garcia-Cao et al., 2004), indicating the specificity of the writers and the corresponding methylation group. In ES cells, this loss of H3K9me3 levels resulted in reduced HP1α binding and aberrantly elongated telomeres (Dang-Nguyen et al., 2013, Garcia-Cao et al., 2004).

The demethylation of H3K9me3 is regulated by KDMs such as including lysine demethylase 3 (KDM3), lysine demethylase 4 (KDM4) and lysine demethylase 7 (KDM7). Of these demethylases, KDM3 and KDM7 are responsible for the demethylation of H3K9me1 and H3K9me2 which promotes transcriptional activation (Yamane et al., 2006, Loenarz et al., 2010). Demethylation of H3K9me1 and H3K9me2 by KDM3 functions by KDM3 binding to DNA through their Zinc finger domain to demethylate H3K9me1 and H3K9me2 (Brauchle et al., 2013) while demethylation of H3K9me1 and H3K9me2 by KDM7 is regulated through the interaction between their PHD domain and the H3K4me3 marks at active chromatin (Horton et al., 2010, Fortschegger and Shiekhattar, 2011). In contrast to KDM3 and KDM7,

KDM4 family proteins are H3K9/K36 demethylases that remove methyl marks from H3K9me2, H3K9me3, H3K36me2 and H3K36me3 (Wei et al., 2017, Yuan et al., 2016, Arifuzzaman et al., 2020).

Previous studies have shown that SETDB1 and SUV39H1/2 methylate H3K9 at the pericentric regions and telomeres to maintain heterochromatin (Rea et al., 2000, Dang-Nguyen et al., 2013, Garcia-Cao et al., 2004). The H3K9me3 then acts as a binding spot for HP1α through their chromodomains and form multimers with SUV39H1/2. Furthermore, as SUV39H1/2 also has a chromodomain, they are further recruited to methylate H3K9, maintaining a heterochromatic environment (Wang et al., 2012, Rea et al., 2000, Lachner et al., 2001). These interactions aid SUV39H1/2 in spreading H3K9me3 to neighbouring nucleosomes (Wang et al., 2012). In addition to the heterochromatic environment created by SUV39H1/2, HP1α also contributes to heterochromatin formation by recruiting other proteins involved in heterochromatin formation, such as histone deacetylase, transcriptional repressors, and chromatin remodeler (Hall et al., 2002). The dissociation of HP1α from chromatin occurs during mitosis and it is driven by the phosphorylation of H3S10 by AURKB (Hirota et al., 2005).

In addition to HP1α, ATRX is another reader of H3K9me3. In ES cells, ATRX contains a PHD-like zinc finger and an ADD domain. For ATRX to deposit newly synthesised H3.3 at heterochromatic regions such as the telomeres, unmodified H3K4 and H3K9me3 PTM marks are required (Wong et al., 2010, Dhayalan et al., 2011, Voon and Wong, 2016). Interestingly, the binding of KDM4 family proteins to H3.3 is increased in paediatric gliomas where the H3.3 glycine at residue 34 is mutated to arginine (Voon et al., 2018). Although the binding affinity of KDM4 proteins to H3.3G34R was increased, the enzymatic activity of

the KDM4 proteins was inhibited by the G34R mutation, leading to increased levels of H3K9me3 and H3K36me3 across the genome (Voon et al., 2018). The simultaneous binding and inhibition of KDM4 by H3.3G34R, is similar to the interactions between H3K27M/PRC2 (Yuan et al., 2011, Fang et al., 2018) or H3K36M/SETD2 (Zhu et al., 2017, de Almeida et al., 2011, Edmunds et al., 2008).These studies show that the histone point mutations can act through inhibition of not only epigenetic writers but also the erasers.

Many studies have indicated that the misregulation of H3K9me3 could contribute to the development of diseases, including neurodegenerative diseases and cancers (Hyun et al., 2017). An aberrant increase in H3K9me3 levels has been found in brain-derived neurotrophic factor genes within mouse Alzheimer models. These genes are essential for synaptic plasticity, and the increased H3K9me3 levels at these genes led to its downregulation, a hallmark of Alzheimer disease (Walker et al., 2013). Furthermore, the aberrant increase of H3K9me3 is also linked to the development of cancers, including breast cancer (Yokoyama et al., 2013, Chi et al., 2010, Hyun et al., 2017). It is tempting to speculate that the increase of H3K9me3 at tumour suppressor genes could repress their expression, allowing for unregulated cell cycle progression (Voon et al., 2018, Mechanic et al., 1991, Wozniak et al., 2007).

6.1.4 Readers Writer and Erasers of H3K36me3

In mammalian cells, a number of histone methyltransferases such as KMT3B, KMT3G, KMT3F and SETD2 are known to methylate H3K36 (Wagner and Carpenter, 2012). Of these methyltransferases, only SETD2 tri-methylates H3K36, while the other methyltransferases are responsible for the mono-methylation and di-methylation of H3K36 (Edmunds et al.,

2008). Although it has been reported that recombinant SETD2 is able to mono-, di- and tri-methylate H3K36 *in vitro*, SETD2 is only able to tri-methylate H3K36 *in vivo* as the loss of SETD2 led to a loss of only H3K36me3 levels (Yuan et al., 2009, Nimura et al., 2009). In addition, decreases of all three forms of H3K36 methylation, *i.e.,* H3K36me1, H3K36me2 and H3K36me3, are found in cells line deficient for KMT3B, KMT3F and KMT3G (Lucio-Eterovic et al., 2010). These studies show that KMT3 proteins are likely required for the mono-methylation and di-methylation of H3K36, whereas SETD2 is required for catalysing H3K36me3 (**Table 6.1**).

The demethylation of methylated H3K36 is regulated by KDM2 and KDM4. Specifically, the demethylation of H3K36me1 and H3K36me2 is regulated by KDM2, while the demethylation of H3K36me2 and H3K36me3 is regulated by KDM4 (Tsukada et al., 2006, Klose et al., 2006). In addition to its activity in H3K36me3 demethylation, KDM4 also demethylates H3K9me3 (Wei et al., 2017, Yuan et al., 2016). These studies suggest that other biological processes, or even histone PTMs, may regulate the methylated and demethylated state of H3K36 by histone methyltransferases and demethylases.

H3K36me3 is widely known to be associated with transcription elongation and prevents aberrant transcription initiation within the gene body (Carrozza et al., 2005, Rahman et al., 2011). In mammalian cells, a complex of various methyltransferases and demethylases interact with both the transcription elongation factors and the phosphorylated S2 residue of C-terminal-RNA polymerase II to maintain a repressed state in newly incorporated nucleosomes to prevent cryptic RNA Polymerase activity (Carrozza et al., 2005, Rahman et al., 2011). This repressed state is maintained through H3K9 and H3K36 methylation and the demethylation of methylated H3K4 (Fang et al., 2010). In addition, the PWWP domain of

both KMT3G and DNMT3A bind to nucleosomes with H3K36me3 and further contribute to repress aberrant transcription (Fang et al., 2010, Dhayalan et al., 2010) (**Table 6.1**).

Interestingly, in addition to its localisation at the gene bodies, H3K36me3 also localises to the gene promoter regions and is important for transcriptional activity (Young et al., 2011, Rahman et al., 2011, Guo et al., 2014, Wen et al., 2014). Here, H3K36me3 inhibits the activity of the PRC2 complex and prevents PRC2-mediated trimethylation of H3K27 methylation and silencing of Arabidopsis Flowering Locus C (*FLC)* vernalization gene (Yuan et al., 2011). The enrichment of H3K27me3 and H3K36me3 is mutually exclusive, and this antagonism is functionally important in regulating transcription. A lack of H3K36me3 results in a fully silenced state at *FLC* even in the absence of cold, suggesting that H3K36me3 is a histone PTM that promotes transcription, and it acts in opposition to H3K27me3 which is required for *FLC* silencing (Yuan et al., 2011).

In addition to the regulation of transcriptional elongation, H3K36me3 has also been associated with DNA damage response (Li et al., 2013, Fnu et al., 2011) and pre-mRNA processing (Hyun et al., 2017, Guo et al., 2014). Recent studies have shed light on the role of H3K36me3 in activating DNA damage response (Sun et al., 2020). Upon the induction of DSB, RAD51, which promotes homologous strand invasion during homologous recombination (HR) repair, is recruited to the chromatin by H3K36me3 at actively transcribed genes (Aymard et al., 2014). The depletion of SETD2, the main H3K36 tri-methyltransferase, severely affects RAD51 binding and impedes HR at such DSBs. In line with this observation, the overexpression of H3K36 demethylase, KDM4A, is found to affect HR repair at DSBs (Pfister et al., 2014). These findings, where H3K36me3 is involved in HR repair, are surprising considering H3K36me3 is a PTM closely associated with gene transcription.

Further investigations are needed to uncover how H3K36me3, that pre-exists at the actively transcribed genes, controls DSB repair (House et al., 2014, Aymard et al., 2014).

H3K36me3 also play a role in large-scale intron retention through regulation of ZMYND11 binding (Guo et al., 2014, Ladendorff et al., 2001, Wen et al., 2014). For ZMYND11 to bind and read H3.3 PTMs through the PWWP domain, both unphosphorylated H3.3S31 together with H3.3K36me3 are required (Wen et al., 2014, Guo et al., 2014). Upon the phosphorylation of H3.3S31, ZMYND11 is ejected from chromatin (Wen et al., 2014). The H3K36me3 is enriched at the exons in the alternative splicing process and are low at intron-less genes (de Almeida et al., 2011). Interestingly, the loss of H3K36me3 at SETD2 target genes through SETD2 depletion reduces H3K36me3 and induces alternative splicing (Guo et al., 2014). In addition to its function in alternative transcriptional splicing, ZMYND11 functions as a tumour suppressor. The loss of ZMYND11 binding led to worsened prognosis in breast cancer patients, while overexpression led to tumour suppression *in vitro* (Wen et al., 2014). Altogether, these studies identify the importance of H3K9me3 and H3K36me3 in regulating chromatin function through reader, writer and eraser proteins.

The misregulation of H3K36me3 has been reported in various diseases, including neurodegenerative diseases and cancer (Hyun et al., 2017). However, the molecular mechanism is currently unknown. Nonetheless, the loss of H3K36me3 through the reduction of KMT3B results in the Sotos syndrome, a neurological disorder characteried by macrocephaly and cognitive and motor skill deficiencies (Kurotaki et al., 2002). In addition, the loss of H3K36me3 through the reduction in SETD2 has been associated with the development of various cancers, including renal cell carcinoma. In addition, the loss of

H3K36me3 caused a loss of ZMYND11 binding, resulting in worsened prognosis in breast cancer patients (Wen et al., 2014).

6.1.5 Family of KDM

A prominent demethylase protein family of H3K9me3 and H3K36me3 is the KDM4 family. To date, five different members of the KDM4 family have been discovered: KDM4A, KDM4B, KDM4C, KDM4D and KDM4E (Labbe et al., 2013). These five members share a similar JmjC domain and a Jumonji N (JmjN) domain. The JmjC domain is critical for demethylase function where it employs an oxygenase mechanism to demethylate specific histone mono-, di- and tri-methylated lysine residues, while the JmjN domain interacts with JmjC to provide structural integrity (Xu et al., 2011, Janke et al., 2017). Interestingly, only KDM4A, KDM4B and KDM4C consist of other domains such as the Tudor and PHD domains. Studies have shown that the Tudor domain is vital for binding H3K4me2/me3 and H4K20me2/me3 through their aromatic residues (Lee et al., 2008, Bock et al., 2011). Although the PHD domain binds unmodified, methylated, and acetylated histone residues on one or more histone tails, the function of this interaction has yet been studied. A summary of the KDM4 family is shown in **Figure 6.1**.

The KDM4A, KDM4B and KDM4C genes are located at 1p34.1, 19p13.3 and 9p24.1, respectively (Labbe et al., 2013). In addition, the KDM4D gene is located at 11q21, where it clusters with both KDM4E and KDM4F genes. Other than KDM4F, which is suggested to be a pseudogene, the expression of KDM4A, KDM4B, KDM4C, KDM4D and KDM4E has been documented (Fang et al., 2010, Xiang et al., 2019, Yuan et al., 2016). The KDM4 family is highly conserved between organisms, suggesting a conserved role in maintaining cell cycle

progression and survival. For example, triple knockout of KDM4A, KDM4B and KDM4C in hematopoietic stem cell lead to the accumulation of H3K9me3 on transcription start sites, resulting in a downregulation of expression of several genes important for the maintenance of hematopoietic cell identity and survival (Agger et al., 2019).

As previously discussed, the family of KDM4 proteins are vital for the demethylation of H3K9me3 and H3K36me3 (Wei et al., 2017, Xiang et al., 2019, Yuan et al., 2016). In paediatric gliomas, H3.3 point mutations are frequently found (Chen et al., 2020, Bjerke et al., 2013). The H3.3K27M, H3.3G34R, H3.3K36M mutations prevent the binding or function of a number of histone writer and eraser proteins (Voon et al., 2018, Lewis et al., 2013, Udugama et al., 2021, Fang et al., 2018). For example, the mutation of H3.3K27M reduced H3K27me2 and H3K27me3 levels but does not affect PRC2 complex recruitment, indicating that the spread of H3K27me2 and H3K27me3 were inhibited. The removal of H3.3K27M restores H3K27me2 and H3K27me3 levels which in turn rescues cell proliferation and prevents the formation of tumors (Harutyunyan et al., 2019). The other mutation, H3.3G34R, preferentially binds KDM4 and inhibits its demethylase activity, leading to genome wide gains in H3K9me3 and H3K36me3 (Voon et al., 2018). This global change H3K9/K36 profile is similar to the chromatin changes found in KDM4 A/B/C triple-knockout cells (Voon et al., 2018). Finally, the H3.3K36M mutation decreases the levels of H3K36me2 and H3K36me3 and increases H3K27me3 levels indicating and impaired PRC2 complex function (Yuan et al., 2011, Schmitges et al., 2011). This change impairs the differentiation of mesenchymal progenitor cells and promotes tumor formation (Lu et al., 2016).

In addition to changing the global chromatin landscape (Voon et al., 2018), H3.3 mutation also affects genome stability. A recent study from our group has shown H3.3G34R promotes

ALT maintenance pathway through the inhibition of KDM4B function (Udugama et al., 2021). Of the five KDM4 proteins, KDM4B has been found to be the key KDM4 protein that is important for controlling telomere function (Udugama et al., 2021). Although telomeres are maintained as a heterochromatic domain, KDM4B binding is required for controlling chromatin accessibility during replication. During replication, KDM4B binds to and removes H3K9me3 (H3.3K9me3) at telomeres to increase chromatin accessibility and to facilitate replication. Loss of KDM4B results in replication stress and DNA damage at telomeric heterochromatin. These findings suggest that ATRX and KDM4B act in cooperation to maintain a balanced chromatin state at telomeres, which is accessible for replication but maintained as a stable chromatin domain that inhibits aberrant transcription.

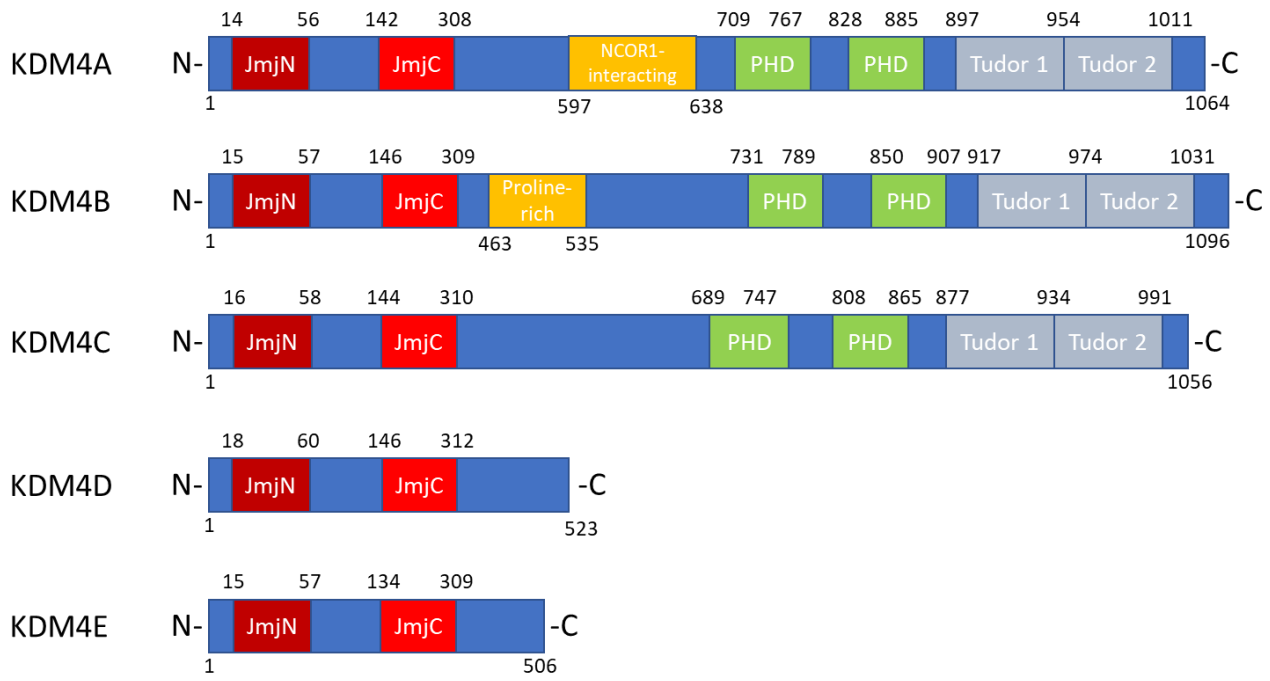

Figure 6.1: KDM4 family and their domains

The different KDM4 family members, gene location and substrates are shown. The domains relevant to each member Is also shown. JmjN domain (Maroon), JmjC domain (Red), plant homeodomain (Green), tudor domain (Grey).

6.1.6 Aims

This chapter investigates the histone epigenetic modifiers that are affected by H3.3S31ph. The role of H3.3S31ph at euchromatic region has been substantially studied (Martire et al., 2019, Sitbon et al., 2020, Armache et al., 2020). However, its function at heterochromatin has not been studied. Previous studies have shown that H3.3S31ph is enriched at heterochromatic regions, where H3.3 is deposited by ATRX/DAXX, such as the pericentric repeats and telomeres of ES cells. The previous chapter (**chapter 5**) has shown the H3K9me3 and ATRX levels were decreased at the telomeres of S31A-H3.3 cells and increased in S31E-H3.3 cells. As the levels of H3K9me3 had changed in S31A and S31E-H3.3 ES cell lines, it is likely that H3.3S31ph regulates the binding of H3K9me3 writer/reader/eraser proteins to maintain heterochromatin formation. A previous study from our lab has shown that KDM4B, a H3K9me3 and H3K36me3 demethylase, is enriched at the telomeres of ES cells (Udugama et al., 2021). Furthermore, the increase in DNA damage suggests a loss of chromatin accessibility and an increase in replication stress, a similar phenotype of KDM4B knockout (Udugama et al., 2021). Thus, in this chapter, the regulation of binding and activity by KDM4B with H3.3S31ph is investigated to elucidate the role of H3.3S31ph in heterochromatin maintenance, ensuring proper chromatin accessibility and preventing replication stress.

6.2 Results

6.2.1 H3.3S31ph regulates KDM4B levels at the telomere

Findings in Chapter 5 have shown that the level of heterochromatin marks including H3K9me3, and ATRX binding are reduced at the telomeres of S31A-H3.3 cells (**Figure 5.2.4** and **5.2.8**). On the other hand, gains of H3K9me3 and ATRX levels are found at the telomeres of S31E-H3.3 cells (**Figure 5.2.4** and **5.2.8**). These findings suggest that H3.3S31 and its phosphorylation promote heterochromatin formation. Given our recent finding that KDM4B, a H3K9/K36 demethylase, is enriched at the telomeres of mouse ES cells (Udugama et al., 2021), the changes in H3K9me3 and ATRX levels in S31A and S31E-H3.3 mutant cells could potentially be linked to KDM4B binding to telomeres.

To investigate the relationship between H3.3S31ph and KDM4B function, we first assessed the enrichment of KDM4B at the telomeres during the cell cycle progression. Mouse ES cells were synchronized and harvested at G1/S, S and M phases, respectively (Wong et al., 2009), and subjected to ChIP/qPCR analyses with antibody against KDM4B. The result showed that KDM4B was enriched at G1/S and S phases but decreased during mitosis (**Figure 6.2.1A**). The binding pattern of KDM4B at telomeres is different from H3.3S31ph, which is only detected during mitosis (Hake et al., 2005, Wong et al., 2009). These findings suggest that H3.3S31ph and KDM4B do not co-exist at telomeres. Thus, we hypothesised that H3.3S31ph may promote heterochromatin maintenance at telomeres in mouse ES cells by preventing binding of KDM4B.

Next, to investigate if the reduction in H3K9me3 level at telomeres was caused by increased KDM4B levels in S31A-H3.3 cells (**Figure 5.2.8iv**), ChIP/qPCR analyses with antibody

against KDM4B were performed. Compared to wild-type-H3.3 cells, KDM4B level was substantially increased at telomeres in S31A-H3.3 cells (**Figure 6.2.1B**). There was no significant change in KDM4B level at telomeres in S31E-H3.3 cell lines. These observations suggest that the gains of KDM4B are likely responsible for the losses of H3K9me3 and ATRX at telomeres in S31A-H3.3 cells (**Figure 5.2.8iv**).

To further investigate whether the H3.3S31ph mark, or lack thereof, may alter the ability of KDM4B to bind and detach during cell cycle progression, the enrichment of KDM4B at the telomeres during different stages of the cell cycle in S31A and S31E-H3.3 mutant mouse ES cells was investigated. Wild-type, S31A and S31E-H3.3 mouse ES cells were synchronized and then harvested at G1/S, mid S, late S and M phases, respectively, prior to ChIP/qPCR analyses with antibody against KDM4B. Compared to the levels of KDM4B at telomeres in wild-type H3.3, KDM4B level was increased at telomeres in S31A-H3.3 cells throughout the cell cycle. The increase in KDM4B binding at telomeres in S31A-H3.3 cells was most prominent at mid S phase, with an approximate 5.7-fold increase (**Figure 6.2.1C**). These observations suggest that H3.3S31ph plays a role in regulating KDM4B binding to telomeres, and this could account for the changes in H3K9me3 levels at the telomeres of S31A and S31E-H3.3 mutant ES cells (**Figure 5.2.8iv**).

Given that H3K36me3 was also a target of KDM4B, the impacts of S31A and S31E substitutions on H3K36me3 levels were also investigated (Xiang et al., 2019, Wei et al., 2017, Voon et al., 2018). ChIP/qPCR on S31A and S31E-H3.3 cells with an antibody specific to H3K36me3 showed a slight decrease of H3K36me3 at the telomeres of S31A-H3.3 cells. This is not surprising considering that the level of H3K36me3 was not an abundant histone mark at telomeres. However, a substantial increase in H3K36me3 level was found at the

telomeres of in S31E-H3.3 cells (**Figure 6.2.1D**). These results provide further evidence that KDM4B binding at telomeres is regulated by H3.3S31ph.

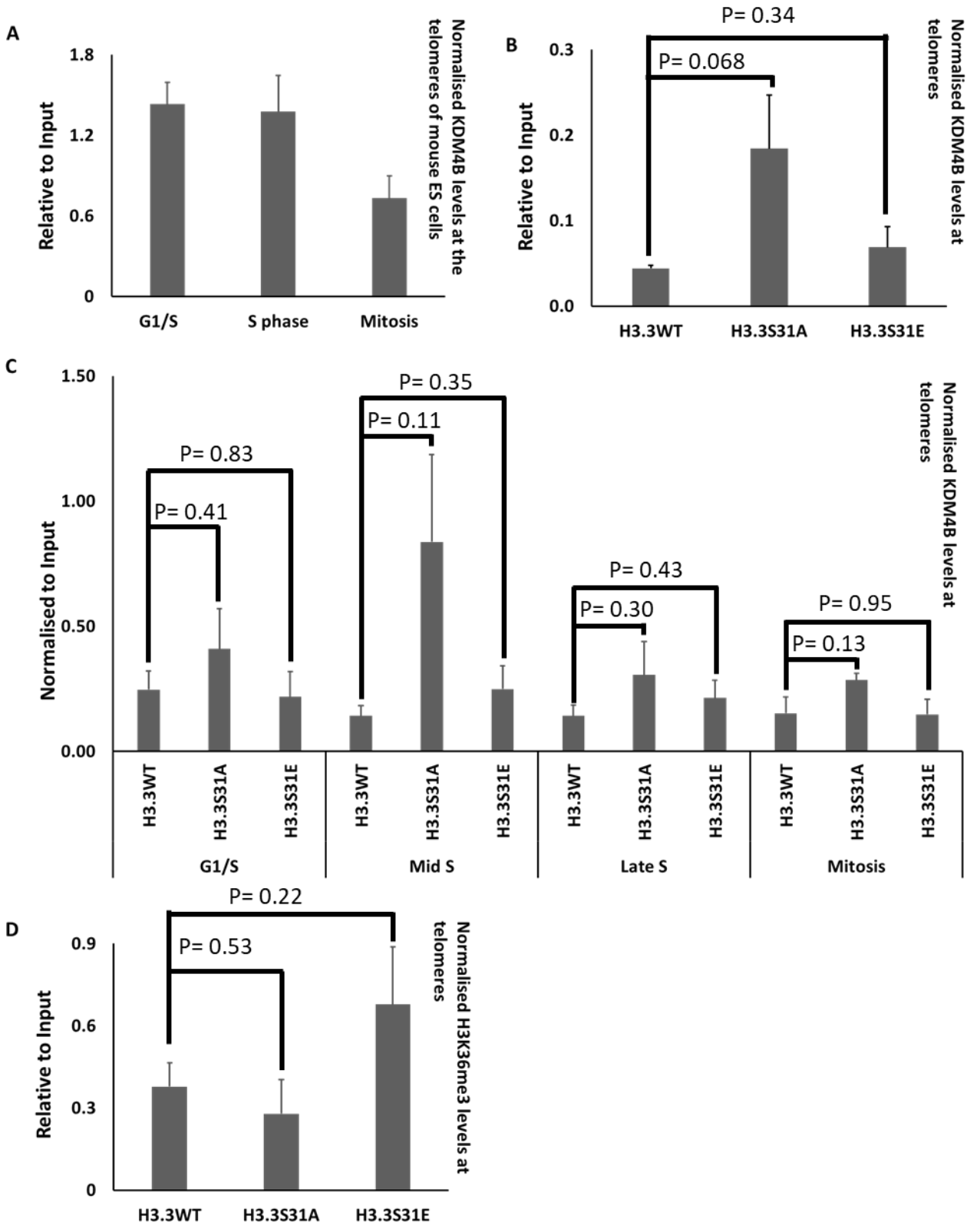
A
Relative to Input
1.8
1.2
0.6
0
G1/S
S phase
Mitosis
Normalised KDM4B levels at the telomeres of mouse ES cells
B
P= 0.34
P= 0.068
Relative to Input
0.3
0.2
0.1
0.0
H3.3WT
H3.3S31A
H3.3S31E
Normalised KDM4B levels at telomeres
C
Normalised to Input
1.50
1.00
0.50
0.00
P= 0.83
P= 0.41
P= 0.35
P= 0.11
P= 0.43
P= 0.30
P= 0.95
P= 0.13
H3.3WT
H3.3S31A
H3.3S31E
G1/S
Mid S
Late S
Mitosis
Normalised KDM4B levels at telomeres
D
P= 0.22
P= 0.53
Relative to Input
0.9
0.6
0.3
0
H3.3WT
H3.3S31A
H3.3S31E
Normalised H3K36me3 levels at telomeres

Figure 6.2.1: KDM4B is enriched during S phase at the telomeres of ES cells

*(**A**) ChIP/qPCR analyses were performed on mouse wild-type ES cells synchronized to G1/S, S and M (mitosis) phases, respectively, with KDM4B antibody. KDM4B levels at the telomeres were enriched at both G1/S and S phase and are lost by mitosis. (**B**) ChIP/qPCR analyses were performed on wild-type, S31A and S31E-H3.3 cell lines with KDM4B antibody. KDM4B level was found to be greatly increased at the telomeres of S31A-H3.3 cells but not in S31E-H3.3 cells. (**C**) ChIP/qPCR analyses were performed using an antibody against KDM4B on wild-type, S31A and S31E-H3.3 cell lines synchronized to G1/S phase, S phase and Mitosis. Compared to wild-type H3.3, an approximate 1.8-fold, 5.7-fold and 2.4-fold increase in KDM4B at the telomeres was observed for G1S, S phase and mitosis for S31A H3.3 cells. In contrast, compared to wild-type H3.3, an approximately 1.6-fold increase in KDM4B at the telomeres was observed for S phase in S31E-H3.3 cells. KDM4B levels at the telomeres of S31E-H3.3 cells during G1S and mitosis were similar to wild-type H3.3 cells. (**D**) ChIP/qPCR analyses were performed with an antibody against H3K36me3 on wild-type, S31A and S31E-H3.3 cell lines. H3K36me3 levels decreased at the telomeres of S31A-H3.3 cells and increased at the telomeres of S31E-H3.3 cells. All results were normalised to input and H3 levels at GAPDH. Error bars represent S.E.M.. N=3. P values (shown in graphs) were calculated using two sample t-test.*

6.2.2 H3.3S31ph regulates KDM4B binding *in vivo*

The increased level of KDM4B together with the loss of H3K9me3 at the telomeres in S31A-H3.3 cells suggest that H3.3S31 and its phosphorylation may regulate KDM4B binding. Therefore, the interaction between H3.3S31A and H3.3S31E mutations with KDM4B was investigated by performing protein immunoprecipitation. To address this, FLAG-tagged KDM4B (FLAG-KDM4B) was expressed in wild-type, S31A and S31E-H3.3 cells followed by immunoprecipitation using an antibody against FLAG. The results showed increased binding between H3.3S31A and KDM4B compared to wildtype H3.3 (**Figure 6.2.2**). In contrast, binding between H3.3S31E and KDM4B was barely detectable (**Figure 6.2.2**). These findings are consistent with the model that KDM4B level is increased at telomeres in S31A-H3.3 cells (**Figure 6.2.1B**), and the high level of KDM4B drives the demethylation of H3K9me3 (**Figure 5.2.8iv**).

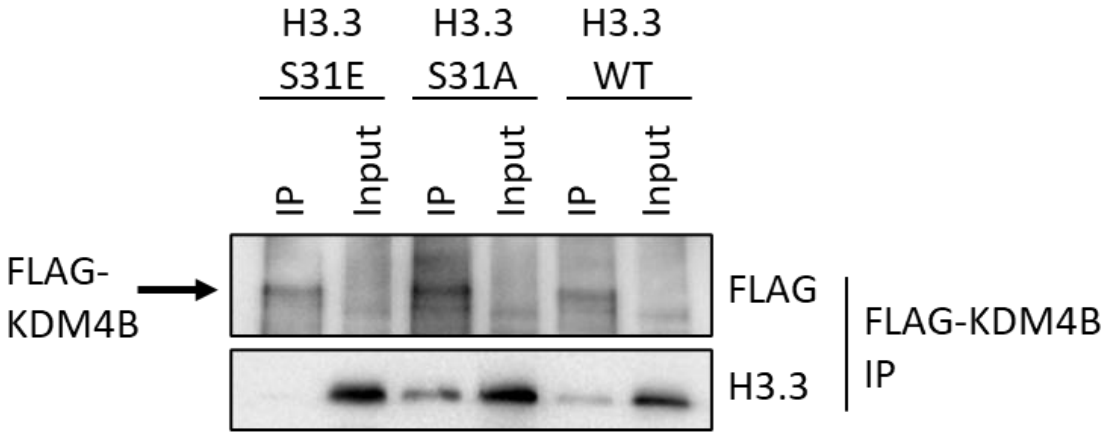

Figure 6.2.2: H3.3S31ph regulates KDM4B binding in ES cells

*(**A**) Wild-type, S31A and S31E-H3.3 cell lines were transfected with FLAG-KDM4B followed by immunoprecipitation with an antibody against FLAG-tag. Immunoblotting with antibodies specific to FLAG-tag and H3.3 were performed, respectively, to determine the binding between KDM4B and, H3.3S31A and H3.3S31E. Compared to wild-type H3.3, a high level of H3.3S31A was bound to FLAG-KDM4B, whereas there was a lower interaction between H3.3S31E and FLAG-KDM4B.*

6.2.3 H3.3S31ph regulates KDM4B function *in vitro*

To further investigate if H3.3S31ph regulates KDM4B activity, four different H3.3S31 peptides carrying the H3.3K36me3 modification were generated. The four H3.3S31 peptides contained i) H3.3-K36me3 (wild-type), ii) H3.3S31A-K36me3, iii) H3.3S31ph-K36me3, and iv) H3.3S31E-K36me3, respectively (**Figure 6.2.3**). The H3.3K36me3 modification was chosen as it is a target of KDM4B, was in close proximity to H3.3S31ph (Wei et al., 2017) and the limitations on peptide length. The *in vitro* demethylation assay was performed using KDM4B recombinant proteins, and the activity of KDM4B was assessed through the demethylation of H3.3-K36me3.

With the generated peptides, *in vitro* demethylase assays were performed with KDM4B protein followed by mass spectrometry analyses of the peptides to determine if KDM4B binding and activity is regulated by H3.3S31ph (**Figure 6.2.4**). KDM4B demethylated K36me3 in H3.3-K36me3 (wildtype, non-phosphorylated) and the H3.3S31A-K36me3 (phospho-null peptide) with equal proficiency (**Figure 6.2.4i and ii**). In contrast, KDM4B was unable to demethylate K36me3 in H3.3S31ph-K36me3 (phosphorylated) and H3.3S31E-K36me3 (phospho-mimic peptide) (**Figure 6.2.4iii and iv**). This indicated that unphosphorylated H3.3S31 promotes KDM4B binding and activity while phosphorylated H3.3S31 inhibits KDM4B binding and activity. Furthermore, these results suggest that the changes in ATRX (**Figure 5.2.8iii**), H3K9me3 (**Figure 5.2.8iv**) and H3.3 (**Figure 5.2.8v**) levels at the telomeres of S31A and S31E-H3.3 mutant cell line were due to the variation of KDM4B binding (**Figure 6.2.1B and 6.2.2**) and activity (**Figure 6.2.4**).

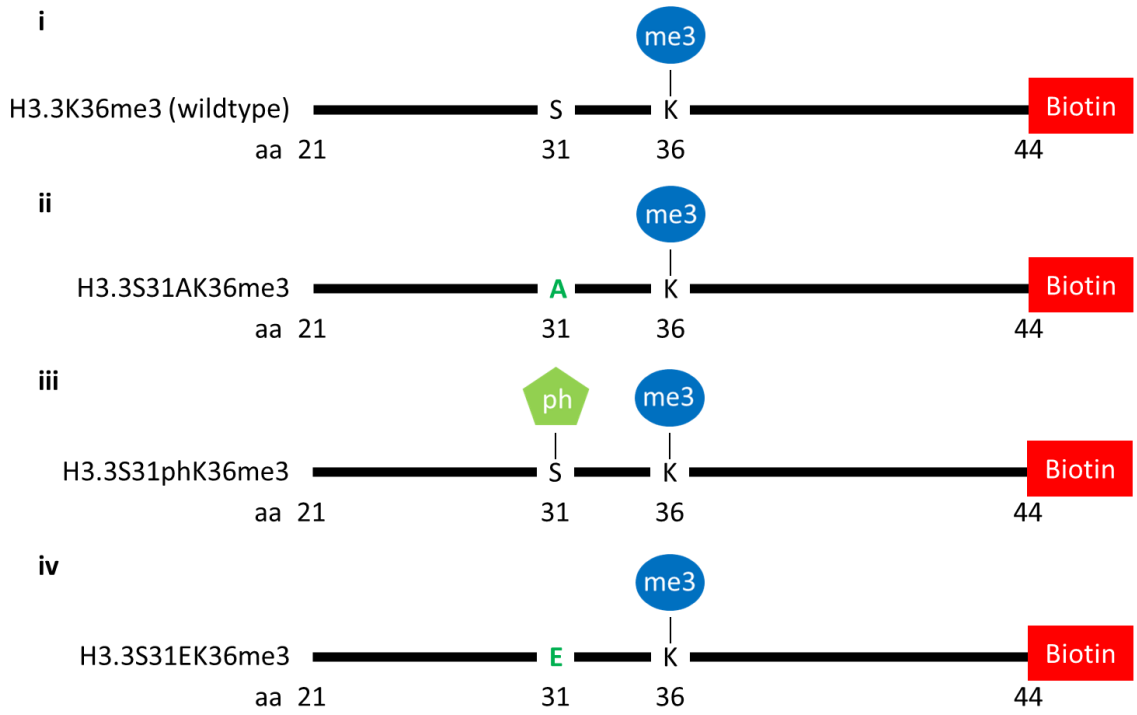

Figure 6.2.3: Schematic of H3.3 peptides generated for in vitro demethylase assay

*(**i**) H3.3-K36me3 (wild-type), (**ii**) H3.3S31A-K36me3, (**iii**) H3.3S31ph-K36me3 and (**iv**) H3.3S31E-K36me3 were generated for in vitro demethylase assay. The region of H3.3 spanning aa 21 to aa 44 was used to generate the peptides. As a positive control for demethylase activity, H3.3-K36me3 (wild-type) was used in the assay. H3.3S31ph-K36me3 and H3.3S31E-K36me3 were used to determine if phosphorylated H3.3S31 prevented KDM4B activity, while H3.3S31A-K36me3 was used to determine if the lack of H3.3S31 phosphorylation promoted KDM4B activity. The peptides also carried a Biotin tag.*

i

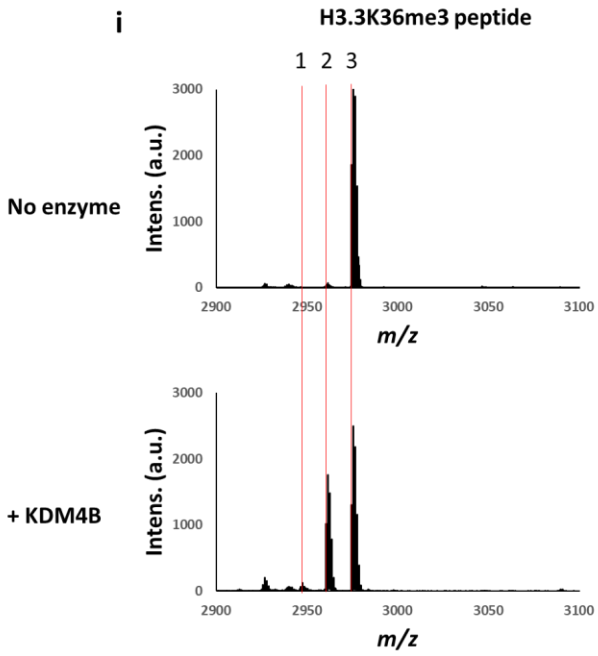

Measured mass (m/z)	1 K36me1 2946.6	2 K36me2 2960.6	3 K36me3 2974.6
H3.3S31	-	1.3	98.7
H3.3S31+4B	2.1	40.3	57.6

ii

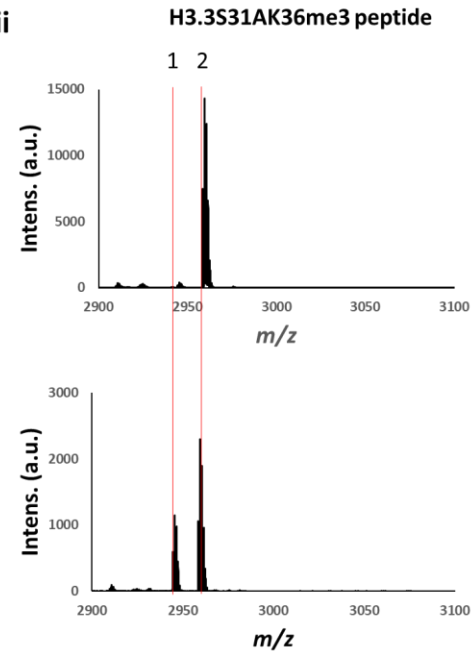

Measured mass (m/z)	K36me1	1 K36me2 2944.5	2 K36me3 2958.6
H3.3S31A	-	1	99
H3.3S31A+4B	-	34.2	65.8

iii

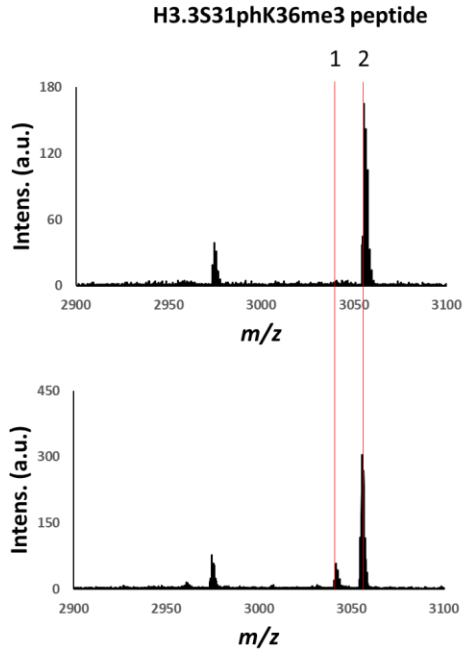

Measured mass (m/z)	K36me1	1 K36me2 3040.6	2 me3 3054.6
H3.3S31ph	-	0	100
H3.3S31ph+4B	-	13.4	86.6

iv

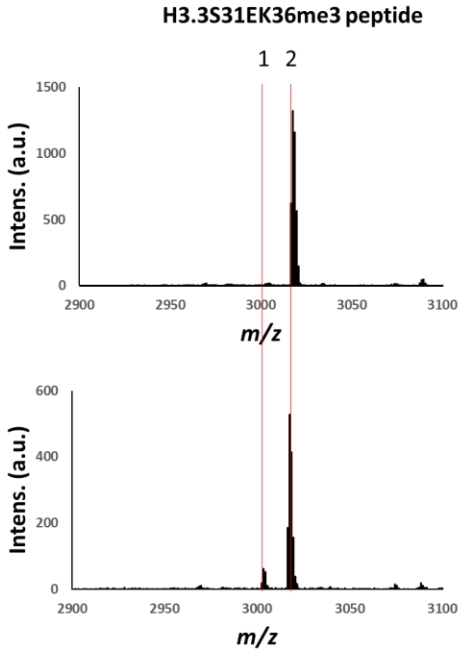

Measured mass (m/z)	K36me1	1 K36me2 3002.5	2 K36me3 3016.6
H3.3S31E	-	0	100
H3.3S31E+4B	-	9.8	90.2

Figure 6.2.4: H3.3S31ph prevents KDM4B-mediated demethylation of H3.3K36me3 in vitro

*(**i**) H3.3K36me3 (wild-type), (**ii**) H3.3S31AK36me3 (**iii**) H3.3S31phK36me3, and (**iv**) H3.3S31EK36me3 peptides were incubated with and without KDM4B recombinant protein prior to being subjected to MALDI-TOF analyses. Following incubation with recombinant KDM4B, K36me3 levels were decreased to 40.3%, 65.8%, 86.6% and 90.2% on H3.3K36me3 (wild-type), H3.3S31AK36me3, H3.3S31phK36me3 and H3.3S31EK36me3 peptides, respectively. In line with the changes in K36me3, higher levels of K36me2 levels were detected with the H3.3K36me3 (wild-type) (57.5%) and H3.3S31AK36me3 (34.2%) peptides. In contrast, when H3.3S31phK36me3 and H3.3S31EK36me3 peptides were used, the increases in K36me2 levels were lower at 13.4% and 9.8%, respectively. These changes suggest that K36me3 demethylation by KDM4B was less efficient on H3.3S31phK36me3 and H3.3S31EK36me3 peptides. Red lines show H3.3K36me1, H3.3K36me2 or H3.3K36me3 between the absence and presence of KDM4B and are labelled corresponding to the tables. A summary of each analysis is shown in the tables provided.*

6.2.4 Knockdown of KDM4B rescues heterochromatin formation in S31A-H3.3 cells

As previously shown, H3.3S31ph and S31E-H3.3 block KDM4B functions (**Figure 6.2.1B, 6.2.2 and 6.2.4iii, iv**) and increased H3K9me3 heterochromatin levels at the telomeres in S31E-H3.3 cells (**Figure 5.2.8iv**). Thus, it is unlikely that the loss of KDM4B in S31E-H3.3 cells will decrease and rescue H3K9me3 levels at the telomeres in S31E-H3.3 cells. However, S31A-H3.3 increased binding (compared to wildtype-H3.3; **Figure 6.2.1B** and **6.2.2**) and KDM4B function (compared to unphosphorylated H3.3S31 peptide) (**6.2.4iii, iv**), decreasing H3K9me3 heterochromatin levels at the telomeres in S31A-H3.3 cells (**Figure 5.2.8iv**). Thus, the rescue of H3K9me3 heterochromatin at telomeres through the loss of KDM4B in S31A-H3.3 cells, but not S31E-H3.3 cells, was next investigated.

The knockdown of KDM4B was performed in wild-type and S31A-H3.3 cells using siRNA oligonucleotides specific to KDM4B (siRNA sequence shown in **Chapter 2.13**). To determine the efficiency of the KDM4B siRNA and the optimal time for KDM4B knockdown, qRT-PCR analyses were performed on the respective RNA extracted from cells after 24h and 48h of KDM4B siRNA knockdown. KDM4B transcripts were decreased by approximately 30% and 60% in both wild-type-H3.3 cells and S31A-H3.3 cells, respectively, after KDM4B knockdown (**Figure 6.2.5**). Given that the loss of KDM4B was similar for wild-type and S31A-H3.3 cells at 24 and 48 hours (**Figure 6.2.5Aii, Bii**), the 24-hour time point was selected for KDM4B knockdown experiments.

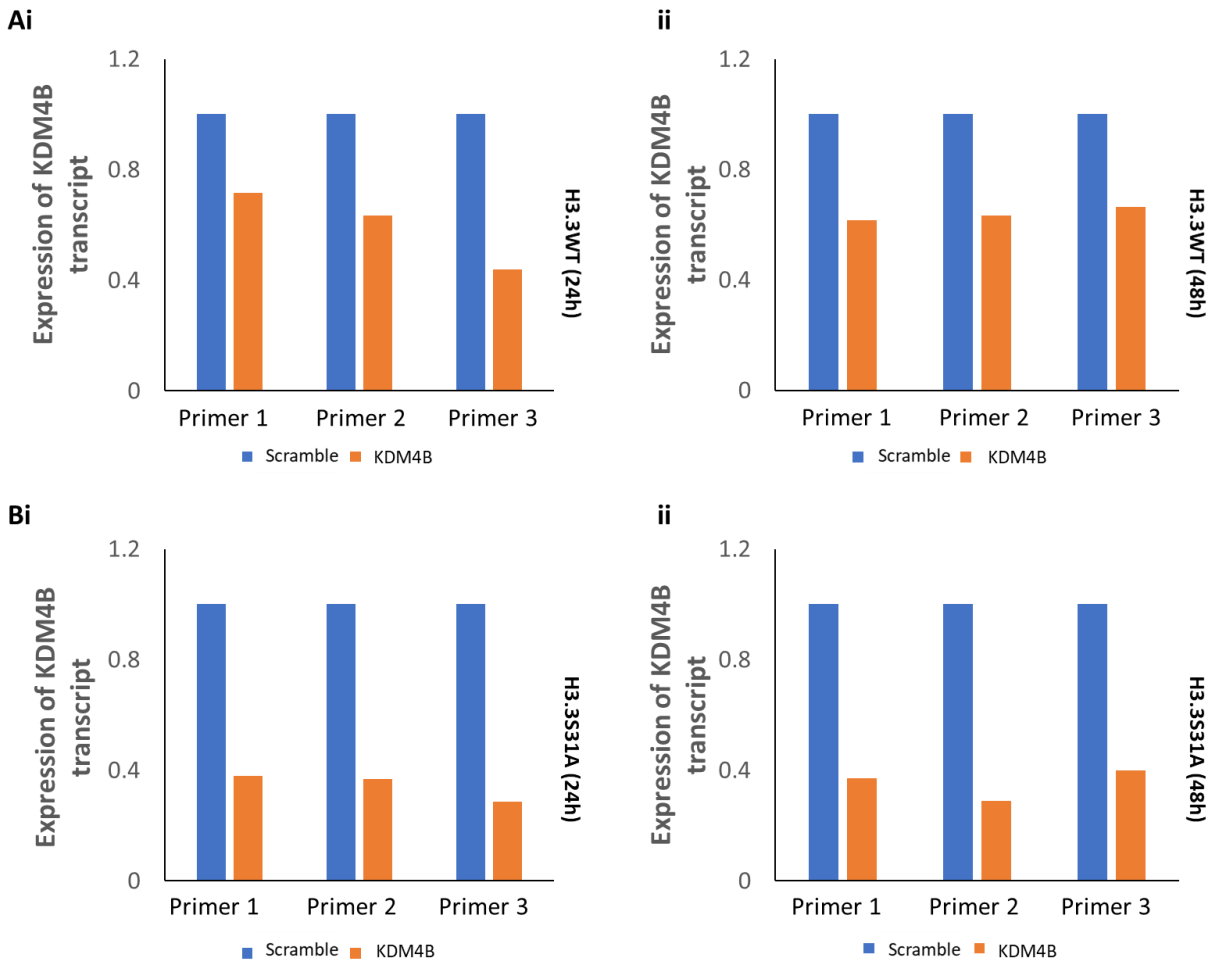

Figure 6.2.5: KDM4B siRNA oligonucleotides depletes KDM4B expression in wild-type and S31A H3.3 cells

*Wild-type and S31A-H3.3 cells were transfected with either control scramble siRNA or KDM4B siRNA oligonucleotides for 24h or 48h before RNA extraction. qRT-PCR was performed, and the KDM4B expression levels were normalised with GAPDH (negative control) and scramble siRNA transfected cells. Three different primer sets specific to the respective KDM4B region was used to determine KDM4B expression (Primer 1: Exon 5, Primer 2: Exon 6/7 and Primer 3: Exon 7/8). (**Ai**) After 24h of KDM4B knockdown, KDM4B expression decreased by approximately 30% in wild-type-H3.3 cells. (**Aii**) No further decrease was observed after 48h of KDM4B knockdown. (**Bi**) After 24h of KDM4B knockdown, KDM4B expression decreased by approximately 60% in S31A-H3.3 cells. (**Bii**) No further decrease was observed after 48h of KDM4B knockdown.*

Next, to investigate if the knockdown of KDM4B rescued H3K9me3 heterochromatin and ATRX binding levels at the telomeres of S31A-H3.3 cells, immunofluorescence analyses were performed using an antibody against ATRX following KDM4B knockdown. ATRX is known to be enriched at heterochromatic regions including the telomeres and pericentric regions where it loads H3.3 onto chromatin (Lewis et al., 2010, Wong et al., 2010, Gibbons et al., 2008, McDowell et al., 1999). However, the substitution of H3.3S31A with wildtype H3.3 resulted in a loss of ATRX at the pericentric regions and the telomeres (**Figure 5.2.4**).

With the depletion of KDM4B, wild-type-H3.3 cells did not show a change in ATRX level at the telomeres (**Figure 6.2.6**). In contrast, the knockdown of KDM4B in S31A-H3.3 cells led to increases in ATRX levels not only at the telomeres but also the pericentric regions of interphase cells. These observations suggest that the gain in KDM4B binding was likely responsible for the loss of ATRX at telomeres in S31A-H3.3 cells. In addition, KDM4B could also be driving the loss of heterochromatin at pericentric region in S31A-H3.3 cells since the depletion of KDM4B also leads to increased ATRX binding.

i

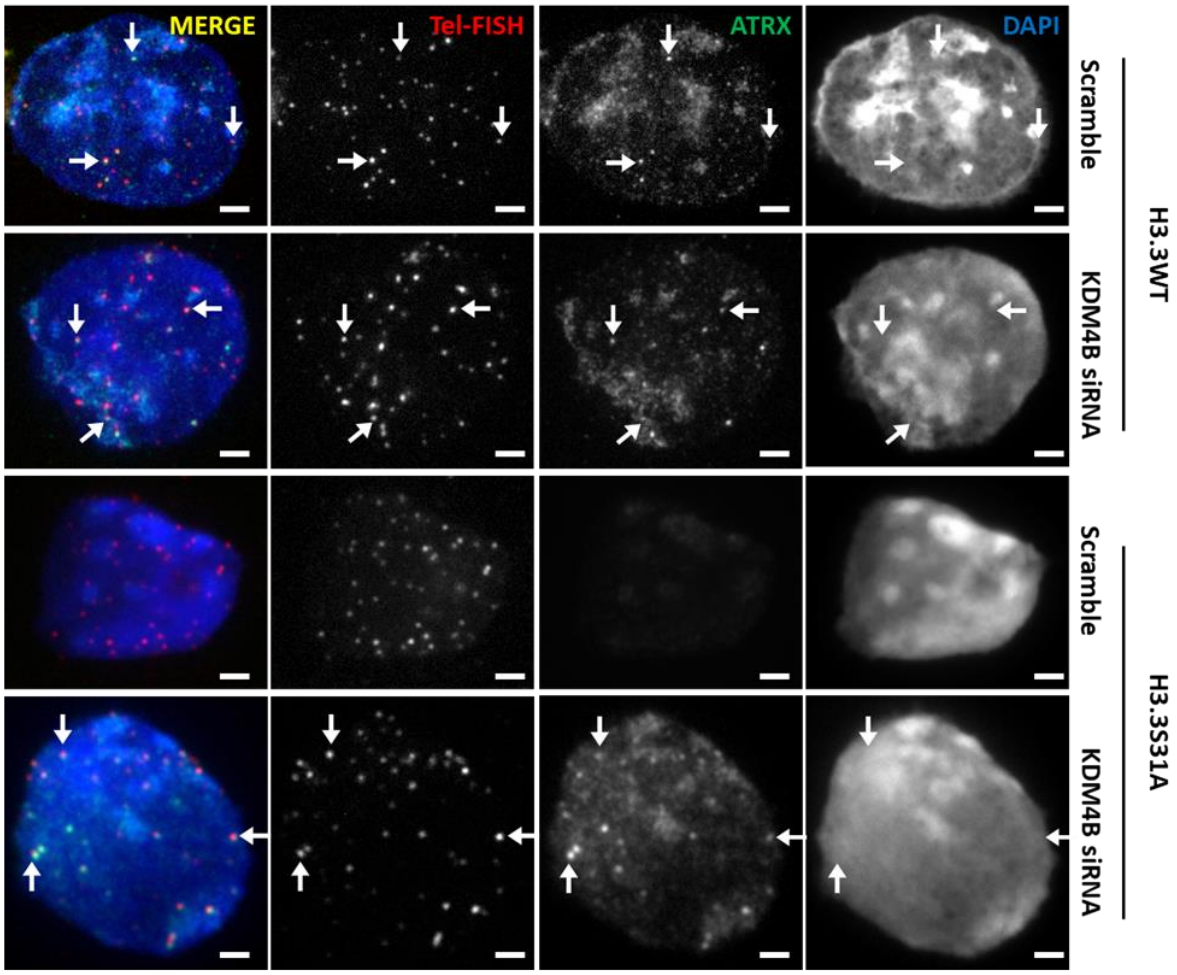
MERGE
Tel-FISH
ATRX
DAPI
Scramble
KDM4B siRNA
Scramble
KDM4B siRNA
H3.3WT
H3.3S31A

ii

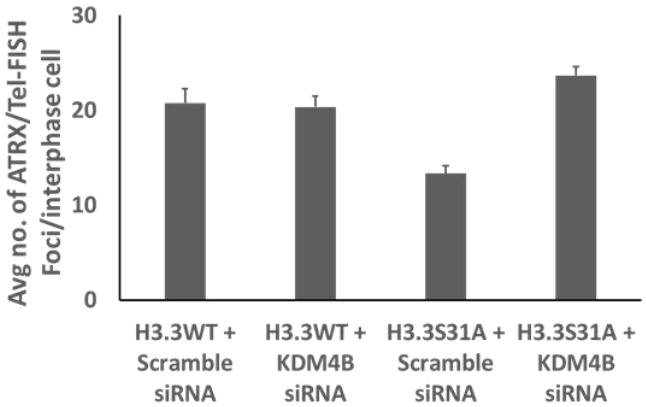
Avg no. of ATRX/Tel-FISH Foci/interphase cell
30
20
10
0
H3.3WT + Scramble siRNA
H3.3WT + KDM4B siRNA
H3.3S31A + Scramble siRNA
H3.3S31A + KDM4B siRNA

Figure 6.2.6: ATRX levels are rescued in S31A-H3.3 cells after KDM4B knockdown

*Immunofluorescence analyses were performed on wild-type and S31A-H3.3 cells after 24h KDM4B knockdown with antibody against ATRX (green) followed by Tel-FISH (red) to determine the enrichment of ATRX. Tel-FISH was used as a telomere marker. (**i**) ATRX colocalised with Tel-FISH signals at the telomeres of interphase wild-type-H3.3 cells (colocalised with Tel-FISH; arrows). The enrichment of ATRX at the telomeres and pericentric regions were similar between scramble and KDM4B knockdown wild-type-H3.3 cells. ATRX was barely detectable in S31A-H3.3 cells. Following KDM4B knockdown, ATRX was enriched at the telomeres (colocalised with Tel-FISH; arrows) and pericentric regions of S31A-H3.3 cells. (**ii**) ATRX/Tel-FISH colocalisation foci were quantified. 30 foci per cell was counted. N= 20. Error bars represent S.E.MDAPI was used as a nuclear counterstain. Scale bar represents 4 µm.*

Previously, the aberrant staining pattern and decreased localisation of PML to the telomeres of S31A-H3.3 cells was shown (**Figure 5.2.6**). To investigate if the increased KDM4B level and activity was directly related to the aberrant staining pattern and decreased localisation of PML at the telomeres, immunofluorescence analyses using specific antibody against PML were performed following KDM4B knockdown. Wild-type-H3.3 cells showed no change in the colocalisation between telomeres and PML bodies following KDM4B knockdown (**Figure 6.2.7**). In contrast, the knockdown of KDM4B in S31A-H3.3 cells led to increased localisation of telomeres to PML bodies (**Figure 6.2.7ii**). These findings suggest that increased KDM4B binding at telomeres inhibit the localisation of telomeres to PML bodies.

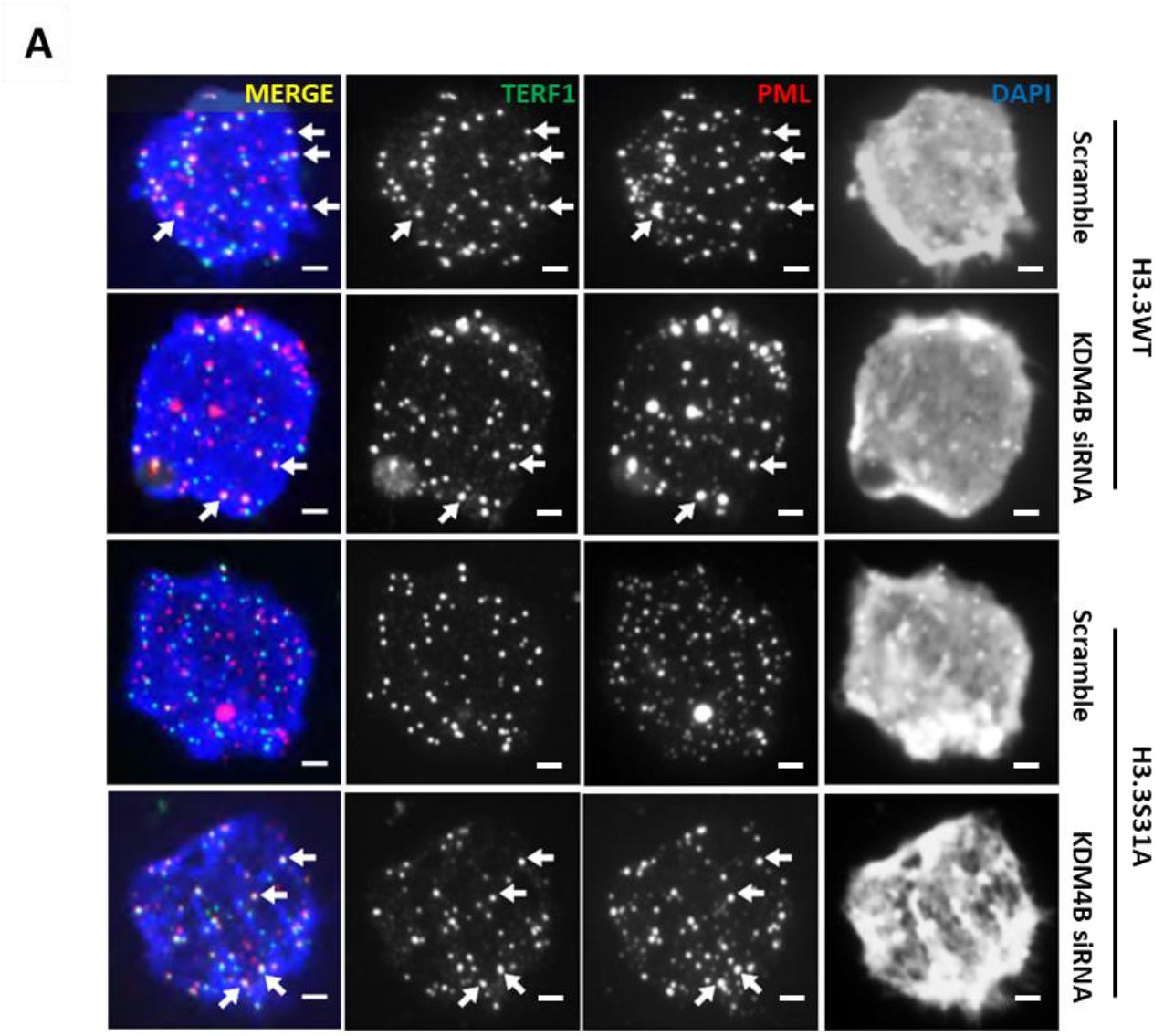
A
MERGE
TERF1
PML
DAPI
Scramble
KDM4B siRNA
Scramble
KDM4B siRNA
H3.3WT
H3.3S31A

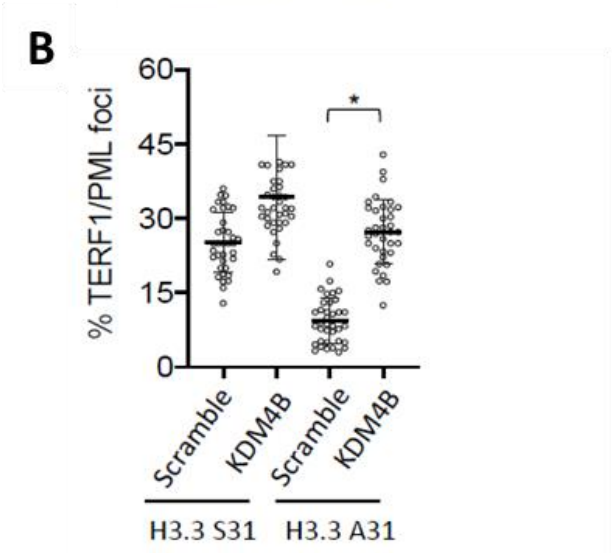
B
% TERF1/PML foci
60
45
30
15
0
*
Scramble
KDM4B
Scramble
KDM4B
H3.3 S31
H3.3 A31

Figure 6.2.7: PML levels are rescued in S31A-H3.3 cells after KDM4B knockdown

*Immunofluorescence analyses were performed on wild-type and S31A-H3.3 cells after 24h KDM4B knockdown with antibody against TERF1 (green) and PML (red) to determine the enrichment of PML. TERF1 was used as a telomere marker. (**Ai**) In interphase cells, PML colocalised with TERF1 at the telomeres of interphase wild-type-H3.3 cells with and without KDM4B knockdown (arrows). In S31A-H3.3 cells, PML colocalisation with TERF1 at the telomeres was low with aberrant staining pattern. With KDM4B knockdown, PML levels and staining pattern in S31A-H3.3 cells were rescued to wildtype levels. DAPI was used as a nuclear counterstain. Scale bar represents 4 µm. (**ii**) The percentage of PML/TERF1 colocalisation foci in wildtype-H3.3 and S31A-H3.3 cells, with and without KDM4B were quantified. P values were calculated using student's T-Test (**: p< 0.05, *: p<0.1, ns : not significant)*

Previous studies have shown that H3K9me3 recruits HP1α to compact chromatin by forming homodimers, condensing chromosome to maintain heterochromatin and prevent transcription (Hirota et al., 2005, Cheutin et al., 2003, Fischle et al., 2005). Thus, the levels of HP1α in S31A-H3.3 cells were investigated after KDM4B knockdown. Immunofluorescence analyses using a specific antibody against HP1α showed that HP1α levels in wild-type-H3.3 cells were similar despite KDM4B knockdown (**Figure 6.2.8**). However, HP1α levels in S31A-H3.3 cells were substantially increased at the pericentric regions and telomeres after KDM4B knockdown (**Figure 6.2.8i**). These results suggest that H3.3S31ph is regulates binding of KDM4B and heterochromatin-related proteins including ATRX and HP1α to maintain the heterochromatin structure at telomeres and pericentric regions

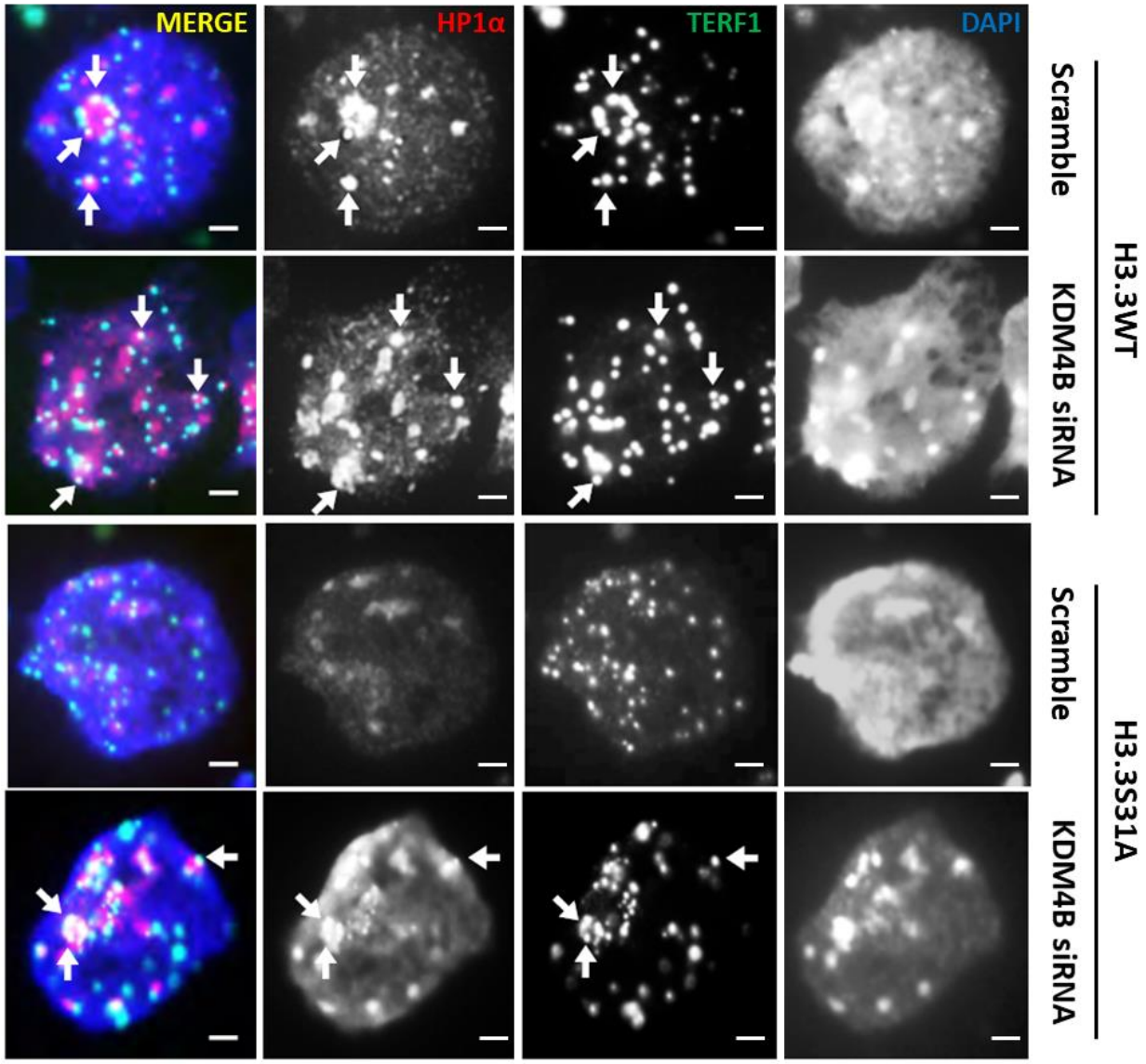

Figure 6.2.8: HP1α levels are rescued in S31A-H3.3 cells after KDM4B knockdown

Immunofluorescence analyses were performed on wild-type and S31A-H3.3 cells after 24h KDM4B knockdown with antibody against HP1α (red) and TERF1 (green) to determine the rescue of HP1α. TERF1 was used as a telomere marker. HP1α levels were unchanged in wild-type-H3.3 cells following KDM4B knockdown. HP1α levels at the telomeres (arrows) and pericentric regions were rescued in S31A-H3.3 cells after KDM4B knockdown. DAPI was used as a nuclear counterstain. Scale bar represents 4 μm.

Finally, to assess the changes of ATRX, H3K9me3 and H3.3 levels at the telomeres of wild-type and S31A-H3.3 cells after KDM4B knockdown, ChIP/qPCR analysis was performed. The results showed that levels of ATRX (**Figure 6.2.9i**), H3K9me3 (**Figure 6.2.9ii**) and H3.3 (**Figure 6.2.9iii**) were increased compared to the levels in cells transfected with scramble siRNA. However, the transient knockdown of KDM4B was insufficient to completely restore ATRX, H3K9me3 and H3.3 levels, and this suggest that a longer period of KDM4B depletion is required for full restoration of heterochromatin levels at the telomere in H3.3 A31 cells.

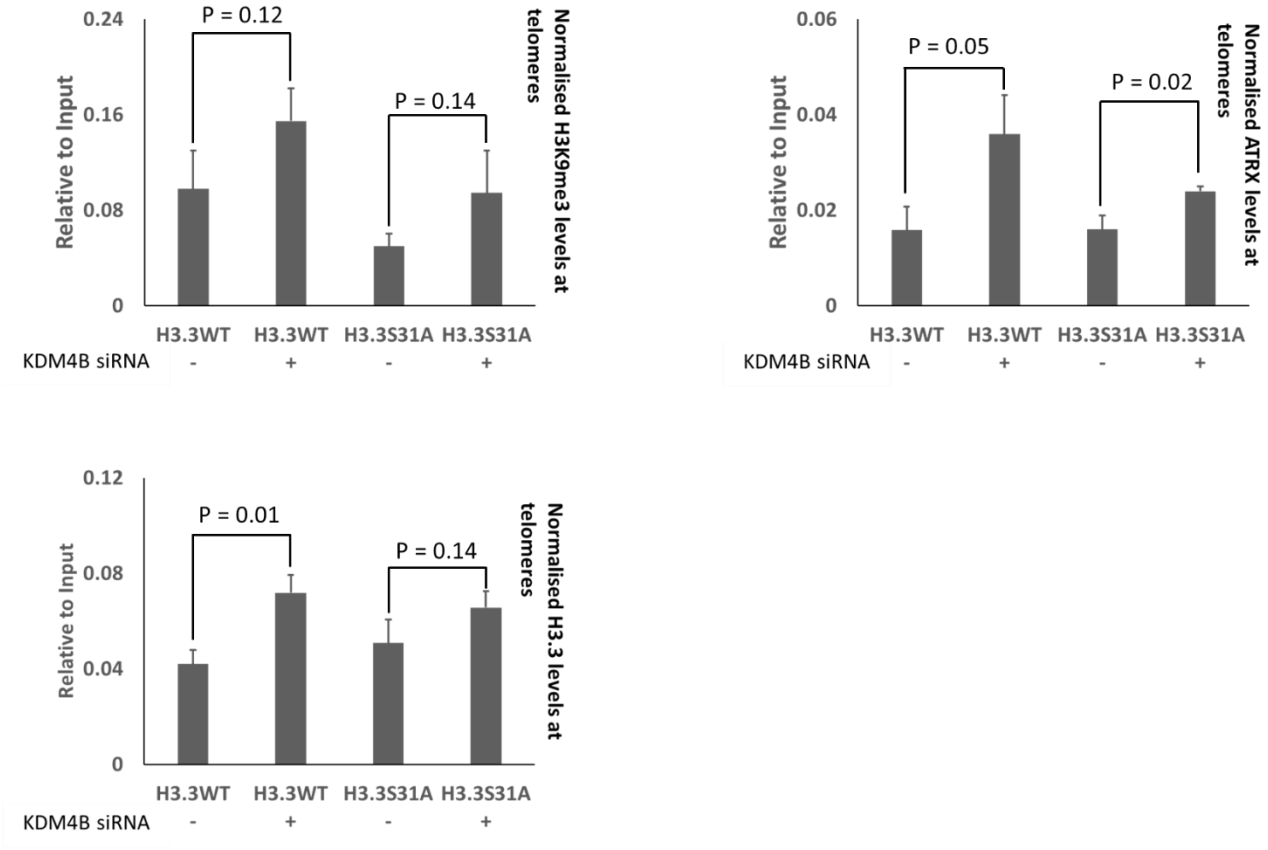

Figure 6.2.9: H3.3S31ph regulates KDM4B to maintain heterochromatin at the telomeres

*ChIP/qPCR analyses were performed on wild-type and S31A-H3.3 cell lines after KDM4B knockdown for 24h, followed by immunoprecipitation with antibodies against ATRX, H3K9me3, and H3.3. Results were normalised to input and H3 levels at GAPDH. Knockdown of KDM4B increased (**i**) ATRX, (**ii**) H3K9me3 and (**iii**) H3.3 levels at the telomeres of wild-type and S31A-H3.3 cell lines when compared to their untreated counterpart. Error bars represent S.E.M.. N=3. P values (shown in graphs) were calculated using two sample t-test.*

6.3 Discussion

Histone H3.3 is a unique histone H3 variant which is loaded at euchromatic regions by the histone chaperone HIRA and at heterochromatin by the histone chaperone ATRX/DAXX (Szenker et al., 2011), indicating the dynamic role of H3.3 in both transcriptional activation and silencing. Unique to H3.3 is a serine reside at position 31 and, both the residue and its phosphorylation are highly conserved between eukaryotes (Hake et al., 2005, Chang et al., 2015, Hinchcliffe et al., 2016, Sitbon et al., 2020, Schulmeister et al., 2007). Recent studies have identified the role of H3.3S31ph in transcriptional activation (Martire et al., 2019, Armache et al., 2020, Sitbon et al., 2020), however, the function of H3.3S31ph at heterochromatic regions has not been established. This chapter has provided evidence for a previously unrecognised role of H3.3S31ph in heterochromatin maintenance through the regulation of KDM4B, a lysine demethylase.

This chapter has shown that unphosphorylated H3.3S31 (and H3.3S31A) promotes KDM4B binding and activity while phosphorylated H3.3S31 (and H3.3S31) inhibits the binding and activity of KD4MB (**Figure 6.2.2** and **6.2.4**). Supporting this discovery, S31A-H3.3 cells showed increased KDM4B binding at the telomeres (**Figure 6.2.1**) and, the depletion of KDM4B in S31A-H3.3 cells enhanced telomeric localisation of PML (**Figure 6.2.7**). In addition, the depletion of KDM4B in S31A-H3.3 cells rescued HP1α (**Figure 6.2.8**) H3K9me3 (**Figure 6.2.9i**), ATRX (**Figure 6.2.6 and 6.2.9ii**), and H3.3 (**Figure 6.2.9iii**), at the telomeres. These results are consistent with a previous finding where the formation of PML bodies around telomeres has been found to be dependent on H3K9me3 and HP1α (Udugama et al., 2021). Thus, the lack of H3.3S31ph in S31A-H3.3 cells promoted uncontrolled KDM4B demethylation activity, leading to losses of H3K9me3 level and PML body recruitment at the telomeres. In this chapter, focus was given to the knockdown of

KDM4B in S31A-H3.3 cell line due to the gain in KDM4B binding and increased KDM4B activity when compared to wildtype-H3.3. However, future experiments examining the knockdown of KDM4B in S31E-H3.3 cell lines will elucidate the function of H3.3S31ph in heterochromatin regulation.

A recent study has proposed that H3.3S31ph attracted factors involved with transcriptional activation of key developmental genes in interphase cells and repulsed factors involved in chromosome condensation in mitotic cells (Sitbon et al., 2020, Clevers, 2006, Liu and Millar, 2010). Supporting this theory, other studies have shown that H3.3S31ph regulate the binding of repressor protein ZMYND11 (Wen et al., 2014, Guo et al., 2014) and the histone acetyltransferase p300 (Martire et al., 2019, Armache et al., 2020). This chapter has shown evidence that H3.3S31ph acts as a switch to regulate KDM4B binding and activity at the telomeres. A previous study has shown that KDM4A, demethylates H3K9me3, preventing HP1α binding, to control chromatin accessibility of a late-replicating heterochromatic satellite region while the overexpression of KDM4A advances S-phase entry (Black et al., 2010, Klose et al., 2006). The results in this chapter support the hypothesis that KDM4B regulates heterochromatin assemblly at telomeres during replication (Udugama et al., 2021). The depletion of KDM4B increased H3K9me3 and HP1α levels at the telomeres, leading to increased replication stress and DNA damage at the telomeres (Udugama et al., 2021). Thus, it is likely that the high levels if DNA damage in S31E-H3.3 cells (**Figure 5.2.9**) were due to the inability of KD4MB to demethylate H3K9me3, leading to high levels of H3K9me3 during replication. This high level of H3K9me3 may inhibit DNA polymerase accessibility, inducing DNA damage at the telomeres. Consistent with this hypothesis, S31E-H3.3 cells showed increased DNA damage at other H3.3S31ph enriched heterochromatin sites such as pericentric heterochromatin repeats (**Figure 5.2.10**). These studies and results suggest

that KDM4B may play a similar role to KDM4A demethylase in antagonising HP1α recruitment to regions including pericentric heterochromatin repeats (Klose et al., 2006).

This thesis proposes that H3.3S31ph acts as a switch to regulate ATRX and H3K9me3 levels and heterochromatin accessibility at DNA repeats such as the telomeres and pericentric regions. The absence of H3.3S31ph at these sites promotes recruitment of KDM4B, reducing H3K9me3 levels to facilitate replication at heterochromatin. ATRX was found to have a function at the telomeres during mitosis to promote the resolution of sister telomeres in mitosis (Ramamoorthy and Smith, 2015). Thus, its increase during mitosis is not surprising in addition to H3.3 loading at the occurs throughout the cell cycle. Following replication completion, H3.3S31 is phosphorylated and it prevents the demethylation of H3K9me3 by KDM4B, facilitating a heterochromatin state until the next G1/S phase (**Figure 6.3.1**). The results have elucidated a molecular pathway whereby H3.3S31ph preserves heterochromatin through the regulation of KDM4B, H3K9me3 and ATRX and, may be useful in investigating if the increased H3.3S31ph observed across the chromosome arms of *ATRX*-mutated ALT-cancer cells follow this molecular pathway. Altogether, this thesis has shown that H3.3S31ph is important for protein binding regulation to maintain heterochromatin, providing insights to the role of H3.3S31ph in regulating genome integrity.

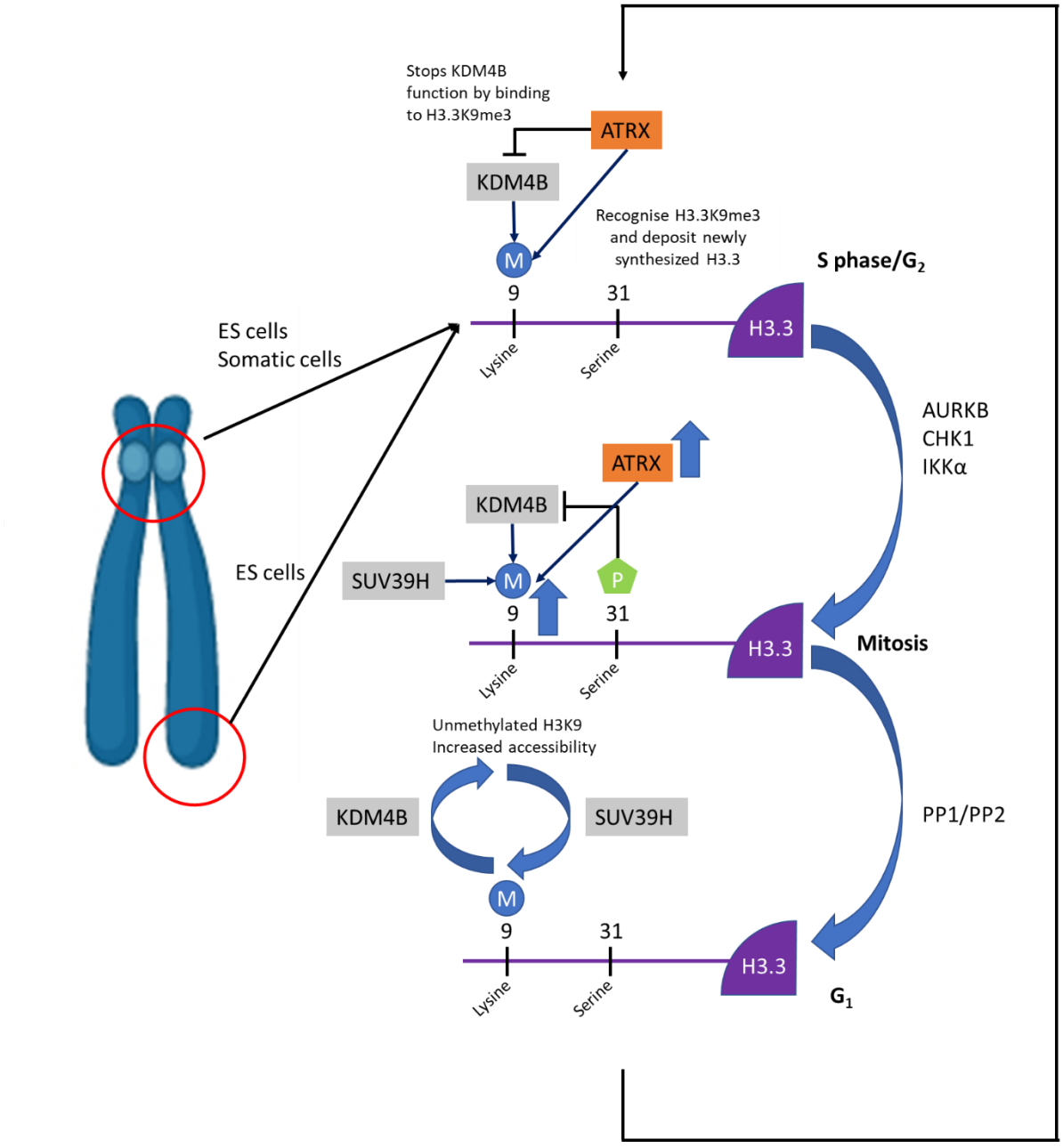
Stops KDM4B
function by binding
to H3.3K9me3
ATRX
KDM4B
Recognise H3.3K9me3
and deposit newly
synthesized H3.3
M
9
31
Lysine
Serine
H3.3
S phase/G2
ES cells
Somatic cells
AURKB
CHK1
IKKα
ATRX
KDM4B
SUV39H
M
P
9
31
Lysine
Serine
H3.3
Mitosis
ES cells
Unmethylated H3K9
Increased accessibility
KDM4B
SUV39H
PP1/PP2
M
9
31
Lysine
Serine
H3.3
G1

Figure 6.3.1: Proposal of H3.3S31ph and its regulation of heterochromatin

Heterochromatic regions such as the telomeres and pericentric regions are enriched with ATRX in interphase cells (Lovejoy et al., 2012, Voon and Wong, 2016, Wong et al., 2010, Xue et al., 2003). To maintain a heterochromatin state, ATRX recognises H3.3K9me3 and unmethylated H3K4 to deposit newly synthesised H3.3 onto chromatin. The presence of ATRX, which promotes the formation of H3K9me3 heterochromatin, prevents KDM4B from demethylating H3K9me3. Despite being maintained as a heterochromatin domain, KDM4B binding at telomeres and pericentric regions is required to increase chromatin accessibility to allow DNA polymerase recruitment and progression during replication at late S/G_2 phase. However, following the completion of replication, KDM4B binding needs to be removed in order to restore the heterochromatin state. Furthermore, presence of H3.3S31ph increases ATRX at the telomeres during mitosis and prevents the binding and activity of KDM4B in removing H3K9me3 at telomeres and pericentric regions. Following the end of mitosis and entry into G1, H3.3S31ph signal is lost and this then allows the binding of KDM4B to telomeres. Overall, we propose a model which ATRX and KDM4B act to maintain a balance of heterochromatin at repetitive DNA including telomeres and pericentric heterochromatin, and H3.3S31ph plays a key role in regulating heterochromatin accessibility through the control of KDM4B function during the progression of cell cycle.

Chapter 7: Final Discussions and Future Directions

7.1 Summary and Conclusions

The proper maintenance of the heterochromatin structure at telomeres is essential for their proper function and for genome protection. Numerous studies have shown that the loss of heterochromatin formation at the telomeres lead to aberrant telomere lengthening, dysregulated transcription, and severe DNA damage (Udugama et al., 2015, Amorim et al., 2016, Garcia-Cao et al., 2004, Benetti et al., 2007, de Lange, 2005). The protection of the telomeres is regulated by the Shelterin complex which prevents DNA damage response activation and aids in the formation of the t-loop to mask the linear ends (de Lange, 2005).

In earlier studies, AURKB has been shown to localise only to the centromeric region, where it functions to ensure proper progression of mitotic events (Ditchfield et al., 2003, Andrews et al., 2004, Gadea and Ruderman, 2005). Although AURKB has been implicated in regulating telomere length (Mallm and Rippe, 2015), the direct role of AURKB remains unknown. This thesis has redefined the role of AURKB in regulating chromosome function by showing that it is required for telomere maintenance in mouse ES cells (Chan et al., 2017). The localisation of AURKB at the telomeres is unique to ES cells, and the loss of AURKB caused MTS formation. This ES cell-specific function of AURKB indicates that AURKB may be required for regulating the unique chromatin environment at the telomere in pluripotent cell types. MTS formation is a well-known phenotype of the depletion of a telomere specific protein, TERF1 (Martinez et al., 2009, Sfeir et al., 2009). The analyses of TERF1 mutants shows that AURKB phosphorylates S404-TERF1, which prevents TERF1-binding to the telomeres. Although the long-term loss of TERF1 binding (including S404E-TERF1 expression) was associated with telomere lengthening (van Steensel and de Lange, 1997, Smogorzewska et al., 2000, Chan et al., 2017), other PTMs on TERF1 may also play a role in TERF1 binding to the telomeres to maintain telomere integrity (Beier et al., 2012,

Lee et al., 2009, McKerlie and Zhu, 2011, Zimmermann et al., 2014). The presence of MTS formation is indicative of an increase in replication fork stalling at the telomeres (Sfeir et al., 2009). This replication fork stalling is prevented by helicases such as BLM RecQ and RTEL1 (Opresko et al., 2002). As the loss of these helicases also causes MTS formation (Ding et al., 2004, Martinez et al., 2009, Lillard-Wetherell et al., 2004), they likely play a role with TERF1 in maintaining telomere integrity. Thus, further investigation of TERF1 by other kinases that regulate its binding and its role in recruiting helicases to prevent replication fork stalling is required.

The localisation of AURKB at the telomeres of ES cell indicates a dynamic function of telomere chromatin maintenance within ES cells. AURKB is a key kinase that phosphorylates H3.3 at various residues, including S10 (Li et al., 2017b), S28 (Goto et al., 2002) and S31 (Li et al., 2017a). H3.3S31 is likely phosphorylated by AURKB at the telomeres considering H3.3S31 is a substrate at the pericentric regions (Li et al., 2017a, Ahmad and Henikoff, 2002). To date, although various studies has shown the enrichment of H3.3S31ph at the pericentric regions (Li et al., 2017a, Schulmeister et al., 2007, Sitbon et al., 2020, Hake et al., 2005, Armache et al., 2020), the enrichment of H3.3S31ph at the telomeres has only been studied in embryonic germ and embryonic stem cells (Wong et al., 2009). However, the role and function of H3.3S31ph in telomere function and heterochromatin function is unknown. Thus, studying the unique role of H3.3S31ph in heterochromatin maintenance is critical for understanding ES cell telomere maintenance and heterochromatin maintenance. The deposition of H3.3 at heterochromatic regions, including the pericentric regions and telomeres, by ATRX/Daxx and, the enrichment of H3.3S31ph at these regions indicates a role of H3.3S31ph in heterochromatin regulation. To investigate the role of H3.3S31ph, endogenous H3.3-null S31A and S31E-H3.3 mutant

cell lines were generated using a H3.3 conditional knockout ES cell model (Tang et al., 2013a). Unlike other studies that have used tagged H3.3 to study the function of H3.3S31 and its phosphorylation (Martire et al., 2019, Sitbon et al., 2020, Armache et al., 2020), our model expressed H3.3 without a tag, as a protein tag could affect H3.3-dependent nucleosome formation and chromatin assembly (Voon and Wong, 2016).

H3.3S31ph is enriched at the telomeres of ES cells (Wong et al., 2009). In addition, ES cells telomeres have highly regulated levels of HMTs SUV4-20H and SUV39H where the loss of SUV4-20H and SUV39H in ES cells caused a loss of H4K20me3 and H3K9me3 levels at the telomeres, resulting in telomere elongation and recombination (Benetti et al., 2007, Wang et al., 2012). Together with our finding that AURKB localises to the telomeres of ES cells (Chan et al., 2017), these studies highlight the importance of telomere chromatin maintenance in ES cells. (Garcia-Cao et al., 2004, Benetti et al., 2007)Our findings show that H3.3S31ph prevents KDM4B binding resulting in increased H3K9me3 levels at the telomeres. In addition, H3.3S31ph was shown to increase SETD2 levels to increase H3K36me3 levels (Armache et al., 2020). As cells undergo differentiation, the telomere chromatin state also changes, with loss of proteins including ATRX (Wong et al., 2010), H3.3 (Wong et al., 2010) and AURB (Chan et al., 2017) and, increased H3K9me3 and H4K20me3 (Garcia-Cao et al., 2004, Benetti et al., 2007, Wong et al., 2009, Wong et al., 2010). It is possible that in differentiated cells, he loss of H3.3 and H3.3S31ph at the telomeres, may drive the maintenance of heterochromatin through other regulatory mechanism including modifications including the phosphorylation of Threonine 6 and 11 which promotes the removal of H3K9me3 by KDM4C (Metzger et al., 2008, Metzger et al., 2010).

The loss of H3S10ph and H3S28ph causes aberrant cell-cycle progression and aberrant chromatin maintenance (Hirota et al., 2005, Li et al., 2017b, Goto et al., 2002, Hochegger et al., 2013). Thus, it was interesting when the expression of S31A and S31E-H3.3 did not cause aberrant cell-cycle progression in mouse ES cells. In contrast to the findings in other cell types, the loss of H3.3S31ph caused a severe loss of heterochromatin, indicated by losses of H3K9me3, ATRX and HP1α, at the telomeres. This thesis shows evidence for a novel role of H3.3S31ph in controlling heterochromatin maintenance at telomeres through regulation of KDM4B demethylase. H3.3S31 acts as a phosphorylation switch which regulates H3K9me3 heterochromatin. The unphosphorylated form of H3.3S31 promotes demethylation by KDM4B, while H3.3S31 phosphorylation prevents KDM4B binding and inhibits its demethylase activity, which in turn preserves H3K9me3 heterochromatin at the telomeres. In addition, this thesis also provides evidence that formation of PML bodies around telomeres require H3.3S31ph. The loss of PML body formation at the telomeres suggests that H3.3S31ph is essential for ATRX/Daxx recruitment to PML bodies (Delbarre et al., 2013, Delbarre et al., 2017). These observations also agree with our recent finding that the formation of PML bodies around telomeres is dependent on H3K9me3 and HP1α (Udugama et al., 2021).

Notably, H3.3S31ph levels are substantially increased across the chromosome in ATRX-mutated cancers that utilise the ALT (Alternative Lengthening of telomeres) telomere maintenance pathway (Chang et al., 2015). Thus, it is tempting to speculate that H3.3S31ph could be important for preventing KDM4B binding and the excessive loss of heterochromatin in the absence of ATRX in these cancers. A recent study has proposed that H3.3S31ph can act either by attracting or repulsing protein factors (Sitbon et al., 2020). Specifically, H3.3S31ph has been shown to regulate binding of chromatin repressor ZMYND11 (a factor

involved in intron retention that recognises H3K36me3) that reads unphosphorylated H3.3S31 and H3.3K36me3. Upon the phosphorylation of H3.3S31, ZMYND11 dissociates from chromatin (Wen et al., 2014), similar to the disrupted binding of KDM4B to H3.3 at telomeres in S31E-H3.3 ES cells. H3.3S31ph may facilitate a specific function within chromatin by acting as a switch that regulates protein binding. It would be interesting to investigate if the cancer driver H3.3K27M and G34R mutations affect H3.3S31ph in paediatric glioblastomas, and if this in turns affects protein associated with H3.3 and contributes to oncogenesis.

Another interesting finding was the lack of changes in H3K27ac in S31A-H3.3 cells (**Figure 5.2.3**). A previous report showed that the expression of HA-tagged S31E-H3.3 in H3.3 depleted *Xenopus laevis* embryos led an increased H3K27ac and decreased H3K27me3 levels. In addition, to the changes in H3K27ac and H3K27me3 levels, H3.3S31ph ejected ZMYND11 form chromatin, allowing transcriptional activation. Contrary to this report, we did not observe significant changes in global H3K27ac and H3K27me3 levels. However, complementing the increased levels of H3K36me3 observed in our S31E-H3.3 cells, increased H3K36me3 levels were observed in H3.3S31E recombinant nucleosomes after incubation with SETD2 (Armache et al., 2020). Our results suggest that in addition to the increased methylation activity by SETD2, H3.3S31E, or H3.3S31ph, prevents KDM4B demethylase activity. This suggests that H3.3S31ph is unique in regulating the H3K36me3, and H3K9me3 through regulating writer proteins to maintain heterochromatin regulation. The changes observed may be due to the different cell types used (*Xenopus laevis* embryos and mouse ES cell). However, more biological replicates of H3K27ac and H3K27me3 levels immunoblotting should be performed to attain a reliable sample number. In addition, it is possible that these changes are more prominent at euchromatic regions, and thus, further

experiments such as ChIP-Seq needs to be performed to elucidate the changes in H3.3 post-translational modification.

Our findings also show that H3.3S31A increases KDM4B binding. As the N-terminal region of H3.3S31A is the same as canonical H3, it is possible that the alanine 31 on H3 promotes KDM4B binding as well. On histone H3, the phosphorylation of other residues on H3 such as Threonine 6 and 11 promotes the removal of H3K9me3 by KDM4C (Metzger et al., 2008, Metzger et al., 2010). In addition, phosphorylation of the Threonine 6 residue on Histone H3 prevents lysine specific demethylase 1-mediated removal of methylated or di-methylated Lysine 4 residue on Histone H3 (Metzger et al., 2010), further promoting transcriptional activcation. Furthermore, the phosphorylation of H3S10 ejects HP1α, which binds H3K9me3 to compact chromatin (Hirota et al., 2005). These studies show that H3 phosphorylation promotes transcriptional activation. Thus, the binding efficiency of KDM4B with canonical H3 at Alanine 31 should be investigated to add insights into the regulation of heterochromatic marks on H3. As H3.3S31ph is enriched at repetitive regions (Wong et al., 2009), the role of H3.3S31ph in preventing KDM4B binding might be site specific. Thus, H3.3S31ph function in preventing KDM4B binding at euchromatic regions should also be investigated as H3.3S31ph ejects ZMYND11 from chromatin for transcriptional activation (Armache et al., 2020), to give a holistic understanding of H3.3S31ph function. Nonetheless, our findings add to previous knowledge of SETD2 and ZMYND11 being regulated by H3.3S31ph by introducing KDM4B as another target of H3.3S31ph function in repelling KDM4B to maintain heterochromatin.

7.2 Future directions

Based on the work presented in this thesis, there are several avenues for further investigation that can be explored. The S31A and S31E-H3.3 ES cell lines have shown to be useful for elucidating the function of H3.3S31ph. In addition to KDM4B, ZMYND11 (Guo et al., 2014, Wen et al., 2014) and p300 (Martire et al., 2019), H3.3S31ph is likely to regulate binding and function of a number of other proteins (including histone readers, writers and erasers). As part of a future study to identify these interacting proteins, protein immunoprecipitation could be performed in wild-type, S31A and S31E-H3.3 cells followed by mass spectrometry analyses. Outcomes from these studies will further inform the role of H3.3S31ph in regulating chromatin function.

Currently, the phospho-null and phospho-mimic mutation of H3.3S31 has not been reported in development, cancers and diseases, suggesting its relevance in development. Although the complete and partial loss of H3.3 has led to rapid cell death in mouse cells (Tang et al., 2013a, Tang et al., 2015), the function of H3.3S31 and its phosphorylation in development has not been studied. To investigate the role of H3.3S31ph in regulating mammalian development, mouse models with complete replacement of H3.3S31 to S31A-H3.3 or S31E-H3.3 should be generated and studied.

Various kinases have been identified to regulate H3.3S31 phosphorylation. Therefore, the regulation by specific kinases may be responsible for the activation of H3.3S31ph at specific location and for specific phenotypes (Armache et al., 2020, Li et al., 2017a, Chang et al., 2015). Thus, inhibition of specific kinases may help elucidate if the regulation of H3.3S31ph by specific kinases would result in a specific phenotype (Chang et al., 2015, Li et al., 2017a).

However, it is important to take into consideration the off-target effects, as these kinases may be critical for other functions (Gadea and Ruderman, 2005, Shimada et al., 2008).

This thesis focused on investigating telomeres as a model to study the function of H3.3S31ph in regulating heterochromatin formation. Further investigations at other heterochromatic regions, including the pericentric regions, where H3.3S31ph is also enriched, would be helpful in informing its function and verifying if it plays a similar role in heterochromatin maintenance at other repetitive DNA regions. Thus, centromere-FISH and ChIP/qPCR of H3K9me3 ATRX and KDM4B at other heterochromatic regions may identify if H3.3S31ph also regulates heterochromatin formation at the pericentric regions.

Chapter 8: Bibliography

ADAM, M., ROBERT, F., LAROCHELLE, M. & GAUDREAU, L. 2001. H2A.Z is required for global chromatin integrity and for recruitment of RNA polymerase II under specific conditions. *Mol Cell Biol,* 21**,** 6270-9.

ADAM, S., POLO, S. E. & ALMOUZNI, G. 2013. Transcription recovery after DNA damage requires chromatin priming by the H3.3 histone chaperone HIRA. *Cell,* 155**,** 94-106.

ADAMS, R. R., MAIATO, H., EARNSHAW, W. C. & CARMENA, M. 2001. Essential roles of Drosophila inner centromere protein (INCENP) and aurora B in histone H3 phosphorylation, metaphase chromosome alignment, kinetochore disjunction, and chromosome segregation. *J Cell Biol,* 153**,** 865-80.

ADAMS, R. R., WHEATLEY, S. P., GOULDSWORTHY, A. M., KANDELS-LEWIS, S. E., CARMENA, M., SMYTHE, C., GERLOFF, D. L. & EARNSHAW, W. C. 2000. INCENP binds the Aurora-related kinase AIRK2 and is required to target it to chromosomes, the central spindle and cleavage furrow. *Curr Biol,* 10**,** 1075-8.

AGGER, K., NISHIMURA, K., MIYAGI, S., MESSLING, J. E., RASMUSSEN, K. D. & HELIN, K. 2019. The KDM4/JMJD2 histone demethylases are required for hematopoietic stem cell maintenance. *Blood,* 134**,** 1154-1158.

AHMAD, K. & HENIKOFF, S. 2002. The histone variant H3.3 marks active chromatin by replication-independent nucleosome assembly. *Mol Cell,* 9**,** 1191-200.

AIHARA, H., NAKAGAWA, T., MIZUSAKI, H., YONEDA, M., KATO, M., DOIGUCHI, M., IMAMURA, Y., HIGASHI, M., IKURA, T., HAYASHI, T., KODAMA, Y., OKI, M., NAKAYAMA, T., CHEUNG, E., ABURATANI, H., TAKAYAMA, K. I., KOSEKI, H., INOUE, S., TAKESHIMA, Y. & ITO, T. 2016. Histone H2A T120 Phosphorylation Promotes Oncogenic Transformation via Upregulation of Cyclin D1. *Mol Cell,* 64**,** 176-188.

AKHMANOVA, A. S., BINDELS, P. C., XU, J., MIEDEMA, K., KREMER, H. & HENNIG, W. 1995. Structure and expression of histone H3.3 genes in Drosophila melanogaster and Drosophila hydei. *Genome,* 38**,** 586-600.

ALLIS, C. D. & JENUWEIN, T. 2016. The molecular hallmarks of epigenetic control. *Nat Rev Genet,* 17**,** 487-500.

AMORIM, J. P., SANTOS, G., VINAGRE, J. & SOARES, P. 2016. The Role of ATRX in the Alternative Lengthening of Telomeres (ALT) Phenotype. *Genes (Basel),* 7.

ANCELIN, K., BRUNORI, M., BAUWENS, S., KOERING, C. E., BRUN, C., RICOUL, M., POMMIER, J. P., SABATIER, L. & GILSON, E. 2002. Targeting assay to study the cis functions of human telomeric proteins: evidence for inhibition of telomerase by TRF1 and for activation of telomere degradation by TRF2. *Mol Cell Biol,* 22**,** 3474-87.

ANDREWS, A. J. & LUGER, K. 2011. Nucleosome structure(s) and stability: variations on a theme. *Annu Rev Biophys,* 40**,** 99-117.

ANDREWS, P. D., OVECHKINA, Y., MORRICE, N., WAGENBACH, M., DUNCAN, K., WORDEMAN, L. & SWEDLOW, J. R. 2004. Aurora B regulates MCAK at the mitotic centromere. *Dev Cell,* 6**,** 253-68.

ANSIEAU, S. & SERGEANT, A. 2003. [BS69 and RACK7, a potential novel class of tumor suppressor genes]. *Pathol Biol (Paris),* 51**,** 397-9.

ARIFUZZAMAN, S., KHATUN, M. R. & KHATUN, R. 2020. Emerging of lysine demethylases (KDMs): From pathophysiological insights to novel therapeutic opportunities. *Biomed Pharmacother,* 129**,** 110392.

ARMACHE, A., YANG, S., MARTINEZ DE PAZ, A., ROBBINS, L. E., DURMAZ, C., CHEONG, J. Q., RAVISHANKAR, A., DAMAN, A. W., AHIMOVIC, D. J., KLEVORN, T., YUE, Y., ARSLAN, T., LIN, S., PANCHENKO, T., HRIT, J., WANG, M., THUDIUM, S., GARCIA, B. A., KORB, E., ARMACHE, K. J., ROTHBART, S. B., HAKE, S. B., ALLIS, C. D., LI, H. & JOSEFOWICZ, S. Z. 2020. Histone H3.3 phosphorylation amplifies stimulation-induced transcription. *Nature,* 583**,** 852-857.

AYMARD, F., BUGLER, B., SCHMIDT, C. K., GUILLOU, E., CARON, P., BRIOIS, S., IACOVONI, J. S., DABURON, V., MILLER, K. M., JACKSON, S. P. & LEGUBE, G. 2014. Transcriptionally

active chromatin recruits homologous recombination at DNA double-strand breaks. *Nat Struct Mol Biol,* 21**,** 366-74.
BAKKENIST, C. J. & KASTAN, M. B. 2003. DNA damage activates ATM through intermolecular autophosphorylation and dimer dissociation. *Nature,* 421**,** 499-506.
BANASZYNSKI, L. A., WEN, D., DEWELL, S., WHITCOMB, S. J., LIN, M., DIAZ, N., ELSASSER, S. J., CHAPGIER, A., GOLDBERG, A. D., CANAANI, E., RAFII, S., ZHENG, D. & ALLIS, C. D. 2013. Hira-dependent histone H3.3 deposition facilitates PRC2 recruitment at developmental loci in ES cells. *Cell,* 155**,** 107-20.
BANNISTER, A. J. & KOUZARIDES, T. 2011. Regulation of chromatin by histone modifications. *Cell Res,* 21**,** 381-95.
BANNISTER, A. J., ZEGERMAN, P., PARTRIDGE, J. F., MISKA, E. A., THOMAS, J. O., ALLSHIRE, R. C. & KOUZARIDES, T. 2001. Selective recognition of methylated lysine 9 on histone H3 by the HP1 chromo domain. *Nature,* 410**,** 120-4.
BARSKI, A., CUDDAPAH, S., CUI, K., ROH, T. Y., SCHONES, D. E., WANG, Z., WEI, G., CHEPELEV, I. & ZHAO, K. 2007. High-resolution profiling of histone methylations in the human genome. *Cell,* 129**,** 823-37.
BAUMANN, P. & CECH, T. R. 2001. Pot1, the putative telomere end-binding protein in fission yeast and humans. *Science,* 292**,** 1171-5.
BAXEVANIS, A. D. & LANDSMAN, D. 1996. Histone Sequence Database: a compilation of highly-conserved nucleoprotein sequences. *Nucleic Acids Res,* 24**,** 245-7.
BAYLISS, R., BURGESS, S. G. & MCINTYRE, P. J. 2017. Switching Aurora-A kinase on and off at an allosteric site. *FEBS J,* 284**,** 2947-2954.
BEIER, F., FORONDA, M., MARTINEZ, P. & BLASCO, M. A. 2012. Conditional TRF1 knockout in the hematopoietic compartment leads to bone marrow failure and recapitulates clinical features of dyskeratosis congenita. *Blood,* 120**,** 2990-3000.
BEJARANO, L., SCHUHMACHER, A. J., MENDEZ, M., MEGIAS, D., BLANCO-APARICIO, C., MARTINEZ, S., PASTOR, J., SQUATRITO, M. & BLASCO, M. A. 2017. Inhibition of TRF1 Telomere Protein Impairs Tumor Initiation and Progression in Glioblastoma Mouse Models and Patient-Derived Xenografts. *Cancer Cell,* 32**,** 590-607 e4.
BENETTI, R., GONZALO, S., JACO, I., SCHOTTA, G., KLATT, P., JENUWEIN, T. & BLASCO, M. A. 2007. Suv4-20h deficiency results in telomere elongation and derepression of telomere recombination. *J Cell Biol,* 178**,** 925-36.
BIAN, C., XU, C., RUAN, J., LEE, K. K., BURKE, T. L., TEMPEL, W., BARSYTE, D., LI, J., WU, M., ZHOU, B. O., FLEHARTY, B. E., PAULSON, A., ALLALI-HASSANI, A., ZHOU, J. Q., MER, G., GRANT, P. A., WORKMAN, J. L., ZANG, J. & MIN, J. 2011. Sgf29 binds histone H3K4me2/3 and is required for SAGA complex recruitment and histone H3 acetylation. *EMBO J,* 30**,** 2829-42.
BIANCHI, A., SMITH, S., CHONG, L., ELIAS, P. & DE LANGE, T. 1997. TRF1 is a dimer and bends telomeric DNA. *EMBO J,* 16**,** 1785-94.
BILAUD, T., BRUN, C., ANCELIN, K., KOERING, C. E., LAROCHE, T. & GILSON, E. 1997. Telomeric localization of TRF2, a novel human telobox protein. *Nat Genet,* 17**,** 236-9.
BISHOP, J. D. & SCHUMACHER, J. M. 2002. Phosphorylation of the carboxyl terminus of inner centromere protein (INCENP) by the Aurora B Kinase stimulates Aurora B kinase activity. *J Biol Chem,* 277**,** 27577-80.
BJERKE, L., MACKAY, A., NANDHABALAN, M., BURFORD, A., JURY, A., POPOV, S., BAX, D. A., CARVALHO, D., TAYLOR, K. R., VINCI, M., BAJRAMI, I., MCGONNELL, I. M., LORD, C. J., REIS, R. M., HARGRAVE, D., ASHWORTH, A., WORKMAN, P. & JONES, C. 2013. Histone H3.3. mutations drive pediatric glioblastoma through upregulation of MYCN. *Cancer Discov,* 3**,** 512-9.
BLACK, B. E., BROCK, M. A., BEDARD, S., WOODS, V. L., JR. & CLEVELAND, D. W. 2007. An epigenetic mark generated by the incorporation of CENP-A into centromeric nucleosomes. *Proc Natl Acad Sci U S A,* 104**,** 5008-13.

BLACK, B. E., FOLTZ, D. R., CHAKRAVARTHY, S., LUGER, K., WOODS, V. L., JR. & CLEVELAND, D. W. 2004. Structural determinants for generating centromeric chromatin. *Nature,* 430**,** 578-82.

BLACK, J. C., ALLEN, A., VAN RECHEM, C., FORBES, E., LONGWORTH, M., TSCHOP, K., RINEHART, C., QUITON, J., WALSH, R., SMALLWOOD, A., DYSON, N. J. & WHETSTINE, J. R. 2010. Conserved antagonism between JMJD2A/KDM4A and HP1gamma during cell cycle progression. *Mol Cell,* 40**,** 736-48.

BLACK, J. C., VAN RECHEM, C. & WHETSTINE, J. R. 2012. Histone lysine methylation dynamics: establishment, regulation, and biological impact. *Mol Cell,* 48**,** 491-507.

BOCK, I., KUDITHIPUDI, S., TAMAS, R., KUNGULOVSKI, G., DHAYALAN, A. & JELTSCH, A. 2011. Application of Celluspots peptide arrays for the analysis of the binding specificity of epigenetic reading domains to modified histone tails. *BMC Biochem,* 12**,** 48.

BOLANOS-GARCIA, V. M. 2005. Aurora kinases. *Int J Biochem Cell Biol,* 37**,** 1572-7.

BONENFANT, D., COULOT, M., TOWBIN, H., SCHINDLER, P. & VAN OOSTRUM, J. 2006. Characterization of histone H2A and H2B variants and their post-translational modifications by mass spectrometry. *Mol Cell Proteomics,* 5**,** 541-52.

BOWMAN, G. D. & POIRIER, M. G. 2015. Post-translational modifications of histones that influence nucleosome dynamics. *Chem Rev,* 115**,** 2274-95.

BRAUCHLE, M., YAO, Z., ARORA, R., THIGALE, S., CLAY, I., INVERARDI, B., FLETCHER, J., TASLIMI, P., ACKER, M. G., GERRITS, B., VOSHOL, J., BAUER, A., SCHUBELER, D., BOUWMEESTER, T. & RUFFNER, H. 2013. Protein complex interactor analysis and differential activity of KDM3 subfamily members towards H3K9 methylation. *PLoS One,* 8**,** e60549.

BROCCOLI, D., SMOGORZEWSKA, A., CHONG, L. & DE LANGE, T. 1997. Human telomeres contain two distinct Myb-related proteins, TRF1 and TRF2. *Nat Genet,* 17**,** 231-5.

BRUSH, D., DODGSON, J. B., CHOI, O. R., STEVENS, P. W. & ENGEL, J. D. 1985. Replacement variant histone genes contain intervening sequences. *Mol Cell Biol,* 5**,** 1307-17.

BURCH, J. B. 2005. Regulation of GATA gene expression during vertebrate development. *Semin Cell Dev Biol,* 16**,** 71-81.

BUSH, K. M., YUEN, B. T., BARRILLEAUX, B. L., RIGGS, J. W., O'GEEN, H., COTTERMAN, R. F. & KNOEPFLER, P. S. 2013. Endogenous mammalian histone H3.3 exhibits chromatin-related functions during development. *Epigenetics Chromatin,* 6**,** 7.

BUVELOT, S., TATSUTANI, S. Y., VERMAAK, D. & BIGGINS, S. 2003. The budding yeast Ipl1/Aurora protein kinase regulates mitotic spindle disassembly. *J Cell Biol,* 160**,** 329-39.

CAHILL, D. P., KINZLER, K. W., VOGELSTEIN, B. & LENGAUER, C. 1999. Genetic instability and darwinian selection in tumours. *Trends Cell Biol,* 9**,** M57-60.

CARMENA, M., RUCHAUD, S. & EARNSHAW, W. C. 2009. Making the Auroras glow: regulation of Aurora A and B kinase function by interacting proteins. *Curr Opin Cell Biol,* 21**,** 796-805.

CARROZZA, M. J., LI, B., FLORENS, L., SUGANUMA, T., SWANSON, S. K., LEE, K. K., SHIA, W. J., ANDERSON, S., YATES, J., WASHBURN, M. P. & WORKMAN, J. L. 2005. Histone H3 methylation by Set2 directs deacetylation of coding regions by Rpd3S to suppress spurious intragenic transcription. *Cell,* 123**,** 581-92.

CASTIGLIA, D., CESTELLI, A., SCATURRO, M., NASTASI, T. & DI LIEGRO, I. 1994. H1(0) and H3.3B mRNA levels in developing rat brain. *Neurochem Res,* 19**,** 1531-7.

CELESTE, A., DIFILIPPANTONIO, S., DIFILIPPANTONIO, M. J., FERNANDEZ-CAPETILLO, O., PILCH, D. R., SEDELNIKOVA, O. A., ECKHAUS, M., RIED, T., BONNER, W. M. & NUSSENZWEIG, A. 2003. H2AX haploinsufficiency modifies genomic stability and tumor susceptibility. *Cell,* 114**,** 371-83.

CELESTE, A., PETERSEN, S., ROMANIENKO, P. J., FERNANDEZ-CAPETILLO, O., CHEN, H. T., SEDELNIKOVA, O. A., REINA-SAN-MARTIN, B., COPPOLA, V., MEFFRE, E., DIFILIPPANTONIO, M. J., REDON, C., PILCH, D. R., OLARU, A., ECKHAUS, M., CAMERINI-OTERO, R. D., TESSAROLLO, L., LIVAK, F., MANOVA, K., BONNER, W. M.,

NUSSENZWEIG, M. C. & NUSSENZWEIG, A. 2002. Genomic instability in mice lacking histone H2AX. *Science,* 296**,** 922-7.
CELLI, G. B. & DE LANGE, T. 2005. DNA processing is not required for ATM-mediated telomere damage response after TRF2 deletion. *Nat Cell Biol,* 7**,** 712-8.
CHAKRAVARTHY, S., PATEL, A. & BOWMAN, G. D. 2012. The basic linker of macroH2A stabilizes DNA at the entry/exit site of the nucleosome. *Nucleic Acids Res,* 40**,** 8285-95.
CHAN, F. L., MARSHALL, O. J., SAFFERY, R., KIM, B. W., EARLE, E., CHOO, K. H. & WONG, L. H. 2012. Active transcription and essential role of RNA polymerase II at the centromere during mitosis. *Proc Natl Acad Sci U S A,* 109**,** 1979-84.
CHAN, F. L., VINOD, B., NOVY, K., SCHITTENHELM, R. B., HUANG, C., UDUGAMA, M., NUNEZ-IGLESIAS, J., LIN, J. I., HII, L., CHAN, J., PICKETT, H. A., DALY, R. J. & WONG, L. H. 2017. Aurora Kinase B, a novel regulator of TERF1 binding and telomeric integrity. *Nucleic Acids Res,* 45**,** 12340-12353.
CHAN, K. M., FANG, D., GAN, H., HASHIZUME, R., YU, C., SCHROEDER, M., GUPTA, N., MUELLER, S., JAMES, C. D., JENKINS, R., SARKARIA, J. & ZHANG, Z. 2013. The histone H3.3K27M mutation in pediatric glioma reprograms H3K27 methylation and gene expression. *Genes Dev,* 27**,** 985-90.
CHANG, F. T., CHAN, F. L., JD, R. M., UDUGAMA, M., MAYNE, L., COLLAS, P., MANN, J. R. & WONG, L. H. 2015. CHK1-driven histone H3.3 serine 31 phosphorylation is important for chromatin maintenance and cell survival in human ALT cancer cells. *Nucleic Acids Res,* 43**,** 2603-14.
CHANG, F. T., MCGHIE, J. D., CHAN, F. L., TANG, M. C., ANDERSON, M. A., MANN, J. R., ANDY CHOO, K. H. & WONG, L. H. 2013. PML bodies provide an important platform for the maintenance of telomeric chromatin integrity in embryonic stem cells. *Nucleic Acids Res,* 41**,** 4447-58.
CHEN, K. Y., BUSH, K., KLEIN, R. H., CERVANTES, V., LEWIS, N., NAQVI, A., CARCABOSO, A. M., LECHPAMMER, M. & KNOEPFLER, P. S. 2020. Reciprocal H3.3 gene editing identifies K27M and G34R mechanisms in pediatric glioma including NOTCH signaling. *Commun Biol,* 3**,** 363.
CHEN, P., WANG, Y. & LI, G. 2014. Dynamics of histone variant H3.3 and its coregulation with H2A.Z at enhancers and promoters. *Nucleus,* 5**,** 21-7.
CHEN, T. & DENT, S. Y. 2014. Chromatin modifiers and remodellers: regulators of cellular differentiation. *Nat Rev Genet,* 15**,** 93-106.
CHEUNG, P., TANNER, K. G., CHEUNG, W. L., SASSONE-CORSI, P., DENU, J. M. & ALLIS, C. D. 2000. Synergistic coupling of histone H3 phosphorylation and acetylation in response to epidermal growth factor stimulation. *Mol Cell,* 5**,** 905-15.
CHEUTIN, T., MCNAIRN, A. J., JENUWEIN, T., GILBERT, D. M., SINGH, P. B. & MISTELI, T. 2003. Maintenance of stable heterochromatin domains by dynamic HP1 binding. *Science,* 299**,** 721-5.
CHI, P., ALLIS, C. D. & WANG, G. G. 2010. Covalent histone modifications--miswritten, misinterpreted and mis-erased in human cancers. *Nat Rev Cancer,* 10**,** 457-69.
CHOW, C. M., GEORGIOU, A., SZUTORISZ, H., MAIA E SILVA, A., POMBO, A., BARAHONA, I., DARGELOS, E., CANZONETTA, C. & DILLON, N. 2005. Variant histone H3.3 marks promoters of transcriptionally active genes during mammalian cell division. *EMBO Rep,* 6**,** 354-60.
CIMINO-REALE, G., PASCALE, E., BATTILORO, E., STARACE, G., VERNA, R. & D'AMBROSIO, E. 2001. The length of telomeric G-rich strand 3'-overhang measured by oligonucleotide ligation assay. *Nucleic Acids Res,* 29**,** E35.
CLAYTON, A. L., HAZZALIN, C. A. & MAHADEVAN, L. C. 2006. Enhanced histone acetylation and transcription: a dynamic perspective. *Mol Cell,* 23**,** 289-96.
CLEVERS, H. 2006. Wnt/beta-catenin signaling in development and disease. *Cell,* 127**,** 469-80.
COOPER, S., DIENSTBIER, M., HASSAN, R., SCHERMELLEH, L., SHARIF, J., BLACKLEDGE, N. P., DE MARCO, V., ELDERKIN, S., KOSEKI, H., KLOSE, R., HEGER, A. & BROCKDORFF,

N. 2014. Targeting polycomb to pericentric heterochromatin in embryonic stem cells reveals a role for H2AK119u1 in PRC2 recruitment. *Cell Rep,* 7**,** 1456-1470.
COSTANZI, C. & PEHRSON, J. R. 1998. Histone macroH2A1 is concentrated in the inactive X chromosome of female mammals. *Nature,* 393**,** 599-601.
COX, S. G., KIM, H., GARNETT, A. T., MEDEIROS, D. M., AN, W. & CRUMP, J. G. 2012. An essential role of variant histone H3.3 for ectomesenchyme potential of the cranial neural crest. *PLoS Genet,* 8**,** e1002938.
CREYGHTON, M. P., CHENG, A. W., WELSTEAD, G. G., KOOISTRA, T., CAREY, B. W., STEINE, E. J., HANNA, J., LODATO, M. A., FRAMPTON, G. M., SHARP, P. A., BOYER, L. A., YOUNG, R. A. & JAENISCH, R. 2010. Histone H3K27ac separates active from poised enhancers and predicts developmental state. *Proc Natl Acad Sci U S A,* 107**,** 21931-6.
CREYGHTON, M. P., MARKOULAKI, S., LEVINE, S. S., HANNA, J., LODATO, M. A., SHA, K., YOUNG, R. A., JAENISCH, R. & BOYER, L. A. 2008. H2AZ is enriched at polycomb complex target genes in ES cells and is necessary for lineage commitment. *Cell,* 135**,** 649-61.
CRISTOFARI, G. & LINGNER, J. 2006. Telomere length homeostasis requires that telomerase levels are limiting. *EMBO J,* 25**,** 565-74.
DANG-NGUYEN, T. Q., HARAGUCHI, S., FURUSAWA, T., SOMFAI, T., KANEDA, M., WATANABE, S., AKAGI, S., KIKUCHI, K., TAJIMA, A. & NAGAI, T. 2013. Downregulation of histone methyltransferase genes SUV39H1 and SUV39H2 increases telomere length in embryonic stem-like cells and embryonic fibroblasts in pigs. *J Reprod Dev,* 59**,** 27-32.
DAUCH, D., RUDALSKA, R., COSSA, G., NAULT, J. C., KANG, T. W., WUESTEFELD, T., HOHMEYER, A., IMBEAUD, S., YEVSA, T., HOENICKE, L., PANTSAR, T., BOZKO, P., MALEK, N. P., LONGERICH, T., LAUFER, S., POSO, A., ZUCMAN-ROSSI, J., EILERS, M. & ZENDER, L. 2016. A MYC-aurora kinase A protein complex represents an actionable drug target in p53-altered liver cancer. *Nat Med,* 22**,** 744-53.
DAURY, L., CHAILLEUX, C., BONVALLET, J. & TROUCHE, D. 2006. Histone H3.3 deposition at E2F-regulated genes is linked to transcription. *EMBO Rep,* 7**,** 66-71.
DAVEY, C. A., SARGENT, D. F., LUGER, K., MAEDER, A. W. & RICHMOND, T. J. 2002. Solvent mediated interactions in the structure of the nucleosome core particle at 1.9 a resolution. *J Mol Biol,* 319**,** 1097-113.
DE ALMEIDA, S. F., GROSSO, A. R., KOCH, F., FENOUIL, R., CARVALHO, S., ANDRADE, J., LEVEZINHO, H., GUT, M., EICK, D., GUT, I., ANDRAU, J. C., FERRIER, P. & CARMO-FONSECA, M. 2011. Splicing enhances recruitment of methyltransferase HYPB/Setd2 and methylation of histone H3 Lys36. *Nat Struct Mol Biol,* 18**,** 977-83.
DE LA BARRE, A. E., GERSON, V., GOUT, S., CREAVEN, M., ALLIS, C. D. & DIMITROV, S. 2000. Core histone N-termini play an essential role in mitotic chromosome condensation. *EMBO J,* 19**,** 379-91.
DE LANGE, T. 2005. Shelterin: the protein complex that shapes and safeguards human telomeres. *Genes Dev,* 19**,** 2100-10.
DECKERT, J. & STRUHL, K. 2001. Histone acetylation at promoters is differentially affected by specific activators and repressors. *Mol Cell Biol,* 21**,** 2726-35.
DELBARRE, E., IVANAUSKIENE, K., KUNTZIGER, T. & COLLAS, P. 2013. DAXX-dependent supply of soluble (H3.3-H4) dimers to PML bodies pending deposition into chromatin. *Genome Res,* 23**,** 440-51.
DELBARRE, E., IVANAUSKIENE, K., SPIRKOSKI, J., SHAH, A., VEKTERUD, K., MOSKAUG, J. O., BOE, S. O., WONG, L. H., KUNTZIGER, T. & COLLAS, P. 2017. PML protein organizes heterochromatin domains where it regulates histone H3.3 deposition by ATRX/DAXX. *Genome Res,* 27**,** 913-921.
DENCHI, E. L. & DE LANGE, T. 2007. Protection of telomeres through independent control of ATM and ATR by TRF2 and POT1. *Nature,* 448**,** 1068-71.
DHAYALAN, A., RAJAVELU, A., RATHERT, P., TAMAS, R., JURKOWSKA, R. Z., RAGOZIN, S. & JELTSCH, A. 2010. The Dnmt3a PWWP domain reads histone 3 lysine 36 trimethylation and guides DNA methylation. *J Biol Chem,* 285**,** 26114-20.

DHAYALAN, A., TAMAS, R., BOCK, I., TATTERMUSCH, A., DIMITROVA, E., KUDITHIPUDI, S., RAGOZIN, S. & JELTSCH, A. 2011. The ATRX-ADD domain binds to H3 tail peptides and reads the combined methylation state of K4 and K9. *Hum Mol Genet,* 20**,** 2195-203.

DING, H., SCHERTZER, M., WU, X., GERTSENSTEIN, M., SELIG, S., KAMMORI, M., POURVALI, R., POON, S., VULTO, I., CHAVEZ, E., TAM, P. P., NAGY, A. & LANSDORP, P. M. 2004. Regulation of murine telomere length by Rtel: an essential gene encoding a helicase-like protein. *Cell,* 117**,** 873-86.

DISSMEYER, N. & SCHNITTGER, A. 2011. Use of phospho-site substitutions to analyze the biological relevance of phosphorylation events in regulatory networks. *Methods Mol Biol,* 779**,** 93-138.

DITCHFIELD, C., JOHNSON, V. L., TIGHE, A., ELLSTON, R., HAWORTH, C., JOHNSON, T., MORTLOCK, A., KEEN, N. & TAYLOR, S. S. 2003. Aurora B couples chromosome alignment with anaphase by targeting BubR1, Mad2, and Cenp-E to kinetochores. *J Cell Biol,* 161**,** 267-80.

DODSON, C. A., KOSMOPOULOU, M., RICHARDS, M. W., ATRASH, B., BAVETSIAS, V., BLAGG, J. & BAYLISS, R. 2010. Crystal structure of an Aurora-A mutant that mimics Aurora-B bound to MLN8054: insights into selectivity and drug design. *Biochem J,* 427**,** 19-28.

DOYON, Y., SELLECK, W., LANE, W. S., TAN, S. & COTE, J. 2004. Structural and functional conservation of the NuA4 histone acetyltransferase complex from yeast to humans. *Mol Cell Biol,* 24**,** 1884-96.

DRANE, P., OUARARHNI, K., DEPAUX, A., SHUAIB, M. & HAMICHE, A. 2010. The death-associated protein DAXX is a novel histone chaperone involved in the replication-independent deposition of H3.3. *Genes Dev,* 24**,** 1253-65.

DU, R., HUANG, C., LIU, K., LI, X. & DONG, Z. 2021. Targeting AURKA in Cancer: molecular mechanisms and opportunities for Cancer therapy. *Mol Cancer,* 20**,** 15.

EDMUNDS, J. W., MAHADEVAN, L. C. & CLAYTON, A. L. 2008. Dynamic histone H3 methylation during gene induction: HYPB/Setd2 mediates all H3K36 trimethylation. *EMBO J,* 27**,** 406-20.

ELSAESSER, S. J. & ALLIS, C. D. 2010. HIRA and Daxx constitute two independent histone H3.3-containing predeposition complexes. *Cold Spring Harb Symp Quant Biol,* 75**,** 27-34.

ELSAESSER, S. J., GOLDBERG, A. D. & ALLIS, C. D. 2010. New functions for an old variant: no substitute for histone H3.3. *Curr Opin Genet Dev,* 20**,** 110-7.

ELSASSER, S. J., HUANG, H., LEWIS, P. W., CHIN, J. W., ALLIS, C. D. & PATEL, D. J. 2012. DAXX envelops a histone H3.3-H4 dimer for H3.3-specific recognition. *Nature,* 491**,** 560-5.

ELSASSER, S. J., NOH, K. M., DIAZ, N., ALLIS, C. D. & BANASZYNSKI, L. A. 2015. Histone H3.3 is required for endogenous retroviral element silencing in embryonic stem cells. *Nature,* 522**,** 240-4.

FAAST, R., THONGLAIROAM, V., SCHULZ, T. C., BEALL, J., WELLS, J. R., TAYLOR, H., MATTHAEI, K., RATHJEN, P. D., TREMETHICK, D. J. & LYONS, I. 2001. Histone variant H2A.Z is required for early mammalian development. *Curr Biol,* 11**,** 1183-7.

FAIRALL, L., CHAPMAN, L., MOSS, H., DE LANGE, T. & RHODES, D. 2001. Structure of the TRFH dimerization domain of the human telomeric proteins TRF1 and TRF2. *Mol Cell,* 8**,** 351-61.

FANG, D., GAN, H., CHENG, L., LEE, J. H., ZHOU, H., SARKARIA, J. N., DANIELS, D. J. & ZHANG, Z. 2018. H3.3K27M mutant proteins reprogram epigenome by sequestering the PRC2 complex to poised enhancers. *Elife,* 7.

FANG, R., BARBERA, A. J., XU, Y., RUTENBERG, M., LEONOR, T., BI, Q., LAN, F., MEI, P., YUAN, G. C., LIAN, C., PENG, J., CHENG, D., SUI, G., KAISER, U. B., SHI, Y. & SHI, Y. G. 2010. Human LSD2/KDM1b/AOF1 regulates gene transcription by modulating intragenic H3K4me2 methylation. *Mol Cell,* 39**,** 222-33.

FERNANDEZ-MIRANDA, G., TRAKALA, M., MARTIN, J., ESCOBAR, B., GONZALEZ, A., GHYSELINCK, N. B., ORTEGA, S., CANAMERO, M., PEREZ DE CASTRO, I. & MALUMBRES, M. 2011. Genetic disruption of aurora B uncovers an essential role for aurora C during early mammalian development. *Development,* 138**,** 2661-72.

FINK, M., IMHOLZ, D. & THOMA, F. 2007. Contribution of the serine 129 of histone H2A to chromatin structure. *Mol Cell Biol,* 27**,** 3589-600.
FISCHER, J. J., TOEDLING, J., KRUEGER, T., SCHUELER, M., HUBER, W. & SPERLING, S. 2008. Combinatorial effects of four histone modifications in transcription and differentiation. *Genomics,* 91**,** 41-51.
FISCHLE, W., TSENG, B. S., DORMANN, H. L., UEBERHEIDE, B. M., GARCIA, B. A., SHABANOWITZ, J., HUNT, D. F., FUNABIKI, H. & ALLIS, C. D. 2005. Regulation of HP1-chromatin binding by histone H3 methylation and phosphorylation. *Nature,* 438**,** 1116-22.
FNU, S., WILLIAMSON, E. A., DE HARO, L. P., BRENNEMAN, M., WRAY, J., SHAHEEN, M., RADHAKRISHNAN, K., LEE, S. H., NICKOLOFF, J. A. & HROMAS, R. 2011. Methylation of histone H3 lysine 36 enhances DNA repair by nonhomologous end-joining. *Proc Natl Acad Sci U S A,* 108**,** 540-5.
FODOR, B. D., SHUKEIR, N., REUTER, G. & JENUWEIN, T. 2010. Mammalian Su(var) genes in chromatin control. *Annu Rev Cell Dev Biol,* 26**,** 471-501.
FORTSCHEGGER, K. & SHIEKHATTAR, R. 2011. Plant homeodomain fingers form a helping hand for transcription. *Epigenetics,* 6**,** 4-8.
FRANCIS, N. J., KINGSTON, R. E. & WOODCOCK, C. L. 2004. Chromatin compaction by a polycomb group protein complex. *Science,* 306**,** 1574-7.
FREY, A., LISTOVSKY, T., GUILBAUD, G., SARKIES, P. & SALE, J. E. 2014. Histone H3.3 is required to maintain replication fork progression after UV damage. *Curr Biol,* 24**,** 2195-2201.
GADEA, B. B. & RUDERMAN, J. V. 2005. Aurora kinase inhibitor ZM447439 blocks chromosome-induced spindle assembly, the completion of chromosome condensation, and the establishment of the spindle integrity checkpoint in Xenopus egg extracts. *Mol Biol Cell,* 16**,** 1305-18.
GARCIA-CAO, M., O'SULLIVAN, R., PETERS, A. H., JENUWEIN, T. & BLASCO, M. A. 2004. Epigenetic regulation of telomere length in mammalian cells by the Suv39h1 and Suv39h2 histone methyltransferases. *Nat Genet,* 36**,** 94-9.
GARCIA, B. A., BARBER, C. M., HAKE, S. B., PTAK, C., TURNER, F. B., BUSBY, S. A., SHABANOWITZ, J., MORAN, R. G., ALLIS, C. D. & HUNT, D. F. 2005. Modifications of human histone H3 variants during mitosis. *Biochemistry,* 44**,** 13202-13.
GASPAR-MAIA, A., QADEER, Z. A., HASSON, D., RATNAKUMAR, K., LEU, N. A., LEROY, G., LIU, S., COSTANZI, C., VALLE-GARCIA, D., SCHANIEL, C., LEMISCHKA, I., GARCIA, B., PEHRSON, J. R. & BERNSTEIN, E. 2013. MacroH2A histone variants act as a barrier upon reprogramming towards pluripotency. *Nat Commun,* 4**,** 1565.
GIAIMO, B. D., FERRANTE, F., HERCHENROTHER, A., HAKE, S. B. & BORGGREFE, T. 2019. The histone variant H2A.Z in gene regulation. *Epigenetics Chromatin,* 12**,** 37.
GIBBONS, R. J., WADA, T., FISHER, C. A., MALIK, N., MITSON, M. J., STEENSMA, D. P., FRYER, A., GOUDIE, D. R., KRANTZ, I. D. & TRAEGER-SYNODINOS, J. 2008. Mutations in the chromatin-associated protein ATRX. *Hum Mutat,* 29**,** 796-802.
GIET, R. & PRIGENT, C. 1999. Aurora/Ipl1p-related kinases, a new oncogenic family of mitotic serine-threonine kinases. *J Cell Sci,* 112 (Pt 21)**,** 3591-601.
GILBERT, N., THOMSON, I., BOYLE, S., ALLAN, J., RAMSAHOYE, B. & BICKMORE, W. A. 2007. DNA methylation affects nuclear organization, histone modifications, and linker histone binding but not chromatin compaction. *J Cell Biol,* 177**,** 401-11.
GIMENEZ-ABIAN, J. F., SUMARA, I., HIROTA, T., HAUF, S., GERLICH, D., DE LA TORRE, C., ELLENBERG, J. & PETERS, J. M. 2004. Regulation of sister chromatid cohesion between chromosome arms. *Curr Biol,* 14**,** 1187-93.
GLOVER, T. W., BERGER, C., COYLE, J. & ECHO, B. 1984. DNA polymerase alpha inhibition by aphidicolin induces gaps and breaks at common fragile sites in human chromosomes. *Hum Genet,* 67**,** 136-42.
GOLDBERG, A. D., BANASZYNSKI, L. A., NOH, K. M., LEWIS, P. W., ELSAESSER, S. J., STADLER, S., DEWELL, S., LAW, M., GUO, X., LI, X., WEN, D., CHAPGIER, A., DEKELVER, R. C., MILLER, J. C., LEE, Y. L., BOYDSTON, E. A., HOLMES, M. C.,

GREGORY, P. D., GREALLY, J. M., RAFII, S., YANG, C., SCAMBLER, P. J., GARRICK, D., GIBBONS, R. J., HIGGS, D. R., CRISTEA, I. M., URNOV, F. D., ZHENG, D. & ALLIS, C. D. 2010. Distinct factors control histone variant H3.3 localization at specific genomic regions. *Cell,* 140**,** 678-91.
GONG, Y. & DE LANGE, T. 2010. A Shld1-controlled POT1a provides support for repression of ATR signaling at telomeres through RPA exclusion. *Mol Cell,* 40**,** 377-87.
GONZALEZ-ROMERO, R., MENDEZ, J., AUSIO, J. & EIRIN-LOPEZ, J. M. 2008. Quickly evolving histones, nucleosome stability and chromatin folding: all about histone H2A.Bbd. *Gene,* 413**,** 1-7.
GONZALO, S., JACO, I., FRAGA, M. F., CHEN, T., LI, E., ESTELLER, M. & BLASCO, M. A. 2006. DNA methyltransferases control telomere length and telomere recombination in mammalian cells. *Nat Cell Biol,* 8**,** 416-24.
GOODARZI, A. A. & JEGGO, P. A. 2012. The heterochromatic barrier to DNA double strand break repair: how to get the entry visa. *Int J Mol Sci,* 13**,** 11844-60.
GOTO, H., YASUI, Y., NIGG, E. A. & INAGAKI, M. 2002. Aurora-B phosphorylates Histone H3 at serine28 with regard to the mitotic chromosome condensation. *Genes Cells,* 7**,** 11-7.
GREAVES, I. K., RANGASAMY, D., RIDGWAY, P. & TREMETHICK, D. J. 2007. H2A.Z contributes to the unique 3D structure of the centromere. *Proc Natl Acad Sci U S A,* 104**,** 525-30.
GREER, E. L. & SHI, Y. 2012. Histone methylation: a dynamic mark in health, disease and inheritance. *Nat Rev Genet,* 13**,** 343-57.
GREIDER, C. W. & BLACKBURN, E. H. 1985. Identification of a specific telomere terminal transferase activity in Tetrahymena extracts. *Cell,* 43**,** 405-13.
GREWAL, S. I. & JIA, S. 2007. Heterochromatin revisited. *Nat Rev Genet,* 8**,** 35-46.
GRIFFITH, J. D., COMEAU, L., ROSENFIELD, S., STANSEL, R. M., BIANCHI, A., MOSS, H. & DE LANGE, T. 1999. Mammalian telomeres end in a large duplex loop. *Cell,* 97**,** 503-14.
GUO, R., ZHENG, L., PARK, J. W., LV, R., CHEN, H., JIAO, F., XU, W., MU, S., WEN, H., QIU, J., WANG, Z., YANG, P., WU, F., HUI, J., FU, X., SHI, X., SHI, Y. G., XING, Y., LAN, F. & SHI, Y. 2014. BS69/ZMYND11 reads and connects histone H3.3 lysine 36 trimethylation-decorated chromatin to regulated pre-mRNA processing. *Mol Cell,* 56**,** 298-310.
HAKE, S. B. & ALLIS, C. D. 2006. Histone H3 variants and their potential role in indexing mammalian genomes: the "H3 barcode hypothesis". *Proc Natl Acad Sci U S A,* 103**,** 6428-35.
HAKE, S. B., GARCIA, B. A., DUNCAN, E. M., KAUER, M., DELLAIRE, G., SHABANOWITZ, J., BAZETT-JONES, D. P., ALLIS, C. D. & HUNT, D. F. 2006. Expression patterns and post-translational modifications associated with mammalian histone H3 variants. *J Biol Chem,* 281**,** 559-68.
HAKE, S. B., GARCIA, B. A., KAUER, M., BAKER, S. P., SHABANOWITZ, J., HUNT, D. F. & ALLIS, C. D. 2005. Serine 31 phosphorylation of histone variant H3.3 is specific to regions bordering centromeres in metaphase chromosomes. *Proc Natl Acad Sci U S A,* 102**,** 6344-9.
HALL, I. M., SHANKARANARAYANA, G. D., NOMA, K., AYOUB, N., COHEN, A. & GREWAL, S. I. 2002. Establishment and maintenance of a heterochromatin domain. *Science,* 297**,** 2232-7.
HANAOKA, S., NAGADOI, A. & NISHIMURA, Y. 2005. Comparison between TRF2 and TRF1 of their telomeric DNA-bound structures and DNA-binding activities. *Protein Sci,* 14**,** 119-30.
HARLEY, C. B., FUTCHER, A. B. & GREIDER, C. W. 1990. Telomeres shorten during ageing of human fibroblasts. *Nature,* 345**,** 458-60.
HARTZOG, G. A. & WINSTON, F. 1997. Nucleosomes and transcription: recent lessons from genetics. *Curr Opin Genet Dev,* 7**,** 192-8.
HARUTYUNYAN, A. S., CHEN, H., LU, T., HORTH, C., NIKBAKHT, H., KRUG, B., RUSSO, C., BAREKE, E., MARCHIONE, D. M., CORADIN, M., GARCIA, B. A., JABADO, N. & MAJEWSKI, J. 2020. H3K27M in Gliomas Causes a One-Step Decrease in H3K27 Methylation and Reduced Spreading within the Constraints of H3K36 Methylation. *Cell Rep,* 33**,** 108390.
HARUTYUNYAN, A. S., KRUG, B., CHEN, H., PAPILLON-CAVANAGH, S., ZEINIEH, M., DE JAY, N., DESHMUKH, S., CHEN, C. C. L., BELLE, J., MIKAEL, L. G., MARCHIONE, D. M., LI, R.,

NIKBAKHT, H., HU, B., CAGNONE, G., CHEUNG, W. A., MOHAMMADNIA, A., BECHET, D., FAURY, D., MCCONECHY, M. K., PATHANIA, M., JAIN, S. U., ELLEZAM, B., WEIL, A. G., MONTPETIT, A., SALOMONI, P., PASTINEN, T., LU, C., LEWIS, P. W., GARCIA, B. A., KLEINMAN, C. L., JABADO, N. & MAJEWSKI, J. 2019. H3K27M induces defective chromatin spread of PRC2-mediated repressive H3K27me2/me3 and is essential for glioma tumorigenesis. *Nat Commun,* 10**,** 1262.

HATEBOER, G., GENNISSEN, A., RAMOS, Y. F., KERKHOVEN, R. M., SONNTAG-BUCK, V., STUNNENBERG, H. G. & BERNARDS, R. 1995. BS69, a novel adenovirus E1A-associated protein that inhibits E1A transactivation. *EMBO J,* 14**,** 3159-69.

HAUF, S., COLE, R. W., LATERRA, S., ZIMMER, C., SCHNAPP, G., WALTER, R., HECKEL, A., VAN MEEL, J., RIEDER, C. L. & PETERS, J. M. 2003. The small molecule Hesperadin reveals a role for Aurora B in correcting kinetochore-microtubule attachment and in maintaining the spindle assembly checkpoint. *J Cell Biol,* 161**,** 281-94.

HEGARAT, N., SMITH, E., NAYAK, G., TAKEDA, S., EYERS, P. A. & HOCHEGGER, H. 2011. Aurora A and Aurora B jointly coordinate chromosome segregation and anaphase microtubule dynamics. *J Cell Biol,* 195**,** 1103-13.

HENDZEL, M. J., WEI, Y., MANCINI, M. A., VAN HOOSER, A., RANALLI, T., BRINKLEY, B. R., BAZETT-JONES, D. P. & ALLIS, C. D. 1997. Mitosis-specific phosphorylation of histone H3 initiates primarily within pericentromeric heterochromatin during G2 and spreads in an ordered fashion coincident with mitotic chromosome condensation. *Chromosoma,* 106**,** 348-60.

HINCHCLIFFE, E. H., DAY, C. A., KARANJEET, K. B., FADNESS, S., LANGFALD, A., VAUGHAN, K. T. & DONG, Z. 2016. Chromosome missegregation during anaphase triggers p53 cell cycle arrest through histone H3.3 Ser31 phosphorylation. *Nat Cell Biol,* 18**,** 668-75.

HIROTA, T., LIPP, J. J., TOH, B. H. & PETERS, J. M. 2005. Histone H3 serine 10 phosphorylation by Aurora B causes HP1 dissociation from heterochromatin. *Nature,* 438**,** 1176-80.

HOCHEGGER, H., HEGARAT, N. & PEREIRA-LEAL, J. B. 2013. Aurora at the pole and equator: overlapping functions of Aurora kinases in the mitotic spindle. *Open Biol,* 3**,** 120185.

HOCKEMEYER, D. & COLLINS, K. 2015. Control of telomerase action at human telomeres. *Nat Struct Mol Biol,* 22**,** 848-52.

HODL, M. & BASLER, K. 2009. Transcription in the absence of histone H3.3. *Curr Biol,* 19**,** 1221-6.

HORTON, J. R., UPADHYAY, A. K., QI, H. H., ZHANG, X., SHI, Y. & CHENG, X. 2010. Enzymatic and structural insights for substrate specificity of a family of jumonji histone lysine demethylases. *Nat Struct Mol Biol,* 17**,** 38-43.

HOUGHTALING, B. R., CUTTONARO, L., CHANG, W. & SMITH, S. 2004. A dynamic molecular link between the telomere length regulator TRF1 and the chromosome end protector TRF2. *Curr Biol,* 14**,** 1621-31.

HOUSE, N. C., KOCH, M. R. & FREUDENREICH, C. H. 2014. Chromatin modifications and DNA repair: beyond double-strand breaks. *Front Genet,* 5**,** 296.

HSU, D. W., CHUBB, J. R., MURAMOTO, T., PEARS, C. J. & MAHADEVAN, L. C. 2012. Dynamic acetylation of lysine-4-trimethylated histone H3 and H3 variant biology in a simple multicellular eukaryote. *Nucleic Acids Res,* 40**,** 7247-56.

HSU, J. Y., SUN, Z. W., LI, X., REUBEN, M., TATCHELL, K., BISHOP, D. K., GRUSHCOW, J. M., BRAME, C. J., CALDWELL, J. A., HUNT, D. F., LIN, R., SMITH, M. M. & ALLIS, C. D. 2000. Mitotic phosphorylation of histone H3 is governed by Ipl1/aurora kinase and Glc7/PP1 phosphatase in budding yeast and nematodes. *Cell,* 102**,** 279-91.

HU, G., CUI, K., NORTHRUP, D., LIU, C., WANG, C., TANG, Q., GE, K., LEVENS, D., CRANE-ROBINSON, C. & ZHAO, K. 2013. H2A.Z facilitates access of active and repressive complexes to chromatin in embryonic stem cell self-renewal and differentiation. *Cell Stem Cell,* 12**,** 180-92.

HUANG, J., WANG, F., OKUKA, M., LIU, N., JI, G., YE, X., ZUO, B., LI, M., LIANG, P., GE, W. W., TSIBRIS, J. C., KEEFE, D. L. & LIU, L. 2011. Association of telomere length with authentic pluripotency of ES/iPS cells. *Cell Res,* 21**,** 779-92.

HYUN, K., JEON, J., PARK, K. & KIM, J. 2017. Writing, erasing and reading histone lysine methylations. *Exp Mol Med,* 49**,** e324.
IOUZALEN, N., MOREAU, J. & MECHALI, M. 1996. H2A.ZI, a new variant histone expressed during Xenopus early development exhibits several distinct features from the core histone H2A. *Nucleic Acids Res,* 24**,** 3947-52.
IWANO, T., TACHIBANA, M., RETH, M. & SHINKAI, Y. 2004. Importance of TRF1 for functional telomere structure. *J Biol Chem,* 279**,** 1442-8.
JANG, C. W., SHIBATA, Y., STARMER, J., YEE, D. & MAGNUSON, T. 2015. Histone H3.3 maintains genome integrity during mammalian development. *Genes Dev,* 29**,** 1377-92.
JANKE, R., IAVARONE, A. T. & RINE, J. 2017. Oncometabolite D-2-Hydroxyglutarate enhances gene silencing through inhibition of specific H3K36 histone demethylases. *Elife,* 6.
JANSE, D. M., CROSAS, B., FINLEY, D. & CHURCH, G. M. 2004. Localization to the proteasome is sufficient for degradation. *J Biol Chem,* 279**,** 21415-20.
JERONIMO, C., WATANABE, S., KAPLAN, C. D., PETERSON, C. L. & ROBERT, F. 2015. The Histone Chaperones FACT and Spt6 Restrict H2A.Z from Intragenic Locations. *Mol Cell,* 58**,** 1113-23.
JIN, Q., YU, L. R., WANG, L., ZHANG, Z., KASPER, L. H., LEE, J. E., WANG, C., BRINDLE, P. K., DENT, S. Y. & GE, K. 2011. Distinct roles of GCN5/PCAF-mediated H3K9ac and CBP/p300-mediated H3K18/27ac in nuclear receptor transactivation. *EMBO J,* 30**,** 249-62.
JOHANSEN, K. M. & JOHANSEN, J. 2006. Regulation of chromatin structure by histone H3S10 phosphorylation. *Chromosome Res,* 14**,** 393-404.
JOHNSSON, A., DURAND-DUBIEF, M., XUE-FRANZEN, Y., RONNERBLAD, M., EKWALL, K. & WRIGHT, A. 2009. HAT-HDAC interplay modulates global histone H3K14 acetylation in gene-coding regions during stress. *EMBO Rep,* 10**,** 1009-14.
JUSTIN, N., ZHANG, Y., TARRICONE, C., MARTIN, S. R., CHEN, S., UNDERWOOD, E., DE MARCO, V., HAIRE, L. F., WALKER, P. A., REINBERG, D., WILSON, J. R. & GAMBLIN, S. J. 2016. Structural basis of oncogenic histone H3K27M inhibition of human polycomb repressive complex 2. *Nat Commun,* 7**,** 11316.
KANG, Y., WANG, J., NEFF, A., KRATZER, S., KIMURA, H. & DAVIS, R. E. 2016. Differential Chromosomal Localization of Centromeric Histone CENP-A Contributes to Nematode Programmed DNA Elimination. *Cell Rep,* 16**,** 2308-16.
KAPOOR, A., GOLDBERG, M. S., CUMBERLAND, L. K., RATNAKUMAR, K., SEGURA, M. F., EMANUEL, P. O., MENENDEZ, S., VARDABASSO, C., LEROY, G., VIDAL, C. I., POLSKY, D., OSMAN, I., GARCIA, B. A., HERNANDO, E. & BERNSTEIN, E. 2010. The histone variant macroH2A suppresses melanoma progression through regulation of CDK8. *Nature,* 468**,** 1105-9.
KARACHENTSEV, D., SARMA, K., REINBERG, D. & STEWARD, R. 2005. PR-Set7-dependent methylation of histone H4 Lys 20 functions in repression of gene expression and is essential for mitosis. *Genes Dev,* 19**,** 431-5.
KARLSEDER, J., BROCCOLI, D., DAI, Y., HARDY, S. & DE LANGE, T. 1999. p53- and ATM-dependent apoptosis induced by telomeres lacking TRF2. *Science,* 283**,** 1321-5.
KARLSEDER, J., KACHATRIAN, L., TAKAI, H., MERCER, K., HINGORANI, S., JACKS, T. & DE LANGE, T. 2003. Targeted deletion reveals an essential function for the telomere length regulator Trf1. *Mol Cell Biol,* 23**,** 6533-41.
KARMODIYA, K., KREBS, A. R., OULAD-ABDELGHANI, M., KIMURA, H. & TORA, L. 2012. H3K9 and H3K14 acetylation co-occur at many gene regulatory elements, while H3K14ac marks a subset of inactive inducible promoters in mouse embryonic stem cells. *BMC Genomics,* 13**,** 424.
KASZAS, E. & CANDE, W. Z. 2000. Phosphorylation of histone H3 is correlated with changes in the maintenance of sister chromatid cohesion during meiosis in maize, rather than the condensation of the chromatin. *J Cell Sci,* 113 (Pt 18)**,** 3217-26.

KIM, M. K., KANG, M. R., NAM, H. W., BAE, Y. S., KIM, Y. S. & CHUNG, I. K. 2008. Regulation of telomeric repeat binding factor 1 binding to telomeres by casein kinase 2-mediated phosphorylation. *J Biol Chem,* 283**,** 14144-52.

KIM, S. H., KAMINKER, P. & CAMPISI, J. 1999. TIN2, a new regulator of telomere length in human cells. *Nat Genet,* 23**,** 405-12.

KIPLING, D. & COOKE, H. J. 1990. Hypervariable ultra-long telomeres in mice. *Nature,* 347**,** 400-2.

KLOSE, R. J., YAMANE, K., BAE, Y., ZHANG, D., ERDJUMENT-BROMAGE, H., TEMPST, P., WONG, J. & ZHANG, Y. 2006. The transcriptional repressor JHDM3A demethylates trimethyl histone H3 lysine 9 and lysine 36. *Nature,* 442**,** 312-6.

KONISHI, A. & DE LANGE, T. 2008. Cell cycle control of telomere protection and NHEJ revealed by a ts mutation in the DNA-binding domain of TRF2. *Genes Dev,* 22**,** 1221-30.

KORNBERG, R. D. 1974. Chromatin structure: a repeating unit of histones and DNA. *Science,* 184**,** 868-71.

KOUZARIDES, T. 2007. Chromatin modifications and their function. *Cell,* 128**,** 693-705.

KRAUSHAAR, D. C., JIN, W., MAUNAKEA, A., ABRAHAM, B., HA, M. & ZHAO, K. 2013. Genome-wide incorporation dynamics reveal distinct categories of turnover for the histone variant H3.3. *Genome Biol,* 14**,** R121.

KRIMER, D. B., CHENG, G. & SKOULTCHI, A. I. 1993. Induction of H3.3 replacement histone mRNAs during the precommitment period of murine erythroleukemia cell differentiation. *Nucleic Acids Res,* 21**,** 2873-9.

KRUG, B., DE JAY, N., HARUTYUNYAN, A. S., DESHMUKH, S., MARCHIONE, D. M., GUILHAMON, P., BERTRAND, K. C., MIKAEL, L. G., MCCONECHY, M. K., CHEN, C. C. L., KHAZAEI, S., KONCAR, R. F., AGNIHOTRI, S., FAURY, D., ELLEZAM, B., WEIL, A. G., URSINI-SIEGEL, J., DE CARVALHO, D. D., DIRKS, P. B., LEWIS, P. W., SALOMONI, P., LUPIEN, M., ARROWSMITH, C., LASKO, P. F., GARCIA, B. A., KLEINMAN, C. L., JABADO, N. & MACK, S. C. 2019. Pervasive H3K27 Acetylation Leads to ERV Expression and a Therapeutic Vulnerability in H3K27M Gliomas. *Cancer Cell,* 36**,** 338-339.

KUROTAKI, N., IMAIZUMI, K., HARADA, N., MASUNO, M., KONDOH, T., NAGAI, T., OHASHI, H., NARITOMI, K., TSUKAHARA, M., MAKITA, Y., SUGIMOTO, T., SONODA, T., HASEGAWA, T., CHINEN, Y., TOMITA HA, H. A., KINOSHITA, A., MIZUGUCHI, T., YOSHIURA KI, K., OHTA, T., KISHINO, T., FUKUSHIMA, Y., NIIKAWA, N. & MATSUMOTO, N. 2002. Haploinsufficiency of NSD1 causes Sotos syndrome. *Nat Genet,* 30**,** 365-6.

LABBE, R. M., HOLOWATYJ, A. & YANG, Z. Q. 2013. Histone lysine demethylase (KDM) subfamily 4: structures, functions and therapeutic potential. *Am J Transl Res,* 6**,** 1-15.

LACHNER, M., O'CARROLL, D., REA, S., MECHTLER, K. & JENUWEIN, T. 2001. Methylation of histone H3 lysine 9 creates a binding site for HP1 proteins. *Nature,* 410**,** 116-20.

LADENDORFF, N. E., WU, S. & LIPSICK, J. S. 2001. BS69, an adenovirus E1A-associated protein, inhibits the transcriptional activity of c-Myb. *Oncogene,* 20**,** 125-32.

LAW, M. J., LOWER, K. M., VOON, H. P., HUGHES, J. R., GARRICK, D., VIPRAKASIT, V., MITSON, M., DE GOBBI, M., MARRA, M., MORRIS, A., ABBOTT, A., WILDER, S. P., TAYLOR, S., SANTOS, G. M., CROSS, J., AYYUB, H., JONES, S., RAGOUSSIS, J., RHODES, D., DUNHAM, I., HIGGS, D. R. & GIBBONS, R. J. 2010. ATR-X syndrome protein targets tandem repeats and influences allele-specific expression in a size-dependent manner. *Cell,* 143**,** 367-78.

LEE, D. F., SU, J., ANG, Y. S., CARVAJAL-VERGARA, X., MULERO-NAVARRO, S., PEREIRA, C. F., GINGOLD, J., WANG, H. L., ZHAO, R., SEVILLA, A., DARR, H., WILLIAMSON, A. J., CHANG, B., NIU, X., AGUILO, F., FLORES, E. R., SHER, Y. P., HUNG, M. C., WHETTON, A. D., GELB, B. D., MOORE, K. A., SNOECK, H. W., MA'AYAN, A., SCHANIEL, C. & LEMISCHKA, I. R. 2012. Regulation of embryonic and induced pluripotency by aurora kinase-p53 signaling. *Cell Stem Cell,* 11**,** 179-94.

LEE, J., THOMPSON, J. R., BOTUYAN, M. V. & MER, G. 2008. Distinct binding modes specify the recognition of methylated histones H3K4 and H4K20 by JMJD2A-tudor. *Nat Struct Mol Biol,* 15**,** 109-11.

LEE, J. H., KIM, E. W., CROTEAU, D. L. & BOHR, V. A. 2020. Heterochromatin: an epigenetic point of view in aging. *Exp Mol Med,* 52**,** 1466-1474.
LEE, S., LEE, J., CHAE, S., MOON, Y., LEE, H. Y., PARK, B., YANG, E. G., HWANG, D. & PARK, H. 2017. Multi-dimensional histone methylations for coordinated regulation of gene expression under hypoxia. *Nucleic Acids Res,* 45**,** 11643-11657.
LEE, T. H., TUN-KYI, A., SHI, R., LIM, J., SOOHOO, C., FINN, G., BALASTIK, M., PASTORINO, L., WULF, G., ZHOU, X. Z. & LU, K. P. 2009. Essential role of Pin1 in the regulation of TRF1 stability and telomere maintenance. *Nat Cell Biol,* 11**,** 97-105.
LEHMANN, O. J., SOWDEN, J. C., CARLSSON, P., JORDAN, T. & BHATTACHARYA, S. S. 2003. Fox's in development and disease. *Trends Genet,* 19**,** 339-44.
LEHNERTZ, B., UEDA, Y., DERIJCK, A. A., BRAUNSCHWEIG, U., PEREZ-BURGOS, L., KUBICEK, S., CHEN, T., LI, E., JENUWEIN, T. & PETERS, A. H. 2003. Suv39h-mediated histone H3 lysine 9 methylation directs DNA methylation to major satellite repeats at pericentric heterochromatin. *Curr Biol,* 13**,** 1192-200.
LEMAN, A. R., DHEEKOLLU, J., DENG, Z., LEE, S. W., DAS, M. M., LIEBERMAN, P. M. & NOGUCHI, E. 2012. Timeless preserves telomere length by promoting efficient DNA replication through human telomeres. *Cell Cycle,* 11**,** 2337-47.
LEWIS, P. W., ELSAESSER, S. J., NOH, K. M., STADLER, S. C. & ALLIS, C. D. 2010. Daxx is an H3.3-specific histone chaperone and cooperates with ATRX in replication-independent chromatin assembly at telomeres. *Proc Natl Acad Sci U S A,* 107**,** 14075-80.
LEWIS, P. W., MULLER, M. M., KOLETSKY, M. S., CORDERO, F., LIN, S., BANASZYNSKI, L. A., GARCIA, B. A., MUIR, T. W., BECHER, O. J. & ALLIS, C. D. 2013. Inhibition of PRC2 activity by a gain-of-function H3 mutation found in pediatric glioblastoma. *Science,* 340**,** 857-61.
LI, B., OESTREICH, S. & DE LANGE, T. 2000. Identification of human Rap1: implications for telomere evolution. *Cell,* 101**,** 471-83.
LI, F., MAO, G., TONG, D., HUANG, J., GU, L., YANG, W. & LI, G. M. 2013. The histone mark H3K36me3 regulates human DNA mismatch repair through its interaction with MutSalpha. *Cell,* 153**,** 590-600.
LI, M., DONG, Q. & ZHU, B. 2017a. Aurora Kinase B Phosphorylates Histone H3.3 at Serine 31 during Mitosis in Mammalian Cells. *J Mol Biol,* 429**,** 2042-2045.
LI, S., DENG, Z., FU, J., XU, C., XIN, G., WU, Z., LUO, J., WANG, G., ZHANG, S., ZHANG, B., ZOU, F., JIANG, Q. & ZHANG, C. 2015. Spatial Compartmentalization Specializes the Function of Aurora A and Aurora B. *J Biol Chem,* 290**,** 17546-58.
LI, W., WANG, P., ZHANG, B., ZHANG, J., MING, J., XIE, W. & NA, J. 2017b. Differential regulation of H3S10 phosphorylation, mitosis progression and cell fate by Aurora Kinase B and C in mouse preimplantation embryos. *Protein Cell,* 8**,** 662-674.
LIANG, G., LIN, J. C., WEI, V., YOO, C., CHENG, J. C., NGUYEN, C. T., WEISENBERGER, D. J., EGGER, G., TAKAI, D., GONZALES, F. A. & JONES, P. A. 2004. Distinct localization of histone H3 acetylation and H3-K4 methylation to the transcription start sites in the human genome. *Proc Natl Acad Sci U S A,* 101**,** 7357-62.
LILLARD-WETHERELL, K., MACHWE, A., LANGLAND, G. T., COMBS, K. A., BEHBEHANI, G. K., SCHONBERG, S. A., GERMAN, J., TURCHI, J. J., ORREN, D. K. & GRODEN, J. 2004. Association and regulation of the BLM helicase by the telomere proteins TRF1 and TRF2. *Hum Mol Genet,* 13**,** 1919-32.
LIN, C. J., CONTI, M. & RAMALHO-SANTOS, M. 2013. Histone variant H3.3 maintains a decondensed chromatin state essential for mouse preimplantation development. *Development,* 140**,** 3624-34.
LIOKATIS, S., STUTZER, A., ELSASSER, S. J., THEILLET, F. X., KLINGBERG, R., VAN ROSSUM, B., SCHWARZER, D., ALLIS, C. D., FISCHLE, W. & SELENKO, P. 2012. Phosphorylation of histone H3 Ser10 establishes a hierarchy for subsequent intramolecular modification events. *Nat Struct Mol Biol,* 19**,** 819-23.
LIU, D., O'CONNOR, M. S., QIN, J. & SONGYANG, Z. 2004a. Telosome, a mammalian telomere-associated complex formed by multiple telomeric proteins. *J Biol Chem,* 279**,** 51338-42.

LIU, D., SAFARI, A., O'CONNOR, M. S., CHAN, D. W., LAEGELER, A., QIN, J. & SONGYANG, Z. 2004b. PTOP interacts with POT1 and regulates its localization to telomeres. *Nat Cell Biol,* 6**,** 673-80.

LIU, F. & MILLAR, S. E. 2010. Wnt/beta-catenin signaling in oral tissue development and disease. *J Dent Res,* 89**,** 318-30.

LIU, Q. & RUDERMAN, J. V. 2006. Aurora A, mitotic entry, and spindle bipolarity. *Proc Natl Acad Sci U S A,* 103**,** 5811-6.

LO, W. S., TRIEVEL, R. C., ROJAS, J. R., DUGGAN, L., HSU, J. Y., ALLIS, C. D., MARMORSTEIN, R. & BERGER, S. L. 2000. Phosphorylation of serine 10 in histone H3 is functionally linked in vitro and in vivo to Gcn5-mediated acetylation at lysine 14. *Mol Cell,* 5**,** 917-26.

LOENARZ, C., GE, W., COLEMAN, M. L., ROSE, N. R., COOPER, C. D., KLOSE, R. J., RATCLIFFE, P. J. & SCHOFIELD, C. J. 2010. PHF8, a gene associated with cleft lip/palate and mental retardation, encodes for an Nepsilon-dimethyl lysine demethylase. *Hum Mol Genet,* 19**,** 217-22.

LOGSDON, G. A., BARREY, E. J., BASSETT, E. A., DENIZIO, J. E., GUO, L. Y., PANCHENKO, T., DAWICKI-MCKENNA, J. M., HEUN, P. & BLACK, B. E. 2015. Both tails and the centromere targeting domain of CENP-A are required for centromere establishment. *J Cell Biol,* 208**,** 521-31.

LOH, Y. H., WU, Q., CHEW, J. L., VEGA, V. B., ZHANG, W., CHEN, X., BOURQUE, G., GEORGE, J., LEONG, B., LIU, J., WONG, K. Y., SUNG, K. W., LEE, C. W., ZHAO, X. D., CHIU, K. P., LIPOVICH, L., KUZNETSOV, V. A., ROBSON, P., STANTON, L. W., WEI, C. L., RUAN, Y., LIM, B. & NG, H. H. 2006. The Oct4 and Nanog transcription network regulates pluripotency in mouse embryonic stem cells. *Nat Genet,* 38**,** 431-40.

LORKOVIC, Z. J., PARK, C., GOISER, M., JIANG, D., KURZBAUER, M. T., SCHLOGELHOFER, P. & BERGER, F. 2017. Compartmentalization of DNA Damage Response between Heterochromatin and Euchromatin Is Mediated by Distinct H2A Histone Variants. *Curr Biol,* 27**,** 1192-1199.

LOVEJOY, C. A., LI, W., REISENWEBER, S., THONGTHIP, S., BRUNO, J., DE LANGE, T., DE, S., PETRINI, J. H., SUNG, P. A., JASIN, M., ROSENBLUH, J., ZWANG, Y., WEIR, B. A., HATTON, C., IVANOVA, E., MACCONAILL, L., HANNA, M., HAHN, W. C., LUE, N. F., REDDEL, R. R., JIAO, Y., KINZLER, K., VOGELSTEIN, B., PAPADOPOULOS, N., MEEKER, A. K. & CONSORTIUM, A. L. T. S. C. 2012. Loss of ATRX, genome instability, and an altered DNA damage response are hallmarks of the alternative lengthening of telomeres pathway. *PLoS Genet,* 8**,** e1002772.

LOWE, B. R., MAXHAM, L. A., HAMEY, J. J., WILKINS, M. R. & PARTRIDGE, J. F. 2019. Histone H3 Mutations: An Updated View of Their Role in Chromatin Deregulation and Cancer. *Cancers (Basel),* 11.

LOYOLA, A., TAGAMI, H., BONALDI, T., ROCHE, D., QUIVY, J. P., IMHOF, A., NAKATANI, Y., DENT, S. Y. & ALMOUZNI, G. 2009. The HP1alpha-CAF1-SetDB1-containing complex provides H3K9me1 for Suv39-mediated K9me3 in pericentric heterochromatin. *EMBO Rep,* 10**,** 769-75.

LU, C., JAIN, S. U., HOELPER, D., BECHET, D., MOLDEN, R. C., RAN, L., MURPHY, D., VENNETI, S., HAMEED, M., PAWEL, B. R., WUNDER, J. S., DICKSON, B. C., LUNDGREN, S. M., JANI, K. S., DE JAY, N., PAPILLON-CAVANAGH, S., ANDRULIS, I. L., SAWYER, S. L., GRYNSPAN, D., TURCOTTE, R. E., NADAF, J., FAHIMINIYAH, S., MUIR, T. W., MAJEWSKI, J., THOMPSON, C. B., CHI, P., GARCIA, B. A., ALLIS, C. D., JABADO, N. & LEWIS, P. W. 2016. Histone H3K36 mutations promote sarcomagenesis through altered histone methylation landscape. *Science,* 352**,** 844-9.

LU, R., YANG, A. & JIN, Y. 2011. Dual functions of T-box 3 (Tbx3) in the control of self-renewal and extraembryonic endoderm differentiation in mouse embryonic stem cells. *J Biol Chem,* 286**,** 8425-36.

LUCIO-ETEROVIC, A. K., SINGH, M. M., GARDNER, J. E., VEERAPPAN, C. S., RICE, J. C. & CARPENTER, P. B. 2010. Role for the nuclear receptor-binding SET domain protein 1

(NSD1) methyltransferase in coordinating lysine 36 methylation at histone 3 with RNA polymerase II function. *Proc Natl Acad Sci U S A,* 107**,** 16952-7.
LUGER, K., MADER, A. W., RICHMOND, R. K., SARGENT, D. F. & RICHMOND, T. J. 1997. Crystal structure of the nucleosome core particle at 2.8 A resolution. *Nature,* 389**,** 251-60.
LUK, E., VU, N. D., PATTESON, K., MIZUGUCHI, G., WU, W. H., RANJAN, A., BACKUS, J., SEN, S., LEWIS, M., BAI, Y. & WU, C. 2007. Chz1, a nuclear chaperone for histone H2AZ. *Mol Cell,* 25**,** 357-68.
LUKE-GLASER, S., POSCHKE, H. & LUKE, B. 2012. Getting in (and out of) the loop: regulating higher order telomere structures. *Front Oncol,* 2**,** 180.
MAEHARA, K., HARADA, A., SATO, Y., MATSUMOTO, M., NAKAYAMA, K. I., KIMURA, H. & OHKAWA, Y. 2015. Tissue-specific expression of histone H3 variants diversified after species separation. *Epigenetics Chromatin,* 8**,** 35.
MALLM, J. P. & RIPPE, K. 2015. Aurora Kinase B Regulates Telomerase Activity via a Centromeric RNA in Stem Cells. *Cell Rep,* 11**,** 1667-78.
MARTENS, U. M., CHAVEZ, E. A., POON, S. S., SCHMOOR, C. & LANSDORP, P. M. 2000. Accumulation of short telomeres in human fibroblasts prior to replicative senescence. *Exp Cell Res,* 256**,** 291-9.
MARTIN, C. & ZHANG, Y. 2005. The diverse functions of histone lysine methylation. *Nat Rev Mol Cell Biol,* 6**,** 838-49.
MARTINEZ, P., THANASOULA, M., MUNOZ, P., LIAO, C., TEJERA, A., MCNEES, C., FLORES, J. M., FERNANDEZ-CAPETILLO, O., TARSOUNAS, M. & BLASCO, M. A. 2009. Increased telomere fragility and fusions resulting from TRF1 deficiency lead to degenerative pathologies and increased cancer in mice. *Genes Dev,* 23**,** 2060-75.
MARTIRE, S., GOGATE, A. A., WHITMILL, A., TAFESSU, A., NGUYEN, J., TENG, Y. C., TASTEMEL, M. & BANASZYNSKI, L. A. 2019. Phosphorylation of histone H3.3 at serine 31 promotes p300 activity and enhancer acetylation. *Nat Genet,* 51**,** 941-946.
MARUMOTO, T., HONDA, S., HARA, T., NITTA, M., HIROTA, T., KOHMURA, E. & SAYA, H. 2003. Aurora-A kinase maintains the fidelity of early and late mitotic events in HeLa cells. *J Biol Chem,* 278**,** 51786-95.
MARZLUFF, W. F., GONGIDI, P., WOODS, K. R., JIN, J. & MALTAIS, L. J. 2002. The human and mouse replication-dependent histone genes. *Genomics,* 80**,** 487-98.
MATTERN, K. A., SWIGGERS, S. J., NIGG, A. L., LOWENBERG, B., HOUTSMULLER, A. B. & ZIJLMANS, J. M. 2004. Dynamics of protein binding to telomeres in living cells: implications for telomere structure and function. *Mol Cell Biol,* 24**,** 5587-94.
MCDOWELL, T. L., GIBBONS, R. J., SUTHERLAND, H., O'ROURKE, D. M., BICKMORE, W. A., POMBO, A., TURLEY, H., GATTER, K., PICKETTS, D. J., BUCKLE, V. J., CHAPMAN, L., RHODES, D. & HIGGS, D. R. 1999. Localization of a putative transcriptional regulator (ATRX) at pericentromeric heterochromatin and the short arms of acrocentric chromosomes. *Proc Natl Acad Sci U S A,* 96**,** 13983-8.
MCKERLIE, M., LIN, S. & ZHU, X. D. 2012. ATM regulates proteasome-dependent subnuclear localization of TRF1, which is important for telomere maintenance. *Nucleic Acids Res,* 40**,** 3975-89.
MCKERLIE, M. & ZHU, X. D. 2011. Cyclin B-dependent kinase 1 regulates human TRF1 to modulate the resolution of sister telomeres. *Nat Commun,* 2**,** 371.
MCMANUS, K. J. & HENDZEL, M. J. 2006. The relationship between histone H3 phosphorylation and acetylation throughout the mammalian cell cycle. *Biochem Cell Biol,* 84**,** 640-57.
MECHANIC, S., RAYNOR, K., HILL, J. E. & COWIN, P. 1991. Desmocollins form a distinct subset of the cadherin family of cell adhesion molecules. *Proc Natl Acad Sci U S A,* 88**,** 4476-80.
MESHORER, E. & MISTELI, T. 2006. Chromatin in pluripotent embryonic stem cells and differentiation. *Nat Rev Mol Cell Biol,* 7**,** 540-6.
METZGER, E., IMHOF, A., PATEL, D., KAHL, P., HOFFMEYER, K., FRIEDRICHS, N., MULLER, J. M., GRESCHIK, H., KIRFEL, J., JI, S., KUNOWSKA, N., BEISENHERZ-HUSS, C.,

GUNTHER, T., BUETTNER, R. & SCHULE, R. 2010. Phosphorylation of histone H3T6 by PKCbeta(I) controls demethylation at histone H3K4. *Nature,* 464**,** 792-6.
METZGER, E., YIN, N., WISSMANN, M., KUNOWSKA, N., FISCHER, K., FRIEDRICHS, N., PATNAIK, D., HIGGINS, J. M., POTIER, N., SCHEIDTMANN, K. H., BUETTNER, R. & SCHULE, R. 2008. Phosphorylation of histone H3 at threonine 11 establishes a novel chromatin mark for transcriptional regulation. *Nat Cell Biol,* 10**,** 53-60.
MICHAELSON, J. S., BADER, D., KUO, F., KOZAK, C. & LEDER, P. 1999. Loss of Daxx, a promiscuously interacting protein, results in extensive apoptosis in early mouse development. *Genes Dev,* 13**,** 1918-23.
MICHISHITA, E., MCCORD, R. A., BERBER, E., KIOI, M., PADILLA-NASH, H., DAMIAN, M., CHEUNG, P., KUSUMOTO, R., KAWAHARA, T. L., BARRETT, J. C., CHANG, H. Y., BOHR, V. A., RIED, T., GOZANI, O. & CHUA, K. F. 2008. SIRT6 is a histone H3 lysine 9 deacetylase that modulates telomeric chromatin. *Nature,* 452**,** 492-6.
MIKKELSEN, T. S., KU, M., JAFFE, D. B., ISSAC, B., LIEBERMAN, E., GIANNOUKOS, G., ALVAREZ, P., BROCKMAN, W., KIM, T. K., KOCHE, R. P., LEE, W., MENDENHALL, E., O'DONOVAN, A., PRESSER, A., RUSS, C., XIE, X., MEISSNER, A., WERNIG, M., JAENISCH, R., NUSBAUM, C., LANDER, E. S. & BERNSTEIN, B. E. 2007. Genome-wide maps of chromatin state in pluripotent and lineage-committed cells. *Nature,* 448**,** 553-60.
MUNOZ-JORDAN, J. L., CROSS, G. A., DE LANGE, T. & GRIFFITH, J. D. 2001. t-loops at trypanosome telomeres. *EMBO J,* 20**,** 579-88.
MUNOZ, P., BLANCO, R., DE CARCER, G., SCHOEFTNER, S., BENETTI, R., FLORES, J. M., MALUMBRES, M. & BLASCO, M. A. 2009. TRF1 controls telomere length and mitotic fidelity in epithelial homeostasis. *Mol Cell Biol,* 29**,** 1608-25.
MURTI, K. G. & PRESCOTT, D. M. 1999. Telomeres of polytene chromosomes in a ciliated protozoan terminate in duplex DNA loops. *Proc Natl Acad Sci U S A,* 96**,** 14436-9.
MUSSELMAN, C. A., KHORASANIZADEH, S. & KUTATELADZE, T. G. 2014. Towards understanding methyllysine readout. *Biochim Biophys Acta,* 1839**,** 686-93.
MUTHURAJAN, U. M., MCBRYANT, S. J., LU, X., HANSEN, J. C. & LUGER, K. 2011. The linker region of macroH2A promotes self-association of nucleosomal arrays. *J Biol Chem,* 286**,** 23852-64.
MYERS, F. A., EVANS, D. R., CLAYTON, A. L., THORNE, A. W. & CRANE-ROBINSON, C. 2001. Targeted and extended acetylation of histones H4 and H3 at active and inactive genes in chicken embryo erythrocytes. *J Biol Chem,* 276**,** 20197-205.
NAKAYAMA, J., RICE, J. C., STRAHL, B. D., ALLIS, C. D. & GREWAL, S. I. 2001. Role of histone H3 lysine 9 methylation in epigenetic control of heterochromatin assembly. *Science,* 292**,** 110-3.
NI, K., REN, J., XU, X., HE, Y., FINNEY, R., BRAUN, S. M. G., HATHAWAY, N. A., CRABTREE, G. R. & MUEGGE, K. 2020. LSH mediates gene repression through macroH2A deposition. *Nat Commun,* 11**,** 5647.
NIMURA, K., URA, K., SHIRATORI, H., IKAWA, M., OKABE, M., SCHWARTZ, R. J. & KANEDA, Y. 2009. A histone H3 lysine 36 trimethyltransferase links Nkx2-5 to Wolf-Hirschhorn syndrome. *Nature,* 460**,** 287-91.
OBRI, A., OUARARHNI, K., PAPIN, C., DIEBOLD, M. L., PADMANABHAN, K., MAREK, M., STOLL, I., ROY, L., REILLY, P. T., MAK, T. W., DIMITROV, S., ROMIER, C. & HAMICHE, A. 2014. ANP32E is a histone chaperone that removes H2A.Z from chromatin. *Nature,* 505**,** 648-53.
OGANESIAN, L. & KARLSEDER, J. 2011. Mammalian 5' C-rich telomeric overhangs are a mark of recombination-dependent telomere maintenance. *Mol Cell,* 42**,** 224-36.
OHISHI, T., HIROTA, T., TSURUO, T. & SEIMIYA, H. 2010. TRF1 mediates mitotic abnormalities induced by Aurora-A overexpression. *Cancer Res,* 70**,** 2041-52.
OHKI, R. & ISHIKAWA, F. 2004. Telomere-bound TRF1 and TRF2 stall the replication fork at telomeric repeats. *Nucleic Acids Res,* 32**,** 1627-37.
OHM, J. E., MCGARVEY, K. M., YU, X., CHENG, L., SCHUEBEL, K. E., COPE, L., MOHAMMAD, H. P., CHEN, W., DANIEL, V. C., YU, W., BERMAN, D. M., JENUWEIN, T., PRUITT, K.,

SHARKIS, S. J., WATKINS, D. N., HERMAN, J. G. & BAYLIN, S. B. 2007. A stem cell-like chromatin pattern may predispose tumor suppressor genes to DNA hypermethylation and heritable silencing. *Nat Genet,* 39**,** 237-42.

OPRESKO, P. L., VON KOBBE, C., LAINE, J. P., HARRIGAN, J., HICKSON, I. D. & BOHR, V. A. 2002. Telomere-binding protein TRF2 binds to and stimulates the Werner and Bloom syndrome helicases. *J Biol Chem,* 277**,** 41110-9.

OSLEY, M. A. 1991. The regulation of histone synthesis in the cell cycle. *Annu Rev Biochem,* 60**,** 827-61.

PALM, W. & DE LANGE, T. 2008. How shelterin protects mammalian telomeres. *Annu Rev Genet,* 42**,** 301-34.

PAN, D., WALSTEIN, K., TAKE, A., BIER, D., KAISER, N. & MUSACCHIO, A. 2019. Mechanism of centromere recruitment of the CENP-A chaperone HJURP and its implications for centromere licensing. *Nat Commun,* 10**,** 4046.

PAPAMICHOS-CHRONAKIS, M., WATANABE, S., RANDO, O. J. & PETERSON, C. L. 2011. Global regulation of H2A.Z localization by the INO80 chromatin-remodeling enzyme is essential for genome integrity. *Cell,* 144**,** 200-13.

PASINI, D., MALATESTA, M., JUNG, H. R., WALFRIDSSON, J., WILLER, A., OLSSON, L., SKOTTE, J., WUTZ, A., PORSE, B., JENSEN, O. N. & HELIN, K. 2010. Characterization of an antagonistic switch between histone H3 lysine 27 methylation and acetylation in the transcriptional regulation of Polycomb group target genes. *Nucleic Acids Res,* 38**,** 4958-69.

PETERS, A. H., KUBICEK, S., MECHTLER, K., O'SULLIVAN, R. J., DERIJCK, A. A., PEREZ-BURGOS, L., KOHLMAIER, A., OPRAVIL, S., TACHIBANA, M., SHINKAI, Y., MARTENS, J. H. & JENUWEIN, T. 2003. Partitioning and plasticity of repressive histone methylation states in mammalian chromatin. *Mol Cell,* 12**,** 1577-89.

PFISTER, S. X., AHRABI, S., ZALMAS, L. P., SARKAR, S., AYMARD, F., BACHRATI, C. Z., HELLEDAY, T., LEGUBE, G., LA THANGUE, N. B., PORTER, A. C. & HUMPHREY, T. C. 2014. SETD2-dependent histone H3K36 trimethylation is required for homologous recombination repair and genome stability. *Cell Rep,* 7**,** 2006-18.

PICKETT, H. A., CESARE, A. J., JOHNSTON, R. L., NEUMANN, A. A. & REDDEL, R. R. 2009. Control of telomere length by a trimming mechanism that involves generation of t-circles. *EMBO J,* 28**,** 799-809.

PIQUET, S., LE PARC, F., BAI, S. K., CHEVALLIER, O., ADAM, S. & POLO, S. E. 2018. The Histone Chaperone FACT Coordinates H2A.X-Dependent Signaling and Repair of DNA Damage. *Mol Cell,* 72**,** 888-901 e7.

PLIATSKA, M., KAPASA, M., KOKKALIS, A., POLYZOS, A. & THANOS, D. 2018. The Histone Variant MacroH2A Blocks Cellular Reprogramming by Inhibiting Mesenchymal-to-Epithelial Transition. *Mol Cell Biol,* 38.

PODHORECKA, M., SKLADANOWSKI, A. & BOZKO, P. 2010. H2AX Phosphorylation: Its Role in DNA Damage Response and Cancer Therapy. *J Nucleic Acids,* 2010.

POKHOLOK, D. K., HARBISON, C. T., LEVINE, S., COLE, M., HANNETT, N. M., LEE, T. I., BELL, G. W., WALKER, K., ROLFE, P. A., HERBOLSHEIMER, E., ZEITLINGER, J., LEWITTER, F., GIFFORD, D. K. & YOUNG, R. A. 2005. Genome-wide map of nucleosome acetylation and methylation in yeast. *Cell,* 122**,** 517-27.

POSTBERG, J., FORCOB, S., CHANG, W. J. & LIPPS, H. J. 2010. The evolutionary history of histone H3 suggests a deep eukaryotic root of chromatin modifying mechanisms. *BMC Evol Biol,* 10**,** 259.

RAHMAN, S., SOWA, M. E., OTTINGER, M., SMITH, J. A., SHI, Y., HARPER, J. W. & HOWLEY, P. M. 2011. The Brd4 extraterminal domain confers transcription activation independent of pTEFb by recruiting multiple proteins, including NSD3. *Mol Cell Biol,* 31**,** 2641-52.

RAISNER, R., KHARBANDA, S., JIN, L., JENG, E., CHAN, E., MERCHANT, M., HAVERTY, P. M., BAINER, R., CHEUNG, T., ARNOTT, D., FLYNN, E. M., ROMERO, F. A., MAGNUSON, S. & GASCOIGNE, K. E. 2018. Enhancer Activity Requires CBP/P300 Bromodomain-Dependent Histone H3K27 Acetylation. *Cell Rep,* 24**,** 1722-1729.

RAMAMOORTHY, M. & SMITH, S. 2015. Loss of ATRX Suppresses Resolution of Telomere Cohesion to Control Recombination in ALT Cancer Cells. *Cancer Cell,* 28**,** 357-69.
RANGASAMY, D., GREAVES, I. & TREMETHICK, D. J. 2004. RNA interference demonstrates a novel role for H2A.Z in chromosome segregation. *Nat Struct Mol Biol,* 11**,** 650-5.
REA, S., EISENHABER, F., O'CARROLL, D., STRAHL, B. D., SUN, Z. W., SCHMID, M., OPRAVIL, S., MECHTLER, K., PONTING, C. P., ALLIS, C. D. & JENUWEIN, T. 2000. Regulation of chromatin structure by site-specific histone H3 methyltransferases. *Nature,* 406**,** 593-9.
RICE, J. C., BRIGGS, S. D., UEBERHEIDE, B., BARBER, C. M., SHABANOWITZ, J., HUNT, D. F., SHINKAI, Y. & ALLIS, C. D. 2003. Histone methyltransferases direct different degrees of methylation to define distinct chromatin domains. *Mol Cell,* 12**,** 1591-8.
RIDGWAY, P., BROWN, K. D., RANGASAMY, D., SVENSSON, U. & TREMETHICK, D. J. 2004a. Unique residues on the H2A.Z containing nucleosome surface are important for Xenopus laevis development. *J Biol Chem,* 279**,** 43815-20.
RIDGWAY, P., RANGASAMY, D., BERVEN, L., SVENSSON, U. & TREMETHICK, D. J. 2004b. Analysis of histone variant H2A.Z localization and expression during early development. *Methods Enzymol,* 375**,** 239-52.
RIOS-DORIA, J., VELKOVA, A., DAPIC, V., GALAN-CARIDAD, J. M., DAPIC, V., CARVALHO, M. A., MELENDEZ, J. & MONTEIRO, A. N. 2009. Ectopic expression of histone H2AX mutants reveals a role for its post-translational modifications. *Cancer Biol Ther,* 8**,** 422-34.
ROCK, K. L., GRAMM, C., ROTHSTEIN, L., CLARK, K., STEIN, R., DICK, L., HWANG, D. & GOLDBERG, A. L. 1994. Inhibitors of the proteasome block the degradation of most cell proteins and the generation of peptides presented on MHC class I molecules. *Cell,* 78**,** 761-71.
ROTHBART, S. B. & STRAHL, B. D. 2014. Interpreting the language of histone and DNA modifications. *Biochim Biophys Acta,* 1839**,** 627-43.
RUCHAUD, S., CARMENA, M. & EARNSHAW, W. C. 2007. Chromosomal passengers: conducting cell division. *Nat Rev Mol Cell Biol,* 8**,** 798-812.
SADIC, D., SCHMIDT, K., GROH, S., KONDOFERSKY, I., ELLWART, J., FUCHS, C., THEIS, F. J. & SCHOTTA, G. 2015. Atrx promotes heterochromatin formation at retrotransposons. *EMBO Rep,* 16**,** 836-50.
SAKAI, A., SCHWARTZ, B. E., GOLDSTEIN, S. & AHMAD, K. 2009. Transcriptional and developmental functions of the H3.3 histone variant in Drosophila. *Curr Biol,* 19**,** 1816-20.
SAKSOUK, N., SIMBOECK, E. & DEJARDIN, J. 2015. Constitutive heterochromatin formation and transcription in mammals. *Epigenetics Chromatin,* 8**,** 3.
SALOMONI, P. & KHELIFI, A. F. 2006. Daxx: death or survival protein? *Trends Cell Biol,* 16**,** 97-104.
SANCHEZ-MOLINA, S., MORTUSEWICZ, O., BIEBER, B., AUER, S., ECKEY, M., LEONHARDT, H., FRIEDL, A. A. & BECKER, P. B. 2011. Role for hACF1 in the G2/M damage checkpoint. *Nucleic Acids Res,* 39**,** 8445-56.
SANSONI, V., CASAS-DELUCCHI, C. S., RAJAN, M., SCHMIDT, A., BONISCH, C., THOMAE, A. W., STAEGE, M. S., HAKE, S. B., CARDOSO, M. C. & IMHOF, A. 2014. The histone variant H2A.Bbd is enriched at sites of DNA synthesis. *Nucleic Acids Res,* 42**,** 6405-20.
SARTHY, J. F., MEERS, M. P., JANSSENS, D. H., HENIKOFF, J. G., FELDMAN, H., PADDISON, P. J., LOCKWOOD, C. M., VITANZA, N. A., OLSON, J. M., AHMAD, K. & HENIKOFF, S. 2020. Histone deposition pathways determine the chromatin landscapes of H3.1 and H3.3 K27M oncohistones. *Elife,* 9.
SAWICKA, A. & SEISER, C. 2012. Histone H3 phosphorylation - a versatile chromatin modification for different occasions. *Biochimie,* 94**,** 2193-201.
SCHEPERS, G. E., TEASDALE, R. D. & KOOPMAN, P. 2002. Twenty pairs of sox: extent, homology, and nomenclature of the mouse and human sox transcription factor gene families. *Dev Cell,* 3**,** 167-70.
SCHMITGES, F. W., PRUSTY, A. B., FATY, M., STUTZER, A., LINGARAJU, G. M., AIWAZIAN, J., SACK, R., HESS, D., LI, L., ZHOU, S., BUNKER, R. D., WIRTH, U., BOUWMEESTER, T.,

BAUER, A., LY-HARTIG, N., ZHAO, K., CHAN, H., GU, J., GUT, H., FISCHLE, W., MULLER, J. & THOMA, N. H. 2011. Histone methylation by PRC2 is inhibited by active chromatin marks. *Mol Cell,* 42**,** 330-41.

SCHNEIDER, R. P., GARROBO, I., FORONDA, M., PALACIOS, J. A., MARION, R. M., FLORES, I., ORTEGA, S. & BLASCO, M. A. 2013. TRF1 is a stem cell marker and is essential for the generation of induced pluripotent stem cells. *Nat Commun,* 4**,** 1946.

SCHOEFTNER, S. & BLASCO, M. A. 2009. A 'higher order' of telomere regulation: telomere heterochromatin and telomeric RNAs. *EMBO J,* 28**,** 2323-36.

SCHOTTA, G., LACHNER, M., SARMA, K., EBERT, A., SENGUPTA, R., REUTER, G., REINBERG, D. & JENUWEIN, T. 2004. A silencing pathway to induce H3-K9 and H4-K20 trimethylation at constitutive heterochromatin. *Genes Dev,* 18**,** 1251-62.

SCHOTTA, G., SENGUPTA, R., KUBICEK, S., MALIN, S., KAUER, M., CALLEN, E., CELESTE, A., PAGANI, M., OPRAVIL, S., DE LA ROSA-VELAZQUEZ, I. A., ESPEJO, A., BEDFORD, M. T., NUSSENZWEIG, A., BUSSLINGER, M. & JENUWEIN, T. 2008. A chromatin-wide transition to H4K20 monomethylation impairs genome integrity and programmed DNA rearrangements in the mouse. *Genes Dev,* 22**,** 2048-61.

SCHULMEISTER, A., SCHMID, M. & THOMPSON, E. M. 2007. Phosphorylation of the histone H3.3 variant in mitosis and meiosis of the urochordate Oikopleura dioica. *Chromosome Res,* 15**,** 189-201.

SCHWARTZENTRUBER, J., KORSHUNOV, A., LIU, X. Y., JONES, D. T., PFAFF, E., JACOB, K., STURM, D., FONTEBASSO, A. M., QUANG, D. A., TONJES, M., HOVESTADT, V., ALBRECHT, S., KOOL, M., NANTEL, A., KONERMANN, C., LINDROTH, A., JAGER, N., RAUSCH, T., RYZHOVA, M., KORBEL, J. O., HIELSCHER, T., HAUSER, P., GARAMI, M., KLEKNER, A., BOGNAR, L., EBINGER, M., SCHUHMANN, M. U., SCHEURLEN, W., PEKRUN, A., FRUHWALD, M. C., ROGGENDORF, W., KRAMM, C., DURKEN, M., ATKINSON, J., LEPAGE, P., MONTPETIT, A., ZAKRZEWSKA, M., ZAKRZEWSKI, K., LIBERSKI, P. P., DONG, Z., SIEGEL, P., KULOZIK, A. E., ZAPATKA, M., GUHA, A., MALKIN, D., FELSBERG, J., REIFENBERGER, G., VON DEIMLING, A., ICHIMURA, K., COLLINS, V. P., WITT, H., MILDE, T., WITT, O., ZHANG, C., CASTELO-BRANCO, P., LICHTER, P., FAURY, D., TABORI, U., PLASS, C., MAJEWSKI, J., PFISTER, S. M. & JABADO, N. 2012. Driver mutations in histone H3.3 and chromatin remodelling genes in paediatric glioblastoma. *Nature,* 482**,** 226-31.

SCRITTORI, L., SKOUFIAS, D. A., HANS, F., GERSON, V., SASSONE-CORSI, P., DIMITROV, S. & MARGOLIS, R. L. 2005. A small C-terminal sequence of Aurora B is responsible for localization and function. *Mol Biol Cell,* 16**,** 292-305.

SEELING, J. M., FARMER, A. A., MANSFIELD, A., CHO, H. & CHOUDHARY, M. 2017. Differential Selective Pressures Experienced by the Aurora Kinase Gene Family. *Int J Mol Sci,* 19.

SEMER, M., BIDON, B., LARNICOL, A., CALISKAN, G., CATEZ, P., EGLY, J. M., COIN, F. & LE MAY, N. 2019. DNA repair complex licenses acetylation of H2A.Z.1 by KAT2A during transcription. *Nat Chem Biol,* 15**,** 992-1000.

SEO, J., KIM, S. C., LEE, H. S., KIM, J. K., SHON, H. J., SALLEH, N. L., DESAI, K. V., LEE, J. H., KANG, E. S., KIM, J. S. & CHOI, J. K. 2012. Genome-wide profiles of H2AX and gamma-H2AX differentiate endogenous and exogenous DNA damage hotspots in human cells. *Nucleic Acids Res,* 40**,** 5965-74.

SFEIR, A. & DE LANGE, T. 2012. Removal of shelterin reveals the telomere end-protection problem. *Science,* 336**,** 593-7.

SFEIR, A., KABIR, S., VAN OVERBEEK, M., CELLI, G. B. & DE LANGE, T. 2010. Loss of Rap1 induces telomere recombination in the absence of NHEJ or a DNA damage signal. *Science,* 327**,** 1657-61.

SFEIR, A., KOSIYATRAKUL, S. T., HOCKEMEYER, D., MACRAE, S. L., KARLSEDER, J., SCHILDKRAUT, C. L. & DE LANGE, T. 2009. Mammalian telomeres resemble fragile sites and require TRF1 for efficient replication. *Cell,* 138**,** 90-103.

SHASTRULA, P. K., SIERRA, I., DENG, Z., KEENEY, F., HAYDEN, J. E., LIEBERMAN, P. M. & JANICKI, S. M. 2019. PML is recruited to heterochromatin during S phase and represses DAXX-mediated histone H3.3 chromatin assembly. *J Cell Sci,* 132.

SHEN, M., HAGGBLOM, C., VOGT, M., HUNTER, T. & LU, K. P. 1997. Characterization and cell cycle regulation of the related human telomeric proteins Pin2 and TRF1 suggest a role in mitosis. *Proc Natl Acad Sci U S A,* 94**,** 13618-23.

SHI, Y., LAN, F., MATSON, C., MULLIGAN, P., WHETSTINE, J. R., COLE, P. A., CASERO, R. A. & SHI, Y. 2004. Histone demethylation mediated by the nuclear amine oxidase homolog LSD1. *Cell,* 119**,** 941-53.

SHIMADA, M., NIIDA, H., ZINELDEEN, D. H., TAGAMI, H., TANAKA, M., SAITO, H. & NAKANISHI, M. 2008. Chk1 is a histone H3 threonine 11 kinase that regulates DNA damage-induced transcriptional repression. *Cell,* 132**,** 221-32.

SHOWELL, C., BINDER, O. & CONLON, F. L. 2004. T-box genes in early embryogenesis. *Dev Dyn,* 229**,** 201-18.

SILVEIRA, A. B., KASPER, L. H., FAN, Y., JIN, H., WU, G., SHAW, T. I., ZHU, X., LARSON, J. D., EASTON, J., SHAO, Y., YERGEAU, D. A., ROSENCRANCE, C., BOGGS, K., RUSCH, M. C., DING, L., ZHANG, J., FINKELSTEIN, D., NOYES, R. M., RUSSELL, B. L., XU, B., BRONISCER, A., WETMORE, C., POUNDS, S. B., ELLISON, D. W., ZHANG, J. & BAKER, S. J. 2019. H3.3 K27M depletion increases differentiation and extends latency of diffuse intrinsic pontine glioma growth in vivo. *Acta Neuropathol,* 137**,** 637-655.

SIMS, R. J., 3RD, NISHIOKA, K. & REINBERG, D. 2003. Histone lysine methylation: a signature for chromatin function. *Trends Genet,* 19**,** 629-39.

SITBON, D., BOYARCHUK, E., DINGLI, F., LOEW, D. & ALMOUZNI, G. 2020. Histone variant H3.3 residue S31 is essential for Xenopus gastrulation regardless of the deposition pathway. *Nat Commun,* 11**,** 1256.

SMOGORZEWSKA, A., VAN STEENSEL, B., BIANCHI, A., OELMANN, S., SCHAEFER, M. R., SCHNAPP, G. & DE LANGE, T. 2000. Control of human telomere length by TRF1 and TRF2. *Mol Cell Biol,* 20**,** 1659-68.

SPELIOTES, E. K., UREN, A., VAUX, D. & HORVITZ, H. R. 2000. The survivin-like C. elegans BIR-1 protein acts with the Aurora-like kinase AIR-2 to affect chromosomes and the spindle midzone. *Mol Cell,* 6**,** 211-23.

STANSEL, R. M., DE LANGE, T. & GRIFFITH, J. D. 2001. T-loop assembly in vitro involves binding of TRF2 near the 3' telomeric overhang. *EMBO J,* 20**,** 5532-40.

STRETTON, S., TECHKARNJANARUK, S., MCLENNAN, A. M. & GOODMAN, A. E. 1998. Use of green fluorescent protein to tag and investigate gene expression in marine bacteria. *Appl Environ Microbiol,* 64**,** 2554-9.

STRICKLAND, S. & MAHDAVI, V. 1978. The induction of differentiation in teratocarcinoma stem cells by retinoic acid. *Cell,* 15**,** 393-403.

STURM, D., WITT, H., HOVESTADT, V., KHUONG-QUANG, D. A., JONES, D. T., KONERMANN, C., PFAFF, E., TONJES, M., SILL, M., BENDER, S., KOOL, M., ZAPATKA, M., BECKER, N., ZUCKNICK, M., HIELSCHER, T., LIU, X. Y., FONTEBASSO, A. M., RYZHOVA, M., ALBRECHT, S., JACOB, K., WOLTER, M., EBINGER, M., SCHUHMANN, M. U., VAN METER, T., FRUHWALD, M. C., HAUCH, H., PEKRUN, A., RADLWIMMER, B., NIEHUES, T., VON KOMOROWSKI, G., DURKEN, M., KULOZIK, A. E., MADDEN, J., DONSON, A., FOREMAN, N. K., DRISSI, R., FOULADI, M., SCHEURLEN, W., VON DEIMLING, A., MONORANU, C., ROGGENDORF, W., HEROLD-MENDE, C., UNTERBERG, A., KRAMM, C. M., FELSBERG, J., HARTMANN, C., WIESTLER, B., WICK, W., MILDE, T., WITT, O., LINDROTH, A. M., SCHWARTZENTRUBER, J., FAURY, D., FLEMING, A., ZAKRZEWSKA, M., LIBERSKI, P. P., ZAKRZEWSKI, K., HAUSER, P., GARAMI, M., KLEKNER, A., BOGNAR, L., MORRISSY, S., CAVALLI, F., TAYLOR, M. D., VAN SLUIS, P., KOSTER, J., VERSTEEG, R., VOLCKMANN, R., MIKKELSEN, T., ALDAPE, K., REIFENBERGER, G., COLLINS, V. P., MAJEWSKI, J., KORSHUNOV, A., LICHTER, P., PLASS, C., JABADO, N.

& PFISTER, S. M. 2012. Hotspot mutations in H3F3A and IDH1 define distinct epigenetic and biological subgroups of glioblastoma. *Cancer Cell,* 22**,** 425-37.
SULLIVAN, K. F., HECHENBERGER, M. & MASRI, K. 1994. Human CENP-A contains a histone H3 related histone fold domain that is required for targeting to the centromere. *J Cell Biol,* 127**,** 581-92.
SUN, Z., ZHANG, Y., JIA, J., FANG, Y., TANG, Y., WU, H. & FANG, D. 2020. H3K36me3, message from chromatin to DNA damage repair. *Cell Biosci,* 10**,** 9.
SZENKER, E., LACOSTE, N. & ALMOUZNI, G. 2012. A developmental requirement for HIRA-dependent H3.3 deposition revealed at gastrulation in Xenopus. *Cell Rep,* 1**,** 730-40.
SZENKER, E., RAY-GALLET, D. & ALMOUZNI, G. 2011. The double face of the histone variant H3.3. *Cell Res,* 21**,** 421-34.
SZOSTAK, J. W. & BLACKBURN, E. H. 1982. Cloning yeast telomeres on linear plasmid vectors. *Cell,* 29**,** 245-55.
TACHIWANA, H., KAGAWA, W., OSAKABE, A., KAWAGUCHI, K., SHIGA, T., HAYASHI-TAKANAKA, Y., KIMURA, H. & KURUMIZAKA, H. 2010. Structural basis of instability of the nucleosome containing a testis-specific histone variant, human H3T. *Proc Natl Acad Sci U S A,* 107**,** 10454-9.
TAGAMI, H., RAY-GALLET, D., ALMOUZNI, G. & NAKATANI, Y. 2004. Histone H3.1 and H3.3 complexes mediate nucleosome assembly pathways dependent or independent of DNA synthesis. *Cell,* 116**,** 51-61.
TALBERT, P. B. & HENIKOFF, S. 2021. Histone variants at a glance. *J Cell Sci,* 134.
TANAKA, T. U., RACHIDI, N., JANKE, C., PEREIRA, G., GALOVA, M., SCHIEBEL, E., STARK, M. J. & NASMYTH, K. 2002. Evidence that the Ipl1-Sli15 (Aurora kinase-INCENP) complex promotes chromosome bi-orientation by altering kinetochore-spindle pole connections. *Cell,* 108**,** 317-29.
TANG, A., GAO, K., CHU, L., ZHANG, R., YANG, J. & ZHENG, J. 2017. Aurora kinases: novel therapy targets in cancers. *Oncotarget,* 8**,** 23937-23954.
TANG, J., WU, S., LIU, H., STRATT, R., BARAK, O. G., SHIEKHATTAR, R., PICKETTS, D. J. & YANG, X. 2004. A novel transcription regulatory complex containing death domain-associated protein and the ATR-X syndrome protein. *J Biol Chem,* 279**,** 20369-77.
TANG, M. C., JACOBS, S. A., MATTISKE, D. M., SOH, Y. M., GRAHAM, A. N., TRAN, A., LIM, S. L., HUDSON, D. F., KALITSIS, P., O'BRYAN, M. K., WONG, L. H. & MANN, J. R. 2015. Contribution of the two genes encoding histone variant h3.3 to viability and fertility in mice. *PLoS Genet,* 11**,** e1004964.
TANG, M. C., JACOBS, S. A., WONG, L. H. & MANN, J. R. 2013a. Conditional allelic replacement applied to genes encoding the histone variant H3.3 in the mouse. *Genesis,* 51**,** 142-6.
TANG, M. C., JACOBS, S. A., WONG, L. H. & MANN, J. R. 2013b. Conditional allelic replacement applied to genes encoding the histone variant H3. 3 in the mouse. *Genesis,* 51**,** 142-146.
TAVERNA, S. D., ILIN, S., ROGERS, R. S., TANNY, J. C., LAVENDER, H., LI, H., BAKER, L., BOYLE, J., BLAIR, L. P., CHAIT, B. T., PATEL, D. J., AITCHISON, J. D., TACKETT, A. J. & ALLIS, C. D. 2006. Yng1 PHD finger binding to H3 trimethylated at K4 promotes NuA3 HAT activity at K14 of H3 and transcription at a subset of targeted ORFs. *Mol Cell,* 24**,** 785-796.
THEODOROPOULOS, P. A., GRAVANIS, A., TSAPARA, A., MARGIORIS, A. N., PAPADOGIORGAKI, E., GALANOPOULOS, V. & STOURNARAS, C. 1994. Cytochalasin B may shorten actin filaments by a mechanism independent of barbed end capping. *Biochem Pharmacol,* 47**,** 1875-81.
TOLSTORUKOV, M. Y., GOLDMAN, J. A., GILBERT, C., OGRYZKO, V., KINGSTON, R. E. & PARK, P. J. 2012. Histone variant H2A.Bbd is associated with active transcription and mRNA processing in human cells. *Mol Cell,* 47**,** 596-607.
TROJER, P. & REINBERG, D. 2007. Facultative heterochromatin: is there a distinctive molecular signature? *Mol Cell,* 28**,** 1-13.
TSAI, Y. C., QI, H. & LIU, L. F. 2007. Protection of DNA ends by telomeric 3' G-tail sequences. *J Biol Chem,* 282**,** 18786-92.

TSUKADA, Y., FANG, J., ERDJUMENT-BROMAGE, H., WARREN, M. E., BORCHERS, C. H., TEMPST, P. & ZHANG, Y. 2006. Histone demethylation by a family of JmjC domain-containing proteins. *Nature,* 439**,** 811-6.

TURINETTO, V. & GIACHINO, C. 2015. Multiple facets of histone variant H2AX: a DNA double-strand-break marker with several biological functions. *Nucleic Acids Res,* 43**,** 2489-98.

UDUGAMA, M., FT, M. C., CHAN, F. L., TANG, M. C., PICKETT, H. A., JD, R. M., MAYNE, L., COLLAS, P., MANN, J. R. & WONG, L. H. 2015. Histone variant H3.3 provides the heterochromatic H3 lysine 9 tri-methylation mark at telomeres. *Nucleic Acids Res,* 43**,** 10227-37.

UDUGAMA, M., HII, L., GARVIE, A., CERVINI, M., VINOD, B., CHAN, F. L., DAS, P. P., MANN, J. R., COLLAS, P., VOON, H. P. J. & WONG, L. H. 2021. Mutations inhibiting KDM4B drive ALT activation in ATRX-mutated glioblastomas. *Nat Commun,* 12**,** 2584.

UEDA, J., HARADA, A., URAHAMA, T., MACHIDA, S., MAEHARA, K., HADA, M., MAKINO, Y., NOGAMI, J., HORIKOSHI, N., OSAKABE, A., TAGUCHI, H., TANAKA, H., TACHIWANA, H., YAO, T., YAMADA, M., IWAMOTO, T., ISOTANI, A., IKAWA, M., TACHIBANA, T., OKADA, Y., KIMURA, H., OHKAWA, Y., KURUMIZAKA, H. & YAMAGATA, K. 2017. Testis-Specific Histone Variant H3t Gene Is Essential for Entry into Spermatogenesis. *Cell Rep,* 18**,** 593-600.

UMENE, K., BANNO, K., KISU, I., YANOKURA, M., NOGAMI, Y., TSUJI, K., MASUDA, K., UEKI, A., KOBAYASHI, Y., YAMAGAMI, W., NOMURA, H., TOMINAGA, E., SUSUMU, N. & AOKI, D. 2013. Aurora kinase inhibitors: Potential molecular-targeted drugs for gynecologic malignant tumors. *Biomed Rep,* 1**,** 335-340.

VAN HOLDE, K. E., SAHASRABUDDHE, C. G. & SHAW, B. R. 1974. A model for particulate structure in chromatin. *Nucleic Acids Res,* 1**,** 1579-86.

VAN HOOSER, A. A., OUSPENSKI, II, GREGSON, H. C., STARR, D. A., YEN, T. J., GOLDBERG, M. L., YOKOMORI, K., EARNSHAW, W. C., SULLIVAN, K. F. & BRINKLEY, B. R. 2001. Specification of kinetochore-forming chromatin by the histone H3 variant CENP-A. *J Cell Sci,* 114**,** 3529-42.

VAN STEENSEL, B. & DE LANGE, T. 1997. Control of telomere length by the human telomeric protein TRF1. *Nature,* 385**,** 740-3.

VAN STEENSEL, B., SMOGORZEWSKA, A. & DE LANGE, T. 1998. TRF2 protects human telomeres from end-to-end fusions. *Cell,* 92**,** 401-13.

VARELA, E., SCHNEIDER, R. P., ORTEGA, S. & BLASCO, M. A. 2011. Different telomere-length dynamics at the inner cell mass versus established embryonic stem (ES) cells. *Proc Natl Acad Sci U S A,* 108**,** 15207-12.

VELDMAN, T., ETHERIDGE, K. T. & COUNTER, C. M. 2004. Loss of hPot1 function leads to telomere instability and a cut-like phenotype. *Curr Biol,* 14**,** 2264-70.

VENKATESH, S. & WORKMAN, J. L. 2015. Histone exchange, chromatin structure and the regulation of transcription. *Nat Rev Mol Cell Biol,* 16**,** 178-89.

VOON, H. P., HUGHES, J. R., RODE, C., DE LA ROSA-VELAZQUEZ, I. A., JENUWEIN, T., FEIL, R., HIGGS, D. R. & GIBBONS, R. J. 2015. ATRX Plays a Key Role in Maintaining Silencing at Interstitial Heterochromatic Loci and Imprinted Genes. *Cell Rep,* 11**,** 405-18.

VOON, H. P. & WONG, L. H. 2016. New players in heterochromatin silencing: histone variant H3.3 and the ATRX/DAXX chaperone. *Nucleic Acids Res,* 44**,** 1496-501.

VOON, H. P. J., UDUGAMA, M., LIN, W., HII, L., LAW, R. H. P., STEER, D. L., DAS, P. P., MANN, J. R. & WONG, L. H. 2018. Inhibition of a K9/K36 demethylase by an H3.3 point mutation found in paediatric glioblastoma. *Nat Commun,* 9**,** 3142.

WAGNER, E. J. & CARPENTER, P. B. 2012. Understanding the language of Lys36 methylation at histone H3. *Nat Rev Mol Cell Biol,* 13**,** 115-26.

WALKER, J. R. & ZHU, X. D. 2012. Post-translational modifications of TRF1 and TRF2 and their roles in telomere maintenance. *Mech Ageing Dev,* 133**,** 421-34.

WALKER, M. P., LAFERLA, F. M., ODDO, S. S. & BREWER, G. J. 2013. Reversible epigenetic histone modifications and Bdnf expression in neurons with aging and from a mouse model of Alzheimer's disease. *Age (Dordr),* 35**,** 519-31.
WANG, F., DAI, J., DAUM, J. R., NIEDZIALKOWSKA, E., BANERJEE, B., STUKENBERG, P. T., GORBSKY, G. J. & HIGGINS, J. M. 2010. Histone H3 Thr-3 phosphorylation by Haspin positions Aurora B at centromeres in mitosis. *Science,* 330**,** 231-5.
WANG, F., PAN, X., KALMBACH, K., SETH-SMITH, M. L., YE, X., ANTUMES, D. M., YIN, Y., LIU, L., KEEFE, D. L. & WEISSMAN, S. M. 2013. Robust measurement of telomere length in single cells. *Proc Natl Acad Sci U S A,* 110**,** E1906-12.
WANG, G. G. & ALLIS, C. D. 2009. "Misinterpretation" of a histone mark is linked to aberrant stem cells and cancer development. *Cell Cycle,* 8**,** 1982-3.
WANG, R. C., SMOGORZEWSKA, A. & DE LANGE, T. 2004. Homologous recombination generates T-loop-sized deletions at human telomeres. *Cell,* 119**,** 355-68.
WANG, T., XU, C., LIU, Y., FAN, K., LI, Z., SUN, X., OUYANG, H., ZHANG, X., ZHANG, J., LI, Y., MACKENZIE, F., MIN, J. & TU, X. 2012. Crystal structure of the human SUV39H1 chromodomain and its recognition of histone H3K9me2/3. *PLoS One,* 7**,** e52977.
WEBER, C. M. & HENIKOFF, S. 2014. Histone variants: dynamic punctuation in transcription. *Genes Dev,* 28**,** 672-82.
WEBER, C. M., RAMACHANDRAN, S. & HENIKOFF, S. 2014. Nucleosomes are context-specific, H2A.Z-modulated barriers to RNA polymerase. *Mol Cell,* 53**,** 819-30.
WEI, J., ANTONY, J., MENG, F., MACLEAN, P., RHIND, R., LAIBLE, G. & OBACK, B. 2017. KDM4B-mediated reduction of H3K9me3 and H3K36me3 levels improves somatic cell reprogramming into pluripotency. *Sci Rep,* 7**,** 7514.
WEI, Y., MIZZEN, C. A., COOK, R. G., GOROVSKY, M. A. & ALLIS, C. D. 1998. Phosphorylation of histone H3 at serine 10 is correlated with chromosome condensation during mitosis and meiosis in Tetrahymena. *Proc Natl Acad Sci U S A,* 95**,** 7480-4.
WEI, Y., YU, L., BOWEN, J., GOROVSKY, M. A. & ALLIS, C. D. 1999. Phosphorylation of histone H3 is required for proper chromosome condensation and segregation. *Cell,* 97**,** 99-109.
WELLS, D., HOFFMAN, D. & KEDES, L. 1987. Unusual structure, evolutionary conservation of non-coding sequences and numerous pseudogenes characterize the human H3.3 histone multigene family. *Nucleic Acids Res,* 15**,** 2871-89.
WEN, H., LI, Y., XI, Y., JIANG, S., STRATTON, S., PENG, D., TANAKA, K., REN, Y., XIA, Z., WU, J., LI, B., BARTON, M. C., LI, W., LI, H. & SHI, X. 2014. ZMYND11 links histone H3.3K36me3 to transcription elongation and tumour suppression. *Nature,* 508**,** 263-8.
WILLEMS, E., DEDOBBELEER, M., DIGREGORIO, M., LOMBARD, A., LUMAPAT, P. N. & ROGISTER, B. 2018. The functional diversity of Aurora kinases: a comprehensive review. *Cell Div,* 13**,** 7.
WONG, H. P. & SLIJEPCEVIC, P. 2004. Telomere length measurement in mouse chromosomes by a modified Q-FISH method. *Cytogenet Genome Res,* 105**,** 464-70.
WONG, L. H., MCGHIE, J. D., SIM, M., ANDERSON, M. A., AHN, S., HANNAN, R. D., GEORGE, A. J., MORGAN, K. A., MANN, J. R. & CHOO, K. H. 2010. ATRX interacts with H3.3 in maintaining telomere structural integrity in pluripotent embryonic stem cells. *Genome Res,* 20**,** 351-60.
WONG, L. H., REN, H., WILLIAMS, E., MCGHIE, J., AHN, S., SIM, M., TAM, A., EARLE, E., ANDERSON, M. A., MANN, J. & CHOO, K. H. 2009. Histone H3.3 incorporation provides a unique and functionally essential telomeric chromatin in embryonic stem cells. *Genome Res,* 19**,** 404-14.
WOZNIAK, R. J., KLIMECKI, W. T., LAU, S. S., FEINSTEIN, Y. & FUTSCHER, B. W. 2007. 5-Aza-2'-deoxycytidine-mediated reductions in G9A histone methyltransferase and histone H3 K9 di-methylation levels are linked to tumor suppressor gene reactivation. *Oncogene,* 26**,** 77-90.
WRIGHT, W. E., TESMER, V. M., HUFFMAN, K. E., LEVENE, S. D. & SHAY, J. W. 1997. Normal human chromosomes have long G-rich telomeric overhangs at one end. *Genes Dev,* 11**,** 2801-9.

WU, G., BRONISCER, A., MCEACHRON, T. A., LU, C., PAUGH, B. S., BECKSFORT, J., QU, C., DING, L., HUETHER, R., PARKER, M., ZHANG, J., GAJJAR, A., DYER, M. A., MULLIGHAN, C. G., GILBERTSON, R. J., MARDIS, E. R., WILSON, R. K., DOWNING, J. R., ELLISON, D. W., ZHANG, J., BAKER, S. J. & ST. JUDE CHILDREN'S RESEARCH HOSPITAL-WASHINGTON UNIVERSITY PEDIATRIC CANCER GENOME, P. 2012. Somatic histone H3 alterations in pediatric diffuse intrinsic pontine gliomas and non-brainstem glioblastomas. *Nat Genet,* 44**,** 251-3.

WU, Y., XIAO, S. & ZHU, X. D. 2007. MRE11-RAD50-NBS1 and ATM function as co-mediators of TRF1 in telomere length control. *Nat Struct Mol Biol,* 14**,** 832-40.

WU, Z. Q., YANG, X., WEBER, G. & LIU, X. 2008. Plk1 phosphorylation of TRF1 is essential for its binding to telomeres. *J Biol Chem,* 283**,** 25503-13.

XIANG, Y., YAN, K., ZHENG, Q., KE, H., CHENG, J., XIONG, W., SHI, X., WEI, L., ZHAO, M., YANG, F., WANG, P., LU, X., FU, L., LU, X. & LI, F. 2019. Histone Demethylase KDM4B Promotes DNA Damage by Activating Long Interspersed Nuclear Element-1. *Cancer Res,* 79**,** 86-98.

XIE, A., PUGET, N., SHIM, I., ODATE, S., JARZYNA, I., BASSING, C. H., ALT, F. W. & SCULLY, R. 2004. Control of sister chromatid recombination by histone H2AX. *Mol Cell,* 16**,** 1017-25.

XU, W., YANG, H., LIU, Y., YANG, Y., WANG, P., KIM, S. H., ITO, S., YANG, C., WANG, P., XIAO, M. T., LIU, L. X., JIANG, W. Q., LIU, J., ZHANG, J. Y., WANG, B., FRYE, S., ZHANG, Y., XU, Y. H., LEI, Q. Y., GUAN, K. L., ZHAO, S. M. & XIONG, Y. 2011. Oncometabolite 2-hydroxyglutarate is a competitive inhibitor of alpha-ketoglutarate-dependent dioxygenases. *Cancer Cell,* 19**,** 17-30.

XUE, Y., GIBBONS, R., YAN, Z., YANG, D., MCDOWELL, T. L., SECHI, S., QIN, J., ZHOU, S., HIGGS, D. & WANG, W. 2003. The ATRX syndrome protein forms a chromatin-remodeling complex with Daxx and localizes in promyelocytic leukemia nuclear bodies. *Proc Natl Acad Sci U S A,* 100**,** 10635-40.

XUE, Y., LIU, Z., CAO, J., MA, Q., GAO, X., WANG, Q., JIN, C., ZHOU, Y., WEN, L. & REN, J. 2011. GPS 2.1: enhanced prediction of kinase-specific phosphorylation sites with an algorithm of motif length selection. *Protein Eng Des Sel,* 24**,** 255-60.

YAMANE, K., TOUMAZOU, C., TSUKADA, Y., ERDJUMENT-BROMAGE, H., TEMPST, P., WONG, J. & ZHANG, Y. 2006. JHDM2A, a JmjC-containing H3K9 demethylase, facilitates transcription activation by androgen receptor. *Cell,* 125**,** 483-95.

YANG, X., KHOSRAVI-FAR, R., CHANG, H. Y. & BALTIMORE, D. 1997. Daxx, a novel Fas-binding protein that activates JNK and apoptosis. *Cell,* 89**,** 1067-76.

YE, J. Z., HOCKEMEYER, D., KRUTCHINSKY, A. N., LOAYZA, D., HOOPER, S. M., CHAIT, B. T. & DE LANGE, T. 2004. POT1-interacting protein PIP1: a telomere length regulator that recruits POT1 to the TIN2/TRF1 complex. *Genes Dev,* 18**,** 1649-54.

YODA, K., ANDO, S., MORISHITA, S., HOUMURA, K., HASHIMOTO, K., TAKEYASU, K. & OKAZAKI, T. 2000. Human centromere protein A (CENP-A) can replace histone H3 in nucleosome reconstitution in vitro. *Proc Natl Acad Sci U S A,* 97**,** 7266-71.

YOKOYAMA, Y., HIEDA, M., NISHIOKA, Y., MATSUMOTO, A., HIGASHI, S., KIMURA, H., YAMAMOTO, H., MORI, M., MATSUURA, S. & MATSUURA, N. 2013. Cancer-associated upregulation of histone H3 lysine 9 trimethylation promotes cell motility in vitro and drives tumor formation in vivo. *Cancer Sci,* 104**,** 889-95.

YOUNG, M. D., WILLSON, T. A., WAKEFIELD, M. J., TROUNSON, E., HILTON, D. J., BLEWITT, M. E., OSHLACK, A. & MAJEWSKI, I. J. 2011. ChIP-seq analysis reveals distinct H3K27me3 profiles that correlate with transcriptional activity. *Nucleic Acids Res,* 39**,** 7415-27.

YU, Y., YONG, J., LI, X., QING, T., QIN, H., XIONG, X., YOU, J., DING, M. & DENG, H. 2005. The proteasomal inhibitor MG132 increases the efficiency of mouse embryo production after cloning by electrofusion. *Reproduction,* 130**,** 553-8.

YUAN, W., XIE, J., LONG, C., ERDJUMENT-BROMAGE, H., DING, X., ZHENG, Y., TEMPST, P., CHEN, S., ZHU, B. & REINBERG, D. 2009. Heterogeneous nuclear ribonucleoprotein L Is a

subunit of human KMT3a/Set2 complex required for H3 Lys-36 trimethylation activity in vivo. *J Biol Chem,* 284**,** 15701-7.
YUAN, W., XU, M., HUANG, C., LIU, N., CHEN, S. & ZHU, B. 2011. H3K36 methylation antagonizes PRC2-mediated H3K27 methylation. *J Biol Chem,* 286**,** 7983-7989.
YUAN, X., KONG, J., MA, Z., LI, N., JIA, R., LIU, Y., ZHOU, F., ZHAN, Q., LIU, G. & GAO, S. 2016. KDM4C, a H3K9me3 Histone Demethylase, is Involved in the Maintenance of Human ESCC-Initiating Cells by Epigenetically Enhancing SOX2 Expression. *Neoplasia,* 18**,** 594-609.
YUEN, B. T., BUSH, K. M., BARRILLEAUX, B. L., COTTERMAN, R. & KNOEPFLER, P. S. 2014. Histone H3.3 regulates dynamic chromatin states during spermatogenesis. *Development,* 141**,** 3483-94.
YUEN, B. T. & KNOEPFLER, P. S. 2013. Histone H3.3 mutations: a variant path to cancer. *Cancer Cell,* 24**,** 567-74.
ZALENSKY, A. & ZALENSKAYA, I. 2007. Organization of chromosomes in spermatozoa: an additional layer of epigenetic information? *Biochem Soc Trans,* 35**,** 609-11.
ZALZMAN, M., FALCO, G., SHAROVA, L. V., NISHIYAMA, A., THOMAS, M., LEE, S. L., STAGG, C. A., HOANG, H. G., YANG, H. T., INDIG, F. E., WERSTO, R. P. & KO, M. S. 2010. Zscan4 regulates telomere elongation and genomic stability in ES cells. *Nature,* 464**,** 858-63.
ZHANG, T., COOPER, S. & BROCKDORFF, N. 2015. The interplay of histone modifications - writers that read. *EMBO Rep,* 16**,** 1467-81.
ZHONG, Z., SHIUE, L., KAPLAN, S. & DE LANGE, T. 1992. A mammalian factor that binds telomeric TTAGGG repeats in vitro. *Mol Cell Biol,* 12**,** 4834-43.
ZHOU, H., KUANG, J., ZHONG, L., KUO, W. L., GRAY, J. W., SAHIN, A., BRINKLEY, B. R. & SEN, S. 1998. Tumour amplified kinase STK15/BTAK induces centrosome amplification, aneuploidy and transformation. *Nat Genet,* 20**,** 189-93.
ZHU, K., LEI, P. J., JU, L. G., WANG, X., HUANG, K., YANG, B., SHAO, C., ZHU, Y., WEI, G., FU, X. D., LI, L. & WU, M. 2017. SPOP-containing complex regulates SETD2 stability and H3K36me3-coupled alternative splicing. *Nucleic Acids Res,* 45**,** 92-105.
ZIMMERMANN, M., KIBE, T., KABIR, S. & DE LANGE, T. 2014. TRF1 negotiates TTAGGG repeat-associated replication problems by recruiting the BLM helicase and the TPP1/POT1 repressor of ATR signaling. *Genes Dev,* 28**,** 2477-91.